Int. J. High Technology Ceramics **2** (1986) 1–31

Review: Fabrication of Engineering Ceramics by Injection Moulding. I. Materials Selection

M. J. Edirisinghe and J. R. G. Evans

Department of Materials Technology, Brunel University,
Uxbridge, Middlesex, England

SUMMARY

The present article, Part I, reviews the literature on ceramic powders and organic polymers used to compound ceramic injection moulding mixtures. The intention is to distil, from a somewhat diverse literature, guidelines for the proper selection of materials, with the aim of facilitating the development of the defect-free moulding of ceramic components. Part II will examine mixing methods, moulding techniques and procedures for removal of the organic vehicle prior to sintering.

1. INTRODUCTION

Recent surveys of the world market for ceramics[1–5] show that, while ceramics in electrical and electronic engineering are well established with a high growth rate,[6] the structural ceramics market is at an earlier stage of development but that the demand for ceramic components in heat engines is poised to reach high levels by the turn of the century.[5]

One of the principal difficulties to be overcome before structural engineering ceramics can be fully exploited, especially in heat engine components, concerns fabrication of shapes from powders. At present the ability to produce complex shapes of high dimensional accuracy, high strength and uniformity with low scrap rates and at reasonable cost eludes the industry. Two techniques, i.e. slip casting and injection moulding, offer versatility. In addition injection moulding offers automated production at high rates.

Int. J. High Technology Ceramics 0267-3762/86/$03·50

In the injection moulding route the following stages in the fabrication process are necessary[7] and need to be developed to a level that precludes the introduction of strength-limiting defects:

1. Compounding, which involves the mixing of ceramic powder with an organic vehicle to confer sufficient fluidity to fill the mould under available machine pressures.
2. Injection of the mould cavity without introducing moulding defects.
3. Removal of the organic vehicle without disrupting the powder body.
4. Sintering of the body to near full density.
5. Final machining.

It is generally considered that for most reciprocating engine components moulding accuracy should be sufficient to dispense with expensive machining. However, the sensitivity of gas turbine efficiency to blade profile and the importance of surface finish suggest the need for a slight final machining for some components.

Only stages 1–3 are novel to the ceramics industry. The present review confines itself to the selection of materials, principally the powder properties and the components of the organic vehicle. A subsequent publication[8] will review machinery development and binder removal methods.

Although injection moulding has been used for natural polymers since the 19th century, in its present form it was first used for fabrication of spark plug insulators in 1937,[9] only to be replaced later by isostatic pressing. There are, however, patented moulding techniques which are conceptual precursors of injection moulding for ceramics. A patent by Miller[10] describes a device in which an extruder is registered with an open mould. Later patents[11] describe a device in which air is used to confer fluidity to a dry powder and to force it into a mould. There is an uninterrupted record of the development of ceramic injection moulding in the patent literature since the 1930s as listed by Hennicke and Neuenfeld.[12] Nevertheless, reports on this technique began to appear in the scientific literature only recently, probably for two major reasons. First, the pressureless sintering to near full density of fine powders of covalently bonded silicon-based ceramics became realistic in the 1970s,[13–17] opening up the possibility of producing complex shapes without expensive high pressure processes or machining. Secondly, the revolution in materials selection for critical engine parts has focussed on ceramics for the reciprocating engines, gas turbine[18,19] and rocket[20] engines. Although ceramic injection moulding techniques are not yet sufficiently developed to qualify as a significant fabrication process, it is clear that many organisations are developing this technique for the net shape fabrication of

complex structural ceramic components.[21–38] Component complexity and the need for large-scale production suggests that the most feasible manufacturing technique is injection moulding.[38]

According to Strivens[39] components with dimensions from 2·5 to 25 mm can be made to a tolerance of 1%. In addition the components produced would have the surface finish demanded for thread guides and wire drawing dies.[40] The only disadvantages are the rather complicated binder removal process and high tooling costs.[41]

A characteristic of published work on ceramic injection moulding is that the literature is frequently silent on crucial experimental detail. This arises from the difficulty of defending proprietry knowledge of optimum organic vehicle components. Neither is there a logical theme to the development of this technology; much work is haphazard in its empirical approach. It is only in recent years that systematic studies[30,35–38] have begun in earnest.

2. CERAMIC POWDER

2.1. Shrinkage considerations

Most of the candidate materials for engineering ceramics applications have been subject to injection moulding studies, principally silica,[42] silicon for the fabrication of reaction-bonded silicon nitride,[43] silicon nitride itself,[44] silicon carbide,[45,46] alumina and zirconia.[47] The powder characteristics have a strong influence on the green density and mechanical strength of the body after binder removal and on the viscosity of the moulding mixture. It is important to achieve a high green density for a given powder not just because the error in firing shrinkage increases as the overall shrinkage increases[39] but because failure to achieve a near-maximum powder volume fraction in a polymer may result in the body slumping or distorting during removal of the organic vehicle. What is perhaps more important than the net green density is the uniformity of powder packing throughout the moulded body. Non-uniform shrinkage during sintering resulting from poor mixing of polymer and ceramic may result in a type of distortion which, as for example in thin aerofoil sections, cannot be corrected by subsequent machining.

There are several contributions to shrinkage in the injection moulding process which must be taken into account in die design. In the first place there is a shrinkage of the moulded body by thermal contraction during cooling in the cavity. Typical coefficients of expansion for polymers used in ceramic moulding, together with shrinkage to be expected by cooling from the melting point to room temperature (20°C) for a typical 35 vol%

TABLE 1

Typical Melting Points and Coefficients of Thermal Expansion for Polymers used in Ceramic Moulding Together with Shrinkage to be Expected for a 35 vol% Formulation with Silicon Nitride[a] on Cooling from Melting Point to Room Temperature

Polymer	*Melting point/°C*	*Thermal expansion coefficient/ MK^{-1}*	*Thermal expansion coefficient of formulation/ MK^{-1}*	*Shrinkage on cooling from melting point to 20°C/%*
Polypropylene	171	80	31	0·5
Low density polyethylene	132	190	69	0·8
Polystyrene	240	70	27	0·6

[a] Thermal expansion coefficient, $3{\cdot}8\,MK^{-1}$.

polymer blend with silicon nitride, are given in Table 1.[48,49] If the polymer is partially crystalline there is a shrinkage associated with solidification. Specific volumes for amorphous and crystalline components of typical polymers are given in Table 2.[50] When the organic vehicle is removed there is a further slight shrinkage associated with the drawing together of particles by capillary action. In a moulding composition there must be excess vehicle to prevent the particles contacting or the composition would be too viscous to enter the mould. Finally, the largest shrinkage contribution is caused by pore removal during sintering.

In practice, using conventional metrology equipment the moulding shrinkage (S_m) can be found from the dimensions of the moulded body L_1 and the mould itself L_0:

$$S_m = \frac{L_0 - L_1}{L_0} \tag{1}$$

The small shrinkage due to polymer removal involves accurate measurements on an extremely fragile body and is normally included in the sintering shrinkage S_s:

$$S_s = \frac{L_1 - L_2}{L_1} \tag{2}$$

where L_2 is the dimension of the as-sintered body.

Thus the final dimensions are related to the die dimensions by

$$S_s = 1 - \frac{L_2}{L_0(1 - S_m)} \tag{3}$$

and since $S_m < 0{\cdot}02\, S_m \approx -\ln(L_1/L_0)$.

TABLE 2
Specific Volumes for Amorphous and Crystalline Components of Polypropylene, Low Density Polyethylene and Polystyrene

Polymer	*Specific volume/$m^3\ Mg^{-1}$*	
	Amorphous	*Crystalline*
Polypropylene	1·128–1·233	0·986–1·032
Low density polyethylene	1·172–1·176	1·060–1·073
Polystyrene	0·950–0·977	0·888–0·898

If the final relative density ρ_s is known the volume fraction V of powder in the moulded body can be related to the sintering shrinkage S_s by

$$1 - \frac{V}{\rho_s} = 3S_s - 3S_s^2 + S_s^3 \tag{4}$$

(The common approximation $1 - (V/\rho_s) = 3S_s$ should be avoided as it introduces a large error: 17% for a linear shrinkage of 15%.)

This equation assumes that shrinkage is uniform in all directions and that there are no volume dilations associated with phase changes during sintering.

2.2. Effect of powder on viscosity

The volume fraction of powder in the injection moulding blend is limited by the viscosity of the powder–fluid mixture which increases steeply as $V > 0{\cdot}5$. The derivation of the filler volume dependence of viscosity has an identical mathematical derivation to the filler volume dependence of the elastic constant for particle-reinforced composites.[51] The first theoretical treatment was due to Einstein[52] but was valid for very dilute systems of spherical particles at volume fractions less than 0·1:[53]

$$\frac{\eta}{\eta_0} = 1 + 2{\cdot}5V \tag{5}$$

where η is the viscosity of the suspension and η_0 the viscosity of the fluid.

Subsequent treatments have attempted to extend the theory to concentrated suspensions and non-spherical particles; these have been reviewed by Rutgers[54] and Frisch and Simha.[55]

Eilers[56] used an equation of the type

$$\frac{\eta}{\eta_0} = \left(1 + \frac{1{\cdot}25V}{1 - (V/V_{max})}\right)^2 \tag{6}$$

where V_{max} is the maximum space filling efficiency for uniform-sized spheres ($V_{max} = 0{\cdot}74$) and this gave a fit with results of experiments for emulsion

systems where particle sizes ranged from 1·6 to 4·7 μm. In fact this particle size range is too large to use $V_{max} = 0{\cdot}74$ and this has been a source of criticism.[57] One important approach was to consider a general power-series equation in volume fraction:

$$\frac{\eta}{\eta_0} = 1 + k_1 V + k_2 V^2 + k_3 V^3 + \cdots \tag{7}$$

where k values are constants and $k_1 = 2{\cdot}5$ from Einstein's treatment.[52] Several workers have established different values for k_2 and k_3 and these attempts have been reviewed by Goodwin.[58] De Bruijn[59] assumed that eqn (7) was a quadratic and that the relative viscosity η/η_0 would become infinite when the volume fraction reached the value for the cubic close-packed spheres. The value of k_2 then becomes 4·7 but increases slowly as the packing fraction decreases. Vand[60] assumed that after collision two particles, considered as monosized spheres, would separate along rectilinear paths and this led to an equation of the form

$$\frac{\eta}{\eta_0} = 1 + 2{\cdot}5V + 7{\cdot}349V^2 \tag{8}$$

This was found[61] to fit experimental data for glass spheres in a glycerol solution up to a concentration of $V = 0{\cdot}5$. Subsequently, Manley and Mason[62] and Mooney[57] have shown that Vand's assumption[60] was not fully justified, as it can be proved that paths of recession of two colliding spheres are curvilinear and mirror images of their paths of approach.

At very high concentrations a large number of terms in eqn (7) would be required to calculate η/η_0 and the higher power terms would have an increasing influence on the value obtained.

Another more acceptable approach was to consider an infinite power-series in a general form of an exponential function:

$$\frac{\eta}{\eta_0} = \exp(2{\cdot}5V) \tag{9}$$

Equation (9) has been modified by including a factor h so that it satisfied disperse systems in general:[54]

$$\frac{\eta}{\eta_0} = \exp\left(\frac{2{\cdot}5hV}{1 - hV}\right) \tag{10}$$

Mooney[57] has developed an identical equation for monodisperse spheres, in which he took into account the crowding of particles in concentrated suspensions:

$$\frac{\eta}{\eta_0} = \exp\left(\frac{2{\cdot}5\,V}{1 - k\,V}\right) \tag{11}$$

where k was called the crowding factor; $k = 1/V_{max}$ where V_{max} is the volume fraction for maximum packing. Spheres in a cubic close-packed lattice ($V_{max} = 0{\cdot}74$) were considered to exhibit infinite viscosity because of mechanical interlocking. Simple cubic packing ($V_{max} = \pi/6$) was taken to provide the greatest density which would permit continuous movement. Thus the lower and upper limits of k are

$$1{\cdot}35 < k < 1{\cdot}91$$

Mooney[57] has pointed out that Vand's theory[60] gives a k value of 0·61 which was well outside the limits of k. He points out that Vand's experimental observations[60] can be made to fit his equation if $k = 1{\cdot}43$.

Brodnyan[63] extended Mooney's equation, shown as eqn (11), to ellipsoidal particles:

$$\frac{\eta}{\eta_0} = \exp \frac{(2{\cdot}5\,V + 0{\cdot}399(p-1)^{1{\cdot}48}\,V)}{1 - k\,V} \tag{12}$$

where p is the axial ratio. This equation was found to fit experimental data up to $V = 0{\cdot}55$. This was extended on an empirical basis by Kitano *et al.*[64] to give a relationship for acicular particles:

$$\frac{\eta}{\eta_0} = 1 - \frac{V}{0{\cdot}54 - 0{\cdot}0125p} \tag{13}$$

Krieger and Dougherty[65] derived an equation by a modification of Mooney's analysis:[57]

$$\frac{\eta}{\eta_0} = (1 - kV)^{-2{\cdot}5} \tag{14}$$

and this has found experimental justification.[66]

The work of Chong *et al.*[67] has shown good fit between experimental results and an equation of the type

$$\frac{\eta}{\eta_0} = \left(1 + \frac{0{\cdot}75V/V_{max}}{1 - (V/V_{max})}\right)^2 \tag{15}$$

for V/V_{max} close to unity.

2.3. Effect of particle size distribution

Equations (5)–(15) are valid for particles of uniform diameter and near spherical shape and it is pertinent to note that modern developments in ceramic powders[68,69] are yielding materials which closely meet those

conditions. In fact the requirement for uniform shrinkage without discontinuous grain growth during sintering imposes the requirement of near uniform particle size, for which, given sphericity, $V_{max} \simeq 0{\cdot}74$. The disadvantage of this approach is the low green density and consequent high sintering shrinkage compared to the more traditional approach of achieving high green density by blending of particle sizes.

Clearly if a range of particle sizes is present the value of the crowding factor k in Mooney's equation[57] changes. Unfortunately, fit with experiment has usually been obtained by choosing rather than deriving a suitable value of k. Theories on the viscosity of polydisperse systems have been developed by Lee[70] and by Farris.[71] Chong[67] has also developed his own equation to consider more complex particle size distributions. In general, the incorporation of more than one particle size leads to a decrease in viscosity for the same volume fraction of powder but it is generally insufficient to replace k with a new, higher packing efficiency.

There are cases in the fabrication of ceramics where a wide distribution of particle sizes can be accommodated without consequent grain growth during sintering. One such case is the fabrication of reaction-bonded silicon nitride where vapour phase reactions refine the grain size during nitriding[72] and Mangels[43,73] has made use of the reduced viscosity of wide size distribution powders to produce injection moulding blends of high powder loading (73·5 vol%).

Farris[71] attempted to predict the viscosity of multimodal suspensions from data for monomodal suspensions. For uniform spherical particles viscosity increased steeply after $V = 0{\cdot}5$, approaching infinity at $V = 0{\cdot}74$. However, if the total volume of particulate filler is split into 25% fines and 75% coarse, very high loading can be obtained without increase in viscosity; this is shown in Fig. 1. If the ratio of the coarse to fine particle diameters is 7:1 the volume of filler can be increased to $V = 0{\cdot}73$ from the monomodal loading of $V = 0{\cdot}59$ without increase in viscosity. Figure 2 shows the proportion of coarse and fine particles to give minimum viscosity for a range of total filler loading, indicating minima in the region of 30% fines.

Strivens[74] attempted to analyse the influence of particle size distributions on the packing characteristics and filler loading in an injection moulding mix. He observed that one intermediate milling time yielded a powder with improved flow behaviour during moulding but this material was not characterised. A patent by Waugh[75] states that better mixing was obtained if fines were added to the mix when using a bimodal powder distribution for investment casting cores. In 1978, Mangels[43] working with silicon powder obtained particle size distributions by dry ball milling and air classifying as shown in Fig. 3, and subsequently showed that a 140 h dry

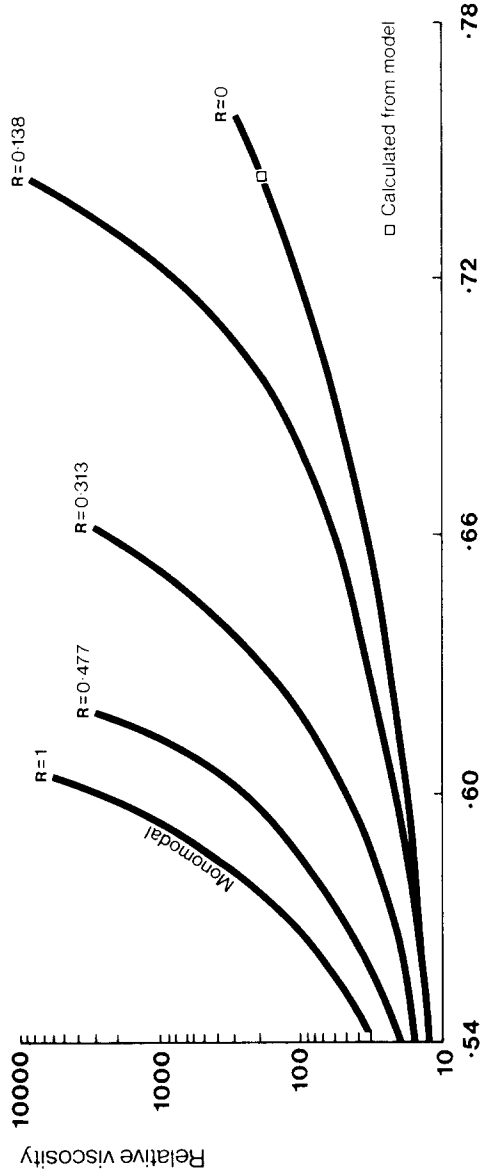

Fig. 1. Calculated and measured viscosities of monomodal and bimodal suspensions; after Farris.[71]
R = (mean fine particle size)/(mean coarse particle size).

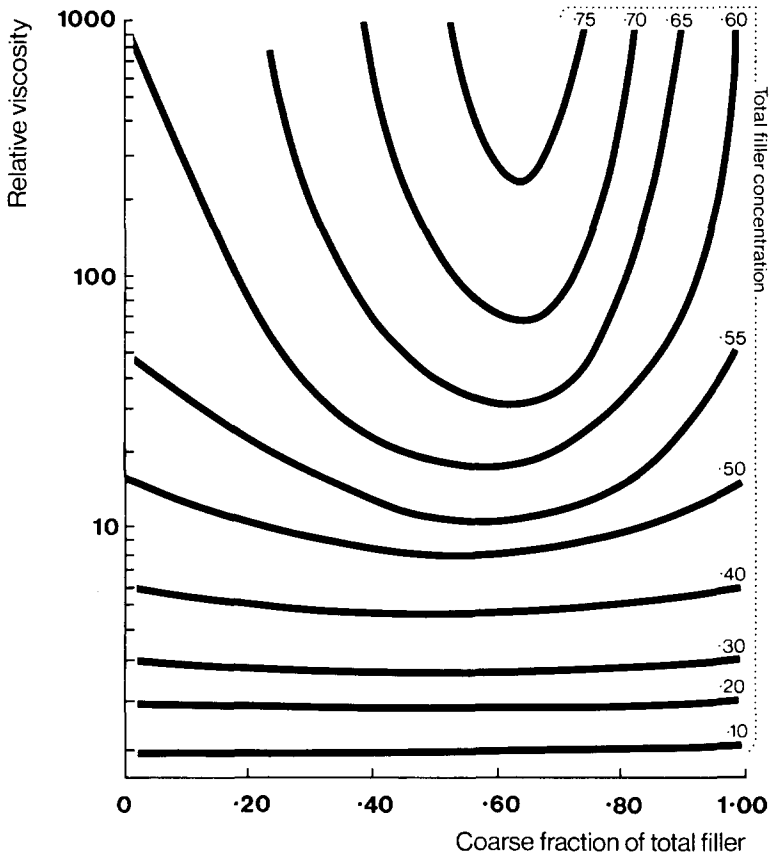

Fig. 2. Comparison of calculated viscosity for bimodal suspension for various blend ratios and concentrations; after Farris.[71]

ball-milled powder with the broadest particle size distribution yielded the best viscosity in a spiral flow mould test.[73] In general, by altering the particle size distribution from a sharp, monomodal type[76] distribution to a very broad distribution the solids content can be increased without increasing the viscosity of the system.[41] Similar requirements have been noted by Adams[77] for slip cast ceramics and there is a similarity with the requirements for achieving high green density in a pressed powder.[78–80]

2.4. Effect of particle size and shape

Matsumoto and Sherman[81] found k, the crowding factor defined by Mooney,[57] to be very sensitive to mean particle size. In contrast, Barsted *et al.*[82] found only a small variation in k over a broader particle size range than that employed by Matsumoto and Sherman.[81] Thus the value of k does not vary systematically with particle size.

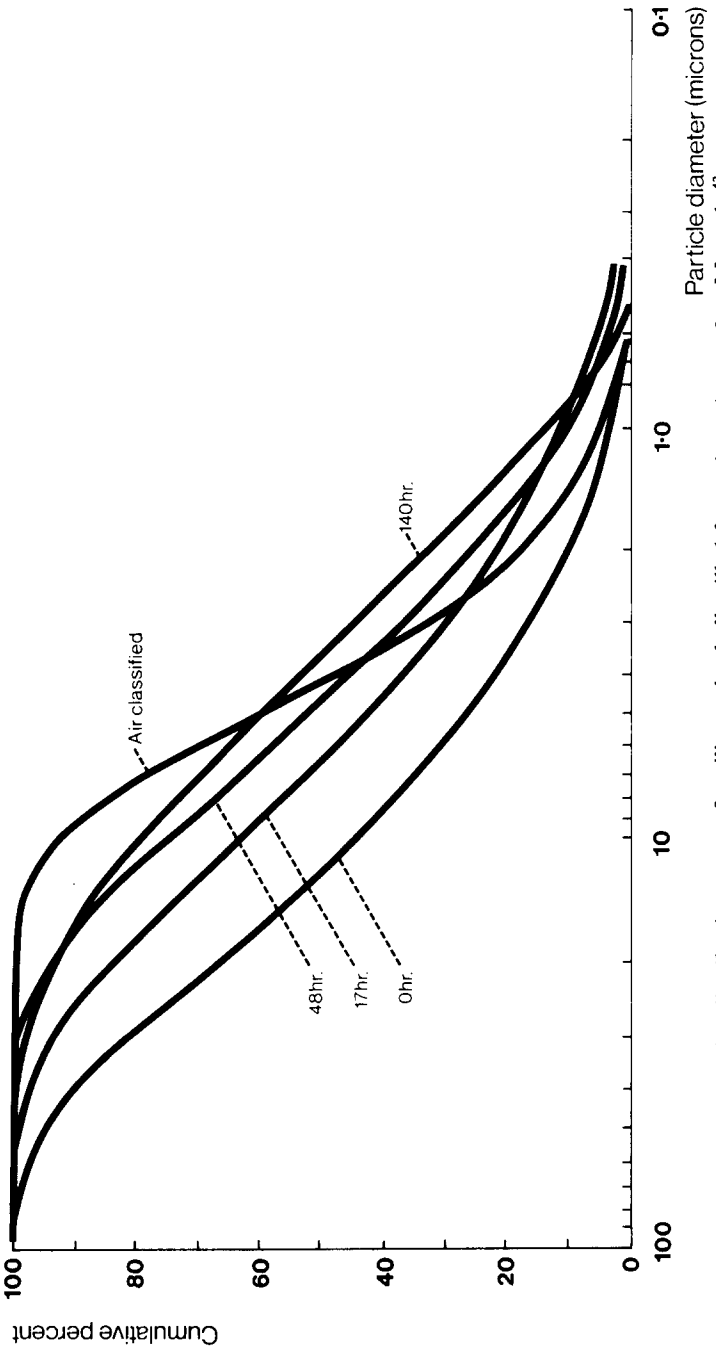

Fig. 3. Particle size distribution curves for silicon, dry ball-milled for various times; after Mangels.[43]

This is not surprising as eqns (5)–(15) do not allow for an effect of overall particle size on viscosity. Yet this effect has been noticed.[83,84] It was found that viscosity sometimes increased as particle diameter decreased and this has been attributed to an adsorbed immobile layer on fine particles which effectively increases particle diameter[83] and hence total filler loading. Willermet *et al.*[46] report a halving of spiral flow length during moulding, caused by a decrease in mean particle diameter from 28 to 10 μm. There does not appear to be a sound explanation for this but the respective particle size distributions were not given.

A further explanation of the effect of particle size on viscosity for a fixed volume loading may be sought from the combined effects of particle size and shape. The effect of non-spherical morphology on the viscosity of suspensions may influence both the packing efficiency of the powder V_{max} and the effective radius of rotating particles in shear. Mangels and Trela[41] therefore preferred a spherical particle morphology to obtain maximum prefired densities. The effect of shape on V_{max} is shown in a study of vibratory compaction of spheres and angular particles.[85] For spherical particles the packing efficiency is not influenced by particle diameter, but as the number of sides of the particle considered as a regular polyhedron decreases, i.e. as the particles become more angular, the effect of particle diameter on the packing efficiency becomes more pronounced and packing efficiency decreases with decreasing particle diameter. This may help to explain the results of Willermet *et al.*[46] mentioned above. An apparent contradiction to this effect was noted by Mutsuddy[47] who found that a higher proportion of angular alumina particles than spherical zirconia particles could be accommodated in injection moulding blends. However, since the particle size distribution of the two powders was different, this is inconclusive.

2.5. Effect of agglomerates

The viscosity of ceramic injection moulding blends is also influenced by the tendency of fine particles to agglomerate. The adhesion forces between particles have been discussed by Rumpf and Schubert.[86] In addition to electrostatic and van der Waals' forces the presence of liquid and solid bridges contribute to high agglomerate strength. The initial drying of powders and the heating associated with processing with a high molecular weight organic vehicle help to reduce the effect of liquid bridges. The presence of solid bridges when a small amount of additive has been incorporated in the powder via a salt by spray drying, such as magnesia in alumina or yttria in zirconia, gives rise to more serious problems. Such agglomerates can only be broken down by milling of the powder or by using mixing devices which impose high shear stress to the blends.

The dispersion of powders in liquids is influenced in part by the wetting characteristics of the liquid on the solid surface. The dispersion of ceramic titanate powders in a range of organic liquids has been related to the hydrogen-bonding capability of the liquid[87] which can be expressed as its cohesive energy density.[88] In systems where it is not possible to change the entire liquid phase the interfacial interactions can be modified by so-called coupling agents added as pre-treatments to the powder or directly to the melt. One of the simplest such surface-active agents is stearic acid which has found frequent use[32] as a minor vehicle component.

The effect of such coupling agents on viscosity is a matter of controversy. Intuitively, if agglomerates are dispersed, the particle size distribution would be evened out and, according to the arguments presented above, the viscosity should increase. This has been observed by Bigg[89] using low density polyethylene and 5–44 μm steel spheres at 60% volume loading. Addition of a silane and a titanate coupling agent increased the viscosity of the blend considerably. However, this effect cannot be attributed entirely to the breakdown of agglomerates since the starting powder was not well agglomerated. Results of such experiments are surprisingly contradictory. Han *et al.*[90] report that both organic and silane coupling agents reduced the viscosity of calcium carbonate-filled polypropylene but that organic titanate coupling agents increased the viscosity of polypropylene–glass systems. Bretas and Powell[91] found that both titanate and silane coupling agents increased the viscosity of polyethylene–40 vol% glass. Other workers[92–94] observed decreases in viscosity due to coupling agents. Much of the confusion may be due to the *ad hoc* way in which the quantity of coupling agent is added; typically 0·2–2 wt% based on the filler.[95] The adsorbed coupling agent may hold a layer of polymer tightly to the particle, thus increasing its effective diameter and the effective volume fraction of filler. The excess coupling agent, being a bulky low molecular weight species, may act as a plasticiser for the polymer.

The confusion that surrounds the role of agglomerates is not helped by the suggestion of Mutsuddy[47] that agglomerates raised the viscosity of injection moulding blends contrary to the above arguments. Precise density determinations are needed to assess the increase in effective volume fraction of powder due to undisplaced gases.

3. OPTIMUM ORGANIC VEHICLE CONTENT

There is at present no simple way of calculating the optimum organic vehicle content for different types of powder from powder characteristics. In a patent Bailey[96] stated that the binder concentration should be at least 2 vol% in excess of the void volume and that it can vary from 102 to 115% of the void volume where the ceramic particles should be just 'floating' in

minimum binder. Mutsuddy[97] has applied a technique used extensively in the printing ink industry and in the characterisation of carbon black fillers for elastomers. A torque rheometer was used to provide a quantitative assessment of the critical powder volume concentration in the plastic forming of ceramic mixes. In this technique, the ceramic powder was mixed with an oil, the oil being added at a constant rate. The volume of oil at which the maximum torque occurred was used to obtain the critical powder volume concentration (CPVC). The CPVC value differs slightly in practice from the optimum powder loading for different powder types but the method considerably shortens an extensive experimental optimisation process.

4. SELECTION OF ORGANIC VEHICLE

For the extrusion of ceramics it is sufficient that an organic vehicle should confer fluidity to the powder. For injection moulding it must also be possible to bring about a change in material properties of the mixture, during residence in the cavity, such that the moulded article has sufficient resistance to shear stresses to withstand knock-out and handling. This change in properties should obviously take place within a reasonable time. Clearly, although dimensional tolerances can be rectified by minor post-sintering machining operations, the distortion of moulded components during ejection or handling results in scrap.

These requirements can be met by the cooling, in the cavity, of thermoplastic, both crystalline and amorphous, or the freezing of water-based polymer solutions. The crosslinking of thermosets by injection into a heated cavity fulfils the same requirements, as indeed does the thermo-gelling of water-soluble polymers.

Organic vehicle systems used to injection mould ceramics are almost exclusively composed of two or more components. The components used can be classified into one of four categories:[98]

1. *Major binder component:* This material determines the general range of final binder properties.
2. *Minor binder component:* Often used is a thermoplastic or oil which is removed early in the binder removal cycle. It is often claimed that this generates pore channels to the interior part allowing easier removal of the other components;[98] however, this is undoubtedly an over-simplification.
3. *Plasticisers:* The function of these minor additives is to increase the fluidity of the ceramic–binder mixture.

4. *Processing aids:* These minor additives are used mainly as surfactants to the ceramic powder. They improve the wetting characteristics between binder and ceramic during mixing.

Selection of the organic vehicle system to suit the ceramic powder is necessary for successful moulding but as yet selection has been more a matter of experience than a scientific development.

4.1. Selection criteria

Qualitatively, the major binder should present the following properties (there is at present insufficient published work to define quantitatively the upper and lower bounds of such properties):

—Confer fluidity upon the powder sufficient for defect-free filling of the cavity.
—Wet the solid powders in order to aid dispersion and remove entrapped gas.
—Show stability under mixing and moulding conditions.
—Confer adequate strength to the body during the initial stage of polymer removal.
—Leave a low residue after burn-out.
—Have an adequate shelf life.
—Be readily available at acceptable cost.

A plasticiser has been referred to as a high boiling solvent possessing an affinity for various kinds of polymers.[99] In the ceramic injection moulding context it should present the following properties:

—Compatibility with the binders: It should not react but form an intimate mixture with the binders increasing the free volume of the polymer and thereby lowering viscosity.
—Low volatility: This ensures the retention of the plasticiser compound during processing which is necessary for consistency of ceramic powder volume loading.

The processing aid may consist of more than one component. Ideally, a low cost processing aid is required and it should perform the following functions:

—Modify adhesive forces between polymer and filler, thus dispersing the organic vehicle components throughout the mix and enhancing deagglomeration of filler particles.
—Reduce melt viscosity.
—Allow easy mould release.

The criteria for the selection of an organic vehicle system is that it will, first, give correct rheological properties to the ceramic–binder mix during injection moulding and, secondly, become amenable to successful removal.

Rheology of these systems has been studied extensively by researchers using the capillary rheometer.[100] Spiral-flow measurements too have been cited by several workers.[46,48,100] The use of spiral flow moulds to assess the mould-filling ability of a material is well established and has greater similarity to the moulding situation than the more exact flow curves obtained by rheometry.[101] Mutsuddy[47] has also used a dynamic oscillatory-type viscometer to minimise particle migration effects that may be present in capillary rheometer measurements wherein the material at the capillary wall may be depleted in powder. However, this method has less similarity to injection moulding conditions.

The major difficulty at present is the task of arriving at a model to relate experimental observations to the flow behaviour during actual injection moulding. Attempts to use models, like the Weir model,[102,103] suitable for straight polymers have been found to be unsuccessful.[100] Computer modelling of fluid flow during injection moulding[104] is being investigated in order to develop models suitable for ceramic–binder systems.

Therefore, qualitative and semi-quantitative guidelines for the ceramic–binder system rheology have been advocated. Firstly, the formulation should have either Bingham or pseudoplastic flow characteristics. It has been found that if the mix has a very high yield stress it extrudes into the mould cavity like a thread of ribbon that coils upon itself, tending to trap air and induce mechanical stresses.[38] On the other hand, a very low yield stress has caused the moulded part to deform in the binder removal stage.[38] Moore[105] described a method by which the yield stress can be estimated from capillary rheometer data but this construction cannot be applied to some high polymer systems.[106] It has been claimed that good flow during injection moulding requires a viscosity of less than 1000 Pa s (10^4 Poise) in the shear range usually encountered in the gates and mould, which ranges between 100–1000 s^{-1}, although it could occasionally reach 10 000 s^{-1}.[47] Thus, it can be inferred that a suitable ceramic–binder system mix should have viscosities below 1000 Pa s in the 100–1000 s^{-1} shear range. Recent work has attempted to define parameters from capillary rheometer results and relate these to the mouldability of formulations.[106] The parameters selected were the gradient of the viscosity shear rate graph, the fluidity, and the rate of change of viscosity with temperature. The analysis was performed at the shear rate and temperature at the nozzle (entry to the mould). Extraction of organic vehicles from injection moulded ceramics is a potentially time-consuming operation. Thermal degradation of the organic vehicles has been widely used and the relevant parameter is the

decomposition rate[107] in the bulk which frequently differs considerably from the decomposition of thin films. The decomposition rate can be controlled by the selection of a proper binder system, containing a mixture of polymers with different decomposition characteristics, in order to broaden the burn-out region.[108,109] Solvent extraction,[110] evaporation[111] and capillary action to remove the organic vehicles[112] have also been used and these impose different criteria. Capillary action requires low viscosity systems such as waxes or oils. Evaporation under reduced pressure was viable with paraffin waxes[111] and solvent extraction has been found to function with partially oxidised waxes blended with coumarone-indene resin.[110]

5. POLYMER SYSTEMS IN USE

Polymer systems may be broadly classified as thermoplastic or thermosetting.

A subsidiary classification could be made according to the demands of the blending and moulding equipment.[8] Some moulding equipment uses low pressures and therefore low viscosity mixtures[112] and is close generically to resin casting, employing mainly oils and waxes. Mixtures of intermediate viscosity, low molecular weight thermoplastics and thermosetting resins can be prepared by using blade-type mixers. The full benefit of high shear mixing and high pressure moulding can only be obtained with high molecular weight thermoplastics.

Much of the published work on organic vehicle formulations is deficient in precise experimental technique and this has often made it difficult to interpret the significance of results.

5.1. Thermoplastic systems

Many thermoplastics which are themselves routinely injection moulded satisfy most of the conditions stipulated in order to be effective binders and have been used extensively, especially for silicon-based ceramics. Japanese patent publications[113] mention a mixture that includes a styrene–butadiene copolymer. In this instance diethyl phthalate was used as a plasticiser and stearic acid as a lubricant. In another instance a mixture of styrene–butadiene copolymer and thermosetting resins has been used.[114] Polyolefins such as polyethylene, polypropylene or polybutene are first recorded in use in the United States.[115] In this case, however, the binder was added in large amounts which gave rise to problems in removal and dimensional control.

Partial substitution with substances like wax, phthalic acid, stearic acid or low boiling point oils has been recommended.[116] A mixture of polystyrene plasticised with light oil and beeswax[116] has also been attempted but when incorporated in large proportions the light oil tended to coagulate during injection moulding. Since a large volume fraction of oil and resin was used in the ceramic mixture a low green density resulted. Diethyl phthalate has been employed as a substitute for light oil.[116]

More recently, atactic polypropylene was used as a successful injection moulding mix.[117,118] It is reported that atactic polypropylene rendered the mix sufficiently fluid for injection moulding and also allowed the thermal decomposition rate to be freely adjusted. The latter effect was made possible by mixing different fractions, having molecular weights of 5000–12 000. This patent goes on to state that an even more effective injection moulding formulation was achieved by adding other thermoplastic resins such as ethylene vinyl acetate, polystyrene and polymethylmethacrylate. Plasticisers and lubricants were also used. The plasticisers included diethyl phthalate, dibutyl phthalate, dioctyl phthalate and diallyl phthalate. The lubricants included stearic acid, paraffin wax and ester wax. Atactic polypropylene, the amorphous waste product from isotactic polypropylene production, has the advantage of being one of the lowest cost polymers on the market. Recent work at Toyota Motor Corporation[36] used polypropylene-based thermoplastic binders, with phthalates as minor additives. After successful injection moulding and vehicle removal, ceramic swirl chambers yielded a Weibull modulus of 20·3. Since the removal stage is just as liable to introduce critical defects as the moulding stage this high Weibull modulus appears to indicate the suitability of polypropylene binder systems.

Litman *et al.*[108] working with silicon powder loadings of up to, or in excess of, 70 vol% experimented with several thermoplastic binders. These included low and high density polyethylene, polystyrene, polypropylene, nylon, acrylonitrile–butadiene–styrene, styrene–acrylonitrile and polyurethane. Only polypropylene was found suitable. Others were rejected on the basis that their melt viscosity was relatively high at standard processing conditions and increased further as the filler was added. They also found that loading of the polypropylene was further improved by adding hydrogenated peanut oil, which acted as a diluent and lubricant, reducing the viscosity significantly. Litman *et al.*[108] have also reported success with a series of low molecular weight polyethylenes and microcrystalline waxes.

Patent literature[119] describes the use of thermoplastic, rubber-related ABAB block copolymers. A is a linear branched polymer that is glassy or crystalline at room temperature and has its softening point in the range

of about 80–250°C. B behaves as an elastomer at processing temperatures. Although the patent[119] claimed almost any thermoplastic was suitable for A blocks, the examples cited used polystyrene. Polybutadiene, polyisoprene and poly(ethylene butylene) were used as B blocks. Plasticisers such as naphthanic or paraffinic oils or waxes were optionally added. In addition, supplementary resins and fillers such as carbon black that increase the stiffness, elastomers that increase the tear strength and anti-oxidants that retard oxidation were used. Processing aids used include methyl acetylricinoleate, stearic acid, polyethylene, polyethylene wax, mixtures of natural waxes and wax derivatives, different types of vegetable fat and partially oxidised polyethylene.

An interesting development has been reported by Burroughs and Thornton[120] and also by Matkin *et al.*[121] whereby the binder used was a silicone resin which was not fully removed prior to sintering but was converted to silica and incorporated in the final microstructure of the body. Such formulations are limited to ceramics where an additional 2 wt% of silica can be tolerated. This is the case for some silicon nitrides prepared by either reaction bonding or sintering but would be unsuitable in high purity refractory oxides.

Swedish research workers[107] have used polyethylene and stearic acid with 57 vol% filler loading of silicon nitride powder. The use of polyethylene has also been described in the patent literature.[96] In this instance it was mixed with polyethylene glycol. Tritolyl phosphate and glycerol monostearate were added to the mixture as release agents. This binder system was particularly successful in the injection moulding of electrical insulating bodies, semi-conductors and cores for metal casting. Mutsuddy[47] chose a low molecular weight ethylene–vinyl acetate copolymer with a melt flow index of 200 and a density of $0{\cdot}920\,Mg\,m^{-3}$ as the major binder. Several plasticisers have been mentioned for ethylene–vinyl acetate copolymers;[122] phthalates and butyl stearate are among them. Moteki[123] has evaluated some phthalates which are compatible with polystyrene and has recommended diethyl phthalate as a compatible plasticiser for alumina–polystyrene formulations. Farrow and Conciatori[124] have successfully injection moulded alumina using polyacetal binders. Low density polyethylene, atactic polypropylene and an ethylene–vinyl acetate copolymer were also added to the mixture. The binder system provided easy and defect-free burn-out.

There are several instances[125–129] where typical thermoplastic systems were used in formulations containing silicon carbide powder. These included polyethylene, acrylic resins, acrylonitrile–butadiene–styrene, nylon, ethylene–acrylic acid copolymers, polystyrene, polybutylene, polysulphone and polyethylene glycol. Polystyrene was found to be particularly

acceptable. Sugano[130] has described the injection moulding of silicon carbide powder using plasticised polystyrene as a vehicle. The author emphasised the importance of plasticisers to control fluidity and draws attention to the effect of high injection temperatures in creating residual stresses in the moulded article which are themselves relieved by plasticiser addition. Sugano also pointed out what is no doubt a universal but unstated observation that ceramic injection moulding formulations do not display die swell typical of high polymers. Nevertheless, recent work in the UK indicated that polystyrene binder systems in silicon powder give rise to poor rheological properties.[131]

A method of producing β-silicon carbide injection moulded components using α-silicon carbide with a particle size not more than 400 mesh has been described.[129] The binder system consisted of poly(*n*-butyl methacrylate), di(*n*-butyl phthalate), epoxy resin and dicyandiamide. Colloidal graphite was included for subsequent siliciding.

In general, thermoplastic systems contain a variety of other minor additions, such as wax, various types of oil and different fatty acids and their derivates. These are claimed to function as minor binders, plasticisers and processing aids. Frequently the quantities added are arbitrary or unstated. In the CATE turbine blade programme[98] the major binder content was 80 vol% of the total organic vehicle content while the minor binder, plasticiser and processing aid contents were 8, 8 and 4, respectively, of the total organic vehicle content.

5.2. Thermosetting systems

One of the first ceramic injection moulding formulations used has been described by Strivens[39] and is given below:

Component	*% Volume*	*Function*
Ceramic powder*	63·0	filler
Epoxy resin	7·3	binder
Coumarone-indene resin	3·2	diluent
Phenylformaldehyde resin	2·2	hardener
Wax	24·3	plasticiser and mould release

This composition was selected after a study of wax–resin systems, during which more than 100 commercially available waxes were investigated. Wax–resin systems could be one of three basic types—compatible, dispersible or incompatible. Compatible systems have been very difficult to injection mould. Also the moulding efficiency generally increased with fineness and

* Steatite body.

stability of the wax–resin mixture. Waxes based on certain glycol esters of montanic acid or on similar oxidised and esterified hydrocarbon long-chain molecules appear superior. Strivens also used many other formulations in his research and these are described in the early patent literature.[74,109]

For silicon carbide powders a thermosetting plastic has often been used as the major binder.[45,46,132] Although it generally involves a longer cycle time in the mould, it possesses the distinct advantage of producing strong bodies in the as-moulded condition. Also it provides the large carbon content needed for reaction sintering.

The typical composition used at the USA Ford Motor Company's Research and Engineering Centre contains:[132]

Component	*% Volume*
Silicon carbide	47
Phenolfurfural–phenolformaldehyde copolymer	47
Graphite	5
Zinc stearate	1

The patent literature[133] gives examples where thermosets such as epoxy resins or phenolic resins were used. The major advantage was that these reduced thermal deformation of the moulded mass during polymer removal. Nevertheless, this required a large proportion of resin.

5.3. Other systems

Sarkar and Greminger[134] draw attention to the advantages of water-soluble polymers, principally methyl, hydroxyethyl and hydroxypropylmethyl cellulose. These materials allow room temperature processing, ease of dispersing the ceramic powder, the benefit of a two-stage vehicle removal with humidity-controlled drying and the low cost of transient polymer, but may be offset by the disadvantage of hydrolysis of some nitride powders intended for high temperature use.

The use of water-soluble polymers such as the cellulose ethers has been developed into a successful injection moulding process for metal powders.[135,136] Advantage was taken of the thermo-gelling properties of such solutions, whereby the composition solidifies upon injection into a die heated to 90°C. Glycerin and boric acid were added to aid mould release.

The cellulose ethers and polyacrylamides have been used by Birchall *et al.*[137] to process cement powders to produce macro-defect-free cement. Such shapes as bottle caps have been compression moulded using this method.[138]

The advantage from the ceramics viewpoint is the ability to remove the

bulk of the binder (water) by controlled humidity drying, leaving a 'porous' body for polymer removal by pyrolysis. The removal stage can thus be reduced from the order of days, for the carefully controlled heating of thermoplastic binder, to hours.[136]

A composite organic vehicle composition, comprising an incompatible mixture of a water-soluble polymer and a sparingly water-soluble organic substance dispersed in emulsion form, has been used in powder moulding processes including injection moulding.[139] It is claimed that such formulations gave rise to high quality articles. The ceramic powder used in these instances has been alumina or magnesia; the water-soluble polymer was polyvinyl alcohol, methyl cellulose or gelatin, and the organic substance was wax, stearic acid or liquid paraffin. It is noteworthy that water-soluble polymer-based blends may suffer loss of strength in high humidities.[140]

Some Soviet investigations[12] have used clay–wax systems as an alternative to clay–water mixtures. The mixture quoted contained porcelain body, paraffin and beeswax. It was kept liquid in the machine and shaping occurred as a result of the liquid wax stiffening in a cooled mould. In this way cups were made complete with handles.

Waxes have been used extensively in moulding formulations.[107,111,124,141] The wetting characteristics of partially oxidised waxes are the most beneficial factor. It has been suggested that in this respect they are very much better than low density polyethylene. At the Ford Motor Company's Research and Engineering Centre an unstated two-component organic system created problems of density variations during moulding due to vaporisation of components.[30] For these reasons the system was abandoned for a more conventional wax binder system[30] which allowed 73·5 vol% loading of silicon powder.[48]

Mouldable ceramic formulations that comprise a mixture of clay, such as kaolin, with inclusion of hard mineral substances, such as quartz, feldspar, dolomite or wollastonite, have been developed by a German company.[142] Metal stearates such as calcium, magnesium, zinc and aluminium stearate were used as agents for improving flow. Electrolytes such as alkali metal carbonates and/or ammonium carbonate were added to assist removal from the mould. The adhesion of the damp ceramic composition to the mould surface was further reduced by the addition of alkyl sulphonates.

Another US patent[143] describes the use of an organic vehicle having a high solid state vapour pressure. The patent defines this type of organic binder as being solid at normal room temperature but having a melting point of about 200°C and a vapour pressure of at least 1 mm within the temperature range from 20°C to the melting point. Examples of suitable organic materials are naphthalene, paradichlorobenzene and camphor.

These binders reduced the time required for removal and also substantially reduced the associated linear shrinkage to 1% over conventional formulations.[143] The sublimation technique was used with ceramic powders such as silica glass, alumina, beryllia, magnesia and mullite, the principal application being precision cores for metal castings. A colloidal ceramic having a particle size of substantially less than 0·1 μm, such as finely divided alumina or silica, was added to inhibit dilatancy. The addition of a thermosetting material such as gum, shellac or silicone resin further improved the reduction of the binder removal time. This composition provided an excellent combination of good plastic flow properties for injection moulding, rapid bake-out of organic binder within 12 h or less without distortion, shrinkage or excessive porosity, and easy burn-out of the thermosetting resin without forming a shell-like layer on the ceramic.

Recent trade information[144] reveals that two types of ceramic binder systems CB-3 and CB-7 are commercially available but no further details of the constituents have been stated.

6. CONCLUSION

The potential for large-scale production of ceramic components for, *inter alia,* heat engines is critically dependent on the development of shaping techniques. Injection moulding is receiving attention as one of the most promising routes. The success of the moulding process is itself dependent on the correct formulation of the organic vehicle component and the achievement of the optimum filler loading. The general rules for the preparation of injection moulding blends in so far as these have been established are set out above. The development of moulding techniques and removal of organic vehicle will be reviewed in a future article.

There is no doubt that developments over the last half century have been haphazard and there are discernible reasons for this. The difficulty of defending hard-won proprietry knowledge for an organic binder system which is ultimately sacrificed has meant that disclosure in the open literature has been limited. Earlier blending and moulding equipment favoured low temperature, low viscosity waxes and oils while modern moulding techniques, borrowed from polymer composite technology, favour high melting point polymers. The requirements for moulding nitride and oxide ceramics are that carbon residue should not be present, whereas the moulding of silicon carbide, in particular reaction-sintered silicon carbide which accounts for a substantial proportion of published work, requires that residual carbon remain prior to sintering. Furthermore, only the moulding of oxide ceramics permits water-based systems. These diverse

requirements lead to the quite different choices of polymer blends described above.

Future developments are likely to be driven by the need to lower the proportion of defective mouldings, to mould artefacts which include thick sections and to incorporate ceramic fibres, potentially with preferred orientation, into mouldings. This will lead to a refinement of polymeric binders for subsequent pyrolysis in air, the use of decomposition in controlled atmospheres and the use of materials for removal by other techniques, notably sublimation or evaporation. Looking further ahead, there are several possibilities for organic vehicle components which decompose to the relevant ceramic and perhaps, ultimately, for the fabrication of a ceramic body by injection moulding a polymer precursor.

REFERENCES

1. Wachtman, J. B. and Mclaren, M. G., New ceramics, in *Advances in Materials Technology Monitor*, UNIDO, Vienna, No. 2, Aug. 1984, 25–45.
2. *Annual Report on High Technology Materials 1984–85*, Technical Insights Inc., New Jersey, 1985.
3. Kantrow, A. M. and Montgomery, S. (Eds) *High Technology Ceramics in Japan*, National Materials Advisory Board Report No. 418, NRC, Washington DC, 1984.
4. Francis, T. L., Advanced ceramics in the United States, *Interceram*, No. 2 (1985) 31–4.
5. Kenney, G. B. and Bowen, H. K., High technology ceramics in Japan: current and future markets, *Am. Ceram. Soc. Bull.*, **62** (1983) 590–6.
6. Fisher, G., New technologies bolster electronic ceramics economics, *Am. Ceram. Soc. Bull.*, **63** (1984) 569–71.
7. Westlake, R. C., Injection moulding complex ceramics, paper presented at 71st AGM of The American Ceramics Society, Joint Session IV, Presentation No. 2-JIV-69, May 1969.
8. Edirisinghe, M. J., Evans, J. R. G., Hornsby, P. R. and Bevis, M. J., to be published.
9. Schwartzwalder, K., Injection moulding of ceramic materials, *Am. Ceram. Soc. Bull.*, **28** (1949) 459–61.
10. Miller, W. J., *Improved machine for the manufacture of pottery*, UK Patent 283 151, 7 March 1929. Date of filing: 23 Dec. 1927.
11. Triggs, W. A., Marks and Clerk, England, *Method of moulding materials*, UK Patent 400 281, 16 Oct. 1933. Date of filing: 16 April 1932.
12. Hennicke, H. W. and Neuenfeld, K., Injection moulding as a shaping method in ceramics, *Ber. Deut. Keram. Ges.*, **45** (1968) 469–73.
13. Prochazka, S., Sintering of silicon carbide, in *Ceramics for High Performance Applications*, Eds J. J. Burke, A. E. Gorum and R. N. Katz, Brook Hill Publishing Co., Chestnut Hill, Massachusetts, USA, 1974, 239–52.
14. Prochazka, S. and Charles, R. J., Strength of boron-doped hot pressed silicon carbide, *Am. Ceram. Soc. Bull.*, **52** (1973) 885–91.

15. Priest, H. F., Priest, G. L. and Gazza, G. E., Sintering of silicon nitride under high nitrogen pressure, *J. Am. Ceram. Soc.*, **60** (1977) 81.
16. Terwilliger, G. R. and Lange, F. F., Pressureless sintering of silicon nitride, *J. Mat. Sci.*, **10** (1975) 1169–74.
17. Giachello, A. and Popper, P., Post-sintering of reaction-bonded silicon nitride, *Ceramurgia International*, **5** (1979) 110–14.
18. Timoney, S. G. (Ed.), *Survey of Technological Requirements for High Temperature Materials: Diesel Engine*, EUR 7660 EN, EEC, Brussels, 1981.
19. Hartley, J., Japan gears up for ceramics, *Am. Ceram. Soc. Bull.*, **61** (1982) 911–12.
20. Schnittgrund, G. D., Injection moulded ceramic rocket engine components, *SAMPE Quart.*, **12** (1981) 8–13.
21. Taylor, H. D., Injection moulding intricate ceramic shapes, *Am. Ceram. Soc. Bull.*, **45** (1966) 768–70.
22. McLean, A. F., Overview of ARPA/ERDA/FORD ceramic turbine programme, in *Ceramics for High Performance Applications—II*, Eds J. J. Burke, E. N. Lenoe and R. N. Katz, Brook Hill Publishing Co., Chestnut Hill, Massachusetts, USA, 1978, 1–34.
23. Heckel, J., Heuer, J., Raeuchle, W. and Tank, E., Designing and testing silicon nitride components at Mercedes–Benz, ibid., 445–80.
24. Poschel, W. H., Siebmanns, W. and Trappmann, K., Development of ceramic parts for a truck gas turbine at MTU, ibid., 481–502.
25. Richerson, D. W., Schuldies, J. J., Yonushonis, T. M. and Johansen, K. M., ARPA/Navy ceramic engine materials and process development summary, ibid., 625–50.
26. Andersson, C. A., Bratton, R. J., Sanday, S. C. and Cohn, A., Progress on ERPI ceramic rotor blade program, ibid., 783–804.
27. Bunk, W., Gugel, E. and Walzer, P., Overview of the German gas turbine programme, in *Ceramics for High-Performance Applications—III*, Eds E. M. Lenoe, R. N. Katz and J. J. Burke, Plenum Press, New York, 1983, 29–50.
28. Kronogard, S. O. and Malmrup, L., Ceramic engine research and development in Sweden, ibid., 51–80.
29. Godfrey, D. J., Parker, D. A., Rhodes, M. L. P. and Smart, R. F., Research on the use of ceramics in diesels, ibid., 81–102.
30. Mangels, J. A., Injection moulding ceramics, *Ceram. Eng. Sci. Proc.*, **3** (1982) 529–37.
31. Handke, H., Injection moulding as a shaping method in the production of fine-ceramic articles, *Ber. Deut. Keram. Ges.*, **51** (1974) 97–101.
32. Mann, D. L., *Injection Moulding of Sinterable Silicon-Base Non-Oxide Ceramics*, Technical Report AFML-TR-78-200, Dec. 1978.
33. McLean, A. F. and Fisher, E. A., *Brittle Materials Design, High Temperature Gas Turbine*, Final Report AMMRG-TR-81-14, March 1981.
34. Giddings, R. A. and Johnson, C. S., *Investigation of Sintered Silicon Carbide for High Temperature Turbine Components*, Final Report NADG 77096-30, Nov. 1980.
35. Storm, R. S. and Lashway, R. W., *Progress in Ceramic Component Fabrication Technology*, American Institute of Aeronautics and Astronautics, Publication No. AA1A-82-1211, 1982.
36. Kamiya, S., Murachi, M., Kawamoto, H., Kato, S., Kawakami, S. and Suzuki, Y., *Silicon Nitride Swirl Lower-Chamber for High Power Turbo-*

charged Diesel Engines, Society of Automotive Engineers, Publication No. 850523, 1985.
37. Brunel University, UK and British Ceramic Research Association Progress Reports on *Fabrication of Engineering Ceramics by Injection Moulding and Sintering at Ordinary Pressure*, May 1985.
38. Mutsuddy, B. C., Injection moulding research paves way to ceramic engine parts, *J. Ind. Res. Dev.*, **25** (1983) 76–80.
39. Strivens, M. A., Injection moulding of ceramic insulating materials, *Am. Ceram. Soc. Bull.*, **42** (1963) 13–19.
40. Bahn, R. and Blechschmidt, H., Forming of non-plastic ceramic materials by injection moulding, *Silikat Tech.*, **10** (1959) 442–5.
41. Mangels, J. A. and Trela, W., Ceramic components by injection moulding, in *Advances in Ceramics*, Vol. 9, Ed. J. Mangels, The American Ceramic Society, Columbus, Ohio, 1984, 220–3.
42. Mostetzky, H. and Hennicke, H. W., Injection moulding of non-plastic ceramic powders, *Ber. Deut. Keram. Ges.*, **52** (1975) 25–30.
43. Mangels, J. A., Development of injection moulded reaction bonded silicon nitride, in *Ceramics for High Performance Applications—II*, Eds J. J. Burke, E. N. Lenoe and R. N. Katz, Brook Hill Publishing Co., Chestnut Hill, Massachusetts, USA, 1978, 113–30.
44. Engel, W., Lange, E. and Muller, N., Injection moulded and duo density silicon nitride, ibid., 527–38.
45. Whalen, T. J., Noakes, J. E. and Terner, L. L., Progress on injection moulded reaction-bonded silicon carbide, ibid., 179–92.
46. Willermet, P. A., Pett, R. A. and Whalen, T. J., Development and processing of injection-mouldable reaction-sintered silicon carbide compositions, *Am. Ceram. Soc. Bull.*, **57** (1978) 744–7.
47. Mutsuddy, B. C., Influence of powder characteristics on the rheology of ceramic injection moulding mixtures, *Proc. Brit. Ceram. Soc.*, **33** (1983) 117–37.
48. Mark, H. F. and Gaylord, N. G. (Eds), *Encyclopedia of Poly. Sci. and Tech.*, Vol. 13, Wiley, New York, 1966, 780.
49. Bandrup, J. and Immergut, E. H. (Eds), *Polymer Handbook*, Wiley, New York, 1975.
50. Mark, H. F. and Gaylord, N. G. (Eds), *Encyclopedia of Poly. Sci. and Tech.*, Vol. 4, Wiley, New York, 1966, 476.
51. Christensen, R. M., *Mechanics of Composite Materials*, Wiley, New York, 1979, 46.
52. Einstein, A., in *Investigations on the Theory of Brownian Movement*, Ed. R. Furth, Dover Publications, New York, 1956, 55.
53. Sommer, K., Viscosity of concentrated suspensions, in *Ceramic Processing before Firing*, Eds G. Y. Onoda and L. L. Hench, Wiley, New York, 1978, 227–33.
54. Rutgers, R., Relative viscosity and concentration, *Rheol. Acta*, **2** (1962) 305–48.
55. Frisch, H. L. and Simha, R., The viscosity of colloidal suspensions and macromolecular solutions, in *Rheology: Theory and Applications*, Vol. I, Ed. F. R. Eirich, Academic Press, New York, 1956, 525–612.
56. Eilers, H., The viscosity of emulsions made of highly viscous materials as a function of the concentration, *Kolloid-Z*, **97** (1941) 313–21.

57. Mooney, M., The viscosity of a concentrated suspension of spherical particles, *J. Coll. Sci.*, **6** (1951) 162–70.
58. Goodwin, J. W., The rheology of dispersions, *Coll. Sci.*, **2** (1975) 246–93.
59. De Bruijn, H., The viscosity of suspensions of spherical particles, *Rec. Trav. Chim.*, **61** (1942) 863–74.
60. Vand, V., Viscosity of solutions and suspensions I, *Phys. Chem.*, **52** (1948) 277–99.
61. Vand, V., Viscosity of solutions and suspensions II, *Phys. Chem.*, **52** (1948) 300–14.
62. Manley, R. St. J. and Mason, S. G., Particle motions in sheared suspensions II: Collision of uniform spheres, *J. Coll. Sci.*, **7** (1952) 354–69.
63. Brodnyan, J. G., The concentration dependence of the Newtonian viscosity of prolate ellipsoids, *Trans. Soc. Rheol.*, **III** (1959) 61–8.
64. Kitano, T., Kataoka, T. and Shirota, T., An empirical equation of the relative viscosity of polymer melts filled with various inorganic fillers, *Rheol. Acta*, **20** (1981) 207–9.
65. Krieger, I. M. and Dougherty, T. J., A mechanism for non-Newtonian flow in suspensions of rigid spheres, *Trans. Soc. Rheol.*, **III** (1959) 137–52.
66. Woods, M. E. and Krieger, I. M., Rheological studies on dispersions of uniform colloidal spheres: I. Aqueous dispersions in steady shear flow, *J. Coll. Interface Sci.*, **34** (1970) 91–9.
67. Chong, J. S., Christiansen, E. B. and Baer, A. D., Flow of viscous fluid through a circular pipe, *J. Appl. Poly. Sci.*, **15** (1971) 369–79.
68. Cannon, W. R., Danforth, S. C., Flint, J. H., Haggerty, J. S. and Marra, R. A., Sinterable ceramic powders from laser-driven reactions II: Powder characteristics and process variables, *J. Am. Ceram. Soc.*, **65** (1982) 330–5.
69. Blendell, J. E., Bowen, H. K. and Coble, R. L., High purity alumina by controlled precipitation from aluminium solutions, *Am. Ceram. Soc. Bull.*, **63** (1984) 797–801.
70. Lee, D. I., The viscosity of concentrated suspensions, *Tran. Soc. Rheol.*, **13** (1969) 273–88.
71. Farris, R. J., Prediction of the viscosity of multimodal suspensions from unimodal viscosity data, *Trans. Soc. Rheol.*, **12** (1968) 281–301.
72. Moulson, A. J., Review of reaction-bonded silicon nitride: Its formation and properties, *J. Mat. Sci.*, **14** (1979) 1017–51.
73. Mangels, J. A. and Williams, R. M., Injection moulding ceramics to high green densities, *Am. Ceram. Soc. Bull.*, **62** (1983) 601–6.
74. Strivens, M. A., Standard Telephones and Cables Ltd, London, *Improvements in or relating to the formation of moulded articles from sinterable materials*, UK Patent 779 242, 17 Jul. 1957. Date of filing: 7 Aug. 1953.
75. Waugh, A., Lexington Labs. Inc., Massachusetts, *Process for forming sintered leachable objects of various shapes*, US Patent 3 549 436, 22 Dec. 1970. Date of filing: 2 Sept. 1966.
76. Barringer, E. A. and Bowen, H. K., Formation, packing and sintering of monodisperse TiO_2 powders, *J. Am. Ceram. Soc.*, **65** (1982) C199–C201.
77. Adams, E. F., Slip cast ceramics, in *High Temperature Oxides*, Part IV, Ed. M. Allen, Academic Press, New York, 1971, 45.
78. Westman, A. E. R. and Hugill, H. R., Packing of particles, *J. Am. Ceram. Soc.*, **13** (1930) 767–9.
79. Lewis, H. D. and Goldman, A., Theorems for calculation of weight ratios

to produce maximum packing density of powder mixtures, *J. Am. Ceram. Soc.*, **49** (1966) 323–7.
80. Ayer, J. E. and Soppet, F. E., Vibratory compaction: I, Compaction of spherical particles, *J. Am. Ceram. Soc.*, **48** (1965) 180–3.
81. Matsumoto, S. and Sherman, P., The viscosity of microemulsions, *J. Coll. Interface Sci.*, **30** (1969) 525–36.
82. Barsted, S. J., Nawakowska, L. J., Wagstaf, I. and Walbridge, D. J., Measurement of steric stabiliser barrier thickness in dispersions of poly-(methyl methacrylate) in aliphatic hydrocarbon, *Trans. Faraday Soc.*, **67** (1971) 3598–603.
83. Sweeney, K. H. and Geckler, R. D., The rheology of suspensions, *J. Appl. Phys.*, **25** (1954) 1135–44.
84. Weltman, R. N. and Green, H., Rheological properties of colloidal solutions, pigment suspensions and oil mixtures, *J. Appl. Phys.*, **14** (1943) 569–76.
85. Ayer, J. E. and Soppet, E., Vibratory compaction: II, Compaction of angular shapes, *J. Am. Ceram. Soc.*, **49** (1966) 207–10.
86. Rumpf, H. and Schubert, H., Adhesion forces in agglomeration processes, in *Ceramic Processing before Firing*, Eds G. Y. Onoda and L. L. Hench, Wiley, New York, 1978, 357–76.
87. Parish, M. V., Garcia, R. R. and Bowen, H. K., Dispersion of oxide powders in organic liquids, *J. Mat. Sci.*, **20** (1985) 996–1008.
88. Kaelbe, D. H., *Physical Chemistry of Adhesion*, Wiley, New York, 1971, 46.
89. Bigg, D. M., Rheological analysis of highly loaded polymeric composites filled with non-agglomerating spherical filler particles, *Poly. Eng. Sci.*, **22** (1982) 512–18.
90. Han, C. D., Van Den Weghe, T., Shete, P. and Haw, J. R., Effects of coupling agents on the rheological properties, processability, and mechanical properties of filled polypropylene, *Poly. Eng. Sci.*, **21** (1981) 196–204.
91. Bretas, R. E. S. and Powell, R. L., Dynamic and transient rheological properties of glass filled polymer melts, *Rheol. Acta*, **24** (1985) 69–74.
92. Boaira, M. S. and Chaffey, C. E., Effects of coupling agents on the mechanical and rheological properties of mica-reinforced polypropylene, *Poly. Eng. Sci.*, **17** (1977) 715–18.
93. Monte, S. J. and Bruins, P. F., New coupling agents for filled polyethylene, *Modern Plastics*, **51** (1974) 68–70, 72.
94. Han, C. D., Sandford, C. and Yoo, H. J., Effects of titanate coupling agents on the rheological and mechanical properties of filled polyolefins, *Poly. Eng. Sci.*, **18** (1978) 849–54.
95. Monte, S. J. and Sugerman, G., Processing of composites with titanate coupling agents, *Poly. Eng. Sci.*, **24** (1984) 1369–82.
96. Bailey, D. F., Doulton and Co. Ltd, London, *Moulding ceramic composition*, US Patent 3 285 873, 15 Nov. 1966. Date of filing: 30 Sept. 1965.
97. Markoff, C. J., Mutsuddy, B. C. and Lennon, J. W., Method for determining critical ceramic powder volume concentration in the plastic forming of ceramic mixes, in *Advances in Ceramics*, Vol. 9, Ed. J. Mangels, The American Ceramic Society, Columbus, Ohio, 1984, 246–50.
98. Quackenbush, C. L., French, K. and Neil, J. T., Fabrications of sinterable silicon nitride by injection moulding, *Ceram. Eng. Sci. Proc.*, **3** (1982) 20–34.
99. Brydson, J. A., *Plastic Materials*, Butterworths, London, 1975, 80.

100. Mutsuddy, B. C. and Kahn, L. R., A practical approach in relating capillary viscosity and spiral-length data for moulding ceramic mixes, in *Advances in Ceramics*, Vol. 9, Ed. J. Mangels, The American Ceramic Society, Columbus, Ohio, 1984, 251–8.
101. ASTM Specification D3123-72, 1978.
102. Weir, F. R., Mouldability of plastics based on melt rheology, Part I—Theoretical development, *SPE Trans.*, **3** (1963) 32–6.
103. Weir, F. R., Doyle, M. E. and Norton, D. G., Mouldability of plastics based on melt rheology, Part II—Practical applications, *SPE Trans.*, **3** (1963) 37–41.
104. Holman, R. A., Biggs, D. M., Mutsuddy, B. C. and Kurth, R. E., Computer modelling of fluid flow, in *Advances in Ceramics*, Vol. 9, Ed. J. Mangels, The American Ceramic Society, Columbus, Ohio, 1984, 259–64.
105. Moore, F., *Rheology of Ceramic Systems*, Institute of Ceramics, UK, 1965, 18.
106. Edirisinghe, M. J. and Evans, J. R. G., to be published.
107. Johnsson, A., Carlstrom, E., Hermansson, L. and Carlsson, R., Rate-controlled thermal extraction of organic binders from injection moulded bodies, *Proc. Brit. Ceram. Soc.*, **33** (1983) 139–47.
108. Litman, A. M., Schott, N. R. and Tozlowski, S. W., Rheological properties of highly filled polyolefin/ceramic systems suited for injection moulding, *Soc. Plas. Eng. Tech.*, **22** (1976) 549–51.
109. Newfield, S. E. and Gac, F. D., *Injection Mouldable Ceramics*, Report LA 6960, Los Alamos Scientific Lab., USA, 1978.
110. Strivens, M. A., Standard Telephones and Cables Ltd, London, *Improvements in or relating to the formation of moulded articles from sinterable materials*, UK Patent 808 583, 4 Feb. 1959. Date of filing: 13 Jul. 1956.
111. Wiech, R. E., *Method and means for removing binder from a green body*, US Patent 4 305 756, 15 Dec. 1981. Date of filing: 14 Jan. 1980.
112. Peltsman, I. and Peltsman, M., Low pressure moulding of ceramic materials, *Interceram*, No. 4 (1984) 56.
113. Shung, M. C., Hitachi Corporation, Japan, *Composition for injection moulding*, Japanese Patent 7883, 17 Jun. 1961. Date of filing: 12 Dec. 1958.
114. Kodeii, H., Hitachi Corporation, Japan, *Method of injection moulding*, Japanese Patent 13913, 21 Aug. 1961. Date of filing: 18 Mar. 1959.
115. Wainer, E., Thompson Products Inc., Ohio, *Methods of moulding non metallic powders*, US Patent 2 593 507, 22 Apr. 1952. Date of filing: 1 Mar. 1949.
116. Bendix Aviation Corporation, Delaware, *Improvements in or relating to the moulding of ceramics*, UK Patent 706 728, 7 Apr. 1954. Date of filing: 30 Oct. 1951.
117. Saito, K., Tanaka, T. and Hibino, T., Tokyo Shibaura Electric Co. Ltd, Japan, *Injection moulding composition*, UK Patent 1 426 317, 25 Feb. 1976. Date of filing: 4 Mar. 1979.
118. Pett, R. A., Rao, V. D. N. and Qaderi, S. B. A., Ford Motor Co., USA, *Mouldable mixture of sacrificial binder and sinterable particulate solids*, US Patent 4 265 794, 5 May 1981. Date of filing: 10 Aug. 1979.
119. Pett, R. A., Qaderi, S. B. A. and Tabar, R. J., Ford Motor Co., USA, *Sacrificial binders for moulding particulate solids*, US Patent 4 267 056, 12 May 1981. Date of filing: 17 Oct. 1979.
120. Burroughs, J. E. and Thornton, H. R., Refractory aerospace structural

components by plastic moulding process, *Am. Ceram. Soc. Bull.*, **45** (1966) 187–92.
121. Matkin, D. I., Denton, I. E., Valentine, T. M. and Warrington, P., The fabrication of silicon nitride by ceramic plastic technology, *Proc. Brit. Ceram. Soc.*, **22** (1973) 291–304.
122. Technical Information on ELVAX, E.I. du Pont and Co. Inc., Delaware.
123. Moteki, A., Studies on the injection moulding of ceramics: II, Various factors in the heat treatment of the injection moulded ceramic products, *Yogyo Kyokai Shi*, **67** (1959) 387–99.
124. Farrow, G. and Conciatori, A. B., Celanese Corp., USA, *Polyacetal binders for injection moulding of ceramics*, Eur. Patent 114746, 1 Aug. 1984. Date of filing: 19 Jan. 1984.
125. Ohnsorg, R. W., The Carborundum Co., USA, *Composition and process for injection moulding ceramic materials*, US Patent 4 144 207, 13 Mar. 1979. Date of filing: 27 Dec. 1977.
126. Ohnsorg, R. W., The Carborundum Co., USA, *Process for injection moulding sinterable carbide ceramic materials*, US Patent 4 233 256, 11 Nov. 1980. Date of filing: 18 Dec. 1978.
127. Smoak, R. H. and Storm, R. S., *Interactive Development of Injection Moulded Sintered Alpha Silicon Carbide Turbine Material*, American Society of Mechanical Engineers, Publication No. 79-GT-77, 1979.
128. Storm, R. S., Ohnsorg, R. W. and Frechette, F. J., Fabrication of injection moulded sintered alpha silicon carbide turbine components, *J. Power Eng.*, **104** (1982) 601–6.
129. Muller-Zell, A. and Schwarzmeier, R., Injection moulding of beta silicon carbide capable of being sintered without pressure, *Keram-Z*, **35** (1983) 524–7.
130. Sugano, T., Materials for injection moulding silicon carbide, in *Proceedings of the 1st Symposium on Research and Development of Basic Technology for Future Industry*, Fine Ceramics Project, Japan Tech. Assoc., Tokyo, 1983, 67–84.
131. Edirisinghe, M. J. and Evans, J. R. G., to be published.
132. Whalen, T. J. and Johnson, C. F., Injection moulding of ceramics, *Am. Ceram. Soc. Bull.*, **60** (1981) 216–20.
133. Strivens, M. A., International Standard Electric Corp., USA, *Formation of ceramic mouldings*, US Patent 2 939 199, 7 Jun. 1960. Date of filing: 7 Aug. 1953.
134. Sarkar, N. and Greminger, G. K., Methylcellulose polymers as multi-functional processing aids in ceramics, *Am. Ceram. Soc. Bull.*, **62** (1983) 1280–8.
135. *Annual Report on High Technology Materials 1984–85*, Technical Insights Inc., New Jersey, 1985, 103.
136. Rivers, R. D., Cabot Corp., USA, *Method of injection moulding powder metal parts*, US Patent 4 113 480, 12 Sept. 1978. Date of filing: 9 Dec. 1976.
137. Birchall, J. D., Howard, A. J. and Kendall, K., Imperial Chemical Industries Ltd, UK, *Cementitious product*, Eur. Patent 0021682, 7 Jan. 1981. Date of filing: 6 Jun. 1980.
138. Birchall, J. D., Howard, A. J. and Kendall, K., A concrete approach to the energy crisis, *The Met. and Mat. Tech.*, **15** (1983) 35–8.

139. Hashimoto, T., Hama, M. and Kobayashi, O., Sumitomo Chemical Co. Ltd, Japan, *Composite binder composition for powder moulding*, UK Patent 2 081 733, 24 Feb. 1982. Date of filing: 5 Aug. 1981.
140. Scott, C. E. and Gilberton, H. J., Effects of humidity on binder strength in green ceramic compacts, *Am. Ceram. Soc. Bull.*, **61** (1982) 579–81.
141. Mangels, J. A., Ford Motor Co., USA, *Improved flow moulding composition*, US Patent 3 926 656, 16 Dec. 1975. Date of filing: 30 Oct. 1974.
142. Hutschenreuther Aktiengesellschaft, FRG, *Mouldable ceramic composition for injection moulding and/or pressing of moulding and a method for production of the compositions*, UK Patent 1 562 666, 12 Mar. 1980. Date of filing: 9 Dec. 1977.
143. Herrmann, E. R., Corning Glass Works, USA, *Method of moulding ceramic articles*, US Patent 3 234 308, 8 Feb. 1966. Date of filing: 21 Nov. 1961.
144. Trade Information, Sanyo Chemical Industries, *Japan Technology Bulletin*, Nov. 1984, 9–10.

Received 2 January 1986; accepted 10 January 1986

Int. J. High Technology Ceramics **2** (1986) 33–45

Microstructure, Oxidation and Creep Behaviour of a β'-Sialon Ceramic

T. Chartier, J. L. Besson

Laboratoire des Matériaux Céramiques, LA CNRS 320, ENSCI,
87065 Limoges Cedex, France

and

P. Goursat

Laboratoire des Céramiques Nouvelles, LA CNRS 320, UER des Sciences,
87060 Limoges Cedex, France

SUMMARY

The ceramic material is fabricated by nitriding, followed by pressureless sintering, a mixture of silicon, aluminium and yttrium oxide powders (80·35:5·60:14·05 wt%). The samples, with 3% porosity, consist mainly of the solid solution β'-$Si_{6-z}Al_zO_zN_{8-z}$ *where* $z = 0{\cdot}4$, *with a small quantity of an yttrium silicate in an intergranular glassy phase. The main impurity elements are iron and calcium.*

The oxidation behaviour has been studied between 1150 and 1500°C. Weight gains are slow up to 1380°C and become rapid at higher temperatures. It is shown that the kinetics of the reaction are controlled by yttrium migration. Creep in 3-point bend tests has been examined in air. The deformation consists of viscoelastic and diffusional components. No cavitation has been observed.

The results are discussed in relation to the microstructure and its evolution during creep and oxidation experiments, and compared with current theories for silicon nitride-based ceramics.

1. INTRODUCTION

Due to the highly covalent Si–N bonding and the high temperature volatility of silicon nitride, the densification of silicon nitride requires the

Int. J. High Technology Ceramics 0267-3762/86/$03·50

use of sintering aids, usually metallic oxides, which by reacting with silicon dioxide present at the surface of the nitride grains, form eutectics that permit liquid-phase sintering. This liquid phase transforms during cooling into an intergranular nitrogen-containing glass, in which the impurities are segregated. The high temperature properties of the material are largely determined by the properties of the intergranular phase, that is, the nature and proportion of the sintering aids and impurities.

The material dealt with in this paper was processed by the Ceraver Company (France) as the starting point of a study that aims to define the minimum quantities of additives (aluminium and yttrium oxide) required to achieve high densification by pressureless sintering, together with good material properties.

2. MATERIAL

Silicon, aluminium and yttrium oxide powders (80·35 wt% Si + 5·60 wt% Al + 14·05 wt% Y_2O_3) are mixed in alcohol, dried and then nitrided between 1150 and 1400°C for 70 h. Table 1 shows the levels of chemical

TABLE 1
Impurity Levels and Grain Size Distribution of the Starting Powders

Powder	*Supplier*	*Purity*			*Granulometry* /μm		
		Ca	*Fe*	*Al*	d_{10}	d_{50}	d_{90}
Silicon	Baudier	<0·35 wt%[a] 0·02–0·14 wt%[b]	<0·6 wt%[a] 0·48–0·58 wt%[b]	≃0·5 wt%[a] 0·02–0·15 wt%[b]	0·35	0·82	1·35
Yttrium oxide	Rhone Poulenc	n.d.	50 ppm	n.d.	1·3	3·0	6·5
Aluminium	Seveau	43 ppm (CaO)	2 000 ppm (Fe_2O_3)		Specific surface area = 5·1 $m^2 g^{-1}$		

[a] Supplier's analysis.
[b] Ceraver analysis.

TABLE 2
Main Characteristics of the Nitrided and Milled Powder

Granulometry (μm)			*Specific surface area*	Si_3N_4 $\frac{\alpha}{\alpha+\beta} \times 100$
d_{10}	d_{50}	d_{90}		
0·23	0·87	1·9	3·04	81·3

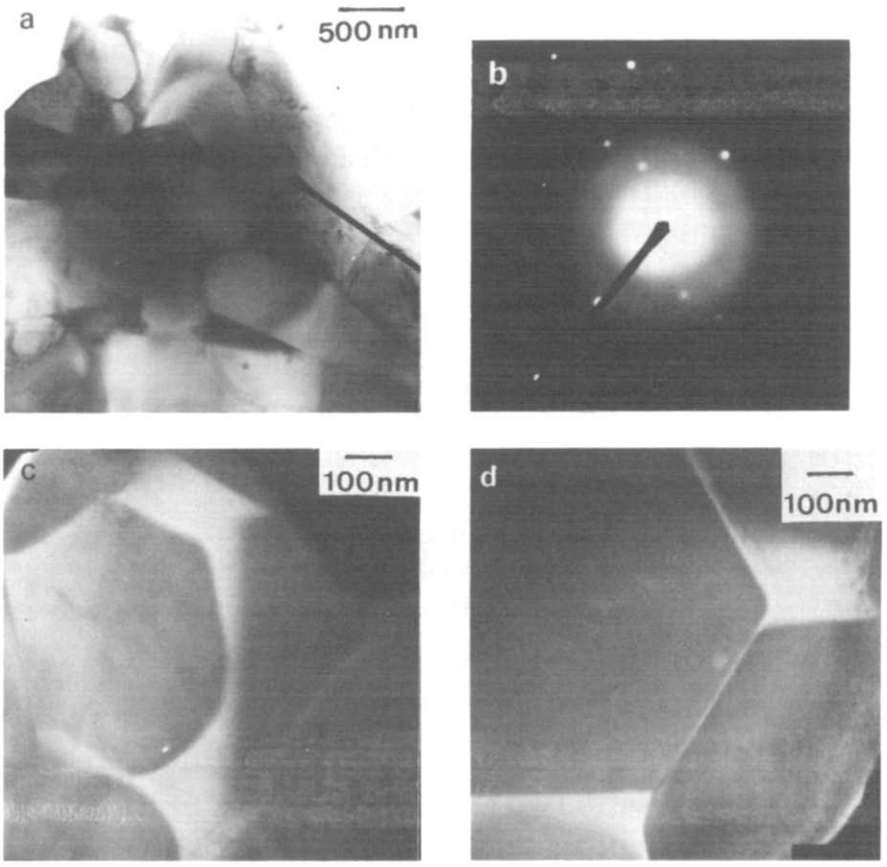

Fig. 1. TEM micrographs of the as-sintered material. (a) Bright field; example of microstructure of the as-sintered material. (b) Electron diffraction pattern of region (a) showing it is non-crystalline. (c) Associated dark field. (d) Another area showing amorphous pockets and glassy grain boundary phase between β'-sialon crystals.

impurities as provided by the manufacturers and determined by Ceraver. The main impurity elements are iron and calcium. After nitridation, the bricks (each weighing 15 kg) are attrition milled in white spirit. The main characteristics of the nitrided and milled powder are given in Table 2. The green samples are fabricated by injection moulding or isostatic pressing and pressureless sintered at 1700°C in a nitrogen atmosphere. The density is greater than 95% theoretical.

Microstructural observations show quite a large amount of glassy phase wetting the grains and forming rather big pockets in places (Fig. 1). The crystalline phases were identified by X-ray diffraction. The major phase is the β'-sialon solid solution. Minor quantities of the yttrium silicate, β-$Y_2Si_2O_7$, are also present. No yttrium aluminium garnet (YAG) was

detected. From the comparison of the a- and c-lattice parameters with those of pure Si_3N_4,[1,2] the composition of the β'-sialon solid solution was determined to be $Si_{5\cdot6}\ Al_{0\cdot4}\ O_{0\cdot4}\ N_{7\cdot6}$.

The test samples were cut using a wire-saw and acid leached with dilute hydrochloric acid to remove the iron contamination resulting from the cutting operation. The samples to be used for mechanical tests were carefully polished and the edges chamfered to reduce the possibility of edge flaws.

3. EXPERIMENTAL RESULTS

3.1. Oxidation

Oxidation behaviour in air was studied in the 1150–1500°C temperature range. Weight gains were detected only above 1300°C. The oxidation reaction is slow up to 1380°C and becomes fast at higher temperatures. The oxidation kinetics follow a parabolic law ($\alpha^2 = (\Delta m_t/\Delta m_\infty)^2 = Kt$, where Δm_t = weight gain at time t, Δm_∞ = weight gain for the complete reaction, and K = parabolic rate constant) throughout the test (24 h) at the lower temperatures. However, above 1380°C departures from the parabolic law are seen (Fig. 2). These departures occur sooner, the higher the temperature.

On polished cross-sections of samples, oxidized at 1200°C and above, a light-grey zone is noticed under the oxide scale (Fig. 3). The extent of this zone grows as the oxidation proceeds. This phenomenon, already

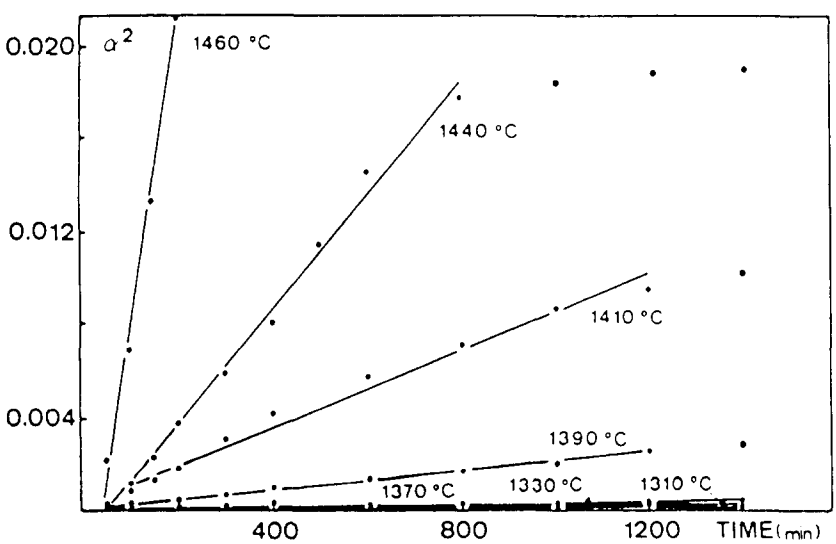

Fig. 2. Oxidation kinetics between 1310 and 1460°C in air.

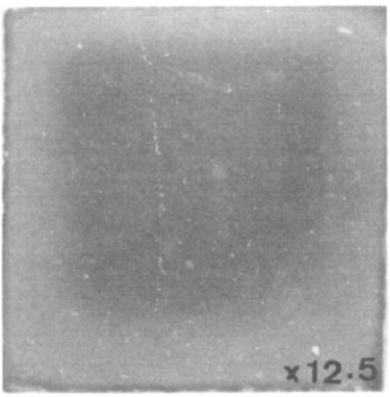

Fig. 3. Optical macrograph of a cross-section of a sample oxidized at 1300°C for 48 h. The lighter zone reveals the depth of oxygen penetration.

observed in the Si_3N_4–SiO_2–Y_2O_3 system,[3] corresponds to a selective oxidation of the intergranular phase. The oxide scale consists of acicular crystals in a glassy phase. The number and the size of the crystals increases with the oxidation temperature. The glassy phase is dense up to 1400°C and becomes gradually microporous and extremely friable after cooling (Fig. 4). The crystalline phases contained in the amorphous phase are cristobalite, a yttrium silicate (β-$Y_2Si_2O_7$ for $T < 1380$°C, δ-$Y_2Si_2O_7$ for $T > 1380$°C) and, in small quantity, for temperatures greater than 1400°C, yttrium aluminate $YAlO_3$. The proportion of yttrium silicate increases quickly with temperature.

Transmission electron microscopy (TEM) investigations of a sample oxidized at 1350°C for 48 h have revealed, in the bulk, microprecipitation resulting from partial devitrification of the intergranular glassy phase, but without a significant change in the total volume of the secondary phases (Fig. 5).

The concentration profiles of yttrium, calcium and aluminium were determined by X-ray microanalysis (EDAX) on a sample oxidized at 1260°C for 48 h (Fig. 6). Starting from the surface, three distinct zones are observed:

(i) a thin scale ($\sim 20\,\mu$m) corresponding to the oxide film in which the calcium and yttrium contents are high;
(ii) a zone depleted of yttrium and where the calcium content is no longer detectable;
(iii) a zone, 60–80 μm in width, where the yttrium concentration increases to reach the bulk concentration.

The entire thickness of these three zones is smaller than the light-grey

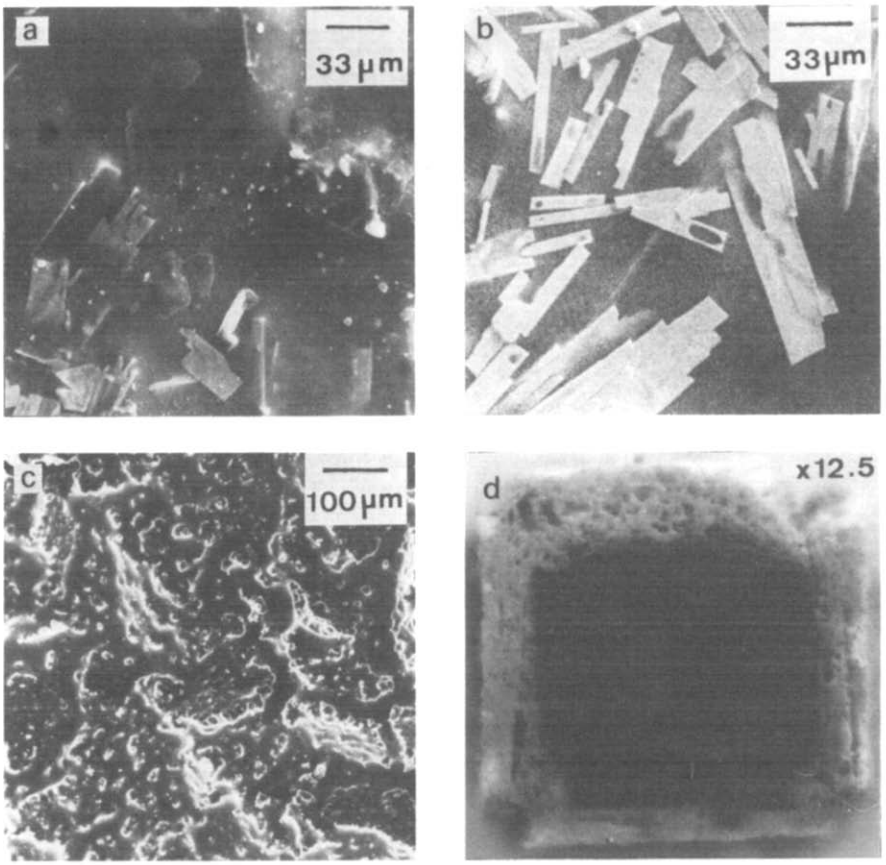

Fig. 4. SEM micrographs of surface of samples oxidized at (a) 1300°C, (b) 1400°C and (c) 1490°C; (d) cross-section of a sample oxidized at 1470°C.

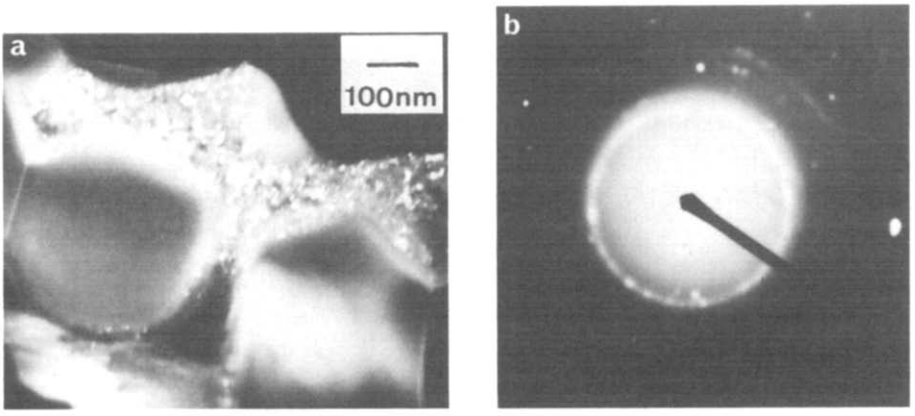

Fig. 5. (a) TEM micrograph of a sample after 48 h at 1350°C, showing microcrystallites in the glassy phase (dark field) (b) Associated electron diffraction pattern showing spotted rings.

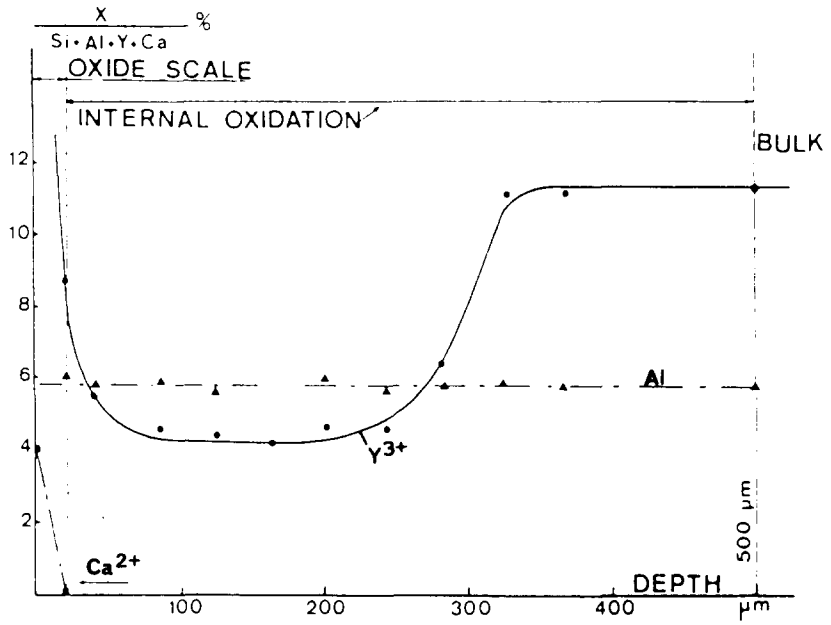

Fig. 6. Concentration profiles for yttrium, calcium and aluminium. Sample oxidized at 1260°C for 48 h.

zone which reflects the progress of the intergranular oxidation and the depth of oxygen penetration. Analyses carried out on the surface of samples oxidized respectively at 1200, 1260 and 1310°C show that the accumulation of yttrium in the oxide scale is already very high when weight gain begins to be detected by thermogravimetry (Table 3).

TABLE 3
Yttrium Concentration at the Surface After Oxidation for 48 h at Various Temperatures

	Bulk	*1 220°C*	*1 260°C*	*1 310°C*
$\frac{Y\%}{Si+Al+Y+Ca}$	12	15·7	26·8	43·3

It was noticed that the aluminium concentration remained uniform throughout the width of the samples and that iron concentrations never reached the detection threshold.

3.2. Creep

Creep in 3-point bend behaviour was investigated in air between 1100 and 1250°C, in the range 70–165 MPa. Below 1100°C, creep deformation was not measurable. A typical creep curve is presented in Fig. 7 ($T = 1150$°C,

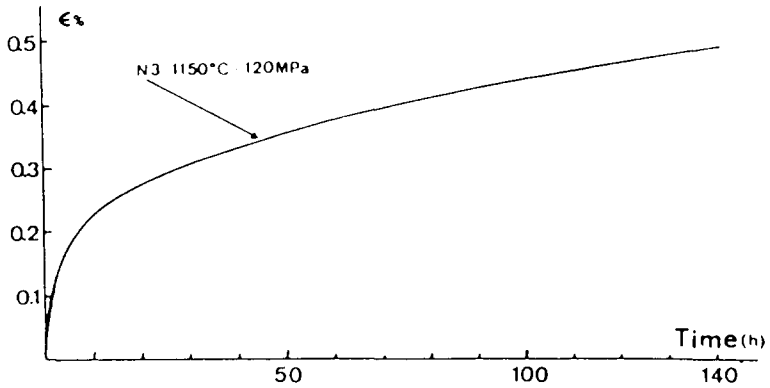

Fig. 7. Representative creep curve (1150°C, 120 MPa).

$\sigma = 120$ MPa). Following a rapid decrease over a few hours (corresponding to the primary stage) the creep rate diminishes very slowly. This stage will be referred to as the 'pseudo-steady-state' stage. Most of the creep tests were pursued until linear creep could be asserted. A true steady-state creep occurs only after a very long time (typically, times greater than 340 h). Tertiary creep was never observed under our experimental conditions. TEM observations of crept samples reveal a marked decrease in the quantity of the vitreous secondary phase. Neither cavitation nor micro-precipitates were observed (Fig. 8). The variation of Young's modulus versus temperature shows a rapid decrease above 1100°C that may be ascribed to the glass transition temperature of the amorphous intergranular phase. This is also the temperature at which the first signs of oxidation are observed.

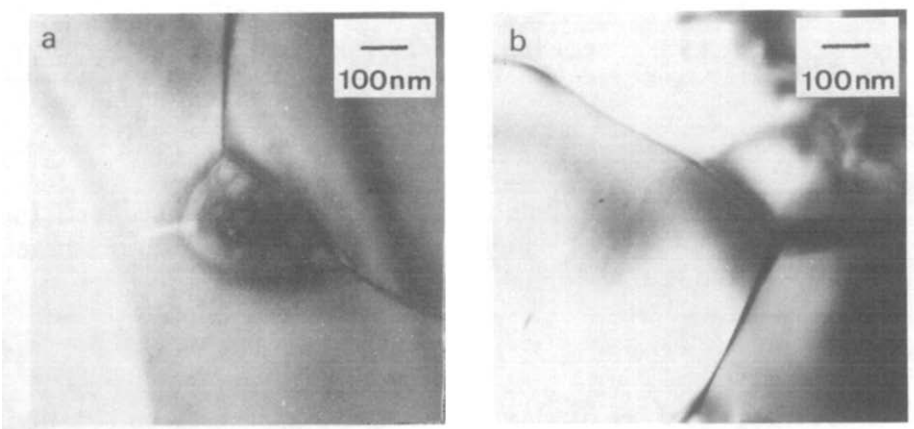

Fig. 8. TEM micrographs of crept samples illustrating the decrease in the amount of glassy phase (cf Fig. 1).

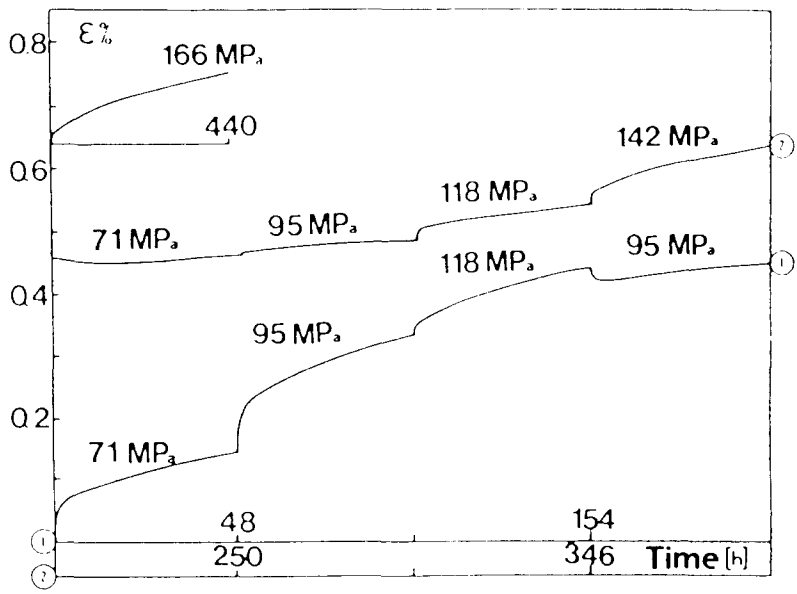

Fig. 9. Creep curve at 1150°C with increasing and decreasing stress increments. Notice negative creep rates for decreasing steps.

Usually, steady-state creep rates can be represented by the phenomenological relation:

$$\dot{\varepsilon} = A(S)\sigma^n \exp -\frac{E}{RT}$$

where σ = applied stress, n = stress exponent, E = apparent activation enthalpy, R = Boltzmann constant, T = absolute temperature and $A(S)$ = some function of the microstructure. If n and E are known identification of the mechanism that accounts for the deformation, and the activation enthalpy of the rate limiting step of the process may be possible. The study of n and E was carried out using, respectively, incremental stress changes at constant temperature and incremental temperature changes at constant stress. Each step lasted 48 h in both cases.

During the first stress steps (pseudo-steady-state stage) negative strain rates were observed when the stress was decreased (Fig. 9). On and after the seventh step (340 h), the creep rates vary linearly and reversibly with log stress. The slope of the line $\dot{\varepsilon}$ (log σ) is then equal to 1.

The growth of the creep rate with temperature also starts to be reversible from the seventh isothermal step (that is, after a creep time of about 340 h). Log $\dot{\varepsilon}$ versus T^{-1} then gives a straight line (Fig. 10). The apparent activation enthalpy was calculated to be $\simeq 780\,\mathrm{kJ\,mol^{-1}}$. An activation enthalpy of the same order of magnitude ($720\,\mathrm{kJ\,mol^{-1}}$) had

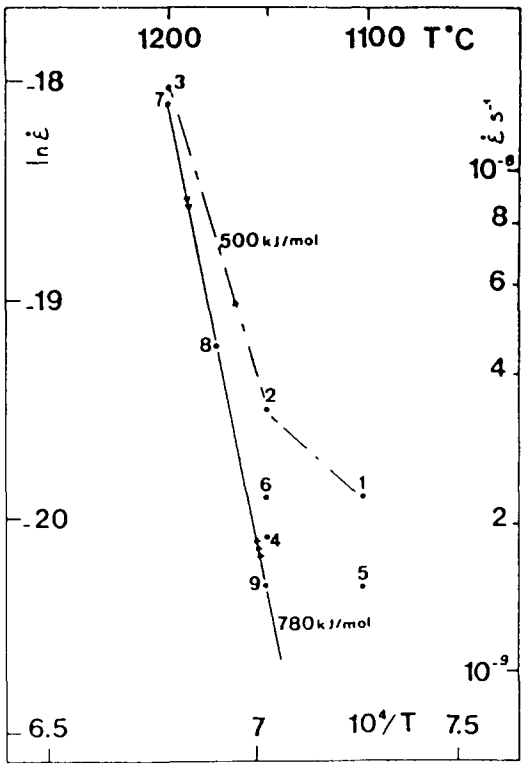

Fig. 10. Plot of $\ln \varepsilon$ versus reciprocal temperature for determination of the apparent activation energy for creep from incremental temperature tests.

been measured for creep in a silicon nitride type ceramic fabricated by hot-pressing from a mixture corresponding to 70 Si_3N_4–25 SiO_2–5 Y_2O_3 mol%.[3]

4. DISCUSSION

It is now well established that the high temperature behaviour of nitrogen ceramics is governed by the presence of secondary intergranular phases. In the present case oxidation and creep resistance begin to deteriorate at 1100°C, which is the glass transition temperature of the amorphous nitrogen-containing phase as indicated by the onset of the rapid decrease of the Young's modulus.

Oxidation starts with the formation of a superficial aluminosilicate film, formed by the reaction between oxygen and sialon which leads to a release of nitrogen, and continues with a selective attack of the intergranular vitreous phase which is more reactive than the grains. Oxygen migrates

inwards towards the bulk and nitrogen towards the outside. A gradient in chemical potential is created between the surface aluminosilicate and the intergranular phase. This induces a migration of the metal cations which react with the aluminosilicate and oxygen to form more complex silicates. This process is now well-established[4] but the details of the mechanism depend on the nature and concentration of the impurities and densification aids.

For the sialon under study, two temperature ranges may be distinguished: the first, from 1150 to about 1380°C, characterized by the formation of a compact and protective superficial oxide coating and a second, above 1380°C, where the oxide scale loses its protective efficiency. In the first range, the weight gain begins to be measurable at 1310°C. The parabolic form of the oxidation kinetics implies a diffusional mechanism. The absence of porosity in the oxide layer or separation at the grain boundaries suggests an ionic intergranular diffusion. From the data plotted in Fig. 2, the activation enthalpy for oxidation between 1300 and 1380°C was calculated to be $440 \pm 40\,\text{kJ mol}^{-1}$. The study of the inward shift to the light-grey front, associated with oxygen diffusion to the bulk, and of the concentration profiles of yttrium and calcium shows that the diffusion of the species commences at 1150°C and it seems likely that the limiting step is the same throughout the first temperature range. An activation enthalpy of $440\,\text{kJ mol}^{-1}$ is too high to be associated with oxygen diffusion for which the literature gives values of about $120\,\text{kJ mol}^{-1}$.[5,6] The alternative is then to assign this enthalpy to the migration of an 'yttrium–nitrogen' or 'calcium–nitrogen' compound species.

In the second range the higher temperature and the rapid accumulation of calcium at the surface lower the viscosity of the vitreous scale. The nitrogen released by the oxidation of the intergranular phase escapes more easily through the silica scale, creating a porosity that facilitates the access of oxygen to the internal interface (Fig. 4(d)). A diffusion regime is observed, for which the higher the temperature, the shorter the duration, and the determination of a rate constant becomes unreliable. In addition, after cooling, the oxide layer is very friable and it is no longer possible to determine concentration profiles for yttrium and calcium. The determination of the limiting step of the oxidation process is then purely speculative.

Concerning creep, Lange *et al.*[7] have proposed that the deformation of nitrogen ceramics is the sum of several components:

(i) a viscoelastic component, which is the main contribution to the strain during the primary stage and arises essentially from the response of the glassy intergranular phase;

(ii) a Coble diffusional component due to a mechanism of solution, migration in the glassy phase and precipitation which accommodates the stresses that arise at the ledges on grain boundaries during grain sliding; this component, characterized by a stress exponent equal to 1, is the major cause of deformation during steady-state creep;
(iii) under certain conditions, a cavitational creep.

The experimental features of creep behaviour of this material may be explained in the light of this theory. Thus, the negative creep rate, observed after a decreasing stress increment, is a consequence of the viscoelastic behaviour of the glassy phase.[8] The long pseudo-steady-state stage corresponds to the superposition of the viscoelastic and the diffusional components. The large decrease in glassy phase content observed in crept specimens explains the gradual decline of the viscoelastic contribution. When steady-state creep is established (for times above 350 h) the only remaining component is a diffusional one.

Because of the high viscosity of the yttrium-containing glassy phase[9] it is believed that the limiting step of the solution–migration–precipitation mechanism, acting during diffusional creep, is the same as for the sialon ceramic material studied in Ref. 3, as suggested by the similar values of activation enthalpy, that is, material transport through the intergranular phase.

Our conclusion is that material transport through the viscous glassy phase is rate-controlling for diffusional creep as well as for viscoelastic creep and oxidation. Hence, the main parameter is the viscosity of the glassy phase. The increase in the apparent activation enthalpy during creep must be related to that of the changes in chemical composition of the glassy phase with time. This view is supported by the fact that the slope of the curve $\ln \dot{\varepsilon}$ vs T^{-1} measured between the points 2 and 3 in Fig. 10 (that is, between 48 to 144 h of creep in air) leads to an 'activation enthalpy' of about 500 kJ mol^{-1}, which compares well with the value of 440 kJ mol^{-1} calculated for the oxidation process after 48 h exposure in air (that is, when a similar composition is reached for the glassy phase).

5. CONCLUSION

Oxidation in air of the β'-sialon material studied is slow up to 1380°C; for higher temperatures, the superficial oxide scale loses its protective efficiency and the oxidation becomes fast. In the lower temperature range the corrosion is intergranular and is accompanied by a migration of yttrium and calcium which accumulate in the oxide scale.

The creep deformation is the sum of a viscoelastic component and a

diffusional one, the relative proportions of which change with time and the characteristics of which are affected by modifications of chemical composition induced by oxidation and by the microstructural changes due to the applied stresses.

The rate-controlling step, for both oxidation and creep, has been ascribed to material transport through the intergranular phase. The activation enthalpy varies from 440 to 780 kJ mol^{-1} depending on the viscosity of the glassy phase which changes with its composition.

This study has allowed us to verify the possibility of fabricating pieces with good thermomechanical properties by injection moulding or isostatic pressing and pressureless sintering. It has established a standard for further studies of the improvements brought in by the choice of starting silicon powders with lower calcium impurity contents and the use of post-sintering thermal treatments.[10]

ACKNOWLEDGEMENTS

We wish to thank MM. L. Minjolle and W. Mustel for fabrication and machining of the samples as part of a collaborative research programme with Ceraver. We are also grateful to Dr P. Lortholary (Service de microscopie, Université de Limoges) for technical assistance. Financial support from the European Communities under contract SUT 111F was greatly appreciated.

REFERENCES

1. Jack, K. H., *J. Mater. Sci.*, **11** (1976) 1135.
2. Roult, G., Brossard, M., Labbe, J. C. and Goursat, P., Int. Conf. Non Oxide Tech. and Eng. Ceramics. Limerick, Ireland. 10–12 July 1985.
3. Bouarroudj, A., Goursat, P. and Besson, J. L., *J. Mater. Sci.*, **20** (1985) 1150.
4. Babini, G. N., Bellosi, A. and Vincenzini, P., *J. Mater. Sci.*, **19** (1984) 3487.
5. Deal, B. E. and Grove, A. S., *J. Appl. Phys.*, **36** (1965) 3770.
6. Tetard, D., Lortholary, P., Goursat, P. and Billy, M., *Rev. Int. Hautes tempér. Réfract.*, **10** (1973) 153.
7. Lange, F. F., Davis, B. I. and Clarke, D. R., *J. Mater. Sci.*, **15** (1980) 601, 611, 616.
8. Karunaratne, B. S. B. and Lewis, M. H., *J. Mater. Sci.*, **15** (1980) 449.
9. Babini, G. N., Bellosi, A. and Vincenzini, P., in *Science of Ceramics 11*, Eds R. Carlsson and S. Karlsson, Swedish Ceramic Society, 1981, 291.
10. Chartier, T., Besson, J. L., Goursat, P. and Mustel, W., in *Science of Ceramics 13*, 9–11 Sept. 1985, Orléans, France. To be published in *Journal de Physique-Colloques (Les Editions de Physique)*.

Received 25 April 1985; amended version received 25 September and accepted 30 September 1985.

Int. J. High Technology Ceramics **2** (1986) 47–63

Mechanical Property Evaluation at Elevated Temperature of Sintered β-Silicon Carbide

M. J. Slavin and G. D. Quinn

Ceramics Research Division, Army Materials Technology Laboratory, Watertown, Massachusetts 02172, USA

SUMMARY

The mechanical properties at room and elevated temperature of sintered β-silicon carbide were evaluated. Testing included room temperature flexural strength, flexural stress rupture at 1200°C, and stepped temperature stress rupture (STSR) experiments. Fractographic examination identified the strength limiting flaw populations. Properties measured on this material are typical of commercial grades of sintered silicon carbide.

1. INTRODUCTION

Silicon-based ceramics have considerable potential for structural applications in heat engines and other energy conversion devices. This study is part of an on-going Department of Energy project to screen the mechanical properties of new materials for heat engine applications.

This report presents findings on a commercially available sintered β-silicon carbide manufactured by the General Electric Co. In 10 years of development this material has evolved from a hot-pressed laboratory grade material to a commercial sintered product.[1–7] It is fabricated from a submicrometer β-silicon carbide powder with small additions (~0·5 wt% each) of boron and carbon, and is sintered in a reducing atmosphere at approximately 2100°C. The boron promotes diffusion while the carbon acts to reduce possible oxide phases (silicon dioxide) and retard grain growth. The sintered product often contains some α-phase silicon carbide

Int. J. High Technology Ceramics 0267-3762/86/$03·50

as a result of phase transformation during sintering. This latter process is dependent upon impurities and sintering conditions and can be very sensitive to conditions of powder preparation, processing, and densification.[3] The presence of the α-phase is not desired because it can manifest itself as large tabular grains that can limit strength.

Earlier studies have suggested that the laboratory hot-pressed and sintered β-silicon carbide materials have excellent high temperature properties up to 1500°C including creep and slow crack growth resistance[8–10] and strength retention.[1,4,9,10] These favorable properties, coupled with the complex shape capabilities of sintering, suggest that β-silicon carbide is a promising heat engine grade ceramic. The purpose of this study was to verify these properties in the commercial form of the material.

2. MATERIAL

The sintered β-silicon carbide was supplied by the General Electric Company's Manufacturing Division, Houston, Texas in the form of eight 50·8 × 50·8 × 12·7 mm tiles in March 1984. Four of these tiles were machined into flexure specimens according to MIL-STD-1942(MR)[11] specimen configuration 'B'. Specimen size was 3·0 × 4·0 × 44·5 mm with a 45° chamfer along the four long edges. Chamfer depths were inadvertently machined to approximately 0·28 mm which is greater than the 0·15 ± 0·05 mm the standard requires. Although this causes only a 1·25% decrease in the cross-sectional area, the strengths reported in this study (based on elastic theory with a rectangular cross-section) are 3·4% lower than if the chamfer were within the prescribed limits.

The average bulk density of the tiles was 3·12 Mg m^{-3} with a standard deviation of 0·03 and is in close agreement with the 3·12 Mg m^{-3} reported by the manufacturer. The elastic modulus and Poisson's ratio as measured via the sonic method were 395 GPa and 0·17, respectively.

The ultrasonic longitudinal wave propagation time C-scan is a powerful characterization tool. The time C-scan shows spatial variation of wave propagation times through the tile thickness with a resolution of ±1 ns. If a tile has constant thickness, the C-scan can be interpreted as a longitudinal velocity C-scan. Figure 1 is a C-scan of a 50·8 × 50·8 × 12·7 mm tile of β-silicon carbide and, allowing for wave distortion near the edges, had a variation in wave propagation time of approximately 5% from the edge to the center of the tile. The Appendix gives an analysis of the C-scan in which the relationship between the tile's thickness, elastic modulus, Poisson's ratio and density as they pertain to the longitudinal wave velocity is evaluated.

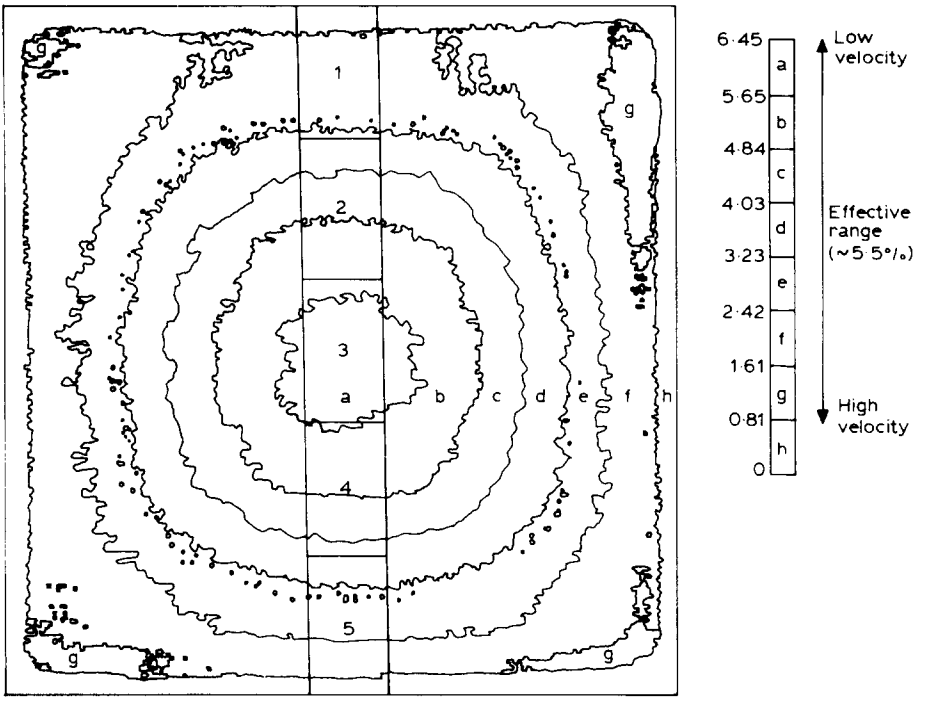

Fig. 1. Time-of-flight C-scan for the sintered β-silicon carbide using a 10 MHz undamped transducer.

The increase in the wave propagation time from the edge to the center of the tile is due to (in order of importance): an increase in thickness, a decrease in elastic modulus, and a decrease in Poisson's ratio. The density, which decreases toward the tile's center, decreases the wave propagation time.

A quantitive analysis of the metallic impurities is given in Table 1. A polished section showing the material porosity (~3%) is shown in Fig. 2. Figure 3 shows the same section etched with boiling Murakami's reagent to delineate the grain boundaries.[6] Tabular grains commonly associated

TABLE 1
Impurity or Additive Content of the Sintered β-Silicon Carbide

Impurity element/wt%[a]												
Al	*B*	*Ca*	*Co*	*Cr*	*Cu*	*Fe*	*Mg*	*Mn*	*Ni*	*Ti*	*Zr*	*V*
0·008	0·5	0·017	—[b]	0·005	0·005	0·003	0·002	~0·001	0·002	0·004	0·16	—[b]

[a] Determined by emission spectroscopy.
[b] Not detected.

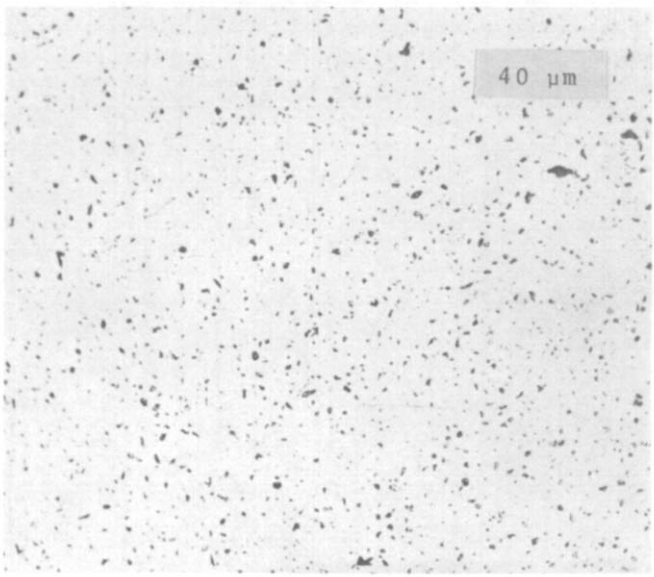

Fig. 2. Polished section of a specimen of β-silicon carbide showing the distribution of porosity.

Fig. 3. Etched section of a specimen showing grain size distribution. Note the long tabular α-grains.

with the α-phase of silicon carbide[1–5] are readily apparent. X-ray diffraction of the silicon carbide showed that the majority of the material is β-silicon carbide with a small percentage of the α-phase and a trace amount of graphite. In a parallel study being carried out at MTL[12] for non-heat engine applications, a 152·4 × 76·2 × 12·7 mm tile had an identical X-ray diffraction pattern and a very similar microstructure (larger α-grains).

3. PROCEDURE

Microhardness testing was performed on a mounted and polished specimen with a load of 19·6 N. Using both Vicker's and Knoop indenters, 10 indentations each were made with a standard microhardness indenter (Miniload II, Leitz, FRG). Fracture toughness was estimated from crack lengths emanating from Vicker's indentations at loads of 19·6 N, 24·9 N, and 34·3 N, using a standard microhardness indenter (Tukon Tester FB, Wilson Mechanical Instrument Co. Inc., New York).

Room temperature flexural testing was used to establish a reference strength and to characterize the strength limiting flaws. A universal testing machine (Model TT-DL, Instron Corp., Canton, Massachusetts) was used with four-point fixtures in accordance with MIL-STD-1942(MR).[11] The spans were 40·0 mm and 20·0 mm and the crosshead speed was 0·5 mm/min. The relative humidity was 35% at 23°C.

The 1200°C flexural stress rupture experiments were carried out in air in several identical test furnaces. These furnaces were constructed with firebrick and employed silicon carbide heating elements as the heat source.[13] Four-point bend fixtures, machined from hot-pressed silicon carbide and having fixed bearing spans of 38·1 mm and 19·0 mm, were used. A simple deadweight lever system applied the load into the furnace. The temperature inside the furnace was allowed to stabilize for 5 min prior to loading. Additional details of this procedure are given in Ref. 14.

A stepped temperature stress rupture (STSR)[15] program was used to quickly screen the material while stressed to a range of temperatures that it may be subjected to in an engine environment. This program assesses where creep or static fatigue may be a problem. The furnace arrangement and loading procedure are identical to the stress rupture tests. The program starts at 1000°C when the load is applied. After 24 h, if the specimen survives, the temperature is raised within approximately 0·5 h to 1100°C. This cycle continues for 1200°C, 1300°C, and 1400°C, but at 1400°C, the specimen cycle time is 72 h. In the event of a failure the furnace is shut down. An arrow labeled with the applied stress denotes the time of failure on the STSR plot.

Specimens that survived the stress rupture or STSR tests were unloaded prior to cool-down. This was done to minimize frictional forces at the knife edges due to unequal specimen-fixture contractions. The survivors were then tested at room temperature to determine the retained strength. They were mounted in the room temperature fixture such that the most highly stressed zone in the high temperature test was again loaded in a tensile manner. Note that the room temperature fixtures have slightly larger inner and outer spans than the high temperature fixtures.

4. RESULTS

The Vicker's indentations produced an average hardness of 23·9 GPa with a standard deviation of 0·4 GPa and the Knoop indentations an average hardness of 20·9 GPa with a standard deviation of 0·3 GPa. This is somewhat lower than the HV9·8 N of 28·0 GPa reported in Ref. 7 but a little higher than the average HK9·8 N of 20·1 GPa with a standard deviation of 0·8 GPa (60 indentations) reported in Ref. 12.

The fracture toughness values were measured from Vicker's indentations and evaluated using the Marshall–Evans formulation.[16] A minimum of five 'good' indentation patterns were obtained for each of the three loads. Some problems with spall and cracks not radiating from the corners were observed. A 'good' indentation pattern consisted of at least three of the four cracks starting from the corners and extending straight from the indent and no spall. Table 2 indicates that the K_{Ic} values averaged 2·8 MPa $m^{0.5}$. This is somewhat lower than other reported values: 3·0 MPa $m^{0.5}$ (double torsion),[17] 3·3 MPa $m^{0.5}$ (single edge notch beam),[12] and 3·1 MPa $m^{0.5}$ (controlled flaw in flexure).[18]

Thirty room temperature four-point fast fracture specimens were tested and had an average flexure stress of 346 MPa with a standard deviation of 34 MPa. This average is appreciably less than values for the laboratory-prepared three-point flexure specimens in Ref. 6, is somewhat less than the 440 MPa four-point results reported in Refs 9 and 10, is also less than

TABLE 2
Fracture Toughness, K_{Ic}, for Varying Indent Loads

Load/N	*Number of indents (n)*	K_{Ic}/*MPa* $m^{0.5}$
19·5	5	2·82
29·4	6	2·81
34·3	6	2·78

Average K_{Ic} = 2·8 MPa $m^{0.5}$, with a standard deviation of 0·2.

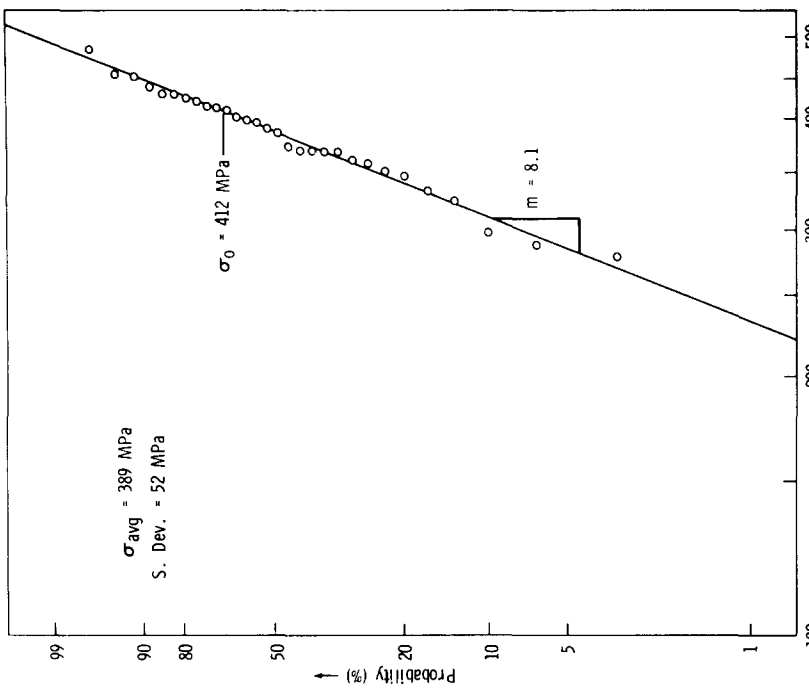

Fig. 5. Weibull plot for the parallel study underway at AMMRC.[12]

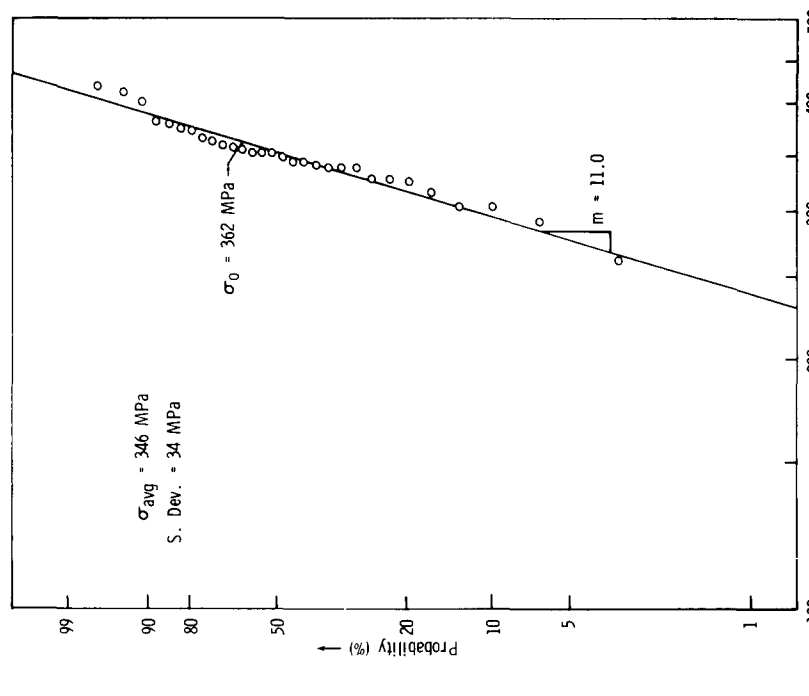

Fig. 4. Weibull plot for the reference flexural strength for this study.

the three-point value of 533 MPa in Ref. 7, but is quite consistent with the four-point value of 389 MPa with a standard deviation of 52 MPa in Ref. 12.

A two-parameter Weibull modulus was determined by a least square fitted line through the strength data when plotted on a standard Weibull format (see Fig. 4). The ranking percentage is $p = i/(N+1)$, where i is the ith data point and N is the total number of specimens. The Weibull modulus, which is the slope of the line, is 11·0 and has a correlation coefficient of 96·5%. Figure 5 is a Weibull plot for the strength data from the parallel study underway at MTL[12] for non-heat engine applications. The Weibull modulus is 8·1 with a correlation coefficient of 98·8%. These moduli are consistent with the reported value of 8 to 15 in Ref. 7.

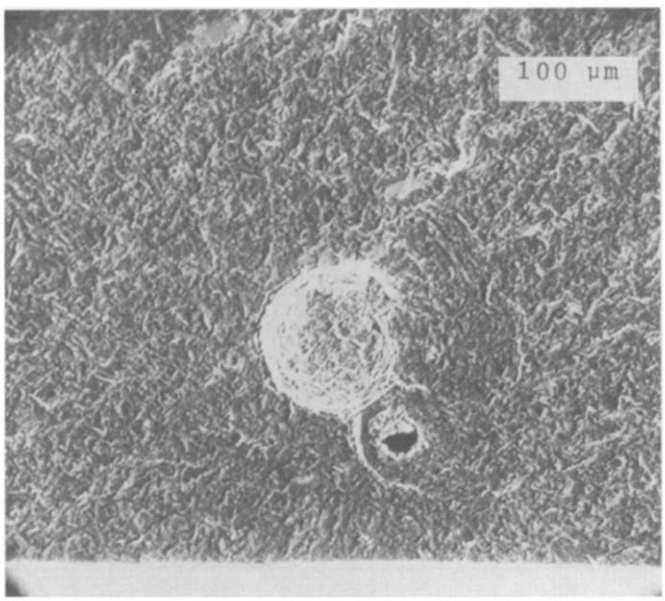

Fig. 6. Fracture surface of a control sample that failed due to the agglomerate and pore: 352 MPa.

All specimens were subjected to a fractographic examination up to a magnification of about 100×. Typical fracture surfaces were then photographed and prepared for SEM examination. The strength-limiting flaws common to the room temperature flexure specimens were: agglomerates and porous zones either at the surface or distributed within the volume (Fig. 6); a few large grains and pores (Fig. 7); and an occasional processing crack (Fig. 8). Thus, although the Weibull plot implies a single flaw population, there are, in fact, several.

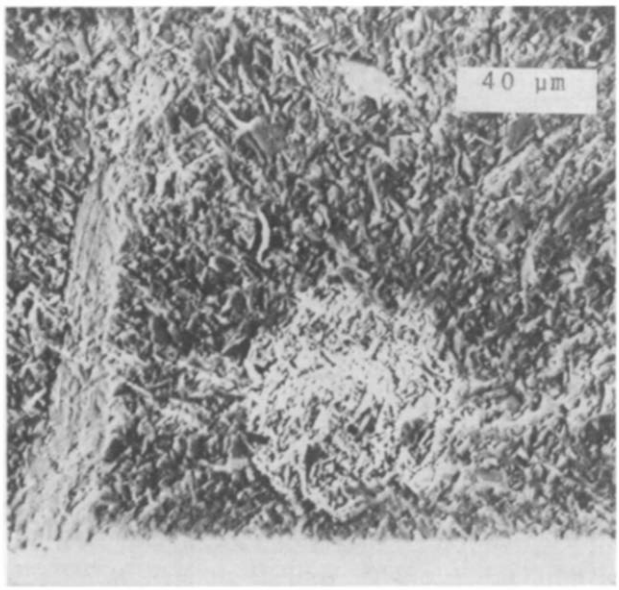

Fig. 7. Fracture surface of a control sample: 356 MPa. The strength-limiting flaw is the combination of the porous area and the grain.

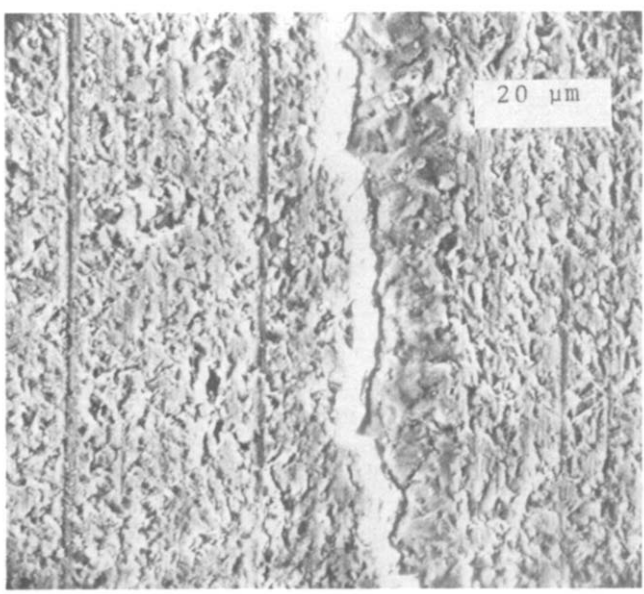

Fig. 8. Tensile surface of a control sample: 341 MPa. The crack runs along the longitudinal axis of the specimen and had an overall length in excess of 4·5 mm.

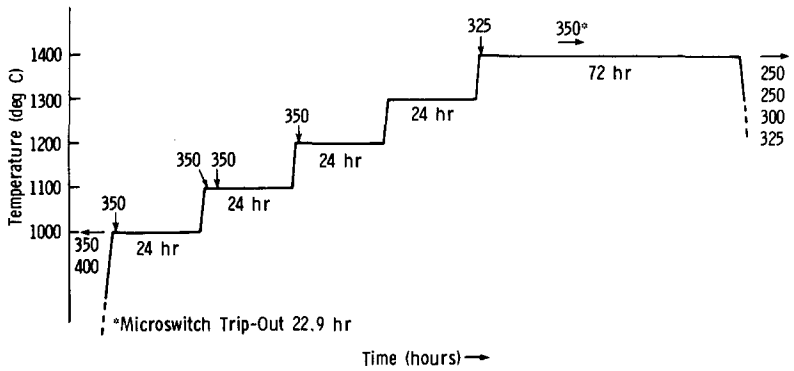

Fig. 9. Stepped temperature stress rupture results.

Twelve specimens were tested via the stepped temperature stress rupture (STSR) procedure and the results are shown in Fig. 9. Two specimens failed on loading with applied stresses of 350 and 400 MPa. Four specimens survived the complete cycle with applied stresses of 250 (2), 300 (1), and 325 MPa (1) and one specimen survived intact at 350 MPa when an inadvertent microswitch trip shut the furnace down after 22·9 h at 1400°C. The five remaining specimens, with applied stresses of 325 (1) and 350 MPa (4) failed in a time-dependent manner at 1000, 1100, 1200, and 1400°C. Permanent deformation of the five survivors was negligible (<0·1% strain). The retained strengths of the four survivors were surprisingly consistent at 401, 448, 402, and 400 MPa for the 250, 250, 300, and

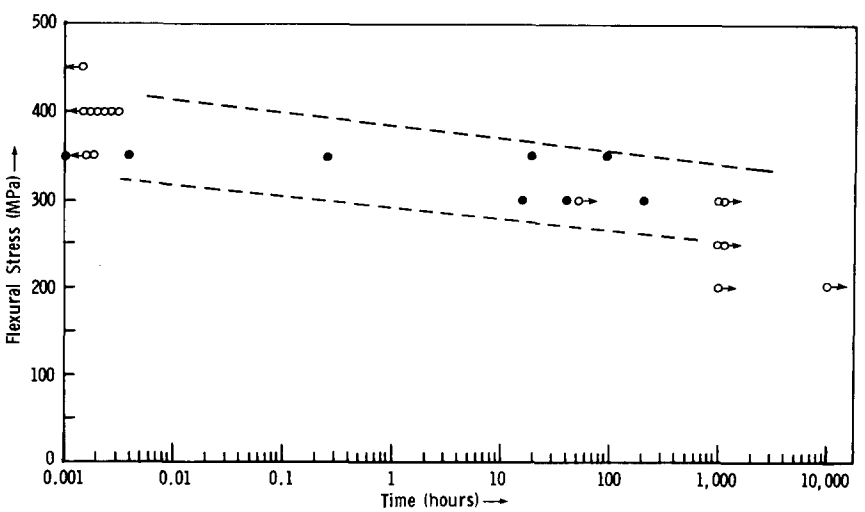

Fig. 10. Flexural stress rupture at 1200°C. The boundary lines approximate the scatter.

350 MPa STSR applied stresses, respectively. The retained strengths are appreciably higher than the reference room temperature strengths (346 MPa average). This may be due either to a flaw healing process or crack blunting.[6]

Twenty-four specimens were tested at 1200°C in the stress rupture experiments (Fig. 10). Nine failed on loading at applied stresses of 350 (2), 400 (6) and 450 MPa (1). Five specimens survived 1000 h at stresses of 200 (1), 250 (2), and 300 MPa (2). One specimen survived 300 MPa for 52·5 h when the furnace malfunctioned and shut down. All surviving specimens had negligible permanent deformation ($\leq 0{\cdot}1\%$ strain) indicating an excellent creep resistance. The retained strengths for the 1000 h survivors were 362, 403, 433, 524 and 524 MPa for the 200, 250, 250, 300 and 300 MPa stress rupture applied stresses, respectively. One specimen which was loaded to 200 MPa survived 10 000 h without failure. Its retained strength at room temperature was 417 MPa and it fractured from a sintering defect. There was only a slight weight change in the specimen since the oxide layer which formed was only 5 μm thick. The retained strengths of all 1200°C survivors were greater than the average room temperature strength. The remaining eight specimens failed in a time-dependent manner from 0·001 h to 210·5 h at applied stresses of 300 and 350 MPa. A static fatigue limit may exist between 200 and 250 MPa.

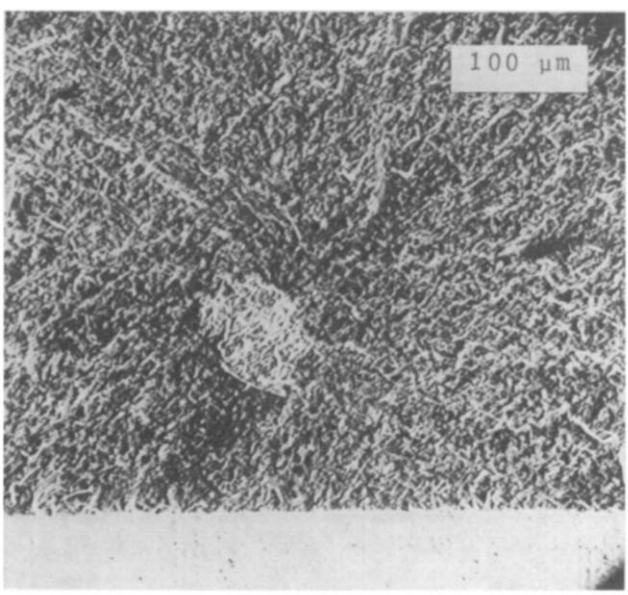

Fig. 11. Fracture surface of a failure on loading during a stress rupture test: 350 MPa. The flaw is a porous area away from the tensile surface.

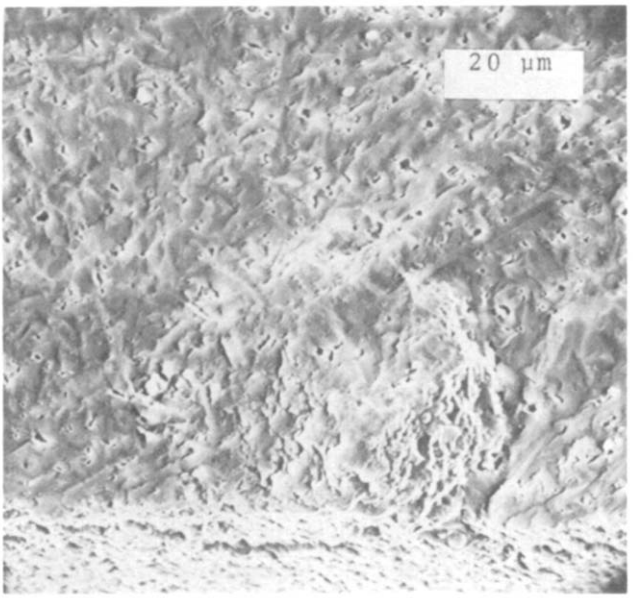

Fig. 12. Fracture surface of a time-dependent failure during a stress rupture test: 300 MPa, $t = 210$ h. Failure occurred at a surface-connected porous area.

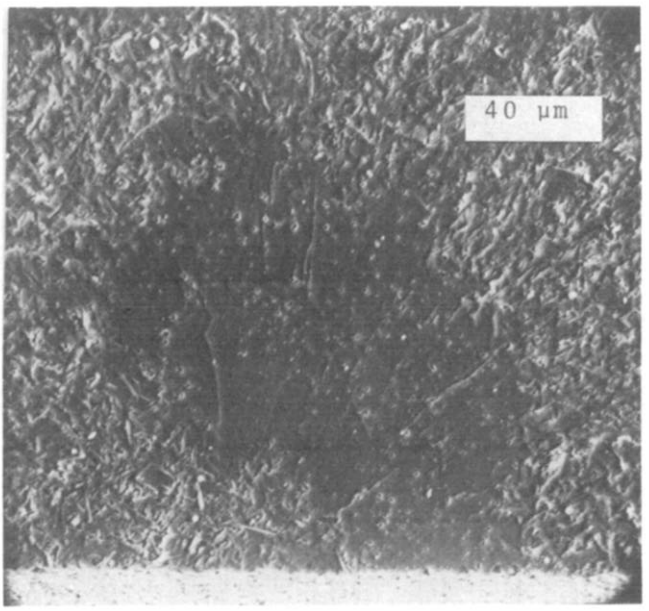

Fig. 13. Fracture surface of a time-dependent failure during a STSR test: 325 MPa, 0·4 h at 1400°C. Failure occurred due to the porous area at the surface which is coincident with a large grain.

The boundary lines on the stress rupture plot (Fig. 10) were drawn to approximate the scatter. None of the specimen fracture surfaces showed any signs of slow crack growth.

The fracture surface characteristics of the stress rupture and STSR time-dependent failures appear identical to those of the fast fracture specimens. The strength-limiting flaws for the failure on loading specimens are volume distributed and are agglomerates (Fig. 11), porous zones, or large grains. The time-dependent failures occurred *exclusively* from surface connected porosity (Figs 12 and 13). This porosity was often an area of small interconnected porosity and not necessarily a discrete void.

5. DISCUSSION

The β-silicon carbide material is subject to static fatigue failure over the 1000–1400°C temperature range for applied flexural stresses of 300–350 MPa, which is at least 85% of the reference fast fracture stress. The scatter in the time to failure of identically loaded specimens was up to five orders of magnitude. The good strength retention at high temperature and the fatigue resistance findings of this study are consistent with earlier reports.[7–10] Double torsion experiments on this material failed to detect any evidence of a time-dependent failure process.[17] That time-dependent failure can occur from surface-connected porous zones, as shown in this report, underscores the desirability of using stress rupture testing.

Although this form of silicon carbide is nominally the β-form, the strength-limiting flaws, the favorable creep and static fatigue resistance, and the enhanced strength of survivors are very similar to results on the sintered α-form of a commercial silicon carbide (Carborundum Corporation, Niagara Falls, New York).[19–21] Indeed, the two materials share a susceptibility of time-dependent failure to primarily surface connected defects, which suggests a stress corrosion phenomenon. Controlled atmosphere experiments would be valuable in clarifying this but were beyond the scope of this screening study.

6. CONCLUSIONS

The sintered β-silicon carbide tested for this program is of a limited production scale and may not necessarily be identical with research laboratory-produced earlier vintages. The Vickers and Knoop microhardness and the Vickers fracture toughness are lower than previously published

data.[7] The room temperature flexural strength is somewhat lower than reported.[9–10]

The intrinsic flaw populations are generally agglomerates and porous zones with a few large grains, inclusions, and process cracks. These flaws are all volume distributed, however. Time-dependent failures occurred only from surface-connected porous zones. There may be an effective stress rupture limit at 1000 h of approximately 250 MPa (~70% of the fast fracture reference strength) at 1200°C. Time-dependent failures occurred throughout the 1000–1400°C temperature range.

The C-scan promises to become a simple, powerful and effective quality control test to find not only large property variations within a tile or component but microstructural variations and severe flaw locations. More in-depth work must be done on the latter two topics for different materials and more complex shapes.

ACKNOWLEDGEMENT

This research was sponsored by the Advanced Materials Development Program Office of Transportation Systems, US Department of Energy IEA DE-AI05-840R 21411 with DOE's Oak Ridge Operation.

APPENDIX

Notation

V_L Longitudinal velocity
d_i Thickness of ith block
t_i Time of flight of ith block
E_i Elastic modulus of ith block
ρ_i Density of ith block
v_i Poisson's ratio for ith block
E_0 Elastic modulus at theoretical density
P Porosity
b Porosity correction factor
ρ_{TH} Theoretical density

The ultrasonic longitudinal wave propagation time C-scan maps point-by-point the wave propagation time through a material. The general equation for the longitudinal wave velocity is:

$$V_L = \frac{2d}{t} = \left[\frac{E}{\rho}\frac{(1-v)}{(1+v)(1-2v)}\right]^{1/2} \tag{A1}$$

which solving for the propagation time becomes

$$t = 2d\rho^{1/2}E^{-1/2}\left[\frac{(1+v)(1-2v)}{(1-v)}\right]^{1/2} \tag{A2}$$

where d, ρ, E, and v are the tile thickness, material density, elastic modulus, and Poisson's ratio, respectively.

The C-scan shown in Fig. 1 shows that (discounting wave distortion at the edges) the wave propagation time, or fly time, increases by approximately 5% from the edge to the center of the tile. Because of this large variation in fly time, it was decided to cut five rectangular blocks through the center of the tile to find the effect of the local material properties on the fly time.

The tile as supplied had a thickness increase from the edge to the center of 1·5%. The five blocks had their densities measured (Archimedes method) and were ultrasonically evaluated for the elastic modulus and Poisson's ratio. The data are shown in Table A1.

TABLE A1
Densities and Sonic Properties of the Machined Blocks

Block i	*Density* $\rho/Mg\,m^{-3}$	ρ_i/ρ_{TH}	*Porosity* P	*Elastic modulus* E/GPa	E_i/E_0	*Poisson's ratio* v
1	3·10	0·967	0·033	404·0	0·907	0·17
2	3·07	0·956	0·044	389·6	0·875	0·16
3	3·05	0·951	0·049	384·4	0·863	0·16
4	3·06	0·954	0·046	388·3	0·872	0·16
5	3·11	0·968	0·032	405·9	0·911	0·16

$\rho_{TH} = 3{\cdot}21\,Mg\,m^{-3}$.
$E_0 = 445\,GPa$.

A decrease in the density corresponding to a decrease in the elastic modulus from the edge to the center of the tile is readily apparent. This relationship, as described by Rice,[22] between the elastic modulus and porosity yields a porosity correction factor, b, of 3·1 and 2·8 for the exponential and linear equations, respectively, assuming an elastic modulus at zero porosity of 445 GPa.* There is no apparent trend in Poisson's ratio versus density through the tile.

This brief analysis does not take into account any secondary microstructure effects on the material properties such as grain size. It was assumed that the porosity is related to the change in theoretical density ($P = 1 - \rho/\rho_{TH}$).

* $E/E_0 = e^{-3{\cdot}1P}$ and $E/E_0 = 1{-}2{\cdot}8P$.

The combined effects of the material properties from block 1 to 3 on the C-scan show a change of +4·0% in the fly time. Using the local properties of the blocks with eqn (A2), the change in fly time is +3·6%. This shows an outstanding agreement even though the 'local' properties are still averages themselves.

A breakdown on change in property required to cause an *increase* in the fly time is:

increased thickness:	major contribution
decreased density	major contribution
decreased elastic modulus:	minor–major contribution
decreased Poisson's ratio:	negligible contribution

Note that the decrease in elastic modulus accompanies the decrease in density which will decrease the fly time.

REFERENCES

1. Prochazka, S. and Charles, R. J., Strength of boron doped hot pressed silicon carbide, *Am. Ceram. Soc. Bull.*, **52**(12) (1973), 885–91.
2. Prochazka, S., Strength of silicon carbide, in *Ceramics for High Performance Applications*, Eds J. Burke, A. Gorum and R. Katz, Brook Hill Publishing Co., Chestnut Hill, Massachusetts, USA, 1974, 239–52.
3. Prochazka, S., Abnormal grain growth in polycrystalline SiC, in *Silicon Carbide—1973*, Proceedings of the Third International Conference on Silicon Carbide, Miami, Florida, September 1973.
4. Prochazka, S. and Charles, R., Strength and microstructure of dense hot pressed silicon carbides, in *Fracture Mechanics of Ceramics*, Vol. 2, Eds R. Bradt, D. Hasselman, and F. Lange, Plenum Press, New York, 1974, 579–98.
5. Prochazka, S., Johnson, C. A. and Giddings, R. A., Atmosphere effects in sintering of silicon carbide, in *Proceedings of International Symposium on Factors in Densification and Sintering of Oxide and Non-Oxide Ceramics*, Eds S. Somiya and S. Saito, Association for Science Documents Information, Tokyo Institute of Technology, Tokyo, Japan, October 1978, 366–81.
6. Johnson, C. A., Crack blunting in sintered SiC, in *Fracture Mechanics of Ceramics*, Vol. 3, Eds R. Bradt, D. Hasselman and F. Lange, Plenum Press, New York, 1978, 99–111.
7. GEC, *Sintride Sintered Silicon Carbide*, General Electric Silicon Carbide Products Operations Brochure, Houston, Texas, 1983.
8. Trantina, G. G. and Johnson, C. A., Subcritical crack growth in boron-doped SiC, *J. Am. Ceram. Soc.*, **58**(7–8) (1975), 344–5.
9. Larsen, D. *Property Screening and Evaluation of Ceramic Turbine Materials*, US Air Force Technical Report AFML-TR79-4188, October 1979.
10. Larsen, D. and Adams, J., *Property Screening and Evaluation of Ceramic Turbine Materials*, US Air Force Technical Report AFWAL TR83-4141, April 1984.

11. US Army MIL-STD-1942(MR), *Flexural Strength of High Performance Ceramics at Ambient Temperature.*
12. Tracy, C. A., Unpublished work, Army Materials and Mechanics Research Center, 1984.
13. Quinn, G. D., *Guide to the Construction of a Simple 1500°C Test Furnace.* Army Materials and Mechanics Research Center, AMMRC TR83-1, January 1983, NTIS ADA 125636.
14. Quinn, G. D., *Characterization of Turbine Ceramics after Long Term Environmental Exposure*, Army Materials and Mechanics Research Center, AMMRC TR80-15, April 1980, NTIS ADA 117463.
15. Quinn, G. D. and Katz, R. N., Stepped temperature stress rupture testing of silicon based ceramics, *Am. Ceram. Soc. Bull.*, **57**(11) (1978), 1057–8.
16. Marshall, D. B. and Evans, A. G., Reply to Comment on 'Elastic/plastic indentation damage in ceramics: the median radial crack system', *Comm. Am. Ceram. Soc.*, **14**(12) (1981), C182–3.
17. Evans, A. G. and Lange, F., Crack propagation and fracture in silicon carbide, *J. Mater. Sci.*, **10** (1975), 1659–64.
18. Larsen, D., *Property Screening and Evaluation of Ceramic Turbine Engine Materials*, US Air Force/IITRI Contract F33615-75C-5196 Interim Report No. 7, March 1979.
19. Quinn, G. D. and Katz, R. N., *Time Dependence of the High Temperature Strength of Sintered Alpha Silicon Carbide*, Army Materials and Mechanics Research Center, AMMRC TN79-5, June 1979.
20. Quinn, G. D., *Stress Rupture of Sintered Alpha Silicon Carbide*, Army Materials and Mechanics Research Center, AMMRC TN81-4, December 1981.
21. Quinn, G. D. and Katz, R. N., Time dependent high temperature strength of sintered α-SiC, *J. Am. Ceram. Soc.*, **63**(1–2) (1980), 117–19.
22. Rice, R. W., Microstructural dependence of mechanical behavior of ceramics, in *Treatise of Materials Science and Technology*, Vol. II, Ed. R. K. MacCrone, Academic Press Inc., New York, 1977, 203–30.

Received 15 October 1985; accepted 16 December 1985

Int. J. High Technology Ceramics **2** (1986) 65–72

Leaching Behavior of Si–Y–Al–O–N Glasses

John W. Wald

Battelle, Pacific Northwest Division, Richland, Washington 99352, USA

Donald R. Messier and Eileen J. DeGuire

Army Materials Technology Laboratory, Watertown, Massachusetts 02172, USA

SUMMARY

Oxynitride glasses in the yttrium sialon family were leach tested under static conditions in deionized water at 40, 90 and 200°C for 28 days. Results indicate a lower silicon release in the compositions tested than that of fused silica glass or crystalline quartz when tested under identical conditions.

1. INTRODUCTION

Interest in oxynitride glasses has recently increased to a significant level as attempts are made to identify and develop new glasses and ceramics for potential applications ranging from electrical insulators to structural components in heat engines.[1] Of specific interest has been the effect of nitrogen on glass physical properties such as glass transition temperature, microhardness, fracture toughness, and thermal expansion.[2,3] Additional studies have also examined the electrical properties of selected oxynitride glasses.[4] Little, if any, detailed work has been reported to date on the chemical durability (leachability) of oxynitride glasses. In a paper on the yttrium sialon glass system, Loehman[5] reported that, while no trend in the degree of leaching with nitrogen content was apparent after testing for 350 h in 95°C distilled water, two of the three glass compositions tested showed lower weight losses than literature values for vitreous silica under

Int. J. High Technology Ceramics 0267-3762/86/$03·50

the same conditions. Other work reported by Loehman[3] indicated that nitrogen increased leach resistance in two additional oxynitride glass systems; the addition of AlN to a sodium–barium–phosphate glass increased its leach resistance by more than a factor of 100, and a high nitrogen content La–Si–O–N glass was reported to be very resistant to alkali attack at elevated temperatures.

In the leach testing reported to date for oxynitride glasses, the main indicator of leachability has been the evaluation of post-test weight loss. Leaching processes are sufficiently complex though, that a simple weight loss determination is insufficient to completely characterize the materials leaching behavior.[6] The experimental work reported here employed static leach test procedures developed to evaluate the chemical durability of proposed nuclear waste materials.[7] As such, emphasis was on the release of specific elements rather than on weight loss alone. The results presented herein compare the behavior of three glass compositions in the Si–Y–Al–O–N system with that of high purity fused silica glass and single crystal quartz, tested under identical conditions of time, temperature, solution, and atmosphere. Also reported is the variation of oxynitride glass leach behavior with temperature and with nitrogen content.

The work reported here is not intended to be a definitive end result, as certainly a more detailed and extensive testing scheme could be developed. But rather, this work presents additional comparative chemical durability data, more detailed than simple weight loss, on a glass system heretofore not extensively tested.

TABLE 1
Chemical Analyses of Oxynitride Glasses (in wt%)

Element	*Glass batch*						
	a		*b*		*h*		
	Nominal	*Analyzed*	*Nominal*	*Analyzed*	*Nominal*	*Analyzed*	
Al[a]	6·0	6·5	12·6	12·7	9·1	9·6	
Si[a]	18·9	18·0	13·2	13·2	14·3	14·3	
Y[b]	39·8	42·6	41·5	43·0	45·1	45·4	
O[c]	32·2	29·3	26·2	24·8	24·4	23·1	
N[d]	3·1	3·3	6·5	6·4	7·1	7·2	
Fe[b]		0·11		0·13		0·09	
B[b]		~0·1		~0·1		~0·1	trace levels

[a] Average of emission spectroscopy and atomic absorption spectroscopy.
[b] Emission spectroscopy.
[c] Vacuum fusion, precision ± 0·8%.
[d] Kjeldahl distillation, precision ± 0·2%.

2. MATERIAL PREPARATION AND TESTING

2.1. Glass preparation

Glasses in the system Si–Y–Al–O–N were prepared from oxide and nitride starting materials that were blended, preslugged, and melted between 1650 and 1700°C in boron nitride crucibles in a nitrogen atmosphere. The preparation and properties of the three glasses used in this study (Table 1) have been discussed in detail elsewhere.[8,9]

Parallelepiped leach samples, with a nominal surface area of 150 mm^2, were prepared from bulk glass of each composition by diamond saw sectioning. Cut samples were ultrasonically cleaned twice in acetone and once in methanol, and stored under vacuum until used.

2.2. Leach testing

Leach testing was conducted on the samples described above using a static leach test technique.[7] Samples of compositions 'b' and 'h' were leach tested in deionized water at 40, 90 and 200°C, while composition 'a' was leach tested only at 200°C. The duration of all tests was 28 days with a sample surface area to leach solution volume ratio (SA/V) of 20 m^{-1}. All tests were conducted by placing the glass leach sample and the appropriate volume of solution inside individual 0·38 mm wall thickness, closed-one-end gold capsules. After loading, each capsule was crimped closed, welded shut, marked, and leak checked, prior to placement in either an autoclave system[10] or convection oven. The chamber of the autoclave was partially filled with deionized water to assure pressure equilibration across the capsule wall during testing. The capsules were heated to 200°C from room temperature and allowed to furnace cool at the end of the test, prior to unloading. Average heating and cooling time was about 4 h. Tests at 40°C and 90°C were conducted by placing the sealed capsules in a mechanical convection oven at the appropriate temperature. Leach solution elemental analyses were performed by inductively coupled argon plasma atomic emission spectroscopy (ICP).

3. RESULTS AND DISCUSSION

Table 1 gives the nominal starting and analyzed final compositions of the three glasses investigated. Since all of the oxides in the glass batches were of high purity (99·5% or higher), the iron contamination must have come from the silicon nitride powder used as the nitrogen-containing component.

The low levels of boron indicate that minimal interaction occurred between the glasses and boron nitride crucibles during melting.

For comparison with previously cited work, the results of weight loss measurements on the samples tested are given in Table 2. In agreement with previous weight loss results, all oxynitride glass compositions tested lost less weight than either silica glass or crystalline quartz. From these same data (comparing the different compositions tested at 200°C) it might

TABLE 2
Weight Loss from Leach Testing in Deionized Water at Various Temperatures
(All specimens were tested with $SA/V = 20\,m^{-1}$)

Sample/comp.	*Leach temperature/°C*	*Weight loss/%*
Silica glass	200	0·56
Quartz	200	0·26
a	200	0·02
b	40	0·02
	90	0·05
	200	0·07
h	40	0
	90	0
	200	0·04

also be concluded, as with previous work, that there is no systematic trend in the degree of leaching with nitrogen content. However, as mentioned earlier, weight loss alone is insufficient to completely characterize the total leaching process. Results of silicon, and yttrium and aluminum elemental release are given in Figs 1 and 2, respectively. The release values shown in the figures have been normalized to the mass fraction in the glass, taking into consideration the SA/V ratio, and are reported in units of normalized grams of element released per square meter.[11] Figure 1(A) illustrates that, in terms of silicon release, the oxynitride glasses are at least a factor of two more durable than either silica glass or crystalline quartz. The durability of the oxynitride glasses improves even more as temperature is lowered. (Although they were not tested, the leach resistances of silica glass and crystalline quartz would also be expected to improve as temperature is lowered.) In terms of nitrogen content, Fig. 1(B) indicates that silicon release is essentially constant up to about 13 at% for this glass system and begins to increase significantly at 15 at%. This effect may have resulted from phase separation or other compositional inhomogeneity in the glass at this high nitrogen level. Yttrium release, shown in Fig. 2, is essentially constant with temperature while aluminum release decreases with temperature. The behavior of aluminum in this case is likely due to

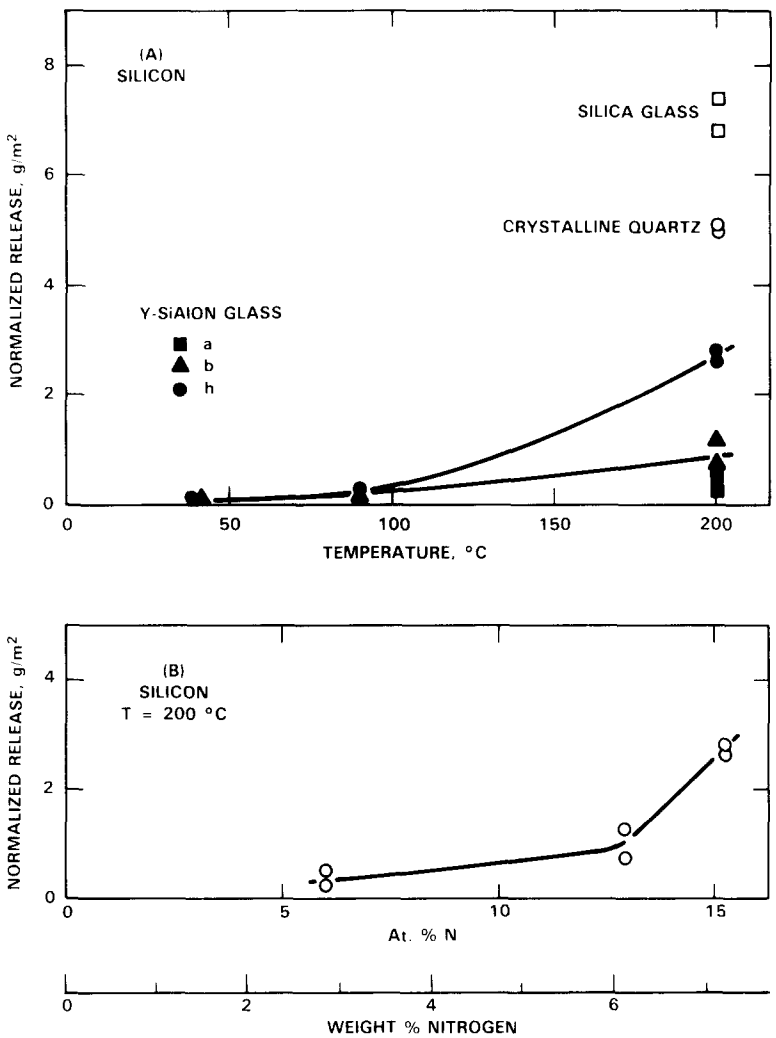

Fig. 1. Silicon release: (A) versus temperature; (B) versus nitrogen level.

the formation of alteration products at the elevated temperature (aluminosilicates), which precipitate from solution onto the sample surface or container walls. At 200°C yttrium release increases up to about 13 at% nitrogen and is essentially constant above this value. Aluminum was below detection limit ($< 0{\cdot}03$ ppm) at all nitrogen levels at this temperature.

Although the results suggest a trend toward increased release of both silicon and yttrium with increasing glass nitrogen content, further work would be needed to confirm such behavior. Reasons for this include the scatter in the test results and the fact that previous work on the glasses[8] gave evidence of minor amounts of crystalline phases in high nitrogen

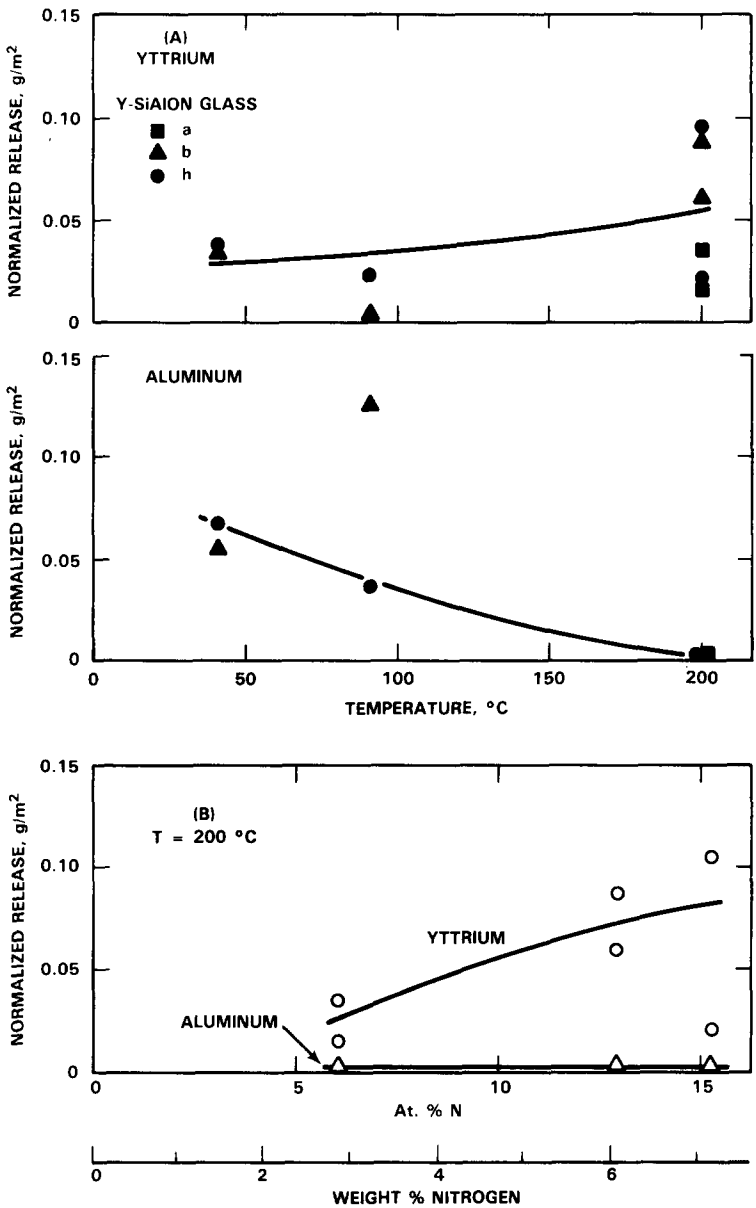

Fig. 2. Yttrium and aluminum release: (A) versus temperature; (B) versus nitrogen level.

(~ 7 wt%) glasses. The presence of such phases could also conceivably increase the leachability of the glass phase.

The leaching process in silicate glasses may be described in terms of solvent attack of Si—O bonds (hydrolysis) to form localized anionic silicate groups which are slowly released to the solution, thereby corroding the surface. In oxynitride glasses it has been reported that nitrogen substitutes

for oxygen in the structural framework, allowing for increased crosslinking of the network through Si–N–Si interactions.[12] This increased crosslinking may have improved leach resistance by greatly reducing the hydrolysis reaction. The effect of yttrium and aluminum on leaching in these glasses, however, should also be considered in light of the known positive effects each has on leach resistance. In studies of soda–lime–silica glasses for solar applications, Buckwalter and McVay have reported that very low concentrations of rare earths can greatly inhibit glass/water interactions.[13] Paul and Zaman have shown that incorporation of aluminum oxide in silicate glasses can also increase the chemical durability of glass.[14] Although increased leach resistance is generally associated with rare earth and aluminum incorporation in the glass system, the magnitude of the effect on leaching compared to fused silica glass is not as great as noted in the current tests. This conclusion would lead to the belief that the high leach resistance noted must for the major part be due to the increased structural integrity resulting from nitrogen incorporation in the structural framework.

4. CONCLUSIONS

The data presented support previously published trends that indicate high chemical durability in nitrogen-containing glasses. Although in the present study no attempt was made to adjust cation ratios as nitrogen concentration was increased (test specimens were adapted from other study areas), each glass tested showed lower normalized silicon release than either fused silica glass or crystalline quartz when tested under identical conditions at 200°C. The enhanced durability in nitrogen-containing glasses is believed to be due to increased cross-linking of the silica network through Si–N–Si interactions and the resultant reduction in the hydrolysis reaction at the glass surface. More fundamental investigations would be required and could be conducted to fully address this belief.

ACKNOWLEDGEMENT

This work was supported by Battelle, Pacific Northwest Division and the Army Materials and Mechanics Research Center.

REFERENCES

1. Jack, K. H., Review: Sialons and related nitrogen ceramics, *J. Mat. Sci.*, **11** (1976) 1135–58.

2. Shillito, K. R., Wills, R. R. and Bennett, R. B., Silicon metal oxynitride glasses, *J. Am. Ceram. Soc.*, **61** (11–12) (1978) 537.
3. Loehman, R. E., Preparation and properties of oxynitride glasses, *J. Non-Cryst. Sol.*, **56** (1983) 123–34.
4. Leedecke, C. J. and Loehman, R. E., Electrical properties of yttrium–aluminum–silicon oxynitride glasses, *J. Am. Ceram. Soc.*, **63** (3–4) (1980) 190–3.
5. Loehman, R. E., Preparation and properties of yttrium–silicon–aluminum oxynitride glasses, *J. Am. Ceram. Soc.*, **62** (9–10) (1979) 491–4.
6. McVay, G. L. and Buckwalter, C. Q., The nature of glass leaching, *Nuc. Tech.*, **51** (1980) 123–9.
7. US Department of Energy, Waste form test methods, in *Nuclear Waste Materials Handbook*, Tech. Rept. No. DOE/TIC–11400, Department of Energy, Richland, Washington.
8. Messier, D. R., Preparation and crystallization of Si–Y–Al–O–N glasses, in *Ceramic Engineering and Science Proceedings*, Vol. 3, No. 9–10, Sept.–Oct. 1982, The American Ceramic Society, Columbus, Ohio, 565–76.
9. Messier, D. R. and Broz, A., Microhardness and elastic moduli of Si–Y–Al–O–N glasses, *J. Am. Ceram. Soc.*, **65** (8) (1982) C–123.
10. Bradley, D. J., McVay, G. L. and Coles, D. G., *Leach Test Methodology for the Waste/Rock Interactions Technology Program*, Tech. Rept. No. PNL–3326, Pacific Northwest Laboratory, Richland, Washington, 1980.
11. Strachan, D. M., Barnes, B. O. and Turcotte, R. P., Standard leach tests for nuclear waste materials, in *Scientific Basis for Nuclear Waste Management*, Vol. 3, Ed. J. G. Moore, Plenum Press, New York, 1981, 347–54.
12. Loehman, R. E., Oxynitride glasses, *J. Non-Cryst. Sol.*, **42** (1980) 433–46.
13. Buckwalter, C. Q. and McVay, G. L., Inhibiting degradation of wet process manufactured solar mirrors, *Solar Energy Mat.*, **3** (1980) 215–24.
14. Paul, A. and Zaman, M. W., The relative influences of Al_2O_3 and Fe_2O_3 on the chemical durability of silicate glasses at different pH values, *J. Mat. Sci.*, **13** (1978) 1499–502.

Received 7 November 1985; accepted 16 December 1985.

Int. J. High Technology Ceramics **2** (1986) 73–78

Wetting of Aluminum Oxide by Liquid Aluminum

H. John and H. Hausner

Technische Universität Berlin, Institut für Nichtmetallische Werkstoffe, Englische Strasse 20, D-1000 Berlin 12, Germany

SUMMARY

The wetting of aluminum oxide by liquid aluminum can be improved considerably by a change of the interfacial energy between the oxide and the metal. The presence of an extremely thin carbon layer at the interface between the oxide and the metal results in a significant decrease of the contact angle.

1. INTRODUCTION

The wetting of aluminum oxide by liquid aluminum has been investigated by several authors using the sessile drop method.[1–8] In general, wetting does not occur below a temperature of 950°C, regardless of whether single crystal or polycrystalline material has been used. At 950°C a slight interaction between the metal and the oxide can already be observed; this is undesirable during the preparation of a fiber reinforced material as it could result in a weakening of the composite. Therefore, experiments with the aim of improving the wettability of the aluminum oxide are of interest. The influence of different parameters on the wetting behavior, e.g. changes in the composition of the metal, the oxide or the gas phase, or variations of the interface between the metal and the oxide, has been investigated extensively by John.[9] Some results of this work are reported below.

2. MATERIAL AND EXPERIMENTAL TECHNIQUES

2.1. Material

Small cylinders of aluminum (99·99%) with a diameter of 3·3 mm and a height of 3·2 mm were used. The samples were machined from aluminum

Int. J. High Technology Ceramics 0267-3762/86/$03·50

rods by using aluminum oxide cutting tools and a diamond wheel. After ultrasonic cleaning in ethanol they were electropolished (36 V, 14 s) in an electrolyte (700 ml methanol, 200 ml perchloric acid, 100 ml butylglycol). The electropolished samples were cleaned in ethanol, etched in a 10% sodium hydroxide solution (35°C) for 3 min, in a 2% hydrofluoric acid solution for 3 min and then washed with water and ethanol.

The aluminum oxide substrates were of polished single crystal material (H. Djevahirdian, SA, Switzerland) of 13 mm diameter and 2 mm thickness, with a purity of 99·99% (main impurities: 100 ppm Si, 120 ppm Mg, 110 ppm Fe) and a surface roughness of $Ra \leq 0{\cdot}01\ \mu m$. They had been fabricated by the Verneuil process and had an orientation of the c-axis of $30 \pm 10°$ from an axis perpendicular to the sample surface.

2.2. Sessile drop apparatus

For the wetting experiments an ultra-high vacuum system (1 μPa) was used. A tantalum heater (inner diameter 25 mm, total length 86 mm) surrounded by tantalum and molybdenum radiation shields was located in a water-cooled stainless steel chamber, which had two windows for the passage of a light beam. In the center of the heater an aluminum oxide plate (99·7% Al_2O_3), parallel to the optical axis, served as a support for the oxide substrate and the metal sample. An optical bench was located on both sides of the vacuum chamber. On one side a xenon high pressure lamp was fixed to the optical bench and illuminated the sample with a light beam 15 mm in diameter. On the opposite side a camera (6 × 6 cm) was attached and pictures could be taken during the various wetting stages. Temperatures inside the tantalum heater were controlled with W 3% Re/W 25% Re thermocouples. Programmed heating and cooling cycles were used in the experiments.

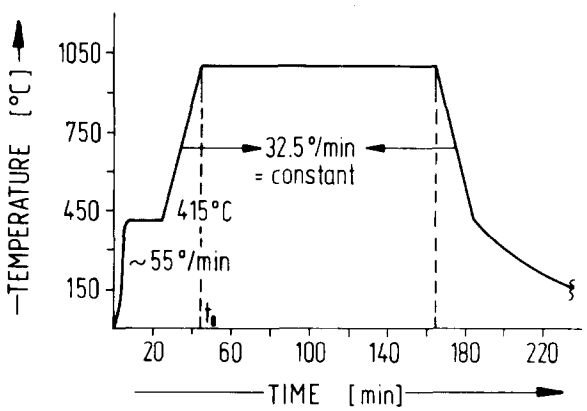

Fig. 1. Heating schedule.

2.3. Experimental technique

The single crystal substrate and the aluminum metal sample were positioned on top of the sample holder with a small manipulator. After pumping down the system to 40 μPa the wetting experiments were carried out according to the heating schedule shown in Fig. 1. The shape of the aluminum droplet was photographed periodically.

The contact angle was determined according to the procedure published by Bartlett and Hall.[10] A critical evaluation of all experimental errors showed that the contact angle could be determined with an accuracy of $\pm 3\%$ in the range between $40° \leq \varphi \leq 140°$.

RESULTS AND DISCUSSION

The time dependence of the contact angle at different temperatures is shown in Fig. 2. Each point of the curve is the median value from three experiments. At each temperature, with the exception of 1150°C, a rather steep decrease in the contact angle can be observed during the first few minutes. This steep decrease has been described in the literature as 'physical wetting' which starts after the sample has transformed completely into the liquid state. After about 15 min the change in the contact angle becomes smaller and remains constant.

At 700°C the change of the contact angle with time is extremely small,

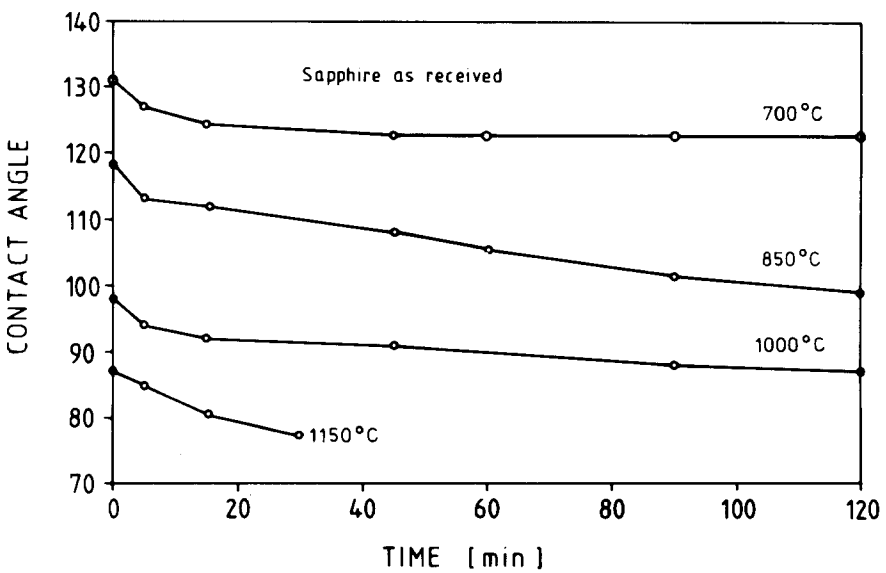

Fig. 2. Time dependence of wetting angle.

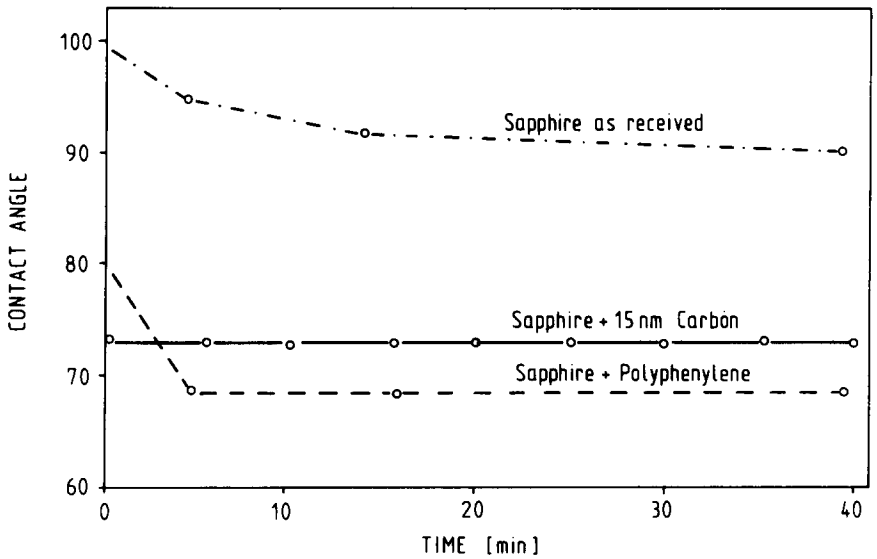

Fig. 3. Time dependence of wetting angle for an as-received sample and for two samples with a thin carbon layer on the surface (1000°C).

but at 1150°C it is significant. It is influenced by an interfacial reaction between the aluminum metal and the oxide, with the formation of suboxides at the low oxygen partial pressure inside the tantalum heater. At 1150°C strong vaporization of the aluminum metal, which limits the duration of the experiment to 30 min, may have an additional influence. Under the experimental conditions the contact angle drops below 90° at a temperature of 1000°C and wetting occurs. During the attempt to improve the wetting behavior of the oxide by the molten metal it could be observed by mass spectrometric analysis of the gas composition in the system that in some experiments an improved wetting behavior was associated with an increased concentration of hydrocarbons, carbon monoxide and carbon dioxide.

This observation led to a series of experiments where the surface of the aluminum oxide was intentionally contaminated with carbon. In Fig. 3 the change of the contact angle with time is shown for an as-received sample and for two samples with a thin carbon layer on the surface. In one case a 15 nm thick layer of carbon had been sputtered onto the substrate surface. The second sample had been treated with a 10% solution of polyphenylene in benzene, dried and used in this condition for the wetting experiment. During the heating-up period the polyphenylene is decomposed; the maximum weight loss occurs between 400 and 700°C, and the residual carbon content is 85·8 m/o. A marked reduction in the contact angle can be observed in the case of both carbon-coated samples.

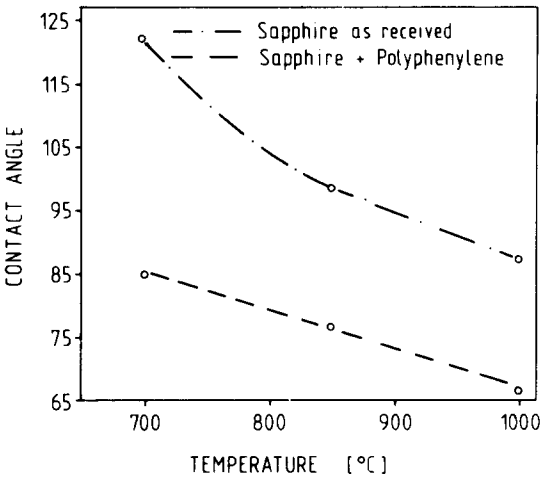

Fig. 4. Wetting angle after 120 min with and without carbon layers at different temperatures.

In Fig. 4 the contact angle at different temperatures is shown for single crystal aluminum oxide (sapphire) with and without a thin carbon layer made from polyphenylene.

It is possible to obtain a contact angle below 90° even at a temperature of 700°C in the case of the coated samples. The difference in the contact angle between the treated and untreated materials is about 20–30° for the whole temperature range.

The improvement in the wettability can be explained by the reaction between aluminum and carbon. Possible reaction products are aluminum carbide or oxycarbides (e.g. Al_2OC or Al_4O_4C). The presence of very small crystals could be observed at the interface between the oxide and the metal.

4. CONCLUSION

The wetting of aluminum oxide by molten aluminum can be achieved at a temperature as low as 700°C, if the surface of the aluminum oxide is first coated with a thin layer of carbon.

REFERENCES

1. Livey, D. T. and Murray, P., 'The Wetting Properties of Solid Oxides and Carbides by Liquid Metals'; *Plansee Proc.*, *2nd Seminar*, *Reutte/Tirol*, 1955, 375–404.
2. Carnahan, R. D., Johnston, T. L. and Li, C. H., Some observations on the wetting of Al_2O_3 by aluminium, *J. Am. Ceram Soc.*, **41** (1958) 343–7.

3. Wolf, S. M., Levitt, A. P. and Brown, J. I., Whiskermetal matrix bonding, *Chem. Eng. Progr.*, **62** (1966) 74–8.
4. Brennan, J. J. and Pask, J. A., Effect of nature of surfaces on wetting of sapphire by liquid aluminum, *J. Am. Ceram. Soc.*, **51** (1968) 569–73.
5. Champion, J. A., Keene, B. J. and Sillwood, J. M., Wetting of aluminium oxide by molten aluminium and other metals, *J. Mat. Sci.*, **4** (1969) 39–49.
6. Šebo, P., Ivan, J., Táborský, L. and Havalda, A., Benetzung von Al_2O_3 durch flüssiges Aluminium, *Kovoré Materiály*, (1973) **2**, 173–80.
7. Köhler, W. T., Van Rensen, E. and Sahm, K., *Entwicklung faserverstärkter Verbundwerkstoffe mit metallischer Matrix*, BMFT-Forschungsbericht T 73–14, 1973.
8. Dawihl, W. and Federmann, H., Einfluß metallischer Aufdampfschichten auf das Benetzungsverhalten von Reinstaluminium auf Al_2O_3-Unterlagen. in *Fachberichte der Tagung Verbundwerkstoffe*, Konstanz, 1974, 450–68.
9. John, H., Thesis, Technische Universität Berlin, 1981.
10. Bartlett, R. W. and Hall, J. K., Wetting of several solids by Al_2O_3 and BeO liquids, *Am. Ceram. Soc. Bull.*, **44** (1965) 444–8.

Received 14 October 1985; amended version received and accepted 23 December 1985.

Int. J. High Technology Ceramics **2** (1986) 79–80

Book Review

Ceramic Heat Exchanger Concepts and Materials Technology. By C. Bliem *et al.*, Noyes Publications, Park Ridge, New Jersey, 1985. 385 pp. Price $45.00.

The publication of this book is particularly timely from the European viewpoint, as the momentum for the subject is building up but is still significantly behind that achieved in N. America and the appearance of books such as this can only help redress the imbalance.

The information in the book is from two sources, 'Evaluation of Selected Advanced Heat Exchangers for Waste Heat Recuperation of High Temperature Streams' by Bliem *et al.* of EG & G, Idaho for the US Department of Energy and 'An Assessment of Ceramic Materials Technology for Heat Exchangers' by Barna *et al.* of EG & G, Federer and Bomar of Oak Ridge National Laboratory, again for the US Department of Energy. These contributions are split clearly into Part I, entitled 'Ceramic Heat Exchanger Concepts' and Part II on 'Materials Technology'. However, valuable as it has been to concentrate subject matter relating to Ceramic Heat Exchangers in one volume, the pitfall of duplication has not been avoided. Consequently, Chapter 3 of Part I and Chapter 2 of Part II could have been condensed into a more effective section on Recuperator Designs, thereby also reducing the number of printed pages. This would undoubtedly have helped the praiseworthy declared aim of the publishers to keep the price at a 'reasonable level' for a specialist hardback. In achieving this aim, direct photo-offset from original reports has been used in part and this generally gives a quite readable text except for some

of the Appendices, where many design calculations are expanded upon. In some instances this does present legibility problems, although the 'whole-food cookery book'-style presentation is not as incongruous as might be expected and is indeed quite refreshing.

Although very short at 3 pages the attempt at the end of Part I to identify Research and Development needs is laudable and is to be commended to other authors as a useful contribution in books of this type. At the end of the book 32 pages are devoted, very usefully, into a collation of Ceramic Material Properties of those materials likely to be, or now being employed, in recuperator tubes. This will prove very valuable to those working in areas concerned with the utilisation of these materials or in materials development itself; however, an index of material grades covered would also have been very helpful.

The stress and environmental problems faced by the ceramic components in recuperators are not in many cases dissimilar to those faced by the same type of materials in, for example, engines. By the same token the 47 pages entitled 'Design-related Materials Technologies' are not out of place and are equally applicable in other areas where ceramics are being used as engineering materials and where problems of non-destructive and proof testing have to be addressed.

A very worthwhile addition to the bookshelf of anyone seriously engaged in work in this area, and the price is reasonable.

P. L. Smith

Int. J. High Technology Ceramics **2** (1986) 81–82

Announcements

CERAMIC MATERIALS & COMPONENTS FOR ENGINES

The Second International Symposium on Ceramic Materials and Components for Engines will be held on April 14–17, 1986 in Lübeck-Travemünde, FRG. It is being sponsored by five national ceramic societies and the Commission of the European Communities, reflecting the growing interest and importance of this rapidly developing technology.

Organised by the German Ceramic Society, the meeting, through a strong international advisory committee which includes S. Sōmiya (Japan), W. Bunk (FRG), H. Hausner (FRG), G. Petzow (FRG) and P. Vincenzini (Italy), is intended to become an important forum for the presentation and discussion of recent advances in the science, technology, applications and reliability of advanced structural ceramic components. Further information may be obtained from: Deutsche Keramische Gesellschaft, e.V. (DKG), Menzenberger Strasse 47, D-5340 Bad Honnef 1, FRG.

CERAMIC MICROSTRUCTURES '86: THE ROLE OF INTERFACES

An International Conference, Ceramic Microstructures '86: The Role of Interfaces, will be held on the Berkeley campus of the University of California on July 28–31, 1986. This conference is the third of a 10-year interval series that started in Berkeley in 1966.

The plenary session will deal with introductory specific overviews of the current status and understanding of ceramic microstructures, with emphasis on the role of interfaces. Subsequent sessions will deal with specific papers on characterization of microstructures, microstructure production and control, effect of interfaces on electrical properties, and the effect of interfaces on mechanical behavior and properties.

Joseph A. Pask and Anthony G. Evans will be co-chairmen of the conference. Members of the International Advisory Committee are H. K. Bowen (USA), D. G. Brandon (Israel), R. J. Brook (UK), L. E. Cross (USA), H. E. Exner (FRG), A. H. Heuer (USA), J. T. Klomp (The Netherlands), F. F. Lange (USA), M. G. Nicholas (UK), K. Okazaki (Japan), M. Ruhle (FRG), S. Sōmiya (Japan), M. W. Swain (Australia), R. R. Tummala (USA) and T. S. Yen (People's Republic of China).

Those who are interested in attending the conference should contact Joseph A. Pask, Department of Materials Science and Mineral Engineering, Hearst Mining Building, University of California, Berkeley, California 94720, USA.

CALENDAR

1986 Meetings

Mar. 17–20	Materials Testing Exhibition, Birmingham, England
Apr. 14–17	Second International Symposium on Ceramic Materials and Components for Engines, Lübeck-Travemünde, FRG
Apr. 16–18	1st World Congress on Particle Technology, Nüremberg, FRG
Apr. 27–May 1	American Ceramic Society Annual Meeting and Exposition, Chicago, Illinois, USA
May 4–9	High Technology Silicon-Based Strctural Ceramics Symposium, Boston, Massachusetts
May 5–7	36th Electronics Components Conference, Seattle, Washington, USA
Jun. 8–11	IEEE International Symposium on the Application of Ferroelectrics, Bethlehem, Pennsylvania, USA
Jun. 11–14	Infared Transmitting Materials Conference, Peebles, Scotland
Jun. 23–27	World Congress on High Tech Ceramics, 6th CIMTEC Meeting, Milan, Italy
Jul. 7–11	Powder Metallurgy 86, International Conference and Exhibition, Düsseldorf, FRG
Jul. 28–31	Ceramic Microstructures '86: Role of Interfaces, University of California, Berkeley, USA
Aug. 3–6	Ceramic Powder Science and Technology: Synthesis Proceesing and Characterization, Boston, Massachusetts, USA
Sept. 9–11	3rd International Conference on Science and Technology of Zirconia, Tokyo, Japan
Nov. 2–5	Joint Meeting of the Basic Science, Electronics and Glass Divisions, American Ceramic Society, New Orleans, Louisiana, USA
Nov. 25–27	The 3rd Annual ME Conference, London, England
Dec. 15–19	Engineering with Ceramics—Institute of Ceramics Basic Science Section Meeting, London, UK

Int. J. High Technology Ceramics (2) (1986)—

Int. J. High Technology Ceramics **2** (1986) 85–98

Mechanical Properties of Y-PSZ After Aging at Low Temperature

Takaki Masaki

Technical Development Department, Toray Industries, Inc.,
2-2, 3-Chome, Sonoyama, Otsu, Shiga 520, Japan

SUMMARY

Y-PSZ (partially stabilized zirconia) materials containing 2·0, 2·5, 3·0, 4·0 and 5·0 mol% of yttrium oxide, which had been prepared by cold isostatic pressing and sintering, hot pressing, or hot isostatic pressing, were aged in air between 200 and 500 °C for 500–9000 h. The materials were examined to determine their mechanical properties and microstructure. It was confirmed that Y-PSZ containing 2·5–5·0 mol% yttrium oxide showed little degradation in strength after 2000 h of aging at 200 °C with no changes in monoclinic/tetragonal ratio and density, when the grain size of the sintered material was less than 0·5 μm and the density was greater than 6·07 Mg m^{-3}.

1. INTRODUCTION

In the ZrO_2–Y_2O_3 system Y-TZP* with nearly 100% tetragonal crystal structure has been actively studied as a sintered material with very high strength and toughness.[1–3] The high toughness of Y-TZP is considered to be due to the martensitic transformation from tetragonal (t) to monoclinic (m) crystal structure near propagating cracks and to the volume expansion associated with this transformation.[4] It was reported for the first time by the author and co-workers[5] that, while having excellent mechanical properties at room temperature, the Y-TZP shows conspicuous degradation in

* Editor's footnote: The author describes the materials with 2–3 mol % yttrium oxide as TZP (tetragonal zirconia polycrystal) but he generally (i.e. 2–5 mol %) designates them as Y-PSZ.

Int. J. High Technology Ceramics 0267-3762/86/$03·50

strength when aged at temperatures as low as 200–300 °C. The strength degradation, which is said to start at the surface, is thought to be due to the transformation from t to m during aging.[6–8] It was reported that the main cause of the transformation is the destabilization of zirconia resulting from the reaction of zirconium dioxide or yttrium oxide with water from the air.[9]

The author has studied the composition, particle size, and density of bodies densified by sintering, hot pressing and hot isostatic pressing (hipping) and examined the effects of aging conditions on the mechanical properties and microstructure in relation to the manufacturing conditions.

2. EXPERIMENTAL PROCEDURES

Zirconium dioxide was admixed with 2·0, 2·5, 3·0, 4·0, and 5·0 mol % yttrium oxide. A mixed solution having a predetermined composition was prepared from hydrous chlorides ($ZrOCl_2$, YCl_3) of 99·9 % ZrO_2, and 99·5 % Y_2O_3 purity, respectively, as starting materials. A zirconium dioxide powder was produced by thermally decomposing the solution, followed by calcining and grinding. The calcination was conducted by keeping the decomposed material at 1000 °C for several hours, and the grinding was done in water, using zirconia balls in a mill lined with polyurethane.

The powder thus obtained was dried and then isostatically pressed into blocks 40 × 30 × 100 mm at a pressure of 100 MPa or 200 MPa. The samples were heated from room temperature to 900 °C at a rate of 100 °C h^{-1} and from 900 °C to the sintering temperature (1350, 1400, 1450, or 1500 °C) at a rate of 30 °C h^{-1}, and were kept at that temperature for 2 to 3 h.

Hot pressing was carried out using a high frequency induction heating apparatus (output 20 kW). The dried powder was put into a carbon die and heated to 1500 °C at a rate of 700 °C h^{-1} under a nitrogen gas atmosphere, and kept at this temperature for 1 h; during heating-up the pressure was maintained at 5 MPa, and then raised to 25 MPa; the hot-pressed sample was 80 mm × 10 mm.

Hipping was carried out on samples pressed at 200 MPa and presintered for 2 h at 1400 or 1450 °C so as to obtain material with a density not less than 97 % of the theoretical density; the unencapsulated sample was raised from room temperature to the maximum temperature at a rate of 700 °C h^{-1} in an argon atmosphere; the gas pressure was adjusted to rise slowly so as to reach 200 MPa at maximum temperature; the samples were treated at 1400 or 1450 °C for 1·5 h.

The densified Y-PSZ samples were aged for 100 to 8000 h in air at 200, 250, 300, 400, and 500 °C in an electric furnace.

Specimens $3 \times 3 \times 24\,mm^3$ were prepared by cutting these samples with a diamond saw after aging. A 3-point-bend test (span 20 mm) was conducted with a loading rate of $0{\cdot}5\,mm\,min^{-1}$. The density was calculated from the volume and weight of the bending test specimens.

The microstructure of the sample was observed by transmission electron microscopy on thin films (less than 500 Å) produced by ion-thinning, and changes in the crystal structure after aging were determined using the X-ray diffraction method:[10]

$$\text{monoclinic/tetragonal ratio} = \frac{m(111) + m(11\bar{1})}{t(111) + m(111) + m(11\bar{1})} \times 100\ (\%)$$

The ZrO_2–Y_2O_3 material powder was chemically analyzed by induction coupled plasma (ICP) emission analysis. The results for the powder containing 2·5 mol % yttrium oxide are shown in Table 1. Although 0·03 % of Na_2O was contained in the powder, this was reduced to 0·01 % or less by

TABLE 1
Chemical Analysis of the 2·5 mol % Y-TZP Powder

	Wt %
SiO_2	0·016
Al_2O_3	0·020
Fe_2O_3	0·005
Na_2O	0·030
MgO	0·001
CaO	0·032
TiO_2	0·021
Y_2O_3	4·52
HfO_2	2·65

evaporation during sintering. Therefore, the purity of the powder including zirconium dioxide and hafnium dioxide is 99·9 %.

The grain size was measured by direct TEM observation and the so-called traverse method.

The theoretical density of Y-PSZ was taken from the value determined by the X-ray diffraction method.[11] The Y-PSZs containing 2·0 mol % and 5·0 mol % yttrium oxide had theoretical densities of $6{\cdot}10\,Mg\,m^{-3}$ and $6{\cdot}03\,Mg\,m^{-3}$, respectively.

3. RESULTS

Figures 1–6 show changes in the bend strength (σ) and monoclinic ratio of the Y-PSZs after aging at 200, 300, 400, and 500 °C.

The density of the sintered material was 97·5–98·7 % of the theoretical density, that of the hot-pressed material 99·6 %, and that of the hipped material 99·8 %.

The average grain size of Y-PSZ is 0·45–0·5 μm for the material sintered at 1500 °C, 0·5 μm for the material hot pressed at 1500 °C, and 0·4 μm for the material hipped at 1450 °C.

Figure 1 shows that the Y-TZPs containing 2–3·0 mol % yttrium oxide degrade greatly in strength when aged at 200 °C. Since the monoclinic ratio increases during aging at 200 °C (Fig. 2) this degradation is considered to be due to the transformation from the t to m structure. The ratio of the monoclinic structure increases with the decrease in mol % of yttrium oxide. However, the Y-PSZ containing 5·0 mol % yttrium oxide shows no deterioration in strength and no change in monoclinic ratio.

Figure 3 shows that the hot-pressed Y-TZP containing 2·0 mol % yttrium

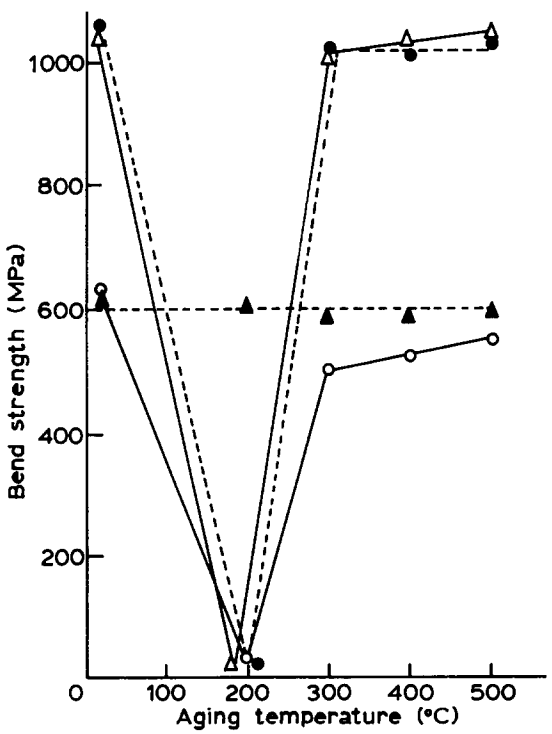

Fig. 1. Change in the bend strength of sintered (1500 °C) Y-PSZ after aging at low temperature for 2000 h. ○, 2·0; ●, 2·5; △, 3·0; ▲, 5·0 mol % yttrium oxide.

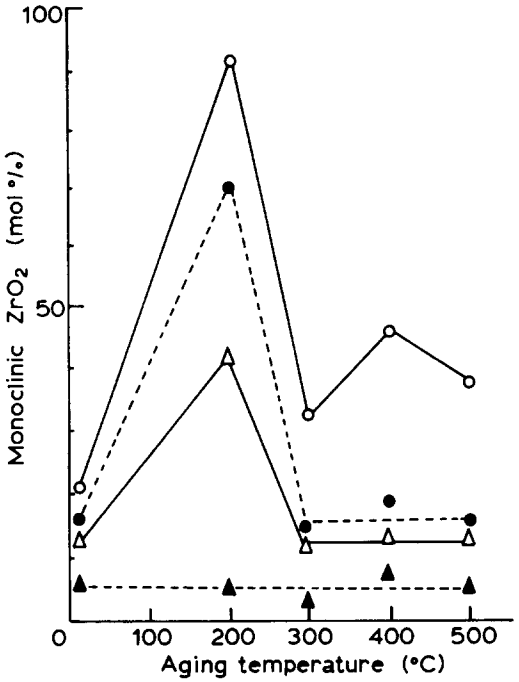

Fig. 2. Change in the monoclinic ratio of the sintered (1500 °C) Y-PSZ after aging at low temperature for 2000 h. ○, 2·0; ●, 2·5; △, 3·0; ▲, 5·0 mol % yttrium oxide.

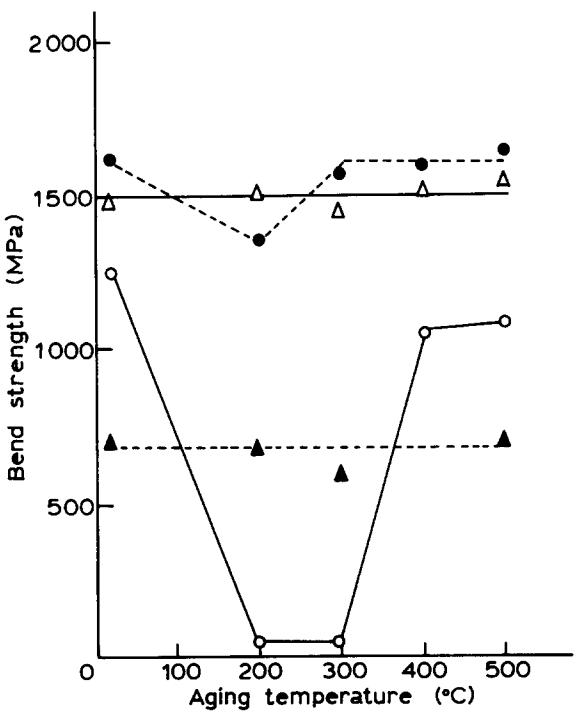

Fig. 3. Change in the bend strength of hot-pressed (1500 °C) Y-PSZ after aging at low temperature for 2000 h. ○, 2·0; ●, 2·5; △, 3·0; ▲, 5·0 mol % yttrium oxide.

oxide degrades greatly in strength when aged at 200 °C and 300 °C, that Y-TZP containing 2·5 mol % yttrium oxide decreases a little in strength, but those containing other molar ratios of yttrium oxide show no changes. Figure 4 shows that only the Y-PSZ containing 2·0 mol % yttrium oxide shows any change in monoclinic ratio. These results prove that a great improvement is achieved when the Y-PSZ is prepared by hot pressing as compared with the sintered material.

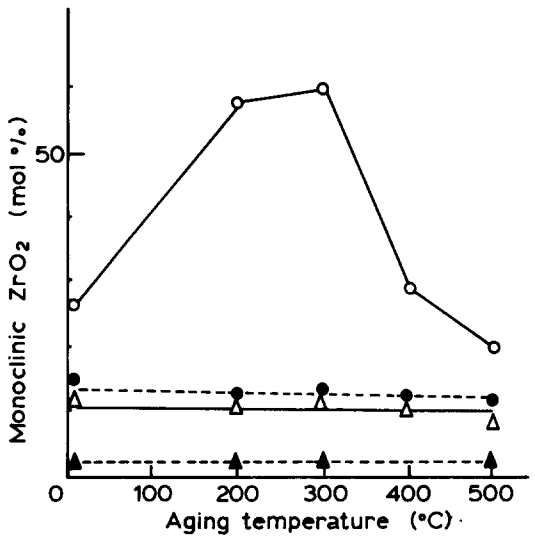

Fig. 4. Change in the monoclinic ratio of the Y-PSZ hot pressed at 1500 °C after aging at low temperature for 2000 h. ○, 2·0; ●, 2·5; △, 3·0; ▲, 5·0 mol % yttrium oxide.

The hipped material shows a similar trend to those prepared by hot pressing (Figs 5 and 6). The Y-TZP containing 2·0 mol % yttrium oxide degrades in strength when aged at 200 °C.

While Fig. 1 shows the dramatic degradation on aging at 200 °C there was no apparent change on aging at 300 °C for compositions containing 2·5, 3 and 5 mol % yttrium oxide. Even after 8000 h there was no degradation, nor any change of the monoclinic ratio; nor were any changes observed after 5000 h at 400 °C and 500 °C.

Figure 7 indicates changes in the strength of the Y-PSZs containing 2·5, 3·0 and 4·0 mol % yttrium oxide, prepared by sintering, hot pressing and hipping, after aging at 200 and 250 °C for 2000 h in relation to density and grain size.

Materials with high densities were obtained by hot pressing and hipping; materials with different grain sizes were prepared at different temperatures.

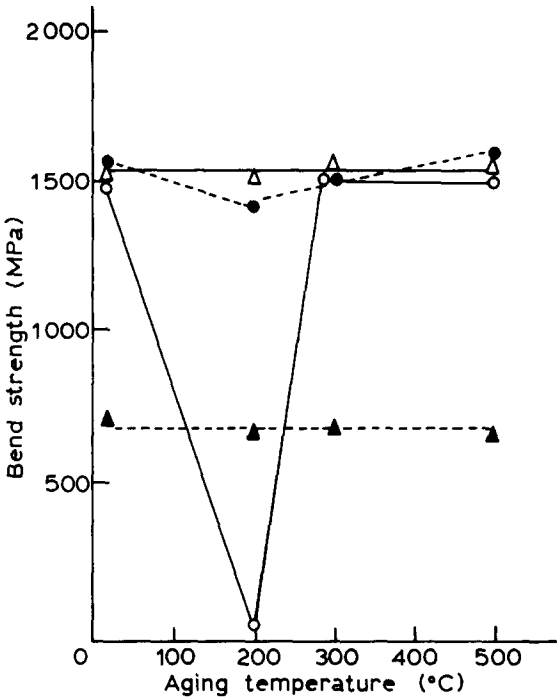

Fig. 5. Change in the bend strength of Y-PSZ hipped at 1400 °C after aging at low temperature for 2000 h. ○, 2·0; ●, 2·5; △, 3·0; ▲, 5·0 mol % yttrium oxide.

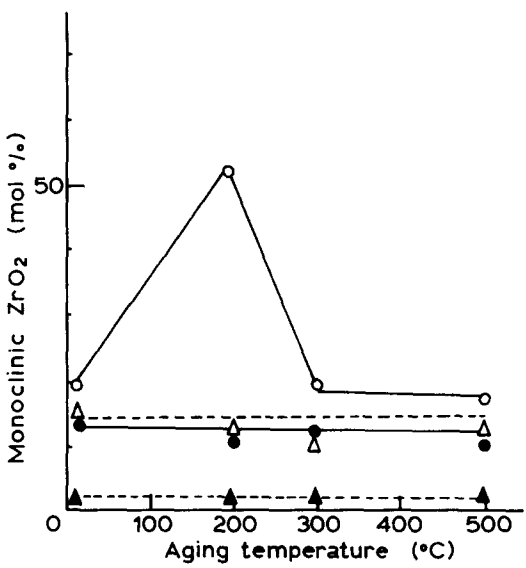

Fig. 6. Change in the monoclinic ratio of the Y-PSZ hipped at 1400 °C after aging at low temperature for 2000 h. ○, 2·0; ●, 2·5; △, 3·0; ▲, 5·0 mol % yttrium oxide.

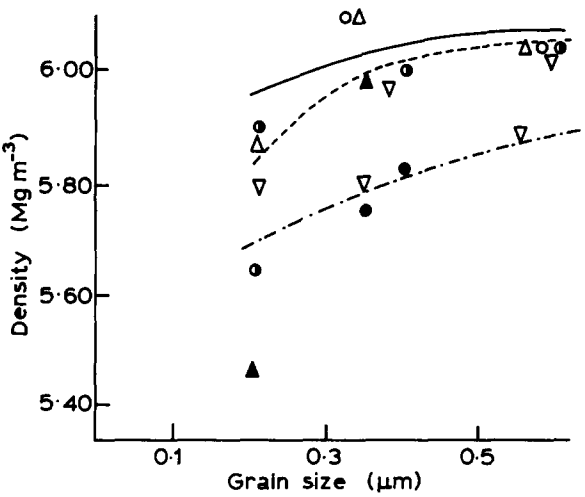

Fig. 7. The interrelation of density and grain size with degradation of the bend strength of Y-PSZ prepared by sintering, hot pressing and hipping, after aging at 200 or 250 °C. ○, ——, 2·5; △, – – –, 3·0; ▽, – · – ·, 4·0 mol % yttrium oxide.

Experiments were carried out on the Y-PSZs with grain sizes of 0·2–0·5 μm and densities of 90–99·7 % of the theoretical density.

The solid circles and triangles show sintered materials, the strength of which decreased greatly after aging; the extent of the black area in each circle corresponds to the degree of degradation in strength.

Figure 7 shows that the higher the content of yttrium oxide (3·0 to 4·0 mol %), the higher the density (not less than 99·6 % of the theoretical density), and the smaller the grain size, the less the degradation in strength after aging. The figure also shows curves of critical densities and grain sizes for degradation after aging with respect to the Y-PSZs containing 2·5, 3·0 and 4·0 mol % yttrium oxide. The area above the curve is a region where degradation after aging is not found.

These results prove that the degradation is associated with the interrelation between the density (or voids), the grain size and the composition. The Y-PSZ containing 4·0 mol % yttrium oxide does not deteriorate after aging.

Figure 8 shows the microstructure of the 2·0 mol % Y-TZP prepared by hot pressing at 1500 °C. The same sample exhibits various microstructures: a uniform granular structure (Fig. 8(a)); a mixed structure (Fig. 8(b)), consisting of fine grains (monoclinic structure) transformed from the tetragonal structure, and t grains; and a structure having clear intra-twins (monoclinic structure) or moiré patterns in the crystal grain (Fig. 8(c)). A material having these microstructures was reported to have a very high fracture toughness.[12]

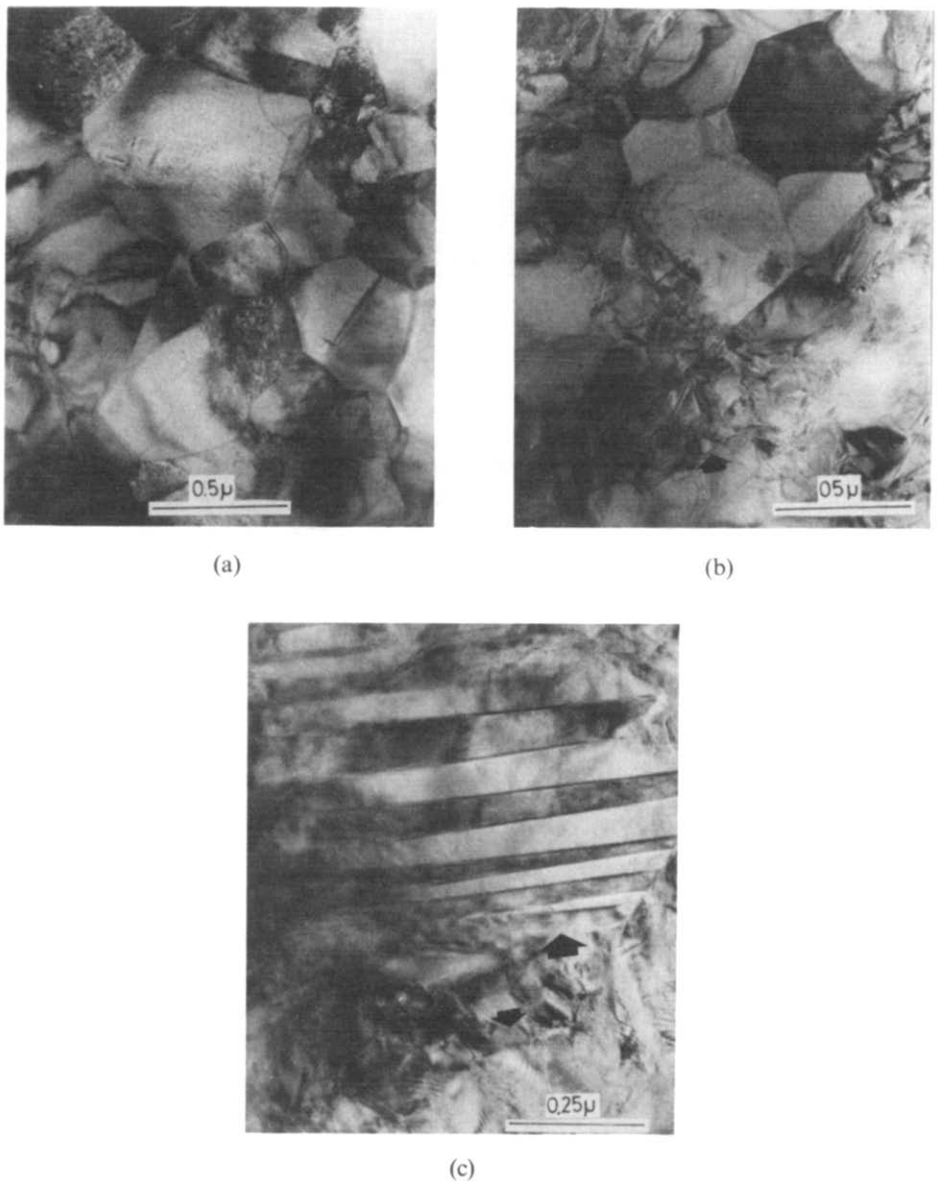

Fig. 8. The microstructures of 2·0 mol% Y-PSZ, hot-pressed at 1500°C. (a) Granular structure; (b) mixed structure of granular and transformed grains, in which a complicated microstructure other than crystal grains can be observed (arrow mark); (c) twins and moiré structure can be observed in the grain (arrow mark).

Figure 9 shows the microstructures of 3·0, 4·0 and 5·0 mol % Y-PSZs. The 3·0 mol % Y-TZP has a uniform granular structure with the t structure, and the 4·0 mol % Y-PSZ, a mixed structure consisting of fine and large grains. The former is of t structure and the latter of c structure. The 5·0 mol % Y-PSZ has a small number of fine grains with t structure and large grains ($\sim 0{\cdot}5\ \mu m$) with c structure.

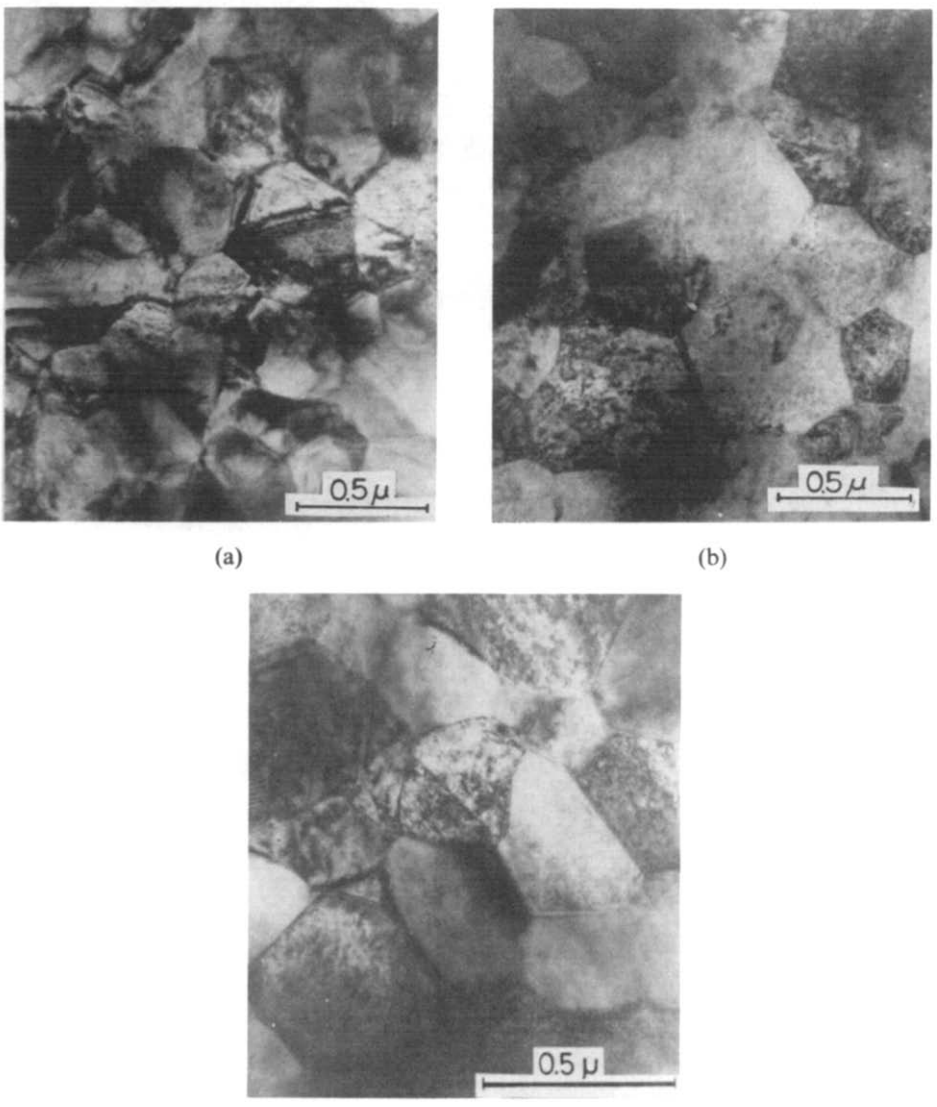

Fig. 9. The microstructure of the Y-PSZ hot-pressed at 1500 °C. (a) 3·0 mol % Y-TZP; (b) 4·0 mol % Y-PSZ; (c) 5·0 mol % Y-PSZ.

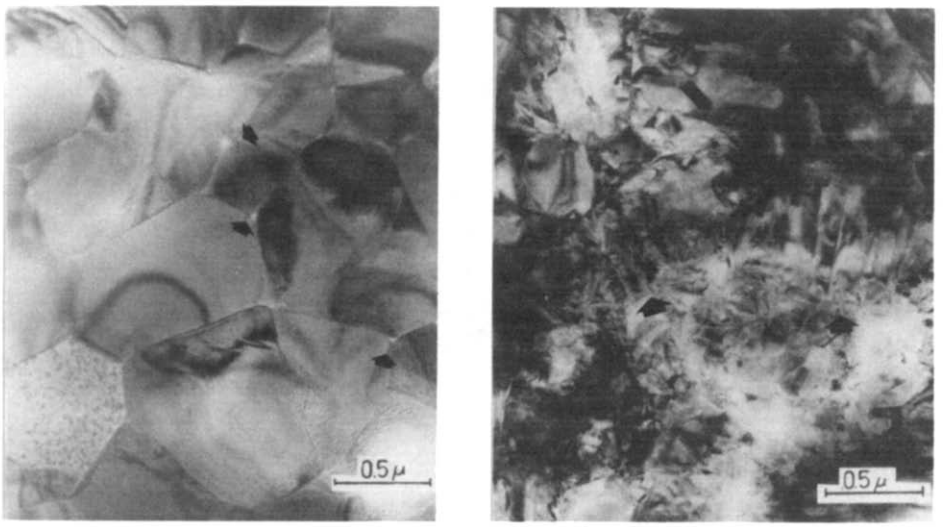

Fig. 10. The microstructures of 2·5 mol % Y-TZP sintered at 1500 °C before and after aging at 200 °C. (a) Microstructure before aging; (b) microstructure after aging at 200 °C for 1000 h, in which many twins and cracks can be observed (arrow mark).

The microstructure of 2·5 mol % Y-TZP, prepared by hot pressing, shows no change in the structure after aging at 200 °C.

Figure 10 shows the microstructure of sintered 2·5 mol % Y-TZP, before and after aging at 200 °C. It is observed that the strength is greatly degraded after aging, and that twins and cracks develop in the microstructure. These changes are considered to be due to the transformation from t to m structure.

4. DISCUSSION

Results of the bend strength (Fig. 1), the monoclinic ratio (Fig. 2), and the observation of the microstructure (Fig. 10), confirm that the degradation of the strength of the Y-TZPs containing 2·0 to 3·0 mol % yttrium oxide after aging at around 200 °C is caused by the transformation from the tetragonal (t) to the monoclinic (m) crystal structure. Changes in microstructure are observed by the increase in twins and cracks. However, the degradation of Y-TZP varies greatly according to the composition, density and grain size of the material. The materials prepared by hot pressing or hipping show no deterioration in strength after low temperature aging, as compared with the sintered material. Almost no deterioration is observed in the 2·5–3·0 mol %

Y-TZPs prepared by hot pressing, as compared with those having almost the same grain size ($\sim 0{\cdot}5\,\mu m$) prepared by sintering.

However, even in a high density material the transformation cannot be prevented when the yttrium oxide composition is as low as 2·0 mol %. From these results, it is confirmed that the degradation after low temperature aging is affected by the composition and property of the material, such as yttrium oxide content, grain size and density. While the degradation in strength is confirmed from the experimental results as being caused by the martensitic transformation from t to m structure, the mechanism of the transformation has been widely studied and discussed;[6] the stability of tetragonal grains is being examined from the points of thermodynamics and kinetics.

The thermodynamic argument is that when the grain size is small, the grain is stabilized because the surface and strain energy become larger than the change in chemical free energy from t to m structure.[13,14]

The kinetic argument is based on the concept that the transformation takes place through heterogeneous nucleation, wherein the nucleus, in the case of the PSZ, is formed mainly by the dislocation of the interface and as the dislocation grows, the transformation develops.[15]

According to the above arguments, as the grain size becomes smaller, the defect on the grain boundaries becomes less, making the nucleation difficult. The fact that the transformation is inhibited by the higher density can be understood qualitatively from the fact that defects and cracks are decreased by the increase in density, whereby nucleation will become difficult. Recently, the author obtained experimental results indicating that there was almost no dependence of the high fracture toughness of high purity Y-TZP upon the grain size.[16] This fact contradicts the concept of the dependence of the transformation upon the grain size, supporting the argument that nucleation is essential for the transformation.

Chen *et al.* proposed a statistic discussion on the relation between nucleation and grain size, explaining that when the grain size is small the nucleation probability decreases.[15]

There are many studies on the aging of Y-TZP and its behavior in aqueous solutions.[17,18] There are reports that the degradation of Y-TZP is accelerated in such aqueous solutions as distilled water, sulfuric acid and caustic soda, as compared with aging in air. The degradation mechanism is considered as follows: a region where zirconia is destabilized is formed by the reaction of OH^- and H^+ in H_2O with Y_2O_3 or ZrO_2; with the region as starting point, the transformation from t to m crystal develops along grain boundaries; as a result, zirconia particles lose coherency with the matrix, causing the great decrease in strength.

The reason why Mg-PSZ is less degraded by low temperature aging than

Y-TZP is possibly that it is difficult for nucleation for the transformation to proceed because, in the case of Mg-PSZ, tetragonal grains are finely precipitated in the cubic matrix, and that since only a small number of tetragonal grains are present on grain boundaries, it is difficult for the transformation to take place along grain boundaries, thus stabilizing the tetragonal grains.

Many methods are proposed in order to avoid the deterioration of Y-TZP after aging.[19,20] Among them are an increase in Y_2O_3 content, small grain size and an increase in the density of the sintered material. Besides these methods, high purification of raw materials is effective for inhibiting the transformation. In particular, when oxides such as TiO_2, Fe_2O_3 and Al_2O_3 are present as impurities or additives, which do not form solid solutions with ZrO_2, strain and thermal stress develop, possibly because these oxides have thermal expansion coefficients and elastic constants different from the matrix. As a result, they will form a starting point at which the transformation occurs along grain boundaries.

On the other hand these oxides act as sintering aids, and hence different results will occur depending on their amount. This problem is an important subject to be studied in the future.

ACKNOWLEDGEMENT

The present author wishes to thank Dr Yukio Murata of the Research Center of Toray, and Taiji Nagata, Fujio Seki, Muneyoshi Nakamura and Yoshihiko Ueda of the technical development department of Toray, for their cooperation in the observation and analysis of the microstructure, the preparation of powders and sintering materials, and the measurement of the mechanical properties.

REFERENCES

1. Masaki, T. and Kobayashi, K., *Jap. Ceram. Soc. Meeting* (1981) 2, 3.
2. Tsukuma, K., Kubota, Y. and Tsukidate, T., in *Advances in Ceramics 12: Science and Technology of Zirconia II*, Eds N. Claussen, M. Rühle and A. H. Heuer, The American Ceramic Society, Columbus, Ohio, 1984, 382–90.
3. Masaki, T., *Jap. Ceram. Soc. Meeting* (1986) 665.
4. McMeeking, R. and Evans, A. G., *J. Am. Ceram. Soc.*, **65**(5) (1982) 242–5.
5. Kobayashi, K., Kuwajima, H. and Masaki, T., *Sol. State Ionics*, **3/4** (1981) 489–93.
6. Matsui, M., Soma, T. and Oda, I., in *Advances in Ceramics 12: Science and Technology of Zirconia II*, Eds N. Clausen, M. Rühle and A. H. Heuer, The American Ceramic Society, Columbus, Ohio, 1984, 371–81.

7. Watanabe, W., Iio, S. and Fukuura, I., ibid., 391–8.
8. Sato, T., Ohtani, S. and Shimada, M., *J. Mater. Sci.*, **20** (1985) 1466–70.
9. Sato, T. and Shimada, M., *J. Am. Ceram. Soc.*, **67**(10) (1984) C212–13.
10. Garvie, R. C. and Nicholson, P. S., *J. Am. Ceram. Soc.*, **55**(6) (1972) 303.
11. Haberko, K. and Pampuch, R., *Ceram. Int.*, **9**(1) (1983) 8–12.
12. Masaki, T., *Jap. Ceram. Soc. Meeting* (1985) 665.
13. Lange, F. F. and Green, D. J., *Advances in Ceramics 3*, Eds A. H. Heuer and L. W. Hobbs, The American Ceramic Society, Columbus, Ohio, 1981, 217–25.
14. Lange, F. F., *J. Mater. Sci.*, **17**(1) (1982) 225–34.
15. Chen, I. W. and Chiano, Y. H., *Acta Metall.*, **31** (1983) 1627–38.
16. Masaki, T., *J. Am. Ceram. Soc.* (1986) in press.
17. Nakajima, K., Kobayashi, K. and Murata, M., in *Advances in Ceramics 12: Science and Technology of Zirconia II*, Eds N. Claussen, M. Rühle and A. H. Heuer, The American Ceramic Society, Columbus, Ohio, 1984, 399–407.
18. Sato, T. and Shimada, M., *Jap. Ceram. Soc. Meeting* (1984) 461.
19. Masaki, T., *Jap. Ceram. Soc. Meeting* (1984) 455.
20. Tsukuma, T., Kubota, Y. and Nobugai, K., *Yogyo-Kyokai-Shi*, **92**(5) (1984) 233–41.

Received 2 October 1985; amended version received 2 January 1986 and accepted 9 January 1986

Int. J. High Technology Ceramics **2** (1986) 99–113

Phase Transformations and Grain Growth in Silicon Carbide Powders

P. A. Kistler-De Coppi and W. Richarz

Department of Chemical Engineering and Industrial Chemistry,
Swiss Federal Institute of Technology, CH-8092 Zurich, Switzerland

SUMMARY

The phase transformations, grain growth and habit changes occurring during annealing of different cubic silicon carbide powders have been studied in a semi-closed silicon carbide–carbon system. Variations in the process parameters—time, temperature, gas atmosphere and impurity content—have been investigated. It has been shown that the time parameter is an important factor that has to be taken into consideration when comparing the results of different experiments. Both the rate of transformation and of grain growth changed dramatically under different process conditions. The presence of certain impurities (aluminium, boron, nitrogen) was found to be the most important factor affecting the phase transformation and polytype distribution as well as the grain growth and resulting particle forms. These impurities stabilize certain modifications and enhance or slow down the grain growth in specific crystallographic directions. They also enhance or lower the rate of transformation. The rates of transformation and grain growth were found to be dependent on the dimension of the specific surface area of the powder. This shows that the rate-controlling step involves surface processes. The observed influences of the individual parameters on the phase transformation and grain growth have been found to act in a cumulative way when occurring simultaneously.

1. INTRODUCTION

Silicon carbide can be found in many different crystallographic modifications. These differ from each other only in their stacking order in the

Int. J. High Technology Ceramics 0267-3762/86/$03·50

[0001] direction. There are four most common silicon carbide polytypes. The only cubic polytype, 3C, is mainly obtained when silicon carbide is synthesized below 2000 °C, the 6H and 4H hexagonal and 15R rhombohedral modifications being usually produced above 2000 °C. Many investigations on polytype formation and transformation have been performed, but the relevant mechanisms are still not fully understood.

In a fairly recent and extensive review[1] of polytypic transformation in silicon carbide the results of many investigations were collected, discussed and compared. Jepps and Page[1] tried to establish a coherent view of the possible mechanics and kinetics of such transformations. Their most important conclusions can be briefly summarized as follows:

- A number of different transformation mechanisms can occur, often in parallel, and these account for the wide range of transformation kinetics observed. The results from single crystal experiments suggest a solid-state mechanism, whilst the transformation kinetics of powdered and compact specimens are more consistent with a vapour or a surface fast transport mechanism. However, it appears that this latter mechanism requires either a pre-existing nucleus of the new polytype to be present, or this nucleus to be formed by solid-state transformation.
- Most measured values for the activation energies of the transformation in powdered samples approximate to the sublimation energy. This is interpreted as indicating that the obtained activation energies are associated with the growth rather than the nucleation stage of transformation.
- The fast material transport responsible for the observed high transformation rates in polycrystalline specimens also results in grain growth and recrystallisation.
- The important role of impurities in the transformation was pointed out. These seem to influence behaviour at all levels: they can possibly stabilize particular structures; they can provide liquid films for rapid transport during transformation. Evidence is given that electronically p-type materials (e.g. boron and aluminium) stabilize layers in hexagonal environments, while n-type materials (e.g. nitrogen and phosphorus) tend to stabilize layers in cubic environments.
- A relatively large number of observations of transformations have been described, but only a few studies have tried to make any form of detailed analysis of reaction kinetics.

Despite the many known facts it is still not possible in the case of real systems to predict the properties of silicon carbide powders. The simultaneous effects of a variation of the process parameters, such as

temperature, time, gas atmosphere, impurity content and starting material, on the phase transformation, grain growth and sintering of the powder are not well known. Also the interactions of various influences (e.g. the influence of impurities on transformation kinetics) are almost unknown.

This investigation tries to obtain more data on the interactions of the various factors found to influence silicon carbide powders. It attempts to answer the question of whether from each β-silicon carbide powder a desired α-silicon carbide powder can be obtained simply by varying the process parameters, or whether the properties of the starting material determine the properties of the resulting powder.

2. EXPERIMENTAL

2.1. Starting materials

Five different manufactured types of β-silicon carbide powder were used as starting materials. Table 1 gives details of these materials and Table 2 summarizes the properties most important to this investigation. The powders differ either in their particle size or in their content of various impurities.

TABLE 1
Starting Materials

Trade name	*Manufacturer*	*Material code*
B 10	H. C. Starck, FRG	HB
A 10	H. C. Starck, FRG	HA
Betarundum ultrafine	Ibiden, Japan	BU
Betarundum standard	Ibiden, Japan	BS
'Experimental' powder	Philips, The Netherlands	PB
'Experimental' powder	Lonza, Switzerland	LB

2.2. Techniques

The experimental arrangement allowed rapid heating of a silicon carbide powder sample ($\simeq 20$ g) in a graphite crucible to the required annealing temperature. The crucible was closed with a lid, but was not gas tight. The crucible was heated with a high frequency generator. The time taken to heat the sample to 2000 °C was less than 3 min. The annealing temperature was varied between 1700 and 2400 °C and was measured with an optical

TABLE 2
Properties of the Starting Materials

Powder code	$S/m^2\,g^{-1}$	$r/\mu m$	*Impurity elements/wt%*				
			Al	*B*	*Fe*	*O*	*N*
HB (β)	14·2	0·7	0·15	0·01	0·02	0·4	0·01
BU (β)	18·7	0·29	0·03	nd	0·03	0·06	0·03
BS (β)	12·2	0·33	0·04	nd	0·03	na	na
PB (β)	0·006	1000	0·03	0·01	0·03	na	na
LB (β)	5·8	1·7	0·79	0·01	0·36	na	na
HA (α)	15·0	0·6	0·02	0·01	0·01	0·4	na

S = specific surface area.
r = mean particle size.
nd = not detected.
na = not analysed.

pyrometer. The time of annealing was varied between 0 and 240 min. After annealing the crucible was quickly removed from the heating zone to a fast-cooling zone. The static gas atmosphere could be argon, nitrogen or carbon monoxide up to 1 atm, or 'vacuum' (0·001 atm). The starting powders were partly doped with aluminium, aluminium oxide, boron, iron oxide, silicon dioxide, or carbon, or a mixture of these.

2.3. Analyses

After annealing, the polytype distribution was measured by X-ray diffraction (automatic diffractometer, Scintag/Seifert) and calculated according to the method of Ruska *et al.*[2] Scanning electron microscope (SEM) pictures of the powder were used to observe the grain growth and resulting habit change. The particle sizes were determined indirectly by calculation from measured values of the specific surface area. The specific surface area was measured by krypton adsorption and calculated with the help of the BET[3] equation.

Spectrochemical analysis (spark emission) was used to establish the impurity content of the powders.

3. RESULTS

A 'standard experiment' was performed initially to serve as a reference. The particle form, modification, rate of transformation and of grain growth,

resulting from the variation of various parameters in the subsequent experiments, have been compared with the properties of the powder obtained in the standard experiment.

Most of the experiments were performed with the powders BU and HB; the other powders were only available in smaller quantities and therefore were used only for special experiments (e.g. powder PB, with an extremely small specific surface area, was used in experiments for establishing the influence of the specific surface area on transformation).

3.1. Standard experiment

The standard experiment was performed with a minimum number of factors affecting the resulting product specifications. The factors related to the manufacturing conditions (e.g. 'history' of the sample) could not be eliminated. The related parameters will be discussed when comparing the behaviour of different β-silicon carbide powders with almost identical specifications.

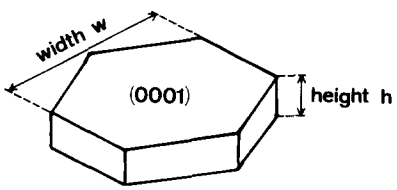

Fig. 1. Form of SiC-grains after annealing of powder BU, standard experiment.

Starting from very pure and fine-grained cubic silicon carbide (BU) the annealing was performed in an argon atmosphere which can be assumed inert. The powder showed the following behaviour (Fig. 1, Table 3):

- The transformation started at about 2000 °C and the resulting powder was predominantly of the 6H type.
- A large grain growth occurred during annealing. Big hexagonal platelets were formed; practically no sintering was observed.

3.2. The influence of the variation of time and temperature

The same powder (BU) as in the standard experiment was used for the following experiments. However, here the time of annealing was varied from 1 to 240 min and the temperature from 1700 to 2400 °C. Figure 2 shows the results for the transformation of 3C. The transformation at low temperature is very slow, so that in the investigated period of time the transformation did not proceed to completion.

TABLE 3
Example: Powder BU Before and After Annealing for 60 min at 2150°C

Treatment	*Polytype distribution*	$S/m^2\,g^{-1}$	$w/\mu m$	$h/\mu m$
—	100% 3C	18·7	0·05	0·05
60 min, 2150°C	90% 6H	0·05	75·0	15·0

S = specific surface area.
w = mean particle width (see Fig. 1).
h = mean particle height (see Fig. 1).

From the Arrhenius plot of the starting transition rates the activation energy of $590 \pm 125\,kJ\,mol^{-1}$ was determined. This value is comparable with values found in the literature.[1] It is also similar to the value for the heat of sublimation of silicon carbide.[1]

The predominantly formed polytype was of the 6H type. The total amount of 4H and 15R was always below 10%.

The higher the temperature the better developed the particles, but the particle size seems to reach a maximum value. Above a certain temperature (>2100°C) this maximum is independent of the annealing temperature. Below 2000°C practically no grain growth was observed. Figure 3 shows the time dependence of the specific surface area of the powder for two different annealing temperatures.

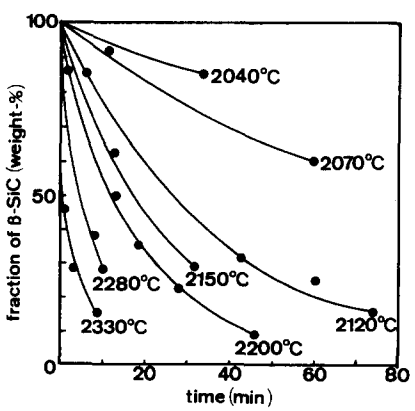

Fig. 2. Transformation of β-SiC at different annealing temperatures (powder BU, argon atmosphere).

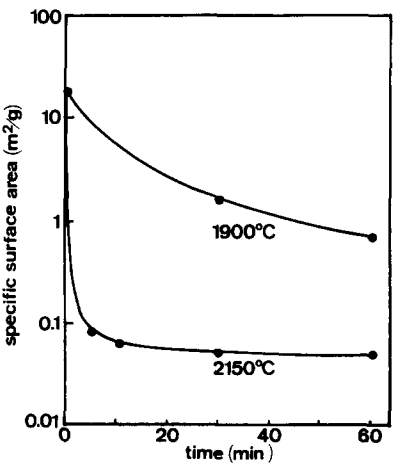

Fig. 3. Specific surface area of silicon carbide powder after annealing at different temperatures (powder BU, argon atmosphere).

These experiments illustrate very clearly that the time factor must be taken into consideration when comparing results which have not been obtained under the same conditions. Many existing contradictions in the literature can be traced to the neglect of the time factor (e.g. the time of annealing).

3.3. Influence of the specific surface area of the powder

The experiments were carried out with the very fine-grained powder BU, the very coarse-grained powder PB and with ground powder PB. The powders PB and BU have very similar specifications except that the particle size is totally different. It could be shown that the rate of transformation was proportional to the dimension of the specific surface area of the powder under otherwise similar conditions (Fig. 4).

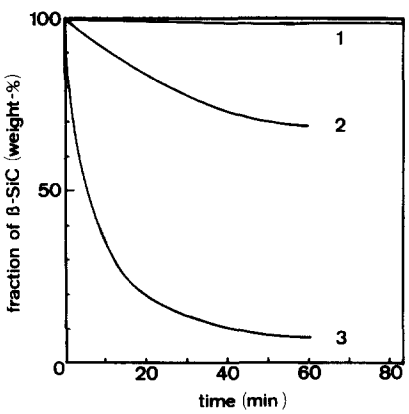

Fig. 4. Transformation of β-silicon carbide powders with different specific surface areas (argon atmosphere, 2200 °C). 1, powder PB, specific surface area = 0·006 $m^2 g^{-1}$; 2, powder PB (ground), specific surface area = 0·8 $m^2 g^{-1}$; 3, powder BU, specific surface area = 18·7 $m^2 g^{-1}$.

A graphical determination of the starting rate of transformation (slope of the transformation curve at the beginning) revealed that the rates are proportional to the starting specific surface areas of the employed powders. Due to the fact that in these experiments the specific surface areas are known exactly only at the start of the experiment, only the initial rates of transformation are compared. The specific surface areas at different stages of reaction could not be determined separately for the different polytypes. Only the overall values could be measured.

Powder annealed at a certain temperature where the transformation proceeded very slowly, due to the small specific surface area available, was

ground and annealed again. The further transformation then occurred much faster than before. These results can be interpreted as showing that the transformation is controlled by surface mechanisms; it is certainly not only an *in situ* rearrangement of the crystal layers.

3.4. Influence of the impurity content of the powder

We next consider if the results found for the powder BU are also valid for the other starting materials consisting of β-silicon carbide. The experiments performed with the powder BU were repeated with the powder HB. Large differences in the resulting properties of the powders have been found (Table 4).

The question arose as to what causes these differences and would it be possible to obtain the same powder after annealing simply by changing the process conditions. The greatest difference between the two powders was in their aluminium content. Therefore, the next experiments were performed with powder BU doped with different amounts of aluminium. With a certain aluminium addition, powder BU could be induced to behave like powder HB with only minor remaining differences. These could be due to a different defect content of the two powders, which was not measured during this investigation.

Other impurity additions were also checked for their influence on the resulting powders. The influence of the following additions were studied: aluminium oxide, aluminium, boron, ferric oxide, silicon dioxide and carbon. Furthermore the transformation was carried out under a nitrogen or carbon monoxide atmosphere, both of which can also be regarded as impurities. Each addition was not restricted to one impurity at a time. The additions were varied between 0 and 2 wt %. It was found that not all of the impurities had the same effects on the behaviour of the powder. Some, such

TABLE 4
Comparison of the Behaviour of Powders BU and HB During Annealing

Powder code	*T*/°C	*Polytype distribution*	*w*/μm	*h*/μm	*S*/m² g⁻¹
BU	2000	90% 6H	75·0	15·0	0·05
HB	1800	20% 4H, 70% 6H	40·0	10·0	0·1

T = starting temperature of transformation.
w = mean particle width (see Fig. 1).
h = mean particle height (see Fig. 1).
S = specific surface area after annealing at 2200 °C.

as aluminium, aluminium oxide, boron and nitrogen, had a very strong influence, others had practically none at all. Oxygen, which is the major impurity in most starting powders, could not be investigated properly, due to the reducing power of the graphite in the annealing environment. No traces of oxygen in the powder could be detected, even after short annealing times.

The impurities which affected the resulting silicon carbide powder most strongly were those which form similar compounds and can presumably be incorporated more easily into the silicon carbide lattice. The effects of the impurities are described below in greater detail.

3.4.1. The rate of transformation

Figure 5 shows the transformation with and without addition of aluminium and aluminium oxide to the powders BU and HB, where the aluminium content of powder HB is higher due to the manufacturing process. It has been found that aluminium enhanced the rate of transformation independently of whether a powder had a relatively high aluminium content or a pure powder was doped with aluminium. Even very small amounts (0·05 wt %) had a significant influence. The rates of formation of both hexagonal polytypes, 4H and 6H, were promoted. No differences in the behaviour of powders doped with aluminium or aluminium oxide were found, only the total amount of aluminium was important.

The addition of boron also had a similar influence, but only the rate of formation of 6H was enhanced, although 4H was the more stable polytype.

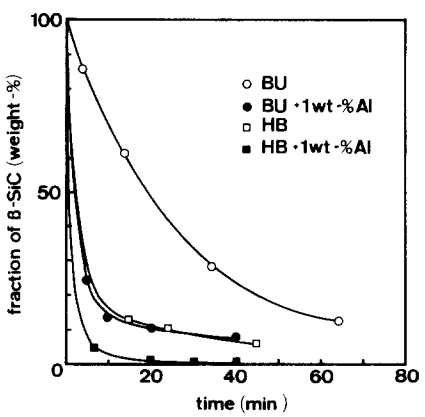

Fig. 5. Influence of the addition of aluminium (in the form of aluminium or aluminium oxide) on the transformation of powders BU and HB (argon atmosphere, 2150 °C).

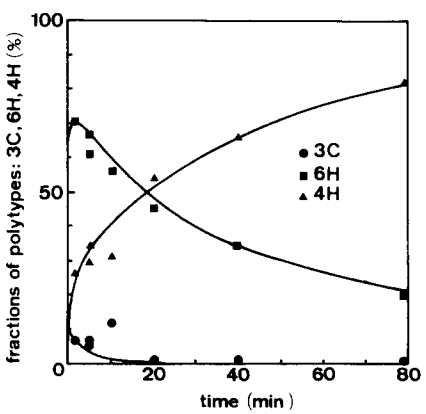

Fig. 6. Amount of different polytypes after annealing of powder BU doped with 2 wt % boron (argon atmosphere, 2150 °C).

Polytype 6H was formed only as an intermediate; after longer annealing times the predominant polytype was 4H. Fig. 6 shows the results.

Annealing the powder in a nitrogen atmosphere enabled comparison of the results with other investigations. It could be clearly demonstrated that nitrogen will retard the transition as shown by Kieffer *et al.*[4]

3.4.2. The polytype distribution at 'equilibrium'

Only the very fine-grained powders, which showed a large transformation rate, reached 'equilibrium states' (that is when no further changes occurred) in polytype distribution. Even if these powders were cooled, ground and annealed again, the polytype distribution did not change any more. Figure 7 shows the polytype distribution for different amounts of impurities of (a) aluminium and (b) boron.

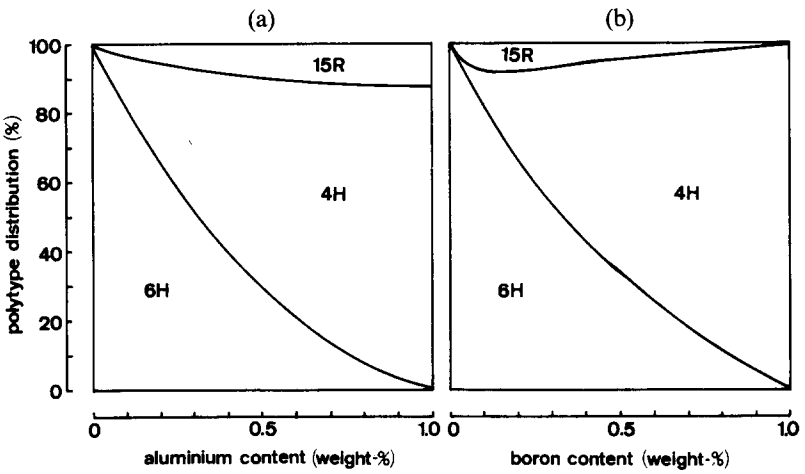

Fig. 7. Polytype distribution after annealing for typically 6 h (equilibrium state) for SiC powders BU, HB, PB, LB, BS and HA doped with different amounts of (a) aluminium and (b) boron.

Almost pure cubic silicon carbide powder (BU), which was transformed to practically pure 6H, can be ground and doped with aluminium and annealed again. The 6H powder is then transformed to 4H, the extent being dependent on the aluminium addition. This shows that some impurities stabilize certain modifications and that the effects of the impurities are not restricted to a kinetical influence only.

In order to distinguish between built-in and superficial impurities, the impurity content of the powder was measured twice after annealing. First without pretreatment and then again after washing the sample and removing superficial impurities (Tables 5 and 6). It was found that practically the

TABLE 5
Boron Content after Different Annealing Conditions of Powders BU and HB Doped with Boron

Boron addition/wt%	*T/°C*	*t/min*	*Boron content/wt%*	
			(1)	*(2)*
1·25	2150	20	0·33	0·13
1·25	2150	20	0·37	0·16
2·0	2150	80	0·62	na
2·0	2000	80	1·00	na

T = temperature of annealing.
t = time of annealing.
(1) = without pretreatment.
(2) = after pretreating with HF/H_2SO_4, $KHSO_4$-melt and HCl.
na = not analysed.

whole amount of aluminium was built into the powder (2 wt% maximum). Boron, on the other hand, could only be incorporated to a much smaller extent (0·5 wt%). The higher the annealing temperature the smaller the impurity content found after the treatment, with the same amount of impurities added before the annealing. A very long annealing time also causes a decrease in impurity content with the chosen experimental set-up.

3.4.3. The particle form

The impurity content was found to have a large influence on the grain

TABLE 6
Aluminium Content after Different Annealing Conditions of Powders BU and HB Doped with Aluminium

Aluminium addition/wt%	*T/°C*	*t/min*	*Aluminium content/wt%*	
			(1)	*(2)*
1·25	2150	40	0·46	0·41
1·25	2150	40	0·47	0·44
1·25	2150	10	0·61	na
1·25	2300	10	0·07	na

T = temperature of annealing.
t = time of annealing.
(1) = without pretreatment.
(2) = after pretreating with HF/H_2SO_4, $KHSO_4$-melt and HCl.
na = not analysed.

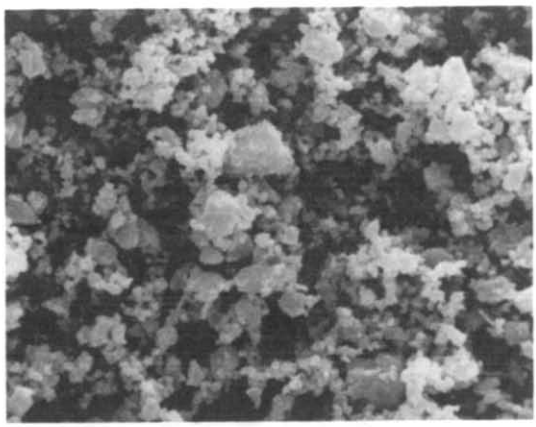

(a)

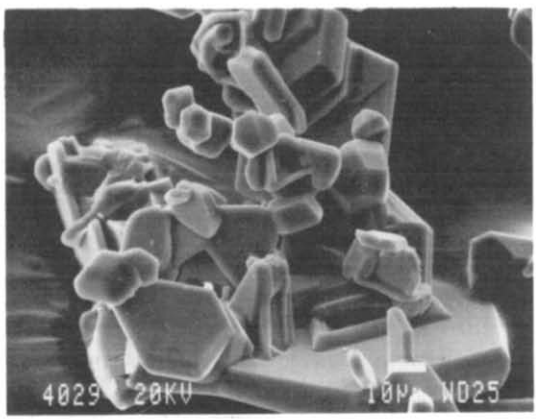

(b)

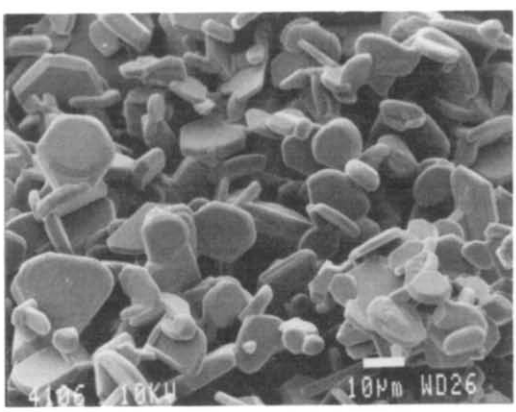

(c)

Fig. 8. (a) BU before annealing, 100 % 3C (magnification × 3000); (b) BU after annealing (31 min, 2150 °C, Ar), 52 % 6H, 29 % 3C (magnification × 530); (c) BU + 4 wt % Al after annealing (60 min, 2000 °C, Ar), 77 % 4H (magnification × 600).

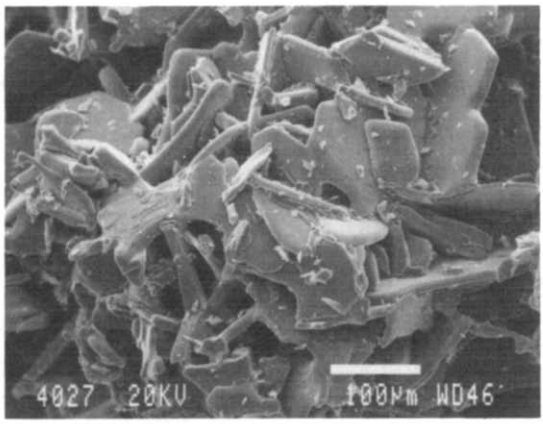

(d)

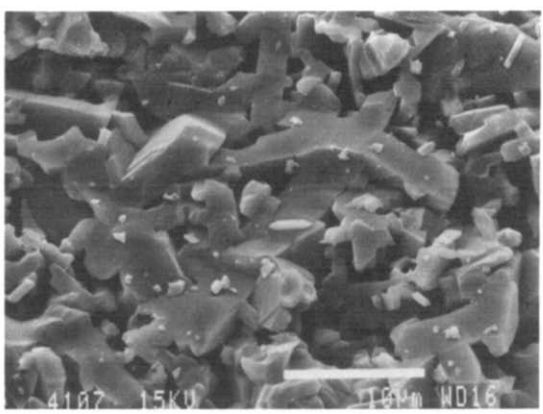

(e)

Fig. 8—*contd.* (d) BU + 2 wt % B after annealing (40 min, 2150 °C, Ar), 34 % 6H, 44 % 4H (magnification × 125); (e) HB + 1 wt % Al + 1 wt % B after annealing (60 min, 2000 °C, Ar), 72 % 4H (magnification × 2000).

growth. SEM-pictures (Fig. 8) show the results. Figure 8(a) represents powder BU before annealing; powder HB has a similar appearance. Figure 8(b) shows the powder BU after annealing for 31 min at 2150 °C in an argon atmosphere. The hexagonal platelets can be seen, as shown diagrammatically in Fig. 1 for the standard experiment. No small particles as in the starting material can be recognized, although 30 % of the powder is still β-silicon carbide. This figure shows that β-silicon carbide particles also have grown under these process conditions.

In contrast to the behaviour of powder BU, there were particles in the powder HB which did not change their habit at all. The whole of powder HB

showed a reduced grain growth. As already mentioned powder HB has a higher aluminium content than powder BU. Figure 8(c) shows powder BU doped with aluminium. Aluminium enhances the growth in the [0001] direction and slows down the growth perpendicular to the [0001] direction; very regular particles of smaller size are formed than in the standard experiment. However, it was not possible to simulate exactly the behaviour of powder HB; small differences remained. In the doped powder BU particles with the size of the starting material were not found; all the grains exhibited grain growth. It seems that only the aluminium incorporated in the grains influences the growth rates. At the beginning of the annealing of the doped powder the aluminium is only superficially distributed. Powder HB with an already higher aluminium content has the aluminium at least partially incorporated in the grains. However, at 'equilibrium' both powders looked the same.

Boron enhances the growth perpendicular to the [0001] direction. Large thin platelets are formed with fairly rounded edges (Fig. 8(d)). The edges appear to be molten. Both aluminium and boron enhance the sintering of the powder, but the strongest sintering was observed with the addition of aluminium and boron simultaneously, as can be seen in Fig. 8(e). In this case practically no single particles can be seen.

4. DISCUSSION

The described experiments show that the factors affecting grain growth, habit changes and transformation are manifold and strongly related to each other. The properties of the resulting powder are influenced by the time and temperature of annealing, and by the rate of heating and cooling, but the most important factor was found to be the impurity content of the powder.

The results obtained in this work confirm many of the conclusions drawn in the review of Jepps and Page.[1] In accordance with their assertions, it was also found that the content of special impurities in the powder is decisive for the formation of certain polytypes. It seems reasonable to assume that pure cubic silicon carbide transforms to the pure 6H polytype in the absence of impurities. All other polytypes are stabilized by different impurities. Furthermore, this work clearly demonstrates that the impurities also influence the rates of transformation and the grain growth. Also the particle form and size and the polytype are strongly influenced by the impurities. In addition the 'history' of the sample affects the behaviour of the resulting powder essentially through the impurity content.

Another important result was that the specific surface area was found to be one of the parameters which control the rates of transformation. The rate

of transformation is proportional to the specific surface area of the powder, under otherwise identical conditions. This is further evidence that the transformation not only proceeds by an *in situ* rearrangement of the layers but also involves surface diffusion mechanisms.

The grain growth starts above 1900 °C; to a great extent, only nucleation is dominant below this temperature. Since for grain growth a certain vapour pressure is needed, this presumably indicates that the vapour phase is involved in the grain growth mechanisms. The starting temperature of grain growth can be shifted by impurities. In contrast to other studies a large grain growth of untransformed powder was also observed under conditions where, in spite of high annealing temperatures, no, or only slow, transformations of β-silicon carbide was observed (e.g. in a nitrogen atmosphere). No relationship between certain polytypes and particle forms was observed.

REFERENCES

1. Jepps, N. W. and Page, T. F., Polytypic transformations in silicon carbide, *J. Cryst. Growth Characterisation*, **7** (1983) 259–307.
2. Ruska, J., Gauckler, L. J., Lorenz, J. and Rexer, H. U., The quantitative calculation of SiC polytypes from measurements of X-ray diffraction peak intensities, *J. Mat. Sci.*, **14** (1979) 2013–17.
3. Brunnauer, S., Emmett, P. H. and Teller, E., Adsorption of gases in multimolecular layers, *J. Am. Chem. Soc.*, **60** (1938) 309–19.
4. Kieffer, R., Gugel, E., Ettmayer, P. and Schmidt, A., Beitrag zur Frage der Phasenstabilität von Siliziumkarbid, *Ber. Deut. Keram. Ges.*, **43** (1966) 621–3.

Received 29 October 1985; amended version received and accepted 6 January 1986

Int. J. High Technology Ceramics **2** (1986) 115–121

Phase Equilibrium Studies in Si_2N_2O-containing Systems: II. Phase Relations in the Si_2N_2O–Al_2O_3–La_2O_3 and Si_2N_2O–Al_2O_3–CaO Systems

G. Z. Cao, Z. K. Huang, X. R. Fu and D. S. Yan (T. S. Yen)

Shanghai Institute of Ceramics, Academia Sinica, Shanghai,
People's Republic of China

SUMMARY

Sub-solidus phase relations have been studied in the Si_2N_2O–Al_2O_3–La_2O_3 and Si_2N_2O–Al_2O_3–CaO systems. The results show that no new compound is found in the Si_2N_2O–Al_2O_3–La_2O_3 system, but there exists a new compound $CaO \cdot Si_2N_2O$ and a continuous cubic solid solution between $3CaO \cdot Si_2N_2O$ and $3CaO \cdot Al_2O_3$ in the Si_2N_2O–Al_2O_3–CaO system. In the Si_2N_2O-rich area of these two systems the excess Si_2N_2O reacts with La_2O_3 and CaO to form Si_3N_4, and either $La_{10}(SiO_4)_6N_2$(H-phase) or $CaSiO_3$, respectively. Several quaternary compatibility regions occur in the Si_2N_2O–Al_2O_3–La_2O_3 system:

$$H\text{–}Si_3N_4\text{–}La_2O_3 \cdot Si_2N_2O\text{–}La_2O_3 \cdot Al_2O_3$$
$$H\text{–}Si_3N_4\text{–}La_2O_3 \cdot Al_2O_3\text{–}La_2O_3 \cdot 11Al_2O_3$$
$$H\text{–}Si_3N_4\text{–}La_2O_3 \cdot 11Al_2O_3\text{–}Al_2O_3$$
$$H\text{–}Si_3N_4\text{–}Al_2O_3\text{–}O'ss$$
$$H\text{–}Si_3N_4\text{–}O'ss\text{–}Si_2N_2O$$

and in the Si_2N_2O–Al_2O_3–CaO system:

$$Si_3N_4\text{–}CaSiO_3\text{–}CaO \cdot Si_2N_2O\text{–}3CaO \cdot Al_2O_3$$
$$Si_3N_4\text{–}CaSiO_3\text{–}3CaO \cdot Al_2O_3\text{–}2CaO \cdot Al_2O_3 \cdot SiO_2$$
$$Si_3N_4\text{–}CaSiO_3\text{–}2CaO \cdot Al_2O_3 \cdot SiO_2\text{–}Al_2O_3$$
$$Si_3N_4\text{–}CaSiO_3\text{–}Al_2O_3\text{–}O'ss$$
$$Si_3N_4\text{–}CaSiO_3\text{–}O'ss\text{–}Si_2N_2O$$

From the results of this work, the sub-solidus phase diagrams of the Si_2N_2O–Al_2O_3–La_2O_3 and Si_2N_2O–Al_2O_3–CaO systems are presented.

Int. J. High Technology Ceramics 0267-3762/86/$03·50

1. INTRODUCTION

In our previous paper[1] the phase relations in the Si_2N_2O–Al_2O_3–Y_2O_3 system were presented. In order to understand the function of rare-earth oxides, lanthanum oxide has been chosen as a component for studying this series of systems. The phase relations in the Si_2N_2O–Al_2O_3–La_2O_3 system may be useful for the investigation of other rare-earth oxide systems and will be beneficial to the utilization of rare-earth oxides as densification aids in high technology ceramics.

As is well known, calcium, as one of the impurities usually occurring in the starting powders of silicon nitride and the sintering aids, is a harmful element which degrades the strength of silicon nitride-based ceramics at high temperatures. The study of the phase equilibrium of CaO-containing systems is beneficial for understanding the behaviour of calcium in advanced ceramics.

Phase relationships previously reported in the Al_2O_3–La_2O_3 system[2] show two stable compounds, $La_2O_3 \cdot Al_2O_3$ and $La_2O_3 \cdot 11Al_2O_3$. In the Si_2N_2O–La_2O_3 system[3,4] there are also two compounds, $2La_2O_3 \cdot Si_2N_2O$ (J-phase) and $La_2O_3 \cdot Si_2N_2O$ (K-phase), paralleling those found in the yttrium oxide-containing system.

In the Al_2O_3–CaO system compounds with the compositions Al_2O_3:CaO = 6:1, 2:1, 1:1, 7:12, 1:3 are well known,[5] and $3CaO \cdot Si_2N_2O$ has been found[6] with the same cubic structure as $3CaO \cdot Al_2O_3$ in the Al_2O_3–CaO system.

The limiting solubility of Al_2O_3 in Si_2N_2O ss in the Si_2N_2O–Al_2O_3 system has been reported to be 15 m/o Al_2O_3.[1]

2. EXPERIMENTAL

The starting materials used were lanthanum oxide, a reagent with 99·9% purity (Shanghai Yuolong Chemical Works), and calcium oxide, obtained by calcining calcium carbonate (99·99% purity) at 1100°C for 2 h. The details of the other starting materials used and all the experimental procedures have been described in the previous paper.[1]

3. RESULTS AND DISCUSSION

3.1. The Si_2N_2O–Al_2O_3–La_2O_3 system

In this system no new phase is found, except the two compounds reported earlier, $2La_2O_3 \cdot Si_2N_2O$ (J-phase) and $La_2O_3 \cdot Si_2N_2O$ (K-phase), with the

same structures as $2Y_2O_3 \cdot Si_2N_2O$ (J-phase) and $Y_2O_3 \cdot Si_2N_2O$ (K-phase), respectively. In the Si_2N_2O-rich side, however, Si_2N_2O reacts with La_2O_3 to form Si_3N_4 and $La_{10}(SiO_4)_6N_2$(H-phase), as in the Si_2N_2O–Al_2O_3–Y_2O_3 system,[1] by the following reactions:

$$10Si_2N_2O + 6La_2O_3 \rightarrow La_{10}(SiO_4)_6N_2 + 4Si_3N_4 + La_2O_3 \cdot Si_2N_2O$$
$$9Si_2N_2O + 5La_2O_3 \rightarrow La_{10}(SiO_4)_6N_2 + 4Si_3N_4$$

These reactions are also extended into the ternary system Si_2N_2O–Al_2O_3–La_2O_3. Therefore, several quaternary compatibility areas are formed as follows:

$$H\text{–}Si_3N_4\text{–}La_2O_3 \cdot Si_2N_2O\text{–}La_2O_3 \cdot Al_2O_3$$
$$H\text{–}Si_3N_4\text{–}La_2O_3 \cdot Al_2O_3\text{–}La_2O_3 \cdot 11Al_2O_3$$
$$H\text{–}Si_3N_4\text{–}La_2O_3 \cdot 11Al_2O_3\text{–}Al_2O_3$$
$$H\text{–}Si_3N_4\text{–}Al_2O_3\text{–}O'ss$$
$$H\text{–}Si_3N_4\text{–}O'ss\text{–}Si_2N_2O$$

On the basis of the experimental results the sub-solidus phase diagrams of the Si_2N_2O–Al_2O_3–La_2O_3 system are as shown in Figs 1 and 2.

The results of this work show the phase diagram of the

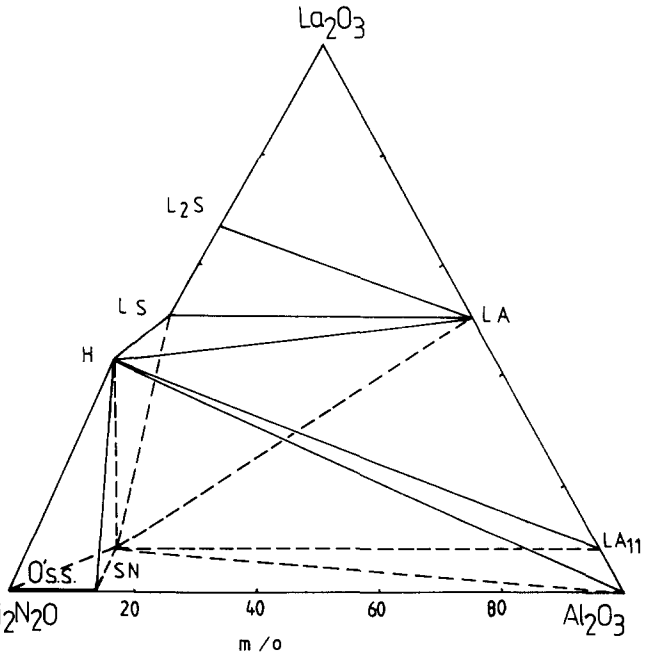

Fig. 1. Sub-solidus diagram of the Si_2N_2O–Al_2O_3–La_2O_3 system. $L_2S = 2La_2O_3 \cdot Si_2N_2O$; $LS = La_2O_3 \cdot Si_2N_2O$; $LA = La_2O_3 \cdot Al_2O_3$; $H = La_{10}(SiO_4)_6N_2$.

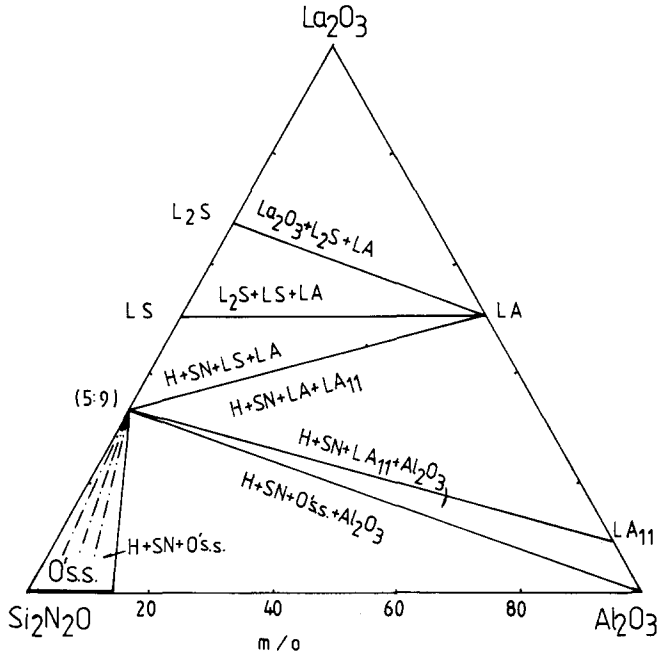

Fig. 2. Sub-solidus diagram of the Si_2N_2O–Al_2O_3–La_2O_3 system. 5:9 ($5La_2O_3 \cdot 9Si_2N_2O = 4Si_3N_4 + La_{10}(SiO_4)_6N_2$).

Si_3N_4–SiO_2–La_2O_3 system to be slightly different from that obtained by Mitomo *et al.*[4]

3.2. The Si_2N_2O–Al_2O_3–CaO system

One new stable compound, $CaO \cdot Si_2N_2O$, was found in this system. Its X-ray data without indexing are shown in Table 1. A continuous cubic solid solution between $3CaO \cdot Si_2N_2O$ and $3CaO \cdot Al_2O_3$ was observed. At the Si_2N_2O-rich end, however, Si_2N_2O also reacts with CaO to form Si_3N_4 and $CaSiO_3$ (which melts at 1415 °C) through the following reactions:

$$2CaO + 3Si_2N_2O \rightarrow Si_3N_4 + CaSiO_3 + CaO \cdot Si_2N_2O$$
$$CaO + 2Si_2N_2O \rightarrow Si_3N_4 + CaSiO_3$$

Such decomposition reactions of excess Si_2N_2O are also liable to occur with the additive Al_2O_3 in the ternary system Si_2N_2O–Al_2O_3–CaO. Therefore, several quaternary compatibility areas are formed as follows:

Si_3N_4–$CaSiO_3$–$CaO \cdot Si_2N_2O$–$3CaO \cdot Al_2O_3$
Si_3N_4–$CaSiO_3$–$3CaO \cdot Al_2O_3$–$2CaO \cdot Al_2O_3 \cdot SiO_2$
Si_3N_4–$CaSiO_3$–$2CaO \cdot Al_2O_3 \cdot SiO_2$–$Al_2O_3$
Si_3N_4–$CaSiO_3$–Al_2O_3–O'ss
Si_3N_4–$CaSiO_3$–O'ss–Si_2N_2O

TABLE 1
X-ray Data for $CaO \cdot Si_2N_2O$

d (obs)/Å	I/I_0	*d (obs)/Å*	I/I_0
4·720	vw	2·145	vvw
4·102	w	2·111	vvw
4·096	vw	2·099	vvw
3·405	ms	2·070	vvw
3·327	ms	2·026	vvw
3·250	vw	1·945	vw
3·176	w	1·907	w
3·089	w	1·881	vw
2·998	m	1·831	vw
2·922	m	1·790	vw
2·882	w	1·734	vw
2·810	w	1·705	vw
2·743	vw	1·675	vw
2·660	s	1·639	w
2·548	ms	1·600	vvw
2·515	m	1·556	m
2·411	w	1·540	vvw
2·350	vs	1·509	vw
2·293	w	1·502	vw
2·249	w	1·476	vvw
2·217	vw	1·447	vw
2·186	vvw		

Key. Notation for I/I_0: w, weak; vw, very weak; vvw, very very weak; m, medium; ms, medium strong; s, strong.

On the basis of the experimental results, the sub-solidus phase diagrams of the Si_2N_2O–Al_2O_3–CaO system investigated are as shown in Figs 3 and 4.

In addition, compositions within the region Al_2O_3–$3CaO \cdot Al_2O_3$–$2Si_2N_2O \cdot CaO$ (Fig. 4) always form the compound $2CaO \cdot Al_2O_3 \cdot SiO_2$ with some nitrogen-containing glass above 1250 °C. Below this temperature the solid-state reaction could not occur and equilibrium could not be reached. Therefore, the phase behaviour in such a region is represented by dashed lines starting from $2CaO \cdot Al_2O_3 \cdot SiO_2$. In the Si_2N_2O-containing systems investigated excess Si_2N_2O decomposes easily and reacts with Y_2O_3, La_2O_3 or CaO to form Si_3N_4 and either H-phase or $CaSiO_3$. According to the following reaction[7,8] in a nitrogen atmosphere at high temperature:

$$4Si_2N_2O \rightarrow Si_3N_4(s) + 4SiO(g) + Si(l,g) + 2N_2(g)$$

the phenomenon of such reactions of excess Si_2N_2O with Y_2O_3, La_2O_3 and CaO is easy to understand.

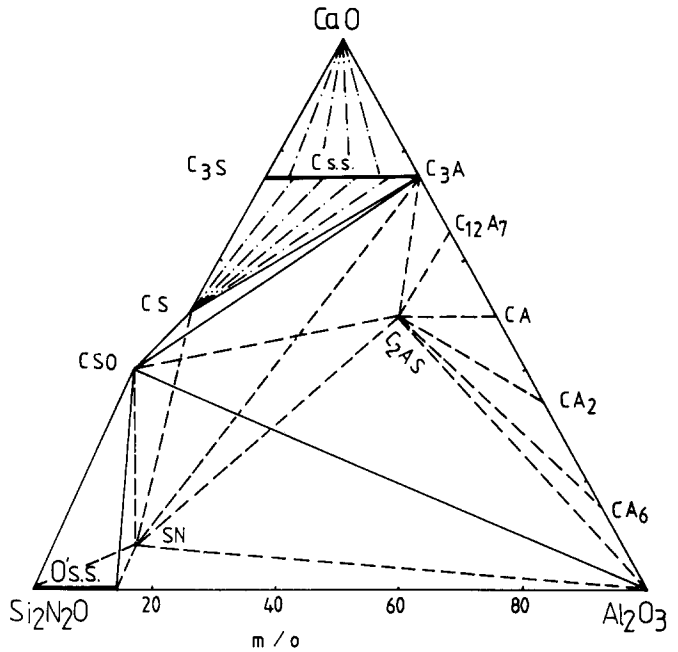

Fig. 3. Sub-solidus diagram of the Si_2N_2O–Al_2O_3–CaO system. $C_3S = 3CaO \cdot Si_2N_2O$; $CS = CaO \cdot Si_2N_2O$; $CSO = CaSiO_3$; $C_2AS = 2CaO \cdot Al_2O_3 \cdot SiO_2$; $CA_6 = CaO \cdot 6Al_2O_3$; $C_3A = 3CaO \cdot Al_2O_3$; $C_{12}A_7 = 12CaO \cdot 7Al_2O_3$; $CA = CaO \cdot Al_2O_3$; $CA_2 = CaO \cdot 2Al_2O_3$.

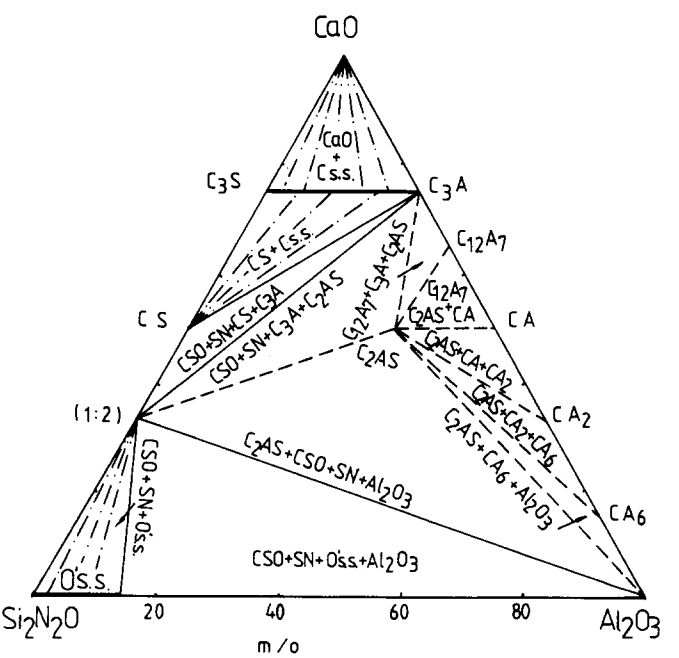

Fig. 4. Sub-solidus diagram of the Si_2N_2O–Al_2O_3–CaO system. 1:2, $CaSiO_3 + Si_3N_4$.

CONCLUSIONS

1. The sub-solidus phase diagrams of the Si_2N_2O–Al_2O_3–La_2O_3 and Si_2N_2O–Al_2O_3–CaO systems are presented. In the former system no new compound is found; in the latter system a new compound $CaO \cdot Si_2N_2O$ and a continuous cubic solid solution between $3CaO \cdot Si_2N_2O$ and $3CaO \cdot Al_2O_3$ are formed.
2. In the Si_2N_2O-rich area of these two systems the excess Si_2N_2O reacts with La_2O_3 and CaO to form Si_3N_4 and either $La_{10}(SiO_4)_6N_2$ (H-phase) or $CaSiO_3$, respectively, in a nitrogen atmosphere at high temperatures, and several quaternary compatibility regions are formed.

REFERENCES

1. Cao, G. Z., Huang, Z. K., Fu, X. R. and Yan, D. S., *Int. J. High Technology Ceramics*, **1**(2) (1985) 119–27.
2. Levin, E. M., Robbins, C. R. and McMurdia, H. F., *Phase Diagrams for Ceramists*, 1969, American Ceramic Society, Columbus, Ohio, 1969, Fig. 2340.
3. Wills, R. R., Stewart, R. W., Cunningham, J. A. and Wimmer, J. M., *J. Mat. Sci.*, **11** (1976) 749–59.
4. Mitomo, M., Izumi, F., Horiuchi, S. and Matsui, Y., *J. Mat. Sci.*, **17** (1982) 2359–64.
5. Roth, R. S., Negas, T. and Cook, L. P., *Phase Diagrams for Ceramists*, 1981, American Ceramic Society, Columbus, Ohio, 1981, Fig. 5141.
6. Huang, Z. K., Sun, W. Y. and Yan, D. S., *J. Mat. Sci. (Letters)*, **4** (1985) 255–9.
7. Huang, Z. K., Greil, P. and Petzow, G., *Ceramics International*, **10**(1) (1984) 14–17.
8. Zabruskova, T. N. and Guzman, I. Y., *Ogneupory*, **2** (1972) 52.

Received 3 December 1985; accepted 5 February 1986.

Int. J. High Technology Ceramics **2** (1986) 123–134

Synthesis of Mullite Powder and its Characteristics

M. G. M. U. Ismail, Zenjiro Nakai, Keiichi Minegishi

Research and Development Division, Chichibu Cement Co. Ltd,
Tsukimicho 2-1-1, Kumagaya, Saitama 360, Japan

and Shigeyuki Sōmiya

Research Laboratory of Engineering Materials, Tokyo Institute of Technology,
4259 Nagatsuda, Midori-ku, Yokohama 227, Japan

SUMMARY

Mullite of stoichiometric composition $3Al_2O_3 \cdot 2SiO_2$ was synthesised using γ-aluminium oxide and colloidal silicon dioxide. γ-Aluminium oxide was hydrolysed at 90°C and peptised using concentrated nitric acid at 95°C under refluxing conditions for 3 h. The boehmite sol formed was cloudy. Colloidal silicon dioxide was dispersed in acidified water using a mechanical blender and gelled by evaporation of excess water. On calcination of the gel at temperatures above 1300°C for 1 h mullite was formed. The mullite synthesised can be sintered in 3 h at 1650°C to 98·1% of its theoretical density, and shows high flexural strength of 385 MPa (determined in three-point bend) at room temperature.

1. INTRODUCTION

There are good summary papers by Davis and Pask[1] and Rodrigo and Boch,[2] and a book edited by Sōmiya.[3]

The high temperature strength and creep resistance[4,5] make mullite ($3Al_2O_3 \cdot 2SiO_2$) a suitable material for use in structural ceramic applications. The usual method of synthesising mullite is the thermal treatment of mixed oxides. The product formed contains excess silicon dioxide or aluminium oxide as a second phase.

Mazdiyasni and Brown[6] reported the synthesis of mullite by hydrolytic decomposition of mixed metal alkoxides, which when hot-pressed at 1500°C

Int. J. High Technology Ceramics 0267-3762/86/$03·50

gave a fully dense ceramic with mixed interlocking needle-like, and polygonal, grains. The average flexural strength at room temperature was 128 MPa which increased to 140 MPa at 1400 °C. Ghate *et al.*[7] prepared mullite by using γ-aluminium oxide and amorphous silicon dioxide as base materials. The gel technique was used for mixing and mullite formed only when treated at 1420 °C for 20 h. The particle morphology of the mullite formed was globular. Metcalfe and Sant[8] synthesised mullite by consecutive precipitation of the hydrolysed product of tetramethyl silicate in the presence of aluminium hydroxide. The flexural strength of the sintered body was in the region of 150 MPa. Mullite has also been synthesised under hydrothermal conditions by Roy,[9,10] Sōmiya *et al.*[11] and Suzuki *et al.*[12] In this process, the mixed silicon and aluminium alkoxides or sols were treated under 50 MPa at 300–400 °C for 2 h, and the product formed calcined at 1300 °C for 1 h to yield mullite. Later Yamaguchi *et al.*[13] reported that direct hydrothermal treatment of the powder prepared by hydrolysis of mixed alkoxides at 600 °C under 20 MPa for durations longer than 2 h led to the formation of mullite. Kanzaki *et al.*[14,15] synthesised mullite possessing high flexural strength (360–450 MPa) by spray pyrolysis of mixed aluminium nitrate and ethyl silicate solutions. The flexural strengths of the sintered mullites synthesised using the processes described in Refs 6–8 and 11–13 were less than 200 MPa. The low strength may be the result of the formation of glassy phases and/or secondary phases.

Most of the methods described above are essentially small-scale methods and seem unsuitable for extensive upscaling because of the high cost of the starting materials (e.g. aluminium and silicon alkoxides) and the difficulties encountered when handling large quantities of gelatinous materials and in the removal of the unwanted by-products. In the present investigation a different approach has been used. γ-Aluminium oxide, which was used as the source of aluminium oxide, was first hydrolysed and peptised to give a clear boehmite sol. Mixing this sol with silicon dioxide sol resulted in a homogeneous mullite sol, which on gelation, followed by calcination, resulted in stoichiometric mullite. The sintered mullite appeared to contain no grain boundary glass.

2. EXPERIMENTAL PROCEDURE

2.1. Starting materials

γ-Aluminium oxide (UA-5605, Shōwa Keikinzoku Co. Ltd, Japan) was used as the source of aluminium oxide. Colloidal silicon dioxide (Nipsil E220A, Nihon Silica Kogyo Co. Ltd, Japan) was the source of silicon dioxide. The

specific surface areas (BET) of the γ-aluminium oxide and the colloidal silicon dioxide were 68 $m^2 g^{-1}$ and 130 $m^2 g^{-1}$, respectively. The impurities present in γ-aluminium oxide were Na (16 ppm), K (5 ppm) and Si (12 ppm). The chemical composition of the colloidal silicon dioxide used was SiO_2 (95·3 %), Al_2O_3 (0·55 %), Na_2O (0·30 %), Fe_2O_3 (0·09 %), TiO_2 (0·09 %) and CaO (0·05 %); loss on ignition, 3·8 %.

2.2. Preparation of boehmite and silicon dioxide sols

Hydrolysis of γ-aluminium oxide was carried out at temperatures above 90 °C under vigorous agitation to form γ-alumina hydrate (γ-$Al_2O_3 \cdot H_2O$), which was peptised using concentrated nitric acid, maintaining a γ-aluminium oxide to concentrated nitric acid molar ratio of 1:0·06. The temperature of peptisation was 95 °C and it was carried out under refluxing conditions. A cloudy sol was formed in 3 h of peptisation at 95 °C.

Colloidal silicon dioxide was dispersed in distilled water under acidic conditions in a mechanical blender. The dispersion formed was slightly cloudy. No settling of silicon dioxide particles was observed even after standing for 12 h.

2.3. Preparation of mullite gel

The boehmite sol formed by peptisation of γ-aluminium oxide was mixed in a blender with the silicon dioxide sol for 30 min. The mullite sol thus formed was gelled to a solid mass by evaporation of the excess water. The pH of the mullite sol before gelation was 1·8.

2.4. Properties

The surface areas of the powders were determined by the standard BET method (model Accusorb 2100E, Micromeritics, USA) which makes use of the nitrogen adsorption/desorption isotherm. The average particle size and the particle size distribution were determined using a laser particle size analyser (Microtrac R model 799-3, Leeds and Northrup, USA).

The crystalline phases in the calcined product were identified by X-ray diffraction (XRD), using Cu–Kα radiation, at 40 kV, 100 A, and a scanning speed of 10° 2θ min^{-1}. For the determination of the lattice parameters of mullite, high purity elemental silicon was used as an internal standard. The reflections selected for the determination of the orthorhombic cell constants were (250), (520), (002) and (331). The crystallite size of the mullite was determined using the (331) reflection.

The differential thermal analysis (DTA) curve of the gel was taken at a

heating rate of 10 °C min^{-1} up to 1400 °C (model MJ800 DR2, Rigaku Denki Co. Ltd, Japan). The infra-red transmission spectrum of mullite was recorded using a JASCO FT/IR-3 Fourier transform infra-red spectrophotometer.

2.5. Microscopic studies

Transmission electron microscope (TEM) micrographs of the mullite powder were obtained after dispersion in water. The microstructures of the sintered polished specimens were observed by scanning electron microscopy (SEM) after thermal etching at 1450 °C, or acid etching using 10% hydrogen fluoride solution for 1 h.

3. RESULTS AND DISCUSSION

3.1. Formation of mullite

The DTA heating curve of the gelled mullite powder was recorded in ambient atmosphere from 20 °C to 1400 °C at a heating rate of 10 °C min^{-1}, and is shown in Fig. 1. The endotherms at 96 °C and 420 °C represent the loss of moisture from the gel, and dehydration of the boehmite to form the spinel phase (γ-Al_2O_3), respectively. The broad endotherm occurring from 540 °C to 1296 °C is associated with the reaction of the spinel phase with amorphous silicon dioxide to form mullite. The exotherm at 1296 °C is an indication of the complete crystallisation of mullite. Similar results were reported by Hoffman *et al.*[16] for diphasic gels prepared by gelling tetraethoxysilane with boehmite sol.

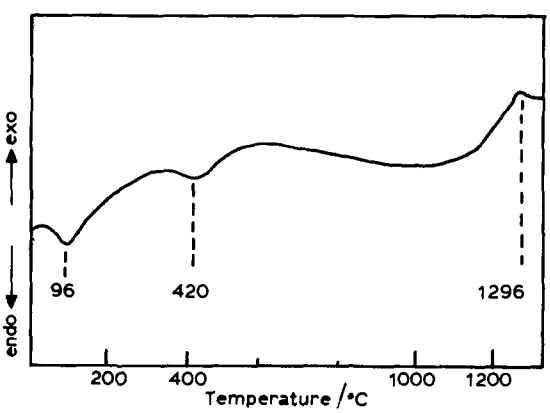

Fig. 1. DTA heating curve of the gelled mullite powder.

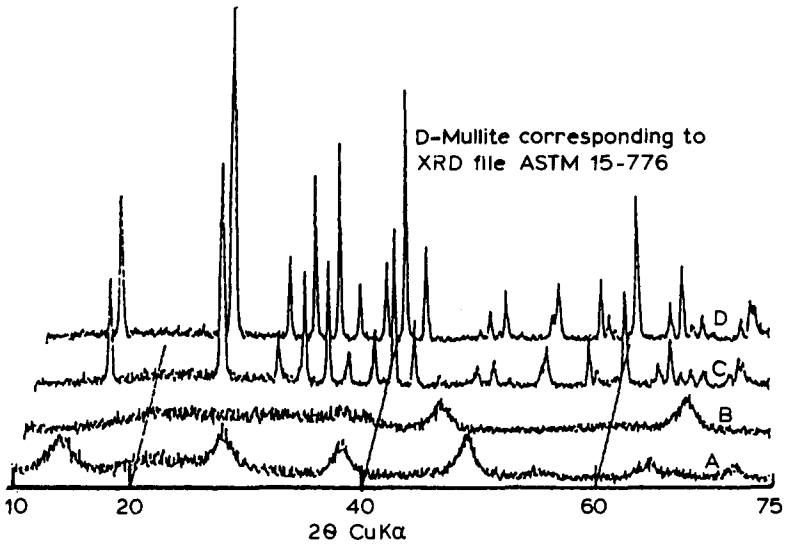

Fig. 2. X-ray diffraction patterns of the gel calcined at different temperatures. A, gel; B, gel at 1000 °C; C, gel at 1300 °C for 1 h; D, gel at 1400 °C for 1 h.

The XRD patterns of the gel mullite, calcined at different temperatures, are shown in Fig. 2. The XRD pattern of the gel shows the presence of boehmite and amorphous silicon dioxide as two discrete phases. These two phases react and at 1000 °C silicon dioxide stabilised δ-aluminium oxide was formed. Amorphous silicon dioxide was also observed. At 1300 °C mullite was observed with traces of δ-aluminium oxide. Similar phenomena were observed by Yoldas[17] in his studies on the Al_2O_3–SiO_2 binary system, and were explained as being due to the stabilisation of active aluminium oxide by silicon dioxide. Only peaks corresponding to mullite were observed when the gel was heated at 1400 °C for 1 h. This phase was retained even after slow cooling and recycling of the same sample several times. This is an indication of the complete solid solution of the mullite.

The chemical composition of the mullite formed is given in Table 1. The lattice parameters of the mullite formed at 1400 °C are $a = 0{\cdot}7566$ nm, $b = 0{\cdot}7684$ nm and $c = 0{\cdot}2887$ nm. The mean crystallite size is 29 nm.

3.2. Infra-red spectra

Infra-red transmission spectra of mullite was observed using potassium bromide discs over the region 1400–400 cm^{-1}. The infra-red transmission spectrum of mullite synthesised at 1400 °C is given in Fig. 3. The observed infra-red-active Al–O tetrahedral vibrations are 1170 cm^{-1}, 865 cm^{-1} and 740 cm^{-1}; Si–O tetrahedral vibrations are 1135 cm^{-1}, 940 cm^{-1} and

TABLE 1
Chemical Composition of the Synthesised Mullite

Constituents	*% by weight*
Al_2O_3	72·0
SiO_2	28·0
Na_2O	0·03
K_2O	0·01
TiO_2	0·13
Fe_2O_3	0·01

505 cm^{-1}; Al–O octahedral vibrations are 580 cm^{-1} and 570 cm^{-1}. The vibrations observed at 1135 cm^{-1}, 740 cm^{-1} and 570 cm^{-1} differ from the frequencies calculated for mullite by MacKenzie.[18] This may be due to the thermal history of the present mullite sample.

3.3. Physical properties of mullite

The surface areas (BET) and calculated average particle sizes of the gel and mullite are given in Table 2. The surface area (BET) of the gel is 277 $m^2 g^{-1}$ which indicates that the gel consists of ultrafine particles of the order of 7 nm

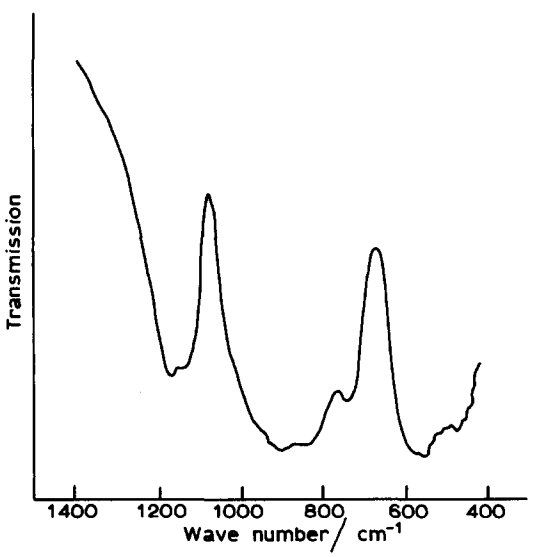

Fig. 3. Infra-red spectrum of mullite recorded using a potassium bromide disc. (Mullite synthesised at 1400°C for 1 h.)

TABLE 2
BET Surface Area and Particle Size Data

Material	*Surface area/$m^2 g^{-1}$*	*Average calculated particle size/nm*
Mullite gel	277	7
Mullite (1 400 °C calcine)	1·7	1 090
Mullite (milled ultrafine powder)	12·0	160

in dimension. On calcination at 1400 °C for 1 h these ultrafine particles undergo sintering, with a decrease in surface area to 1·7 $m^2 g^{-1}$. The average particle size of the mullite formed at 1400 °C for 1 h, as determined by particle size analysis, was 7·5 μm; 90 % of the particles were smaller than 26 μm and 10 % of the particles were smaller than 1·4 μm. This indicates the presence of particle agglomerates. Milling of mullite was carried out in an attrition mill using zirconia balls. The particle size distribution of the milled mullite is shown in Fig. 4. The average measured particle size of the milled mullite was 1·3 μm, with 90 % of the particles smaller than 3·0 μm, and 10 % smaller than 0·5 μm. The surface area (BET) was 12 $m^2 g^{-1}$, and agglomeration is again indicated.

The TEM micrographs of mullite powder synthesised at 1400 °C are shown in Fig. 5. The synthesised mullite shows a chunky habit. Von Lohre and Urban[19] found that mullite prepared in the absence of a glassy phase invariably led to a 'chunky' habit, whereas the needle-like morphology formed only in the presence of a liquid phase.

The thermal conductivity of the synthesised mullite was 0·0864 W $m^{-1} k^{-1}$

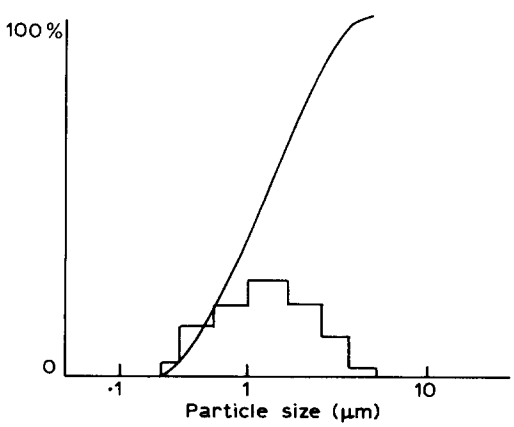

Fig. 4. Particle size distribution of milled calcined mullite powder.

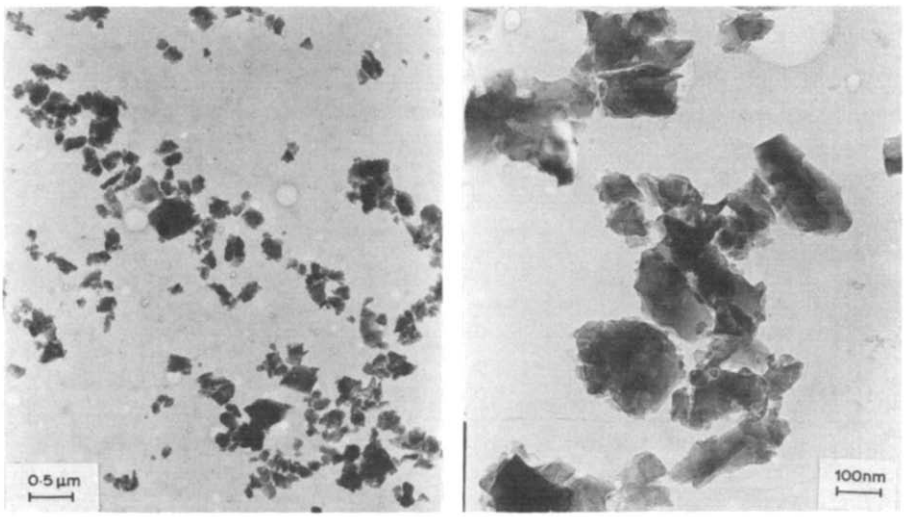

Fig. 5. TEM micrographs of mullite synthesised at 1400 °C for 1 h.

and the coefficient of linear expansion was $5{\cdot}54 \times 10^{-6}\,°C^{-1}$ (25–1500 °C).

3.4. Sintering of mullite powder

Mullite powder was cold isostatically pressed at 200 MPa, and sintered at different temperatures. The green density of the pressed powder compact was 51 % of theoretical (assumed as $3{\cdot}19\,Mg\,m^{-3}$). The powder sintered to 98 % theoretical density after 3 h at 1650 °C. The SEM micrographs of the polished and thermally etched specimens under different magnifications are shown in Fig. 6. The dihedral angles formed by rectangular grains were $> \pi/3$ and indicate the absence of a glassy phase[20] along the grain boundaries. The SEM micrographs of a specimen etched with 10 % hydrogen fluoride are shown in Fig. 7.

The flexural strength of the sintered specimens was determined by the three-point bend method, using test pieces 4 mm × 3 mm × 40 mm in dimension. The mean flexural strength at room temperature was 385 MPa.

4. CONCLUSIONS

Mullite of stoichiometric composition has been synthesised, using a sol–gel route, from γ-aluminium oxide and colloidal silicon dioxide. Formation of mullite from the gel at temperatures as low as 1300 °C indicates that the

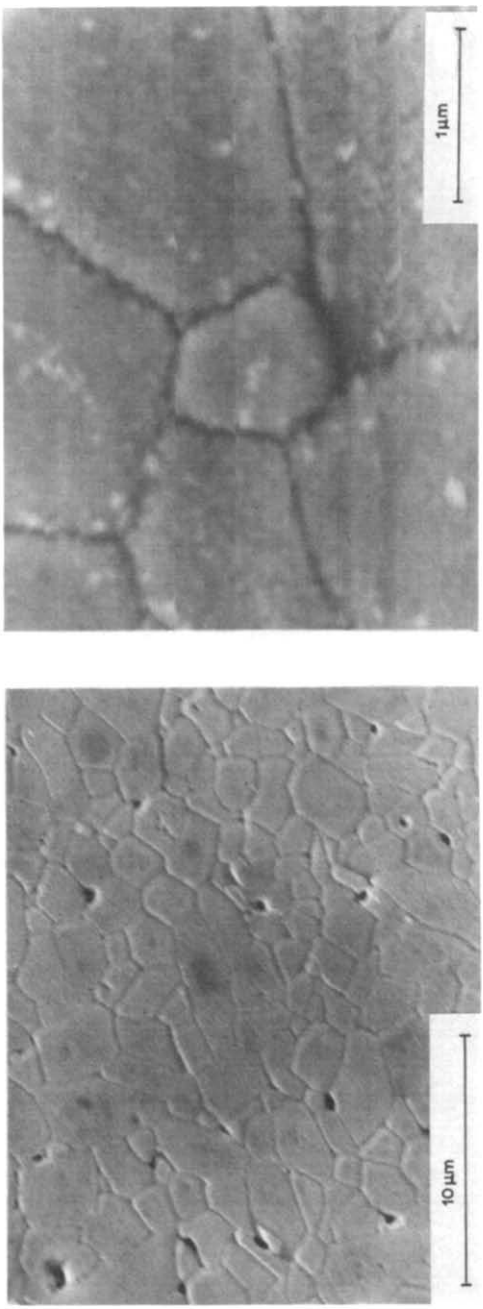

Fig. 6. SEM micrographs of mullite sintered at 1650 °C for 3 h and thermally etched.

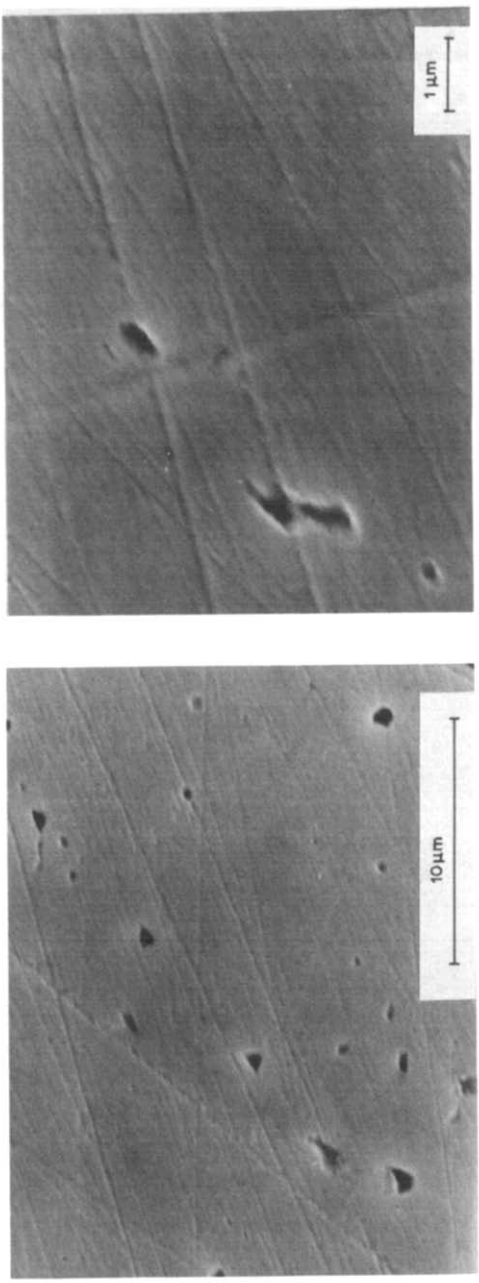

Fig. 7. SEM micrographs of mullite sintered at 1650 °C for 3 h, polished and etched using 10 % hydrogen fluoride for 1 h.

mixing of aluminium oxide and silicon dioxide is homogeneous. In contrast the gel of Ghate *et al.*,[7] formed by mixing γ-aluminium oxide and silicon dioxide, required treatment for 20 h at 1400 °C for complete reaction.

The flexural strength at room temperature of mullite formed by sintering at 1650 °C for 3 h was 385 MPa. The SEM micrographs of thermally and 10 % hydrogen fluoride etched specimens appeared to show no glassy phase along the grain boundaries, but further experiments are needed to confirm the absence of glass.

REFERENCES

1. Davis, R. F. and Pask, J. A., Mullite, in *High Temperature Oxides, Part IV*, Ed. A. M. Alper, Academic Press, New York, 1971, 37–76.
2. Rodrigo, P. D. D. and Boch, P., High purity mullite ceramics by reaction sintering, *Int. J. High Technology Ceramics*, **1**(1) (1985) 3–30.
3. Sōmiya, Shigeyuki (Ed), *Mullite*, Uchida Rokakuho Publishing Co., Tokyo, 1985, 140.
4. Lessing, P. A., Gordon, R. S. and Mazdiyasni, K. S., Creep of polycrystalline mullite, *J. Am. Ceram. Soc.*, **58**(3–4) (1975) 149.
5. Dokko, P. C., Pask, J. A. and Mazdiyasni, K. S., High temperature mechanical properties of mullite under compression, *J. Am. Ceram. Soc.*, **60**(3–4) (1977) 150–5.
6. Mazdiyasni, K. S. and Brown, L. M., Synthesis and mechanical properties of stoichiometric aluminium silicate (mullite), *J. Am. Ceram. Soc.*, **55**(11) (1972) 548–52.
7. Ghate, B. B., Hasselman, D. P. H. and Spriggs, R. M., Synthesis and characterisation of high purity fine grained mullite, *Am. Ceram. Soc. Bull.*, **52**(9) (1973) 670.
8. Metcalfe, B. L. and Sant, J. H., The synthesis, microstructure and physical properties of high purity mullite, *Trans. Brit. Ceram. Soc.*, **74**(6) (1975) 193–201.
9. Roy, R., Aids in hydrothermal investigation, II. Methods of making mixtures for both 'dry' and 'wet' phase equilibrium studies, *J. Am. Ceram. Soc.*, **39** (1956) 149.
10. Aramaki Shigeo and Roy, R., Revised phase diagram for the system Al_2O_3–SiO_2, *J. Am. Ceram. Soc.*, **45**(5) (1962) 229–42.
11. Sōmiya Shigeyuki, Yoshimura Masahiro, Suzuki Matsuo and Yamaguchi Toshihide, Hydrothermal processing of mullite powders from alkoxides, in *Mullite*, Ed. S. Sōmiya, Uchida Rokakuho Publishing Co., Tokyo, 1985, 63–87.
12. Suzuki Matsuo, Hiraishi Shun-ichi, Yoshimura Masahiro and Sōmiya Shigeyuki, Preparation of mullite powder by calcination of the products hydrothermally treated from mixed alkoxides or mixed sols, *Yogyo-Kyokai-shi*, **92**(6) (1984) 32.
13. Yamaguchi Toshihide, Suzuki Matsuo, Hiraishi Shun-ichi, Yoshimura Masahiro and Sōmiya Shigeyuki, Hydrothermal crystallisation of alumino

silicate fine powder prepared by hydrolysis of mixed alkoxides, *J. Mat. Soc. Japan*, **21** (1984) 241–4.
14. Kanzaki, S., Tabata, H., Kumazawa, T. and Ohta, S., Sintering and mechanical properties of stoichiometric mullite, *J. Am. Ceram. Soc.*, **68**(1) (1985) C6–C7.
15. Kanzaki, S. and Tabata, H. Sintering and mechanical property of spray pyrolyzed mullite powder, in *Mullite*, Ed. S. Sōmiya, Uchida Rokakuho Publishing Co., Tokyo, 1985, 51–61.
16. Hoffman, David W., Roy, Rustom and Komarneni, S., Diphasic xerogels. A new class of materials: phases in the system Al_2O_3–SiO_2, *J. Am. Ceram. Soc.*, **67**(7) (1984) 468.
17. Yoldas, Bulent E., Microstructure of monolithic materials formed by heat treatment of chemically polymerised precursors in the Al_2O_3–SiO_2 binary, *Am. Ceram. Soc. Bull.*, **59**(4) (1980) 479.
18. MacKenzie, K. J. D., Infrared frequency calculations for ideal mullite ($3Al_2O_3 \cdot 2SiO_2$), *J. Am. Ceram. Soc.*, **55**(2) (1972) 68.
19. Von Lohre, W. and Urban, H., Contribution to the morphology of mullite, *Ber. Deut. Keram. Ges.*, **37**(6) (1960) 249–51.
20. Raj, Rishi, Morphology and stability of the glass phase in glass–ceramic systems, *J. Am. Ceram. Soc.*, **64**(5) (1981) 245.

Received 12 December 1985; accepted 6 January 1986.

Int. J. High Technology Ceramics **2** (1986) 135–142

Preferred Orientation of the Transformed Monoclinic Phase in Fracture Surfaces of Y–TZP Ceramics

A. W. Paterson

National Institute for Materials Research, CSIR, PO Box 395, Pretoria 0001, South Africa

and

R. Stevens

Department of Ceramics, University of Leeds, Leeds LS2 9JT, England

SUMMARY

X-ray diffraction (XRD) has been used in a study of yttria–tetragonal zirconia polycrystalline (Y–TZP) ceramics to assess the extent of transformation to the monoclinic phase of fracture surfaces. Comparison of powder diffraction patterns and those obtained from fracture surfaces indicated that there are changes in the relative intensities of the $(111)_m$ *and* $(11\bar{1})_m$ *reflections and also shifts in the angles at which the reflections appear.*

From the experimental data, lattice parameters for the monoclinic phase are recalculated, using four reflections, by an iterative technique. Using the new calculated lattice parameters the position of a fifth reflection is predicted accurately.

The integrated intensity of the $(11\bar{1})_m$ *reflection is increased compared with the* $(111)_m$ *reflection. The ratio of the integrated intensities is expected to be about 1·5, but is found to be as high as 7·5. This can give rise to an error in the predicted monoclinic phase content; a correction is proposed.*

The preferred orientation is considered to arise because of the importance of the shear component of the martensitic transformation. The importance of this finding for an understanding of the fracture process is discussed.

1. INTRODUCTION

X-ray diffraction (XRD) techniques form the basis of phase analysis of predominantly tetragonal zirconia polycrystalline ceramics (TZP). The

Int. J. High Technology Ceramics 0267-3762/86/$03·50

transformation of the tetragonal phase to monoclinic symmetry on grinding or on fracture has received attention,[1,2] in particular in the determination of a 'depth of transformation'. A certain amount of doubt concerning the application of these techniques to TZP materials has arisen following the study of Rühle and his co-workers.[3] In an *in-situ* transmission electron microscopy (TEM) fracture study they showed that the monoclinic phase appears in irregular clusters in the crack-tip wake and that some tetragonal grains near the crack or on the crack plane do not transform. It is therefore difficult to assign a 'depth of transformation' in such a system. It should be remembered that such work takes place in a thin, electron transparent section and does not have the elastic constraint present in the bulk ceramic.

In this study it was noted that there is a substantial deviation of the relative intensities of the $(11\bar{1})_m$ and $(111)_m$ reflections from those anticipated in powder XRD and structure factor calculations.[4,5] It is suggested that this deviation arises from the monoclinic phase, formed during the fracture process, having a preferred orientation. In addition, a shift in the position of the $(11\bar{1})$ reflection was noted and this shift is analysed in terms of a distortion of the monoclinic cell from that expected, as a consequence of constraint in the development of the fracture surface.

2. EXPERIMENTAL

Powder XRD analysis was performed on commercially available yttria-doped zirconia powders (MEL, Manchester, UK and Toyo-Soda Co., Tokyo, Japan) that were thermally treated at 1600 °C for sufficient time to ensure equilibrium distribution of the Y_2O_3, and to increase the crystallite size, thereby producing some monoclinic phase.

XRD was carried out on the fracture surfaces of single edge notched bar (SENB) specimens consequent to a study of the sintering behaviour, fracture toughness, and the extent of the tetragonal to monoclinic transformation possible.[6]

A Philips diffractometer using Cu–Kα radiation in continuous scan mode was used. The integrated intensities of the required *hkl* reflections were determined by planimetry.

3. RESULTS AND DISCUSSION

3.1. Recalculation of lattice parameters of the monoclinic phase in fracture surfaces

Initial results showed a significant shift in the $(11\bar{1})_m$ reflection obtained from the fracture surfaces when compared with those obtained using powder XRD samples (Fig. 1).

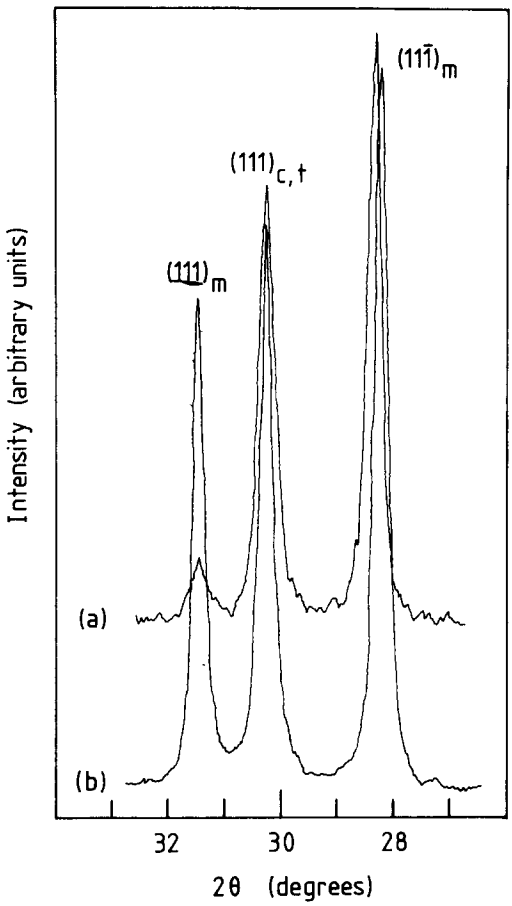

Fig. 1. XRD traces for (a) a TZP fracture surface and (b) Y_2O_3–ZrO_2 powder of the same composition, i.e. 2 mol% Y_2O_3. Note changes in the relative intensities of the $(111)_m$ and $(11\bar{1})_m$ and differences in the position of the $(11\bar{1})_m$ reflection.

An interactive program was developed which permitted the calculation of the systematic variation of the lattice parameters, starting with the values given by JCPDS card 13-307 (baddeleyite). After modification of a lattice parameter value, the *d*-spacings anticipated from the current values were then calculated and compared with the experimental values. This was done for four reflections: (002), (200), (020) and $(11\bar{1})$. Finally, when a good correspondence between the calculated and experimental values (better than 0·001 Å) was obtained, the *d*-spacing for the $(111)_m$ reflection was calculated and compared with the measured value. This provides an independent check of the iterative method described, using all four lattice parameters. The initial lattice parameters, the final lattice parameters and the calculated and measured *d*-spacings for the (111) reflection are given in Table 1.

TABLE 1

Lattice parameters	*JCPDS 13-307*	*Recalculated*
a	5·147 7 Å	5·127 5 Å
b	5·203 Å	5·200 Å
c	5·315 6 Å	5·301 8 Å
β	99·383°	98·505°
Unit cell volume	140·47 Å^3	139·81 Å^3

Calculated $(111)_m$ *d*-spacing = 2·847 Å
Measured $(111)_m$ *d*-spacing = 2·844 Å

It is apparent from Table 1 that the prediction of the *d*-spacing of the (111) reflection using the modified lattice parameters is satisfactory.

From these results it can be seen that compared with standard monoclinic zirconia the monoclinic cell in TZP fracture surfaces is slightly distorted, having a shorter *c* axis tilted slightly towards the normal. The *a* lattice parameter is also shorter, the overall effect resulting in a 'strained' structure.

The unit cell volume of the monoclinic phase in the fracture surface is smaller than that calculated for baddeleyite powder. This suggests that the distortion of the monoclinic cell arises in order to minimise the matrix strain energy increase resulting from the transformation in the fracture surface. This also suggests a lower barrier to transformation than would be anticipated from consideration of the volume change in pure phases.[7]

3.2. Preferred orientation of the monoclinic phase in fracture surfaces

The TZP materials investigated in this study had no monoclinic phase present prior to fracture. Figure 1(a) shows the XRD trace of a fracture surface. The three reflections, in order of increasing 2θ, are $(11\bar{1})_m$, $(111)_{c,t}$ and $(111)_m$. It is apparent from a comparison of the relative intensities of the monoclinic reflections with those in the powder sample (Fig. 1(b)) that the $(11\bar{1})_m$ plane is found parallel to the fracture surface more often than would be anticipated from random transformation of tetragonal grains.

Table 2 shows the ratio of the relative intensities of $(11\bar{1})_m$ to $(111)_m$ for a number of TZP ceramics sintered using a variety of temperatures and times. The results indicate that for both small or extensive amounts of transformation, preferred orientation of the monoclinic phase can be detected in the fracture surface.

This raises certain difficulties in the accurate computation of the monoclinic phase content, since the validity of the expressions used[8–10] relies on the assumption that transformation in the fracture surface is

TABLE 2

Composition	*Treatment*		$\frac{I(11\bar{1})_m}{I(111)_m}$	X_m	X_m *corrected*	V_m	V_m *corrected*
	Temperature/ °C	*Time/ h*					
2·5Y	1675	2	7·125	28·5	26·0	34·8	32·1
2·5Y	1400	2[a]	4·51	8·4	7·7	10·9	10·0
2·5Y	1400	2[b]	4·88	6·6	6·1	8·7	7·9
2Y	1400	2	6·5	20·6	18·7	25·8	23·6
2Y	1575	2	6·61	55·3	52·4	62·4	59·6
2Y	1575	1	7·33	39·6	36·6	46·7	43·7

[a] Notch width 500 μm.
[b] Notch width 100 μm.

crystallographically random. The net effect of this is to give an overestimate of the monoclinic phase content by a few percent. A correction may be applied:

$$I_T = 1{\cdot}255I(111) + 0{\cdot}833I(11\bar{1})$$

where I_T is the corrected intensity of $I(111)_m + I(111)_m$, based on the assumption that the expected relative intensity ratio is 1·5 for randomly oriented grains (see Appendix). The results are calculated for the uncorrected and corrected integrated intensities using the equation of Toraya *et al.*:[8,9]

$$V_m = \frac{PX_m}{1 + (P-1)X_m}$$

where X_m = the monoclinic intensity relative to the total intensity of the $(111)_m$, $(11\bar{1})_m$, $(111)_{c,t}$ reflections; P = the experimental constant for these systems (about 1·31); and V_m = the volume fraction of monoclinic phase. The experimental results and relevant corrections are listed in Table 2.

These results indicate that the $(11\bar{1})_m$ plane is preferentially developed parallel to the crack plane 2·5–5 times more often than would be the case if grains transformed randomly. This suggests an important implication and gives evidence to the effect that the directional component of the shear transformation is very important in the toughening process. An indication of the nature of the directional component can be deduced from a comparison of the areas of $(111)_t$, $(111)_m$ and $(11\bar{1})_m$ planes in the unit cell. These results are shown in Table 3.

The deviatoric component of the transformation can be considered to give rise to toughening of TZP materials ahead of a stationary crack.[11] This model is preferred to the hydrostatic, crack wake model[12] in the light of the

TABLE 3

Plane	*Area*/Å^2	$\Delta A(111)_t$/%
$(111)_t$	22·70	—
$(111)_m$	24·55	+8·2
$(11\bar{1})_m$	22·2	−2·3

preferred orientation observed in the fracture surfaces. It appears that the transformation occurs in grains oriented in such a way that the maximum volumetric expansion occurs parallel to the tensile stress field, thus reducing the strain energy associated with the untransformed grains ahead of the crack. The relatively small number of grains that transform into other orientations may do so through autocatalytic mechanisms (suggested by Rühle *et al.*[3]) or as a result of crack deviation from the plane, microcracking and other phenomena. These represent some 20–25 % of all transformation events.

The distinctive difference between partially stabilised zirconia (PSZ) transformation toughening and TZP transformation toughening appears to reside in the difference in importance of the hydrostatic and deviatoric components of the shear transformation, the latter being of major importance in the TZP system and relatively less important in the PSZ materials.[12]

The results of the present study have been applied to the interpretation of the experimentally determined toughening increment, ΔK_{1c}^{T}, in TZP materials using the equation proposed by Seyler *et al.*[11] in a modified form.[6]

4. CONCLUSIONS

(i) The lattice parameters of the monoclinic phase in TZP fracture surfaces are modified, compared with the powder XRD value, in a manner that reduces the unit cell volume.

(ii) There is a tendency for the $(11\bar{1})$ plane of monoclinic grains to be generated parallel to the crack surface more often than would be the case if transformation of tetragonal grains took place irrespective of their orientation.

(iii) This preferred orientation can be interpreted in terms of the directional nature of the transformation, which occurs so as to minimise the volume increase in the plane of the crack, and more importantly, to maximise it in the direction of the tensile stress field in order to reduce strain energy ahead of the crack tip.

ACKNOWLEDGEMENT

Dr A. W. Paterson was supported financially by the National Institute for Materials Research, CSIR, South Africa, while at the University of Leeds where this research was undertaken.

APPENDIX: ESTIMATION OF THE CORRECTION FACTOR FOR THE CALCULATION OF THE MONOCLINIC PHASE IN SURFACES WITH A PREFERRED ORIENTATION OF THE PHASE

In a random sample 40% of the integrated intensity of $(111)_m$ and $(11\bar{1})_m$ reflections is generated from $(111)_m$. Thus the ratio of the intensity of $(11\bar{1})_m$ to $(111)_m$ is approximately 1·5.

In a non-random sample, the total intensity can be considered to be made up of a random contribution and a non-random contribution due to preferred orientation; the 'random' contribution can be calculated from the intensity of the $(111)_m$ reflection if this intensity is considered to arise randomly.

Thus, $I(11\bar{1})_{mR}$, the random contribution from the $(11\bar{1})_m$ reflection is $I(111)_m \times 1{\cdot}5$. Hence, the non-random contribution, $I(11\bar{1})_{mNR}$, is $I(11\bar{1})_{m\,total} - I(11\bar{1})_{mR}$. If this contribution had arisen randomly its intensity, $I(11\bar{1})_{m\,corr}$, would be

$$\begin{aligned} &0{\cdot}5 \times I(11\bar{1})_{mNR} + 0{\cdot}5 \times 0{\cdot}66 \times I(11\bar{1})_{mNR} \\ &\quad = 0{\cdot}83 \times (I(11\bar{1})_{mNR}) \\ &\quad = 0{\cdot}83(I(11\bar{1})_{m\,total} - I(111)_m \times 1{\cdot}5) \end{aligned}$$

Thus the total corrected intensity I_{mT} can be written

$$\begin{aligned} I_{mT} &= I(111)_m + I(11\bar{1})_{mR} + I(11\bar{1})_{m\,corr} \\ &= I(111)_m + (I(111)_m \times 1{\cdot}5) + (0{\cdot}83 \times (I(11\bar{1})_{m\,total} - I(111)_m \times 1{\cdot}5)) \\ &= 1{\cdot}255I(111)_m + 0{\cdot}833I(11\bar{1})_m \end{aligned}$$

This equation leads to a correction of ~1% at 10% transformation and ~5% at the 60% transformation level.

REFERENCES

1. Kosmac, T., Wagner, R. and Claussen, N., X-ray determination of transformation depths in ceramics containing tetragonal ZrO_2, *J. Am. Ceram. Soc.*, **64** (1981) C72–3.
2. Garvie, R. C., Hannink, R. H. J. and Swain, M. V., X-ray analysis of the transformed zone in partially stabilized zirconia, *J. Mat. Sci. Lett.*, **1** (1982) 437–40.

3. Rühle, M., Kraus, B., Strecker, A. and Waidelich, D., *In-situ* observations of stress-induced phase transformations in ZrO_2-containing ceramics, in *Advances in Ceramics 12*, Eds N. Claussen, M. Rühle and A. H. Heuer, The American Ceramic Society, Columbus, Ohio, 1983, 256–74.
4. Evans, P. A., Stevens, R. and Binner, J. G. P., Quantitative X-ray diffraction analysis of polymorphic mixes of phase zirconia, *Brit. Ceram. Trans. J.*, **83** (1984) 39–43.
5. Porter, D. L. and Heuer, A. H., Microstructural development in MgO-partially stabilized zirconia (Mg-PSZ), *J. Am. Ceram. Soc.*, **62** (1979) 298–305.
6. Paterson, A. W. and Stevens, R., Comparison of indentation and notched bar toughness of TZP materials and their relevance to models of the fracture process, *Int. J. High Technology Ceramics*, **2** (1986) in press.
7. Rühle, M. and Heuer, A. H., Phase transformation in ZrO_2-containing ceramics: II, The martensitic reaction in t-ZrO_2, in *Advances in Ceramics 12*, Eds N. Claussen, M. Rühle and A. H. Heuer, The American Ceramic Society, Columbus, Ohio, 1983, 14–32.
8. Toraya, H., Yoshimura, M. and Sōmiya, S., Calibration curve for quantitative analysis of the monoclinic–tetragonal ZrO_2 system by X-ray diffraction, *J. Am. Ceram. Soc.*, **67** (1984) C119–21.
9. Toraya, H., Yoshimura, M. and Somiya, S., Quantitative analysis of monoclinic-stabilized cubic ZrO_2 systems by X-ray diffraction, *J. Am. Ceram. Soc.*, **67** (1984) C183–4.
10. Garvie, R. C. and Nicholson, P. S., Phase analysis in zirconia systems, *J. Am. Ceram. Soc.*, **55** (1972) 303–5.
11. Seyler, R. J., Lee, S. and Burns, S. J., A thermodynamic approach to toughness in PSZ, in *Advances in Ceramics 12*, Eds N. Claussen, M. Rühle and A. H. Heuer, The American Ceramic Society, Columbus, Ohio, 1983, 213–24.
12. Evans, A. G., Toughening mechanisms in zirconia alloys, in *Advances in Ceramics 12*, Eds N. Claussen, M. Rühle and A. H. Heuer, The American Ceramic Society, Columbus, Ohio, 1983, 193–212.

Received 30 January 1986; accepted 29 March 1986.

Int. J. High Technology Ceramics **2** (1986) 143–155

Coaxial Resonator Method to Determine Dielectric Properties of High Dielectric Constant Microwave Ceramics

E. Kemppinen and S. Leppävuori

Microelectronics Laboratory, Department of Electrical Engineering,
University of Oulu, Finland

SUMMARY

The performance of a resonator incorporating a ceramic depends strongly on the dielectric properties of the ceramic. This paper discusses the measurement of these properties using the coaxial resonator method at high UHF frequencies. It is possible to calculate the dielectric constant with an accuracy better than 1%. If the conductivity of the metal coating on the resonator is known, it is also possible to calculate the loss tangent of the ceramic core.

The measured Q_0-values, which depended on losses in both the silver coating and the barium nonatitanate dielectric of the $\lambda/4$ resonators, were compared with the theoretically calculated maximum values, on the basis that the ceramic is lossless and the conductivity of the coating corresponded with that of bulk silver. Typically, 70–90% of the theoretical maximum values were attained. The loss tangent of the $Ba_2Ti_9O_{20}$ ceramic was between 1×10^{-4} and 2×10^{-4} at 1 GHz. The temperature coefficient of resonance frequency was 4 ppm $°C^{-1}$.

Measurements yield useful data suitable for practical design purposes. In addition, the dimensions of the resonators are small, ranging from a few millimetres to a few centimetres, depending on the frequency, dielectric constant, and desired Q_0-value.

The method can be used as a quality control technique for the ceramic manufacturing process.

1. INTRODUCTION

Low loss microwave ceramics are extremely useful for miniaturizing microwave and UHF components. The importance of these materials has

Int. J. High Technology Ceramics 0267-3762/86/$03·50

increased recently with the greater demand for small portable telecommunications equipment employing UHF frequencies. The use in such applications makes it necessary to know the merits of the electrical performance of the materials employed. There are, however, difficulties in obtaining absolute values of dielectric properties at microwave and UHF frequencies, and particularly in comparing values measured in one laboratory with those from another.

There are two major reasons for this: (i) measurement problems themselves, and (ii) lack of control over ceramic composition and microstructure. The present paper addresses some of the difficulties but concentrates on a method, viz. the coaxial resonator method, which has a number of advantages over others, and which has been used by the authors in the context of microwave ceramics and device development projects.

Different methods have been used to determine the dielectric properties of low loss, high frequency ceramics. The important electrical parameters that are measured are the complex dielectric constant ($\varepsilon_r' + i\varepsilon_r''$), which yields the loss tangent ($\tan d = \varepsilon_r''/\varepsilon_r'$), and the variation of complex dielectric constant with temperature.

Commonly, three methods have been exploited, viz, the rod resonator method developed by Hakki and Coleman,[1] the waveguide method,[2] and the microstrip transmission line method.[3] In all three methods the ceramic samples are in the form of cylinders with aspect ratios such that they resonate with an external electromagnetic field. Knowing the geometry of the sample and the electromagnetic field configuration, it is possible to calculate the complex dielectric constant from the measured resonance curves. In practice, however, this is difficult, especially in the case of the second and third methods, because of the effects of radiation from the resonator.

The three methods referred to above are most suitable for frequencies above about 4 GHz since below this frequency the size of the dielectric resonator becomes impracticably large, so that it is difficult to manufacture them reliably. Internal defects and an uneven distribution in density may increase the losses even though changes in the real part of the dielectric constant may be small. For example, in the case of the rod resonator method, at a frequency of 1 GHz, the approximate dimensions of a barium nonatitanate dielectric cylindrical resonator would be 65 mm in diameter and 36 mm in height.

The advantage of the microstrip transmission line method is that it gives a true Q-factor for the resonator in the environment where it is normally to be used;[4] to some extent this also applies to the waveguide method. From the ceramist's standpoint it is important to have a reliable measurement method for both the development of microwave ceramics and for quality control in their manufacture.

Because of the problems related to the unwieldy size of the dielectric rod resonators at the upper end of the UHF range, above 500 MHz other types of resonators can be used in order to determine the electrical properties of the ceramics. In this paper the coaxial resonator method which employs a much smaller size sample than required by the above-mentioned methods is described. In addition, it is possible to obtain data that can be used for practical electronic circuit design in which the circuits contain coaxial or other types of TEM resonator.

2. SPECIMEN MANUFACTURE AND THEORY OF CERAMIC-FILLED COAXIAL RESONATORS

Ceramic resonator cores with a central cylindrical hole were cold-pressed from calcined ceramic powder in a steel mould and then sintered with an appropriate temperature/time profile to a peak temperature of 1350 °C. In the sintering process the shrinkage was around 20 %. Starting materials and the fabrication route are detailed elsewhere.[5]

Thick film silver paste was brushed on to the surface of the sintered resonator and fired-on at temperatures in the range 900–930 °C, depending on the ceramic and silver, to give a high conductivity coating. Two silver coatings were applied and separately fired-on to ensure that the thickness of the layer was more than ten times the skin depth, that is more than about 20 μm.

Because of the high dielectric constant of microwave ceramics, three basic TEM coaxial resonator types are possible. These are:

1. $\lambda/4$ resonator—where all the surfaces, with the exception of one end, are covered with metal;
2. $\lambda/2$ resonator—where all the surfaces are covered with metal but where, in the middle of the outer conductor, there is a small opening for coupling; and
3. $\lambda/2$ resonator—where all the surfaces, except for both the ends, are covered with metal.

In this paper emphasis is on the $\lambda/4$ type, since this is of practical importance, for example, in miniature UHF filter design. The second type was used for the accurate determination of the dielectric constant ε_r' of the ceramic core. The practical value of the third type of resonator may be less than the others, except for ceramics with a very high dielectric constant, since the measured Q-values are reduced by the imperfect reflections from both open-circuited ends. However, it has the advantage that there are no conduction losses at the ends. In the present study it was employed to

demonstrate that it is possible to determine the dielectric constant fairly accurately using it.

2.1. Q-values for the dielectric $\lambda/4$ coaxial resonators

The unloaded Q_0-value of the resonator is given by

$$1/Q_0 = 1/Q_c + 1/Q_d + 1/Q_r \tag{1}$$

where Q_c is the Q-value due to the conductor losses, Q_d that due to the dielectric losses of the ceramic core, and Q_r that due to radiation losses. In this study the most important factors in determining Q_0 are Q_c and Q_d. The Q_r-factor is considered insignificant because the calculated dielectric constant (see Table 1) of the $\lambda/4$ resonator is nearly equal to that of the $\lambda/2$ resonator with short-circuited ends, implying that the fringing fields are negligible.[6]

TABLE 1
Dielectric Constants of $Ba_2Ti_9O_{20}$ as Determined by the Various Resonator Methods

Resonator type	*Frequency range/MHz*	*Dielectric constant*	*Standard deviation*
$\lambda/4$ resonator	900	36·86	0·14
$\lambda/2$ short-circuited ends	1 800	36·63	0·02
$\lambda/2$ open-circuited ends	1 800	37·12	0·25
Rod resonator	8 300	37·41	0·20

It is possible to calculate the Q_c-value for a coaxial $\lambda/4$ resonator of inner radius a, outer radius b, and length L from the definition of Q and well-known coaxial transmission line theory,[7] assuming a sinusoidal propagation in the z-direction, as follows:

$$Q_c = 2\omega W_e/P_c \tag{2}$$

$$W_e = \frac{\varepsilon_0 \varepsilon_r'}{4} \int_0^L \int_0^{2\pi} \int_a^b \frac{V_0^2}{(\ln b/a)^2} \cdot \frac{1}{r} (2A \sin kz)^2 \, dr \, d\phi \, dz \tag{3}$$

$$P_c = \frac{R_m}{2} \int_0^L \oint_{a,b} \frac{Y_0^2 V_0^2}{(\ln b/a)^2} \cdot \frac{1}{r} (2A \sin kz)^2 \, dr \, d\phi \, dz$$

$$+ \frac{R_m}{2} \int_0^{2\pi} \int_a^b \frac{Y_0^2 V_0^2}{(\ln b/a)^2} \cdot \frac{1}{r} (2A)^2 \, dr \, d\phi \tag{4}$$

where W_e is the time-average electric field energy in the core volume and P_c represents the losses caused by the resistivity of the silver coating on the curved surfaces and the one end. A is a normalization factor, k the propagation constant, R_m the surface resistance, Y_0 the free space admittance and V_0 the voltage difference between the conductors. In the above equations ε_0 is the permittivity of vacuum, ω the angular frequency and r, ϕ and z cylindrical co-ordinates with the z-axis along the axis of the cylinder and the origin at the coated end. A little manipulation yields the result[8]

$$Q_c \frac{\delta}{\lambda} = \frac{1}{4 + \dfrac{2L(1 + b/a)}{b \ln b/a}} \tag{5}$$

where δ is the skin depth ($\delta = (\pi f \sigma \mu_0)^{-1/2}$), σ the conductivity of the silver coating, μ_0 the magnetic permeability of vacuum and λ the wavelength in the dielectric.

Figure 1 illustrates a set of curves calculated from eqn (5) for Q_c at 900 MHz for various dielectric constants and cross sections. In eqn (5) the conductivity of bulk silver ($\sigma = 61\ \mathrm{MS\,m^{-1}}$) has been used in calculating

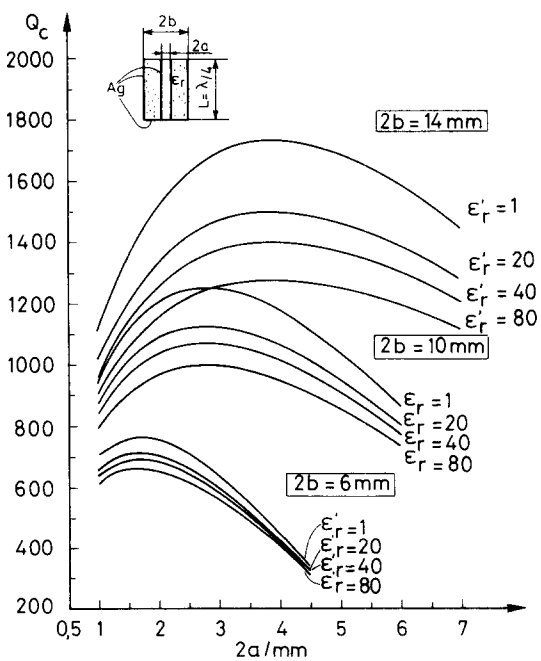

Fig. 1. Q_c-values for a $\lambda/4$ coaxial resonator for different dielectric constants and cross sections (assuming tan $d = 0$ and $\sigma = \sigma_{Ag} = 61\ \mathrm{MS\,m^{-1}}$) at a frequency of 900 MHZ.

the skin depth. The Q_c-value is at a maximum when the ratio b/a is about 3·6; this can be verified by fixing b and by setting the derivative of eqn (5) with respect to a to zero.

If the dielectric core were totally lossless and with no radiation from the open end, these Q_c-values would be the highest achievable by the $\lambda/4$ type coaxial resonators, according to eqn (1).

2.2. Determination of the dielectric constant

The determination of the dielectric constant ε_r' from the resonance frequency and the length of the core is straightforward. It is also very accurate in the case of $\lambda/2$ resonators because of the exact boundary conditions at the short-circuited ends. The following formulae are valid:

$$\lambda/4 \text{ case: } \varepsilon_r' = (c/4Lf_r)^2 \tag{6}$$

$$\lambda/2 \text{ case: } \varepsilon_r' = (c/2Lf_r)^2 \tag{7}$$

where c is the velocity of light in vacuum, f_r the resonance frequency, and L the length of the core. The dielectric constant can also be calculated from the harmonic frequencies using the same principle.

2.3. Determination of loss tangent and skin depth

Because there are two unknowns, loss tangent and skin depth, in eqn (1) for the Q_0-value, to determine them two simultaneous equations must be solved. In the present study this was achieved from measurements on two resonators of equal cross sections but of different lengths.

If the lengths of the resonators are L and $3L$, then the resonance frequency of the first resonator resonating in the $\lambda/4$ mode would be expected to be the same as that of the second resonator resonating at the $3\lambda/4$ mode. It can be shown from the basic definition, eqn (2), that the theoretical Q_c-value of the $3\lambda/4$ coaxial resonator is the same as that indicated by eqn (5) except for a factor '3' in the numerator. Because the loss tangent and skin depth must be equal at the same frequency, the following two equations can be written by combining eqns (1) and (5):

$$\frac{1}{Q_0} = \frac{\delta}{\lambda}(4 + LB) + \tan d \tag{8}$$

$$\frac{1}{Q_0'} = \frac{\delta}{\lambda}(4 + 3LB) + \tan d \tag{9}$$

where Q_0 and Q_0' are the measured Q_0-values of the two resonators of lengths L and $3L$, respectively, and

$$B = 2\frac{1 + b/a}{b \ln b/a}$$

is the shape factor depending only on the cross-sectional geometry. From these equations the following solutions can be obtained:

$$\delta = \frac{3\lambda}{8}\left(\frac{1}{Q_0} - \frac{1}{Q_0'}\right) \tag{10}$$

$$\tan d = \frac{1}{Q_0} - \frac{3}{8}\left(\frac{1}{Q_0} - \frac{1}{Q_0'}\right)(4 + LB) \tag{11}$$

When using this method it is essential that the quality of the ceramic and the metal paste are the same for both resonators. If this is not so the loss tangent or the skin depth in both eqns (8) and (9) cannot be regarded as equal, which invalidates the procedure. The length of the resonators can be adjusted by lapping so that the test frequencies are equal.

3. RESULTS

The unloaded Q_0-values were measured with a Hewlett Packard 8410 network analyser. The measuring jig and the shape of a typical resonance curve are illustrated in Fig. 2. The coupling between the two probes coupled to the electric field was better than 45 dB without the resonator on the jig.

In making the measurement of the Q_0-values, the normal -3 dB method was used. Because of the appreciable coupling ($S_{21} = -20\,\text{dB} \cdots -25\,\text{dB}$, where S_{21} is the forward transmission scattering parameter and $|S_{21}|^2 = P_L/P_A$, where P_L is the power at the load and P_A is the maximum available power from the generator) the final Q_0-values were calculated as follows:[9]

$$Q_0 = \frac{f_r}{f_2 - f_1} \cdot \frac{1 + K}{K} \tag{12}$$

where the correction factor K is

$$K = 10^{(-S_{21}/20)} - 1 \tag{13}$$

where $S_{21} < 0$, f_r is the resonance frequency, and f_1 and f_2 are the lower and upper -3 dBs frequencies, respectively.

In Fig. 3a the typical results of the measured Q_0-values at 900 MHz are shown, together with the theoretical maximum values calculated from eqn

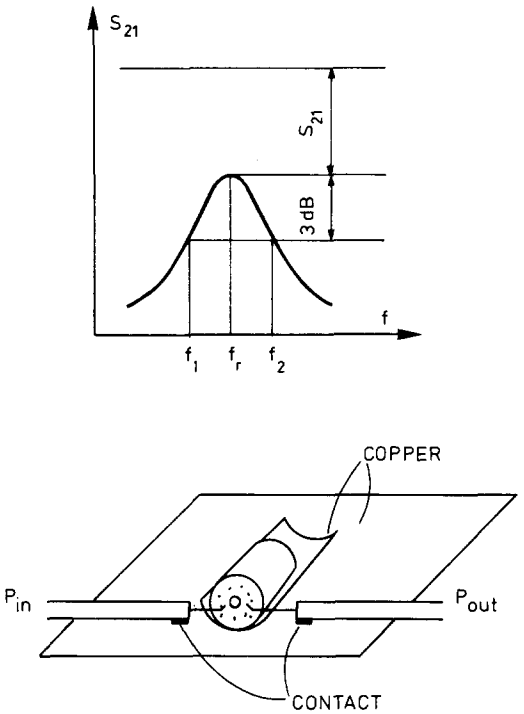

Fig. 2. The coaxial resonator measuring system and a typical resonance curve.

(5) ($\sigma = \sigma_{Ag} = 61\,\mathrm{MS\,m^{-1}}$, and $\tan d = 0$). The measured values were in the range 70–90 % of the theoretical, the closeness of the theoretical being dependent on the quality of the ceramic and silver coating pastes. The Q_c-value, according to eqn (5), is proportional to the square root of the conductivity. For that reason the resulting Q_0-values are different for the different pastes that were used in the study. Figure 3b illustrates the measured Q_0-values at 900 MHz for four commercially available pastes, as well as the calculated curve from eqn (5) under the same conditions as shown in Fig. 3a.

On measuring the Q_0-values at around 900 MHz of seven different groups of resonators, each group containing between eight and 15 resonators, all of which had been manufactured in a similar manner, it was found that the standard deviation of the Q_0-values in each group was from 3 to 10 % of the mean value.

When the desired Q_0-value of a $\lambda/4$ coaxial resonator with a high ε_r' at, say, 900 MHz is about 1000, and the loss tangent of the ceramic is approximately 1×10^{-4}, it is self-evident from eqns (1) and (5) that the conductor losses dominate, and special attention has to be paid to the quality and the conductivity of the covering paste. On the other hand, as can be concluded

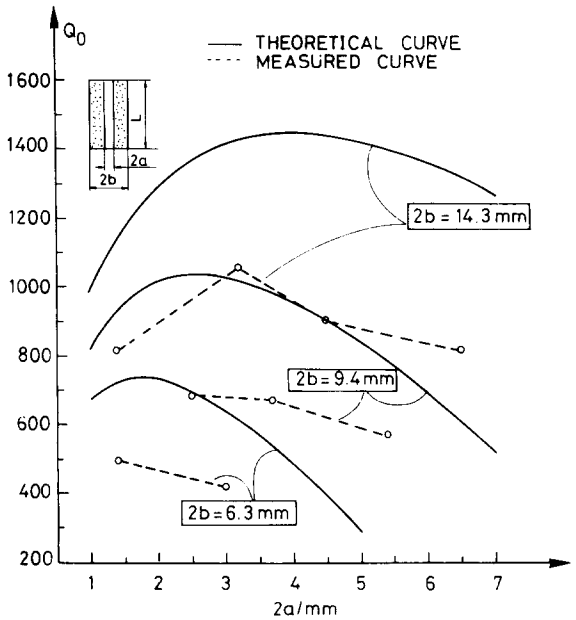

Fig. 3a. Measured and calculated Q_0-values from eqn (5) at 900 MHz ($\tan d = 0$, $\sigma = \sigma_{Ag} = 61\,\mathrm{MS\,m^{-1}}$) for barium nonatitanate coaxial resonators of different cross sections. The covering paste was 'Dupont 8032' randomly selected for initial trials.

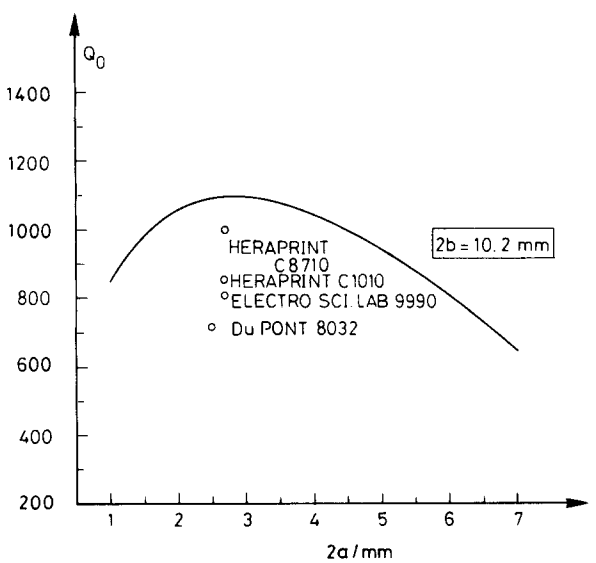

Fig. 3b. Comparison between Q_0-values for different commercially available silver pastes at 900 MHz. The calculated curve from eqn (5) ($\tan d = 0$, $\sigma = \sigma_{Ag} = 61\,\mathrm{MS\,m^{-1}}$) for barium nonatitanate is also shown.

from eqn (1), the higher the desired Q_0-value, the greater is the significance of losses arising in the ceramic core.

The dielectric constant of the ceramic core was calculated using eqn (6) for the $\lambda/4$ resonator and using eqn (7) for both the $\lambda/2$ type resonators. These values are compared with those obtained by the rod resonator method[1] in Table 1. In making the measurements, a coupling between the resonator and the probes (S_{21}) that was as loose as possible was used in order to prevent the probes from having any effect on the resonance frequency.

It can be seen that in the case of the $\lambda/4$ resonator and the short-circuited $\lambda/2$ resonator, the dielectric constants ε_r' are nearly equal. The slightly higher dielectric constant in the case of the $\lambda/4$ resonator is most probably explained by the weak fringing fields at the open end: the effect is most marked in the case of the open circuited $\lambda/2$ resonator because of the action of the fringing fields at both ends.

It should be noted that the dielectric constant ε_r' is affected by the final density of the resonator; the more porous the sample the lower the dielectric constant. For this reason the rod resonator method gives higher dielectric constants than the coaxial method because a higher density can be achieved for the simple cylindrical specimen than for the coaxial resonator specimens. When measuring the dielectric constant ε_r', the accuracy of the short-circuited $\lambda/2$ coaxial resonator measuring method can be made better than 1%, providing specimen geometry is carefully controlled, particularly parallelism of the ends.

In the L and $3L$ measurements to determine the loss tangent of the ceramic core and the skin depth of the covering silver paste, two resonators with Q_0-values, as indicated in Table 2, were utilised. The calculation of the unknown factors is based on eqns (10) and (11) as outlined above.

The calculated skin depth of 2·2 μm is 0·2 μm greater than that calculated for bulk silver. It can therefore be deduced that the conductivity of the paste is 83% that of silver, and by using it (and preparing it in the same way)

TABLE 2

Determination of Loss Tangent and Skin Depth Using Two Barium Nonatitanate Coaxial Resonators of Different Lengths (the shorter resonator resonates at $\lambda/4$-mode and the longer one at $3\lambda/4$-mode: the silver paste was 'Herraprint C8710')

Resonance mode	*2a/mm*	*2b/mm*	*L/mm*	*f/MHz*	Q_0	Q_0'	$\delta/\mu m$	*tan d*
$\lambda/4$	2·7	10·2	11·5	1058	912			
							2·2	$1{\cdot}4 \times 10^{-4}$
$3\lambda/4$	2·7	10·2	34·6	1055		1031		

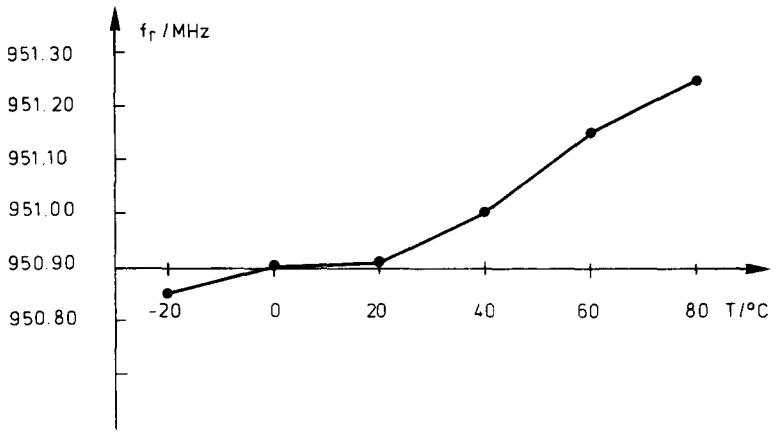

Fig. 4. The variation of resonance frequency of a barium nonatitanate coaxial $\lambda/4$ resonator with temperature.

approximately 90% of the theoretical Q_0-value can be achieved, provided the ceramic is totally lossless. Figure 1 shows the maximum achievable Q_0-values (i.e. for pure Ag coating on lossless ceramic) for different geometries.

The temperature coefficients of the resonance frequency of the coaxial resonators were measured in the temperature range $-20°C$ to $+80°C$. It should be noted that because of the silver coating the measured values are characteristic of the entire resonator system, which is significant from the point of view of practical application. The variation in resonance frequency with temperature of a typical barium nonatitanate coaxial $\lambda/4$ resonator is shown in Fig. 4.

The temperature coefficient of the pure barium nonatitanate coaxial $\lambda/4$ resonator is 4 ppm $°C^{-1}$ which is a very good value for many practical applications. The value can be increased by carrying out suitable doping.[5]

4. CONCLUSION

The objective of the study was to assess the coaxial resonator method for the evaluation of dielectric properties of low loss ceramics at microwave frequencies. This paper describes a practical, and, in many cases, a sufficiently accurate method for evaluating the dielectric properties of low loss ceramics. It is especially suitable at high UHF and low microwave frequencies, where the sample size for methods employing cylindrical dielectric resonators becomes impracticably large. The drawback of the coaxial method is that in eqns (8) and (9) there are two unknown factors, the loss tangent of the ceramic and skin depth of the coating. Both of these

depend on the overall fabrication process and when one of these is known, the other can be calculated. At 1 GHz the skin depth of the silver coating was calculated to be 2·2 μm, indicating the conductivity of the paste to be approximately 83% that of pure silver. By the same principle the loss tangent of the core was evaluated to be $1{\cdot}4 \times 10^{-4}$. Using the best of the silver pastes on a resonator with an outer diameter of 10·2 mm and an inner diameter of 2·7 mm, a Q_0-factor of 1000 was attained, which is approximately 90% of the calculated maximum value.

For the determination of the dielectric constant ε_r' of the ceramic the coaxial resonator method is very satisfactory. For ceramics having high dielectric constants the $\lambda/4$ coaxial resonators can be used with reasonable accuracy but a small increase in ε_r' may be obtained when eqn (6) is used because of the effect of the open end. The temperature coefficient of resonance frequency was found to be 4 ppm $°C^{-1}$. The values obtained by this method can be used immediately as practical design data.

ACKNOWLEDGEMENTS

The work on this project was undertaken at the Microelectronics Laboratory at the University of Oulu, Finland, and was financed by The Finnish Academy of Sciences.

REFERENCES

1. Hakki, B. W. and Coleman, P. O., A dielectric resonator method of measuring inductive capacities in the millimetre range, *IRE Trans. MTT*, July 1960, 402–10.
2. Plourde, J. K. and Chung-li Ren, Application of dielectric resonators in microwave components, *IEEE Trans. MTT*, **MTT-27**(8) (August 1981) 754–70.
3. Khanna, A. and Garault, Y., Determination of loaded, unloaded and external quality factors of a dielectric resonator coupled to a microstrip line, *IEEE Trans. MTT*, **MTT-31**(3) (March 1983) 261–4.
4. Kemppinen, E. and Leppävuori, S., An X-band doppler module made by thick film techniques. *Proc. 5th European Hybrid Microelectronics Conference*, Stresa, Italy, 1985.
5. Jaakola, T., Möttönen, J., Uusimäki, A., Rautioaho, R. and Leppävuori, S., Comparison of sintering behaviour and resulting microstructure of pre-heated and reaction sintered Nd-doped $Ba_2Ti_9O_{20}$ ceramics for use in microwave resonators, Report S86, 1985, Department of Electrical Engineering, University of Oulu, Finland.
6. Matthaei, G., Young, L. and Jones, E. M. T., *Microwave Filters, Impedance-Matching Networks, and Coupling Structures*, Artech House Inc., Dedham, Massachusetts, 1980.

7. Collin, R. E., *Foundations for Microwave Engineering*, McGraw-Hill Kogakusha Ltd, New York, 1966.
8. *The Microwave Engineers' Handbook and Buyers' Guide*, Horizon House Inc., Massachusetts, 1964.
9. Zverev, A. I., *Handbook of Filter Synthesis*, John Wiley & Sons Inc., New York, 1967.

Received 3 March 1986; accepted 27 March 1986

Int. J. High Technology Ceramics **2** (1986) 157–159

Symposium Report

2ND INTERNATIONAL SYMPOSIUM ON CERAMIC MATERIALS AND COMPONENTS FOR ENGINES, TRAVEMÜNDE, NEAR LUBECK, FRG (14–17 APRIL, 1986)

This meeting followed the 1st Symposium held in Hakone, Japan, in October, 1983. The symposium was under the patronage of the German Ministry for Research and Technology (BMFT) and was co-sponsored by most national ceramic societies. The excellent administration was carried out by the German Ceramic Society (DKG), whilst the technical aspects were in the able hands of the Conference Chairman, Professor Bunk.

The great interest in the subject may be judged from the size of the attendance and the amount of information made available. More than 600 people from all over the world attended the symposium, which offered approximately 40 lectures and over 100 posters, as well as an exhibition with displays from several firms, covering raw materials, component manufacture and application of ceramics in engines (Daimler Benz and Volkswagen).

All activities took place in one very large hotel, which also accommodated most of the participants. There was ample space for the posters, which were displayed throughout the entire conference and could be viewed at any time (authors were available for discussion at set times); a very good scheme because it allowed poster authors to look at the other posters. The quality of posters varied greatly, the worst consisting of nothing more than the pinned-up typed sheets of the manuscript. Similar displays have been noticed at other conferences and it is highly desirable that conference organisers should give guidance as to what is to be expected.

Int. J. High Technology Ceramics (2) (1986)—

Similarly, the standard of the slides used in lectures was often greatly inadequate. Many lecturers used 'typescripted' transparencies on the overhead projectors, which were barely readable from the front and quite undecipherable from the back of the lecture theatre. Again, it is felt that organisers could help by issuing instructions.

Professor Bunk opened the meeting with a progress review of the German ceramic engine project, pointing out that there was now a satisfactory supply of raw materials, and that prototypes of all envisaged ceramic components, e.g. turbine rotors, combustion chambers, valve gear cylinder liners, piston crowns, port liners, etc., have been produced by one or several ceramic manufacturers in silicon nitride, silicon carbide, aluminium titanate or zirconia. The port liner made of aluminium titanate has now been introduced into commercial models of Audi and Porsche. Professor Bunk was responsible for this project during the years 1974–85 with a total spending of 71M DM on a 50/50 basis with industry. A much larger general materials programme has now started which up to 1994 will have a budgeted expenditure of 200M DM. The ceramic part will be concerned with powder processing, reliability of components, composites and the joining of ceramics to metals.

At the Hakone conference, the Japanese announced the introduction of a ceramic turbocharger into a commercial car model. It would appear that there was some delay, but since October 1985, Nissan's Fair Lady incorporates a ceramic turbocharger with its advantage of providing greater acceleration resulting from the lower density of the ceramic. In the USA, Ford were carrying out extensive tests on ceramic turbochargers in cars and Cummins continue with their activity on the uncooled diesel engine for trucks.

In conclusion, it should be said that none of the lectures and posters indicated a dramatic breakthrough but steady progress was being made, although the rate of progress is now probably somewhat slower than was hoped for some years ago.

The full proceedings of the Symposium will be published by the DKG in a volume priced at 145 DM. It was announced that the 3rd Symposium will be held in the USA in 1988.

HANNOVER INDUSTRIAL FAIR (9–16 APRIL, 1986)

This event overlapped with the previously reported symposium. The participants of the symposium must be grateful to the organiser for providing

transport from Travemünde to Hannover, which enabled them to visit this important industrial exhibition during the two days preceding the symposium. From the ceramic point of view, two out of the 24 halls were of particular interest: those devoted to 'Research and Technology' and 'New Materials'. In the first mentioned hall, universities, research institutes and private research organisations exhibited their work and willingly discussed projects with potential customers. Daimler Benz, which now includes Dornier, Motor Turbo Union and AEG, and Volkswagen, indicated their interest in exploring the use of ceramics in gas turbines and reciprocating engines. On a long-term basis, Dornier is experimenting with the production of hydrogen by electrolysis of water, making use of the ionic conductivity of zirconia.

The 'New Materials' exhibition hall was devoted to all types of materials, but ceramics were the most prominent. Besides Feldmühle Hoechst Ceramtec (formerly Rosenthal Technik) and ESK, there were foreign exhibitors from the USA, Japan, UK and France. The main interest centred on engineering ceramics and cutting tools.

Paul Popper

Int. J. High Technology Ceramics **2** (1986) 161–162

Book Review

Ceramic Materials for Advanced Heat Engines: Technical and Economic Evaluation. By D. C. Larsen, L. R. Johnson, J. W. Adams, A. P. S. Teotia and L. G. Hill. Noyes Publications, Park Ridge, New Jersey, 1985. 380 pp. ISBN 0-8155-1029-2. Price: $45.00.

This book is a compilation of two reports, one on the properties of ceramics and a second on an economic analysis of structural ceramics, produced for the Air Force Wright Aeronautical Laboratories and the Department of Energy, respectively. As such, both the strength and weakness of the publication can be traced to the source literature.

The first part of the book is divided into 13 sections, dealing in a most comprehensive manner with the property evaluation and materials characterisation of candidate materials, notably the many forms of silicon nitride and silicon carbide which are available. Of the many properties evaluated the fracture toughness was omitted.

Microstructural characterisation has been limited to optical microscopy, surprising in that the grain size of many of these materials is close to the limit of resolution. Also, since so many of the reported properties depend on the presence of a second phase, particularly a grain boundary phase, it is unusual that electron optical techniques have not been utilised. A specific criticism may be levelled at the standard of the micrographs which is generally very low and in several cases, appalling. At least half of the micrographs could be usefully omitted.

The section on the zirconia ceramics is limited to PSZ-type materials and although SEM was employed to examine fracture surfaces little or no useful information is gained from examination of the micrographs. In the fast developing field of zirconia-based engineering ceramics the properties of the TZP ceramics and the two phase ZrO_2–Al_2O_3 have not been reported.

The second section of the book, dealing with the economic evaluation of

Int. J. High Technology Ceramics (**2**) (1986)—

ceramic materials for engine applications, gives an interesting insight into the possibilities available for ceramics, particularly applied to the US market and where Japan and to a lesser extent Germany are seen as the technological competitors. There are chapters in this section which make interesting reading, particularly on strategic materials, and several translated articles from Japanese newspapers.

As a whole the book suffers from lacking a unified theme. There is a most useful compilation of mechanical data, but little insight is given as to where or how these data might be employed or related to the poorly described microstructures. It is a medium priced book, which might be considered for a library reference section, and would have proved far more useful to a wide section of the ceramics community if the micrographs describing the materials tested had been of a higher quality and had been better reproduced.

R. Stevens

Int. J. High Technology Ceramics **2** (1986) 163–164

Announcement

ISO3: 3RD INTERNATIONAL CONFERENCE/EXHIBITION ON ISOSTATIC PRESSING

Cold isostatic pressing (CIP) and hot isostatic pressing (HIP) collectively are predicted to grow 30–50% in the years ahead, having in the past decade established themselves as viable processes for powder consolidation, and also in the case of HIP, as an indispensable tool for the full densification of castings and rejuvenation of components used in the aerospace industry. Current and future areas of application for CIP and HIP, plus the manufacturing economics of the two processes, will be discussed at the 3rd International Conference on Isostatic Pressing which is to be held at the London Marriott Hotel, Grosvenor Square, London, on November 10–12, 1986.

The conference will cover all aspects of the process, including the development of equipment, process controls, and materials being produced by CIP and HIP. Topics include:

Cold isostatic pressing
—Recent advances in CIP equipment
—Tooling developments for CIP
—Tubular ceramic/metal products
—Cylinder liners
—Refractory nozzles/crucibles
—Filters/porous components
—Non-ferrous alloys
—Tool preforms
—Structural ceramics
—Structural PM parts

Hot isostatic pressing
—Recent advances in HIP equipment
—Process economics
—Densification/healing of castings/hardmetals
—Diffusion bonding/welding
—Rejuvenation (turbine blades)
—High pressure impregnation
—PM superalloys/titanium/aluminium alloys
—High alloy steels
—Cermets/ceramics/composites
—Magnets
—Medical implants
—Rapidly solidified/amorphous alloys

As at previous isostatic pressing conferences organised by MPR there will also be an exhibition area where companies can display their latest developments in presses, tooling, and finished products. The exhibition will as usual form the focal point of the conference and will be used for receptions, coffee breaks, etc.

Further details may be obtained from: Conference Manager, ISO3, MPR Publishing Services Ltd, Old Bank Buildings, Bellstone, Shrewsbury, England SY1 1HU. Tel. 0743 64675. Telex 35213 MPRG.

Int. J. High Technology Ceramics **2** (1986) 167–177

Improvement of Thermal Stability of Yttria-Doped Tetragonal Zirconia Polycrystals by Alloying with Various Oxides

Tsugio Sato, Shiro Ohtaki, Tadashi Endo and Masahiko Shimada

Department of Applied Chemistry, Faculty of Engineering, Tohoku University, Sendai, Miyagi 980, Japan

SUMMARY

Yttria-doped tetragonal zirconia polycrystals doped with 0–12 mol% of CaO, MgO, CeO_2 and TiO_2 were sintered at 1400–1600°C for 3 h, and the mechanical properties and thermal stability of the sintered bodies were evaluated. The degree of the tetragonal-to-monoclinic phase transformation by annealing in humid air or hot water decreased with both increasing amounts of CeO_2 or TiO_2 and decreasing grain size of ZrO_2. Alloying with TiO_2 accelerated the grain growth and depressed densification, but alloying with less than 6 mol% of CeO_2 caused no significant changes in grain size and mechanical properties.

1. INTRODUCTION

Partially stabilized zirconia has excellent mechanical properties such as high strength and high fracture toughness. The martensitic phase transformation from the metastable tetragonal to the stable monoclinic phase is believed to relieve the fracture stress in the vicinity of a crack front.[1–3] Therefore, it is essential to retain the tetragonal phase at room temperature subsequent to sintering to obtain high strength and tough zirconia ceramics. Maximum strength and toughness have been attained with fully tetragonal zirconia polycrystals (TZP), fabricated by doping with 2–3 mol% of Y_2O_3.[3] However, it has been reported that both the strength and the fracture toughness of Y-TZP were greatly degraded by annealing at low temperatures (150–300°C) in air.[4] The loss of fracture

Int. J. High Technology Ceramics 0267-3762/86/$03·50

toughness and strength by annealing is caused by the formation of microcracks accompanying the tetragonal-to-monoclinic phase transformation, which starts from the surface and is particularly enhanced in the presence of water.[5-9] The free energy change of the tetragonal-to-monoclinic phase transformation ($\Delta G_{t\to m}$) can be described by

$$\begin{aligned}\Delta G_{t\to m} &= (G_c^m - G_c^t) + (G_{se}^m - G_{se}^t) + (G_s^m - G_s^t) \\ &= \Delta G_c + \Delta G_{se} + \Delta G_s \end{aligned} \quad (1)$$

where G_c^m and G_c^t, G_{se}^m and G_{se}^t and G_s^m and G_s^t are the chemical free energies, the strain free energies and the surface free energies of the monoclinic and tetragonal phases, respectively. It is expected that the tetragonal-to-monoclinic phase transformation can be controlled by increasing ΔG_c, ΔG_{se} and ΔG_s. It was reported that the degree of the phase transformation depended on the Y_2O_3 content, grain size, etc.; the rate of the phase transformation actually decreased[5-7] with increasing Y_2O_3 content, dispersing Al_2O_3 and decreasing the grain size of ZrO_2.[5-9] It should be noted, however, that increasing the thermal stability sometimes results in loss of strength and fracture toughness, i.e. increasing the Y_2O_3 content to more than 4 mol% prevents the phase transformation during low temperature annealing but causes a significant loss in the fracture toughness.[3] In the present study, Y-TZP doped with various amounts of CaO, MgO, CeO_2 and TiO_2 were fabricated and the characteristics of the sintered bodies such as thermal stability and mechanical properties were evaluated.

2. EXPERIMENTAL

Zirconia powders containing 0, 2, 3, 4 and 6 mol% of Y_2O_3 were supplied by Toyo Soda Co. Ltd. All other chemicals were of analytical grade and were used without further purification. Starting powders were prepared by mixing $ZrO_2(Y_2O_3)$ powders and CaO, MgO, CeO_2 and TiO_2 powders by ball milling with plastic balls in a plastic container in acetone; all powders were then dried. The powders were uniaxially pressed at 100 MPa to form pellets, 5 mm in diameter and 5 mm in thickness, and then sintered at 1400, 1450, 1500 and 1600°C for 3 h in air. The sintered bodies were annealed in a stream of humid air at 100–400°C for 50 h or in water at 130°C for 7 days. The partial pressure of water in air was adjusted to 1·54 and 3·35 kPa by bubbling air through the saturated aqueous solutions of $Ca(NO_3)_2 \cdot 4H_2O$ at 25°C and distilled water at 25°C, respectively.

The phases in the surface of the sample were identified by X-ray diffraction analysis using Ni-filtered Cu–Kα radiation. Scans of 2θ between

27° and 33° were conducted to estimate the monoclinic to (tetragonal + cubic) zirconia ratio, and those between 55° and 62° were used to discriminate between the tetragonal and cubic phase. The bulk density of the sintered bodies was measured by Archimedes' technique. The average grain size was determined from scanning electron micrographs of the fracture surface using the intercept method.[10] Vickers microhardness (H_v) was measured by Vickers indentation with loads from 2 to 5 N. Young's modulus (E) was determined by Knoop indentation with loads of 5 N. Fracture toughness (K_{IC}) was measured using the indentation technique[11] at loads from 10 to 20 N.

3. RESULTS AND DISCUSSION

3.1. Characteristics of as-sintered materials

The phase, grain size, relative density and mechanical properties of as-sintered bodies of ZrO_2–3 mol% Y_2O_3 alloyed with various amounts of CaO, MgO, CeO_2 and TiO_2 sintered at 1500°C for 3 h in air are summarized in Table 1 and Fig. 1. The phases of zirconia in ZrO_2–3 mol% Y_2O_3 alloyed with CeO_2 and TiO_2 were fully tetragonal and those in ZrO_2–3 mol% Y_2O_3 alloyed with CaO and MgO were mixtures of tetragonal

TABLE 1
Phase, Grain Size and Relative Density of As-sintered Bodies of ZrO_2–3 mol% Y_2O_3 Ceramics Alloyed with Various Oxides Sintered at 1500°C for 3 h

Additive	*Content/mol%*	*Phase*[a]	*Grain size/μm*	*Relative density/%*
None	—	t	1·1	99·0
	—	t	0·8	99·3
TiO_2	2	t	2·4	98·1
	5	t	5·1	98·4
	10	t	10·6	96·5
CeO_2	2	t	1·1	99·7
	5	t	1·3	99·3
	10	t	1·4	99·0
CaO	2	t + c	0·5	99·0
	4	t < c	0·5	98·4
	6	t ≪ c	—	95·4
MgO	2	t + c	0·9	98·3
	4	t < c	—	98·5
	6	t ≪ c	—	96·3

[a] t: tetragonal, c: cubic.

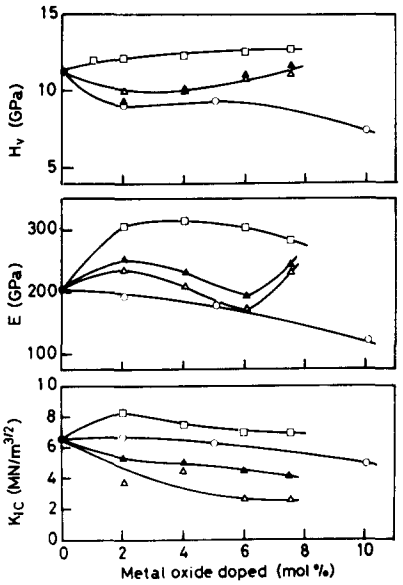

Fig. 1. Vickers microhardness, Young's modulus and fracture toughness of ZrO_2–3 mol% Y_2O_3 ceramics alloyed with various oxides. Metal oxide: CeO_2, □; TiO_2, ○; MgO, ▲; CaO, △.

and cubic. Alloying with CeO_2 resulted in no significant difference in the relative density and grain size, but the values of H_v, E and K_{IC} increased a little. Alloying with TiO_2 resulted in a great increase of grain size and a decrease of relative density. It caused no significant change in K_{IC}, but the values of H_v and E decreased. Alloying with CaO and MgO degraded the value of K_{IC} due to decreasing the tetragonal-ZrO_2 content.

3.2. Tetragonal-to-monoclinic phase transformation in ZrO_2(Y_2O_3) ceramics alloyed with various oxides

ZrO_2–3 mol% Y_2O_3 ceramics alloyed with various amounts of CaO, MgO, CeO_2 and TiO_2 sintered at 1500°C for 3 h were annealed in a stream of air with a partial water vapor pressure of 1·540 kPa at 200°C for 50 h or in water at 130°C for 15–140 h. The amount of monoclinic ZrO_2 formed on the surface of the samples is shown in Figs 2 and 3. Figure 2 shows that the tetragonal-to-monoclinic phase transformation was depressed with increasing amounts of metal oxides added. However, the mechanism controlling the phase transformation seemed to be different. Since no decrease in the rate of the phase transformation to attain equilibrium was found in the ZrO_2–3 mol% Y_2O_3 ceramics alloyed with CaO and MgO, the depression of the phase transformation might be attributed to the

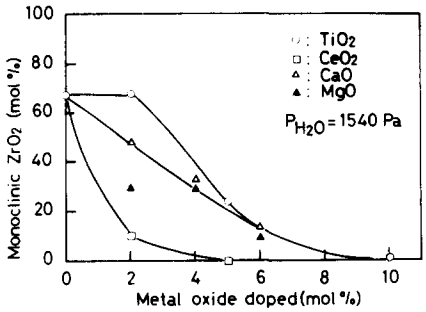

Fig. 2. Amount of monoclinic ZrO_2 formed in ZrO_2–3 mol% Y_2O_3 ceramics alloyed with various oxides by annealing in humid air at 200°C for 50 hours.

smaller amount of the tetragonal-ZrO_2 content in the sintered bodies. It should be noted that the cubic-ZrO_2 content increased with increasing amounts of CaO and MgO added. On the other hand, since ZrO_2–3 mol% Y_2O_3 ceramics alloyed with CeO_2 and TiO_2 were composed entirely of the tetragonal phase as listed in Table 1, CeO_2 and TiO_2 seem to stabilize the tetragonal phase. CeO_2 appeared to be the best oxide for stabilizing the tetragonal ZrO_2 because it caused no significant degradation in sinterability and mechanical properties.

ZrO_2–3 mol% Y_2O_3 ceramics alloyed with various amounts of CeO_2 were sintered at 1400, 1450, 1500 and 1600°C for 3 h to fabricate sintered bodies having different grain sizes. The sintered bodies were annealed in moist air with a partial water vapor pressure of 3·35 kPa at 100–400°C for 50 h. The amount of monoclinic ZrO_2 formed on the surface of the sample is shown in Fig. 4 as a function of annealing temperature. The amount of monoclinic ZrO_2 was at a maximum around 200°C. Both the amount of

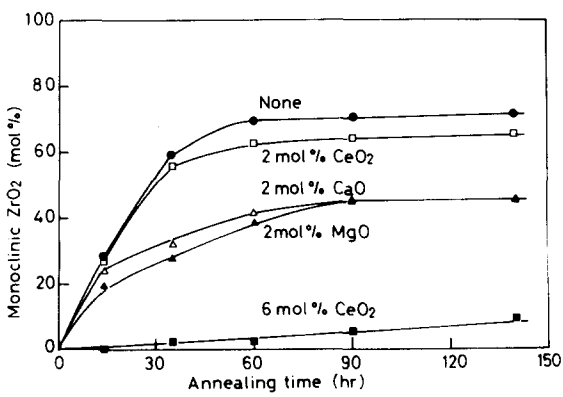

Fig. 3. Time dependence of the amount of monoclinic ZrO_2 formed in ZrO_2–3 mol% Y_2O_3 ceramics alloyed with various oxides by annealing in water at 130°C.

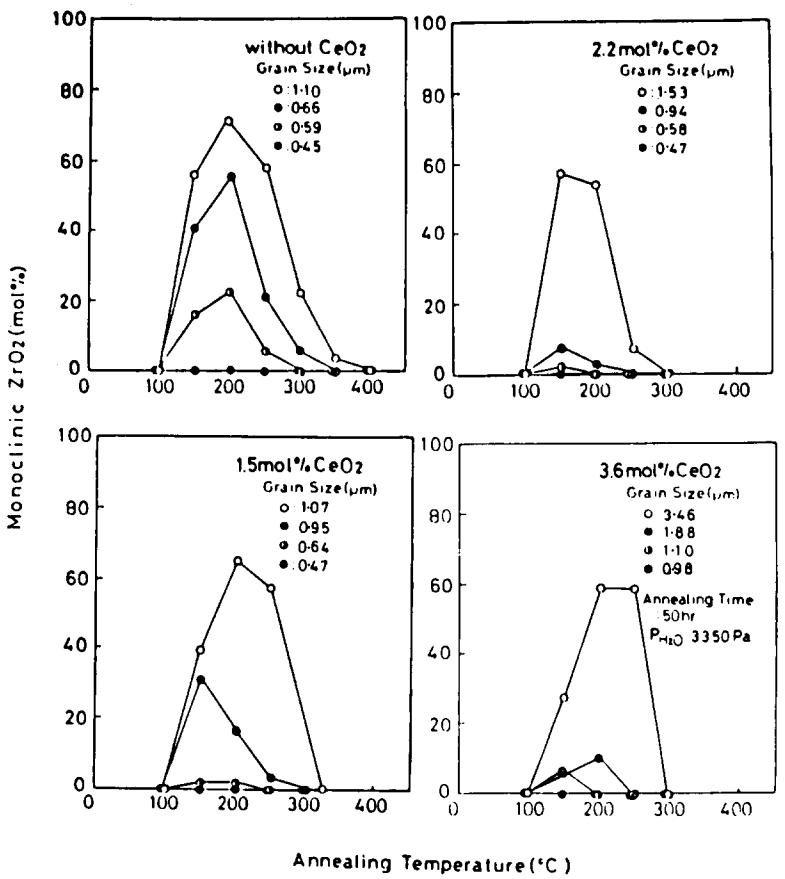

Fig. 4. Relationship between the amount of monoclinic ZrO_2 formed in ZrO_2–3 mol% Y_2O_3 ceramics alloyed with different concentrations of CeO_2 and annealing temperature as a function of grain size.

monoclinic ZrO_2 and the critical temperature (T_c), below which the monoclinic phase was formed, decreased with increasing amount of CeO_2 added and decreasing grain size, as was expected from eqn (1), i.e. ΔG_c increases with increasing amount of CeO_2 added and ΔG_s is inversely proportional to the grain size as given by eqn (2):

$$\begin{aligned}\Delta G_s &= (A_m\gamma_m - A_t\gamma_t)/V \\ &= 6(\gamma_m - g_s\gamma_t)/d \end{aligned} \tag{2}$$

where A_m and A_t are the interfacial surface areas and γ_m and γ_t are the specific surface energies of the monoclinic and tetragonal states, respectively; $V(V = \pi d^3/6)$ is the transformed volume, d is the diameter of the transformed grain and $g_s = A_t/A_m$.

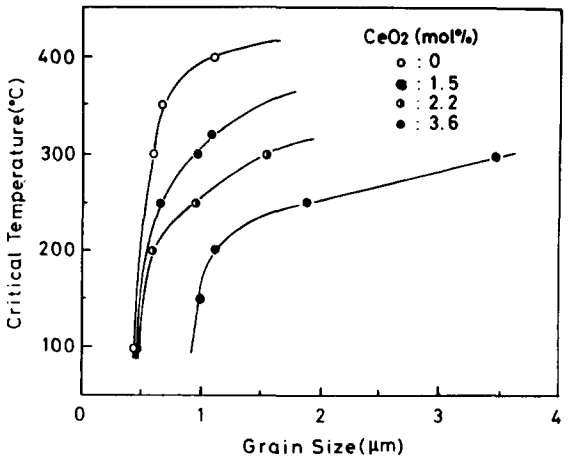

Fig. 5. Relationship between critical temperature and grain size.

By assuming that the value of ΔG_{se} is zero at equilibrium, eqn (1) can be expressed as

$$\Delta G_c + 6(\gamma_m - g_s\gamma_t)/d = 0 \tag{3}$$

If ΔG_c, γ_m and γ_t are expressed as a linear function of temperature (eqns (4)–(6)), eqn (7) can be obtained for the relationship between T_c and the grain size:

$$\Delta G_c = \Delta H_c^\circ - T\Delta S_c^\circ \tag{4}$$

$$\gamma_m = \gamma_m^\circ - \Gamma_m T \tag{5}$$

$$\gamma_t = \gamma_t^\circ - \Gamma_t T \tag{6}$$

$$T_c = \{d + 6(\gamma_m^\circ - g_s\gamma_t^\circ)/\Delta H_c^\circ\}/\{d\Delta S_c^\circ/\Delta H_c^\circ + 6(\Gamma_m - g_s\Gamma_t)/\Delta H_c^\circ\}$$
$$= (d - B)/(dA + C) \tag{7}$$

The relationship between T_c and the grain size is plotted in Fig. 5 and the constants A, B and C determined using the values of T_c and the grain size

TABLE 2
Values of Constants in Eqn (7) and the Grain Sizes Corresponding to $T_c = 298$ K

Concentration of CeO_2/mol%	$A/m\,K^{-1}$	$B/\mu m$	$C/nm\,K^{-1}$	$d/\mu m$ ($T_c = 298$ K)
0	1·38	0·395	−0·474	0·431
1·5	1·55	0·387	−0·508	0·438
2·2	1·55	0·243	−0·118	0·431
3·6	1·70	0·774	−1·18	0·856

as listed in Table 2. Using these values, it is possible to construct a modified phase diagram indicating whether or not the tetragonal-to-monoclinic phase transformation would occur from the surface of the sintered body. The relationship between T_c and the amount of CeO_2 in ZrO_2–3 mol% Y_2O_3 ceramics is illustrated in Fig. 6 as a function of grain size. It is seen that T_c decreases with decreasing grain size and increasing amount of CeO_2. To confirm these results, ZrO_2–3 mol% Y_2O_3 ceramics alloyed with

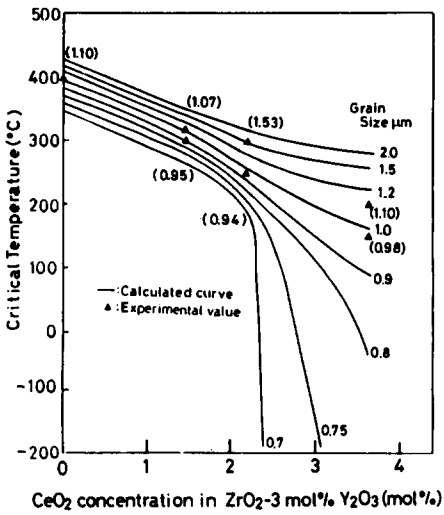

Fig. 6. Relationship between critical temperature and concentration of CeO_2 as a function of grain size.

various amounts of CeO_2 having various grain sizes were annealed in water at 100°C for 7 days; the amount of monoclinic ZrO_2 formed is shown in Fig. 7. The shaded part indicates the region where the tetragonal-to-monoclinic phase transformation did not occur at all. It is obvious that the stability of the tetragonal ZrO_2 strongly depends on both the amount of CeO_2 alloyed and the grain size, especially for grain sizes below 1 μm. It is important to note that the phase transformation is completely controlled by a grain size less than 0·4 μm without any addition of CeO_2. The thermal stability of the tetragonal phase was also evaluated by using zirconia ceramics alloyed with different concentrations of Y_2O_3 and CeO_2. The amount of the monoclinic phase formed by annealing in water at 100°C for 7 days is shown in Fig. 8. The degree of phase transformation decreased with increasing concentration of both Y_2O_3 and CeO_2, i.e. the amount of CeO_2 that could completely control the phase transformation decreased from 12 to 0 mol% on increasing the Y_2O_3 concentration from 0 to 6 mol%.

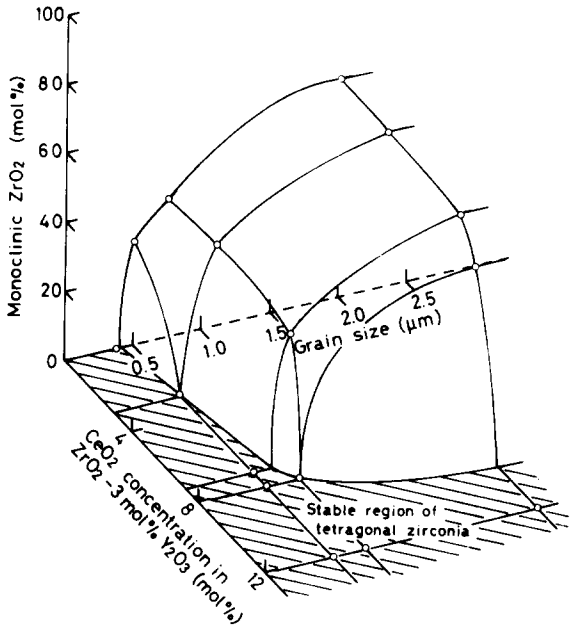

Fig. 7. Relationship of the amount of monoclinic phase formed in ZrO_2–3 mol% Y_2O_3 by annealing in water at 100°C for 7 days, grain size, and CeO_2 concentration.

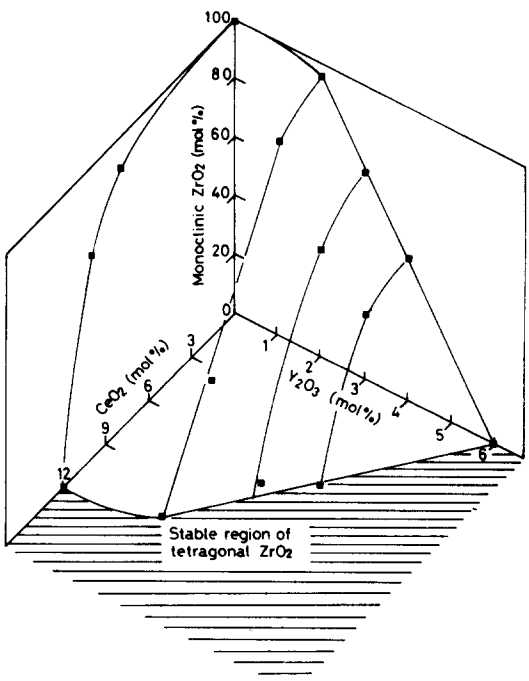

Fig. 8. Relationship of the amount of monoclinic phase formed by annealing in water at 100°C for 7 days and the concentrations of Y_2O_3 and CeO_2.

4. CONCLUSIONS

1. Alloying with TiO_2 stabilized the tetragonal-ZrO_2 phase in $ZrO_2(Y_2O_3)$ ceramics.
2. Alloying CeO_2 stabilized the tetragonal-ZrO_2 phase in $ZrO_2(Y_2O_3)$ ceramics without loss of the mechanical properties.
3. The stability of the tetragonal phase in $ZrO_2(Y_2O_3$–$CeO_2)$ ceramics increased with increasing amounts of Y_2O_3 and CeO_2 and decreasing grain size.

ACKNOWLEDGEMENTS

The authors are indebted to the management of Toyo Soda Co. Ltd for supplying the starting powders used in the present study. The authors would also like to express their appreciation to Mr H. Matsuo for his contributions to the experiments. This work was partly supported by a Grant of Aid for Scientific Research of the Ministry of Education.

REFERENCES

1. Garvie, R. C., Hannink, R. H. J. and Pascoe, R. T., Ceramic steel?, *Nature* (*London*), **258** (1975) 703–4.
2. Porter, D. L. and Heuer, A. H., Mechanism of toughening partially stabilized zirconia ceramics (PSZ), *J. Am. Ceram. Soc.*, **60** (1977) 183–4.
3. Lange, F. F., Transformation toughening, *J. Mater. Sci.*, **17** (1982) 225–34, 235–9, 240–6, 247–54, 255–62.
4. Kobayashi, K., Kuwajima, H. and Tsukidate, T., Thermal and mechanical properties of ZrO_2–Y_2O_3 solid electrolyte after aging, *Solid State Ionics*, **3–4** (1981) 489–93.
5. Sato, T. and Shimada, M., Crystalline phase change in yttria-partially-stabilized zirconia by low-temperature annealing, *J. Am. Ceram. Soc.*, **67** (1984) C212–13.
6. Sato, T., Ohtaki, S. and Shimada, M., Transformation of yttria partially stabilized zirconia by low temperature annealing in air, *J. Mater. Sci.*, **20** (1985) 1466–70.
7. Sato, T. and Shimada, M., Transformation of yttria-doped tetragonal ZrO_2 polycrystals by annealing in water, *J. Am. Ceram. Soc.*, **68** (1985) 356–9.
8. Sato, T. and Shimada, M., Transformation of ceria-doped tetragonal zirconia polycrystals by annealing in water, *Am. Ceram. Soc. Bull.*, **64** (1985) 1382–4.
9. Tsukuma, K. and Shimada, M., Thermal stability of Y_2O_3-partially stabilized zirconia (Y-PSZ) and Y-PSZ/Al_2O_3 composites, *J. Mater. Sci. Lett.*, **4** (1985) 857–61.

10. Fullman, R. L., Measurement of particle sizes in opaque bodies, *Trans AIME*, **197** (1953) 447–52.
11. Niihara, K., Morena, R. and Hasseleman, D. P. H., Evaluation of K_{IC} of brittle solid by the indentation method with low crack-to-indent ratios, *J. Mater. Sci.*, **1** (1982) 13–16.

Received 3 January 1986; accepted 5 May 1986

Int. J. High Technology Ceramics **2** (1986) 179–193

The Effect of Post-Creep Thermal Treatment on Cavitation Damage

R. A. Page and J. Lankford

Southwest Research Institute, 6220 Culebra Rd, San Antonio, Texas 78284, USA

SUMMARY

Small-angle neutron scattering measurements have shown that nucleation and growth of grain boundary cavities occurs, in many ceramics, during the early stages of creep. Subsequent failure generally transpires by cavity coalescence to form cracks, followed by growth of the cracks. The effect on creep cavity populations of thermal treatment, both with and without pressure, has been investigated by comparing cavity distributions obtained from small-angle scattering measurements performed before and after the thermal treatments. The results of these measurements indicate that creep cavities can be removed if sufficient temperature and pressure are applied. From the results obtained on a sintered alumina and a hot-pressed silicon carbide, it appears that hydrostatic pressures approximately equal to the creep stress are required to afford substantial cavity sintering. The use of insufficient pressure not only fails to sinter the cavities formed during prior creep but has also been shown to lead to the nucleation of additional cavities, thus, apparently, increasing the level of damage.

1. INTRODUCTION

Creep failure of polycrystalline ceramics frequently occurs by grain boundary cavitation, which involves the individual processes of cavity nucleation, cavity growth, and cavity coalescence. The early stages of creep are generally dominated by cavity nucleation and growth. In this regime, increases in the number and/or size of cavities are responsible for reductions in the remaining creep life. Hence, if in some way the number and/or size of

Int. J. High Technology Ceramics 0267-3762/86/$03·50

cavities were reduced, one would expect to regain at least a significant portion of the lost lifetime.

The operative cavitation mechanism in ceramics is thought to vary with the grain boundary microstructure.[1] Ceramic systems with glass-free grain boundaries are thought to cavitate by diffusive growth, while a viscous mechanism has been postulated for systems that contain a glassy grain boundary phase. Examination of the pore growth theories suggests a means by which the pores may be removed. For diffusive growth, the rate of increase of cavity radius, $\dot{R}$, is approximately[2]

$$\dot{R} \sim \frac{2\pi D_g Z(\sigma_n - P - 2\gamma/R)\Omega S}{kTlR} \tag{1}$$

where D_g is the grain boundary diffusion coefficient, Z is the grain boundary thickness, Ω the atomic volume, l the cavity spacing, R the cavity radius, σ_n the normal stress on the grain boundary, P the hydrostatic pressure, γ the surface energy, k is Boltzman's constant, T is temperature, and S is approximately unity for expected values of R/l. For viscous growth, the rate of increase of cavity radius is given similarly by[3]

$$\dot{R} = \frac{(2\sqrt{3}l^2 - \beta\pi R^2)h^2[\sigma_n - 2\gamma_s K(1 - 0{\cdot}9\alpha^2)]}{12\pi\eta l^2 \beta R[0{\cdot}96\alpha - \ln\alpha - 0{\cdot}23\alpha^4 - 0{\cdot}72]} \tag{2}$$

where $\alpha = R/l$, β is a geometrical parameter equal to one for a penny-shaped cavity and two thirds for an oblate spheroid cavity, η and h are the viscosity and thickness, respectively, of the glassy phase, and

$$K = \frac{1}{R} + \frac{2}{h}\left[\frac{\gamma_b - \gamma_i}{\gamma_s}\right] \tag{3}$$

where γ_s, γ_b and γ_i are the energies of the glassy-film-free surface, the grain boundary, and the glassy film/grain boundary interface, respectively. It is evident from eqns (1) and (2) that in the absence of a normal traction across the grain boundary ($\sigma_n = 0$), the surface tension will act to sinter the cavities. Hence, the theory suggests that thermal hold periods with no applied load should provide a means by which the cavities can be reduced in size, if not totally eliminated. Additionally, the application of a hydrostatic pressure during the thermal treatment should accelerate cavity sintering.

This paper presents the results of a series of experiments designed to determine the extent of cavity sintering that can be expected during thermal hold periods at the creep temperature, both with and without an applied hydrostatic pressure. To evaluate fully cavity sintering it is necessary to determine both the size, or size distribution, and the number of cavities, and to do so with a large enough sample so that the results have statistical

significance. Small-angle neutron scattering (SANS) is the only technique presently available that can provide a statistically significant measure of both the number and the size of cavities, and it has been used successfully to characterize cavity distributions in metals[4-9] and ceramics,[10-12] arising from irradiation, fatigue, and creep. Hence, SANS was employed in the cavity characterizations performed in this study.

2. EXPERIMENTAL

2.1. Materials

Two materials were included in this study: a hot-pressed silicon carbide (NC 203, Norton Company, Worcester, MA, USA) and a sintered alumina (Lucalox, General Electric Lamp Glass Division, Cleveland, OH, USA). References 11 and 12 should be referred to for a detailed description of the microstructures of these two materials. Suffice it to say that the results of the previous characterizations indicated: (a) that the hot-pressed silicon carbide contained a thin, continuous grain boundary phase, it thus being representative of the liquid-phase sintered materials in which cavity growth is thought to occur by a viscous hole growth process; and (b) that the sintered alumina contained no glassy grain boundary phase, and was thus representative of the single-phase materials in which cavity growth is most likely a grain boundary diffusion process. Additionally, the microstructures of both materials were shown to be stable at the temperature employed for both creep and post-creep thermal treatment in this study.

2.2. Creep tests

Compression creep specimens were fabricated in the form of right-circular cylinders, 6·4 mm in diameter and 12·7 mm long. Creep testing was performed at 1600 °C in a servo-controlled hydraulic test machine equipped with a controlled environment (titanium-gettered argon) resistance furnace. The silicon carbide and alumina specimens were crept at compressive stresses of 570 and 140 MPa, respectively. The individual test durations are listed in Table 1. At the completion of each test the specimens were rapidly cooled to room temperature before being unloaded in order to freeze in the cavity distribution present at the test temperature.

A comparison of the effects of post-creep thermal treatment ideally should be performed on specimens with identical initial states of damage. Unfortunately, well-characterized specimens with identical creep strains were not available for these comparisons. However, it is believed that the

TABLE 1
Creep Conditions of Samples Examined

Sample number	*Material*	*Temperature/°C*	*Stress/MPa*	*Time/h*	*Creep strain*
A-1	Alumina	1 600	140	6·0	0·016 8
A-2	Alumina	1 600	140	8·8	0·033 8
A-3	Alumina	1 600	140	3·3	0·027 0
A-4	Alumina	1 600	140	3·5	0·028 0
S-1	Silicon carbide	1 600	570	25	0·018 7
S-2	Silicon carbide	1 600	570	37	0·018 9
S-3	Silicon carbide	1 600	570	12	0·007 98

variation in creep strain of the specimens employed in this study would not qualitatively affect the reported results.

2.3. SANS measurements

Rectangular flats, 5 mm × 12·7 mm, were ground and polished on opposite sides of the specimens following creep. This procedure yielded specimens approximately 3·7 mm thick, as measured between the parallel flats. Final polishing was performed such that grain pullout was minimized and a similar surface finish was achieved on each specimen.

The small-angle scattering measurements, which were performed on the 30-m instrument at the National Center for Small-Angle Scattering Research at Oak Ridge National Laboratory,[13] utilized an incident neutron wavelength, λ, of 0·475 nm, and sample to detector distances of 9 m and 16·5 m. This yielded intensity data at scattering vectors, $\mathbf{q}$, from 0·037 nm^{-1} to 0·2 nm^{-1}, where $\mathbf{q} = 4\pi \sin\theta/\lambda$ and 2θ is the scattering angle. Parasitic scattering effects arising from electronic background and the empty specimen holder, as well as non-uniform detector sensitivity, were corrected for as described in Reference 7. The corrected data were radially averaged and then converted to a macroscopic differential scattering cross-section, $d\Sigma/d\Omega$, by calibration in reference to the scattering cross-section of voids in a well-characterized irradiated aluminum sample.[4]

2.4. Post-creep thermal treatment

Following the SANS characterization of the creep cavity distribution, one sample of each material was held for 24 h at 1600 °C, the creep temperature, with no applied load, one sample of each material was held for 24 h at 1600 °C with an applied hydrostatic stress of 34 MPa, and one sample of

TABLE 2
Thermal Treatments

Sample number	*Material*	*Treatment conditions*		
		Temperature/°C	*Pressure/MPa*	*Time/h*
A-1	Alumina	1 600	—	24
A-2	Alumina	1 600	34	24
A-3	Alumina	1 600	240	4
A-4	Alumina	No thermal treatment performed		
S-1	Silicon carbide	1 600	—	24
S-2	Silicon carbide	1 600	34	24
S-3	Silicon carbide	1 600	240	4

each material was held for 4 h at 1600 °C with an applied hydrostatic stress of 240 MPa. It should be noted that the latter pressure was well above the alumina creep stress level, but only about half that for the silicon carbide creep tests. In addition to the six samples which received post-creep treatments, a single alumina sample was left in the as-crept condition to determine the repeatability of the SANS measurements. The post-creep thermal treatments employed for each sample are listed in Table 2. Following these treatments, the cavity distributions were again characterized by SANS as described above.

3. RESULTS

At the present time there exists no precise method to define the degree of damage based on a knowledge of the cavitation state. Nonetheless, it is possible to identify a number of parameters upon which the damage state should depend. If we confine ourselves to the early stages of creep, which is the regime where SANS is most effective, damage accumulation is truly a bulk phenomenon, and bulk parameters such as cavity density (number of cavities per unit volume) and volume fraction (total cavity volume per unit volume) should be of critical importance in defining damage. (During the intermediate and final stages of creep, local parameters such as the size of the largest cavity or cavity cluster, or the average spacing within a cluster, may be more appropriate measures of damage.) Changes in the bulk cavitation parameters will therefore be stressed in the following section. Measurements of average cavity size will also be included for added insight.

It should be noted that assessing relative degrees of damage in various specimens is a process fraught with possible ambiguity. For example, the

cavitated volume may increase while cavity density decreases; this would certainly be accompanied by an increase in average cavity size ($\bar{R}$), as well as in the actual number of cavities of this size. On the other hand, suppose V_c/V decreases, and so does N_c/V; if the latter is accomplished principally by the sintering of the smaller cavities in the distribution, $\bar{R}$ will increase, while the number of such cavities will remain roughly constant, or even decrease. In

TABLE 3
Cavity Parameters Calculated from the SANS Data

Sample number	*Sample condition*	$V_c/10^{-3}V$	$(N_c/V)/\mu m^3$	R_G/nm	R_p/nm
A-1	Crept	0·082 3	0·053 3	80·9	71·8
A-1	Crept and annealed without pressure	0·096 2	0·084 0	80·6	61·1
A-2	Crept	0·100	0·067 2	79·5	71·3
A-2	Crept and hipped (34 MPa)	0·131	0·118	80·3	54·6
A-3	Crept	0·155	0·181	79·6	55·8
A-3	Crept and hipped (240 MPa)	0·058 1	0·036 2	87·8	71·1
A-4	Crept	0·090 5	0·085 4	80·8	63·4
A-4	Crept	0·091 0	0·085 2	81·6	63·4
S-1	Crept	6·49	9·85	72·4	57·6
S-1	Crept and annealed without pressure	5·60	16·1	67·5	42·1
S-2	Crept	4·85	5·38	73·2	64·3
S-2	Crept and hipped (34 MPa)	4·03	8·55	68·6	42·1
S-3	Crept	1·89	4·61	74·4	47·5
S-3	Crept and hipped (240 MPa)	1·65	5·12	71·9	42·0

the first case cited, an increase in $\bar{R}$ reflects a real increase in cavitated volume, while in the second, it does not. In a similar manner, a decrease in $\bar{R}$ would represent an increase in either the actual, or the relative, number of small cavities present.

The results of the SANS measurements are listed in Table 3. The methods used for determining the cavity volume fraction, V_c/V, the cavity density, N_c/V, the radius of gyration, R_G, and the Porod radius, R_p, are described in the Appendix.

3.1. Data repeatability

As mentioned in Section 2, specimen A-4 was employed to check the repeatability of the SANS results. This sample's cavity distribution was originally measured together with the other as-crept samples and then remeasured, without undergoing any post-creep treatment, with the hipped specimens. Comparison of the results of the two separate measurements of specimen A-4 indicates that the SANS measurements are indeed highly repeatable; maximum variation between the two sets of measurements was less than 1 %.

3.2. Post-creep treatment of sintered alumina

As shown in Table 3, thermal treatment of the alumina for 24 h at 1600 °C in the absence of a hydrostatic pressure did not remove, and in fact actually increased, cavity damage, resulting in a 16 % increase in the cavity volume fraction, a 58 % increase in the cavity density, a 15 % decrease in R_p, and no change in R_G. The use of a hydrostatic pressure of 34 MPa worsened the damage state still further, yielding a 31 % increase in cavity volume fraction, a 75 % increase in cavity density, and a 23 % decrease in R_p. Application of a hydrostatic pressure of 240 MPa, on the other hand, resulted in a dramatic reduction in both the cavity density and volume fraction; after 4 h at 240 MPa, the cavity density and volume fraction had decreased by 80 and 63 %, respectively. This decrease resulted in a cavity density and volume fraction substantially below that present prior to creep.

Cavity size distributions for the alumina samples are presented in Fig. 1. These distributions clearly show the increase in total cavity number which occurred upon either pressureless annealing or low pressure hipping, Fig. 1(a) and (b). It also is evident that the largest increase occurred near the peak of the distributions. Thus, the observed decrease in R_p was the result of an actual increase in the number of smaller cavities, rather than a decrease in the number of larger cavities through sintering. The distributions in Fig. 1(c), on the other hand, clearly show the reduction in cavity density brought about by higher pressure hipping; a slight shift of the distribution toward larger diameters is also apparent. In combination, these observations suggest that removal of the smaller cavities occurred more efficiently, and also that growth of some of the largest cavities had occurred.

3.3. Post-creep treatment of hot-pressed silicon carbide

Thermal treatment of the silicon carbide for 24 h at 1600 °C in the absence of a hydrostatic pressure provided mixed results (Table 3); the cavity volume

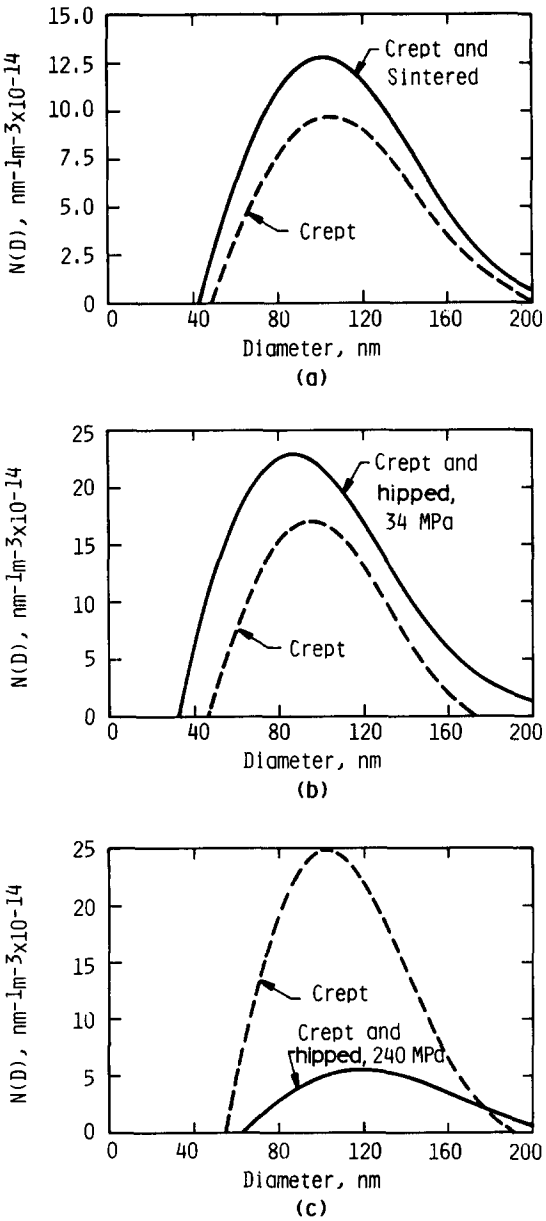

Fig. 1. Cavity size distributions for alumina specimens before and after post-creep treatment, illustrating the effect of (a) annealing without pressure, (b) hipping at 34 MPa, and (c) hipping at 240 MPa.

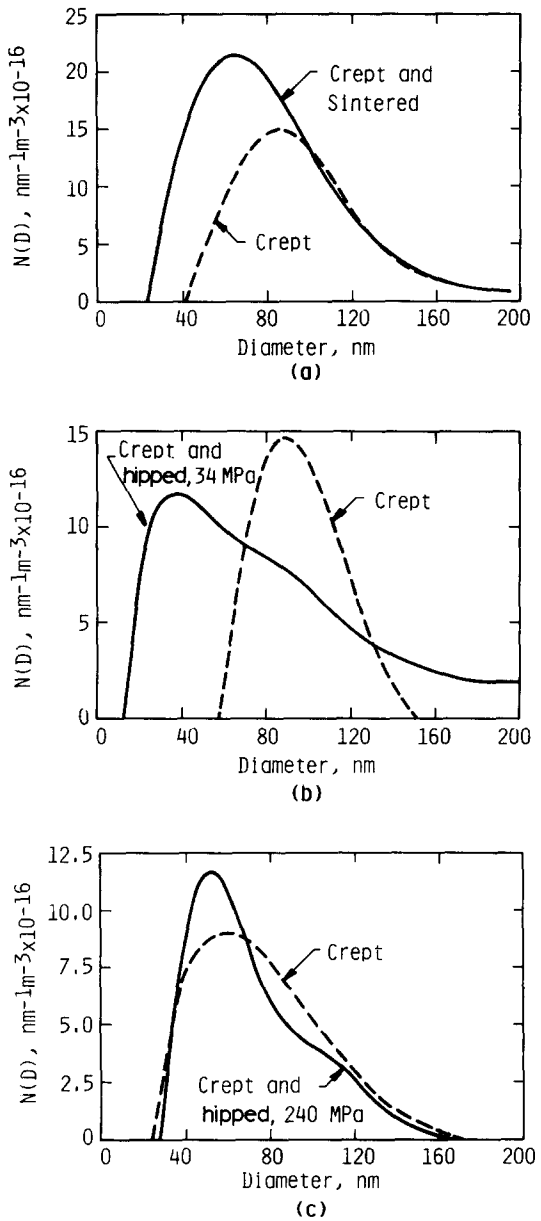

Fig. 2. Cavity size distributions for silicon carbide specimens before and after post-creep treatment, illustrating the effect of (a) annealing without pressure, (b) hipping at 34 MPa, and (c) hipping at 240 MPa.

fraction, R_G, and R_p decreased by 14, 7, and 27%, respectively, while the cavity density increased by 64%. Thermal treatment with a moderate hydrostatic pressure (34 MPa) yielded results very similar to those obtained with no pressure; cavity volume fraction, R_G, and R_p decreased by 17, 6, and 35%, respectively and cavity density increased by almost 59%. Application of a relatively high hydrostatic pressure resulted in a 15% decrease in cavity volume fraction, a slight decrease in R_G and R_p, and a 10% increase in cavity density.

Cavity size distributions for the silicon carbide samples are presented in Fig. 2. Comparison of the size distributions obtained following creep with those following the post-creep thermal treatments, Fig. 2(a), indicates that the increase in cavity density which occurred during thermal treatment was the result of the formation of additional cavities ranging from 20 to 100 nm in diameter. The number of cavities larger than 100 nm in diameter remained essentially constant during thermal treatment. The evolution of the cavity distribution during the low pressure hipping, Fig. 2(b), was considerably more complex. The number of small (≤ 60 nm) and large (≥ 130 nm) cavities and the total number of cavities increased, while the number of cavities between 60 nm and 130 nm decreased. This behavior suggests that three processes—cavity sintering, cavity growth and cavity nucleation—occurred simultaneously. Hipping at the higher pressure eliminated most, if not all, of the cavity nucleation and growth observed at the lower pressure. The only significant alteration of the cavity distribution upon hipping at 240 MPa, Fig. 2(c), was a reduction in the number of intermediate sized cavities (70–110 nm), and a subsequent increase in the number of small cavities (< 70 nm) which, most likely, occurred through sintering.

4. DISCUSSION

The results presented above indicate that removal of prior creep damage in the form of grain boundary cavitation is possible if the proper combination of time, temperature, and hydrostatic pressure is employed. This is clearly demonstrated by the response of the alumina hipped at 1600°C and 240 MPa. Four hours of this pressure/temperature combination reduced the cavitation level to a point below that present prior to creep. However, the results also suggest that the wrong choice of conditions can lead to increased, rather than decreased, damage levels. An increased damage level was quite obvious in the alumina samples that were annealed with no applied pressure, or hipped at 34 MPa. In both instances the cavity density and volume fraction increased as a result of the thermal treatment. An increased

damage level also probably occurred in the silicon carbide samples that were annealed with no applied pressure or hipped at 34 MPa. Although the cavity volume fraction decreased slightly, the cavity density increased dramatically during treatment. It is therefore important that a judicious choice of treatment conditions be made.

The observed removal of cavities during the 240 MPa hipping of sintered alumina is entirely consistent with our present understanding of cavity growth/sintering and, therefore, requires no further discussion. The nucleation of cavities observed during pressureless annealing and hipping (34 MPa) of both alumina and silicon carbide, however, deserves additional comment. The obvious question that comes to mind is whether the nucleation of cavities, as identified by SANS, could be an artifact of the measurement technique. Previous studies[11,12] have shown that the two materials included in this study are microstructurally stable at 1600 °C and, additionally, have demonstrated quite good correlation between SANS-generated cavitation parameters and similar parameters obtained independently by electron microscopy and precision density measurements. It thus can be concluded that the SANS measurements are truly indicative of an increase in the number of cavities of approximately 100 nm or less in radius. An obvious alternative to the proposed nucleation would be the shift of cavities from above, to below, the upper SANS detection limit, thus increasing the number of cavities detected, but with no actual increase in the number present. A simple calculation performed for sample S-1 indicates that if the additional cavities, which number 9·77 μm^{-3}, were the result of the shrinkage of cavities from slightly above ($R \approx 100$ nm) to slightly below ($R \approx 75$ nm) the upper detection limit, then a net density change of 2·4 % would occur. Although a density change of this magnitude would be easily detectable, precision density measurements performed before and after the thermal treatments showed no measurable change. Thus, it is apparent that the measured cavity increase could not have come from the sintering of larger cavities and, therefore, must have resulted from cavity nucleation, as postulated.

The most logical explanation of cavity nucleation during thermal treatment centers around the presence of local residual stresses which were either locked in following the creep loading, or induced by local rearrangements during treatment. Residual microstresses have been shown to nucleate cavities in metals during subsequent annealing,[14-16] and a similar process could be operating in the ceramic materials of this study. At this point, however, such arguments are purely speculative. Additional work is needed to identify the mechanism of cavity nucleation in ceramics during thermal annealing.

One can also speculate as to the reasons for the absence of significant

cavity shrinkage during most of the thermal treatments. Similar results have been obtained by Stevens and Flewitt[17] in a nickel–2 % chromium alloy. The presence of an internal gas pressure is one possible means of balancing the surface tension and thus inhibiting cavity shrinkage. However, we doubt that this is the present case. An alternative, and more reasonable explanation for the lack of sintering, can be obtained from the concepts of matrix constraint. As pointed out by Raj and Ghosh,[18] cavity growth in a polycrystalline material can be constrained by the surrounding uncavitated material. In this situation the cavity growth rate is controlled by the bulk creep rate. Since the creep rates at 1600 °C and zero (or low) applied pressure should be near zero, it is likely that matrix constraint severely inhibits cavity sintering. If matrix constraint is indeed important, one would expect significant cavity shrinkage rates only at high hydrostatic pressures, which could produce significant matrix creep, as was observed for the alumina sample hipped at 240 MPa. Conversely, 240 MPa is insufficient pressure to produce significant creep, and attendant cavity shrinkage, in the silicon carbide initially crept at 570 MPa. Higher stresses or temperatures thus would be needed for cavity removal in this material.

5. CONCLUSIONS

The following conclusions can be drawn from the results obtained in the present investigation:

1. Removal of creep damage, that is, grain boundary cavities, can be achieved at the creep temperature, provided a sufficient hipping stress is employed.
2. Reduction of the damage level occurs by a reduction in both the cavity volume fraction and the number of cavities.
3. Thermal treatments performed with insufficient hydrostatic pressure can lead to an increased damage level, which occurs primarily through cavity nucleation during the thermal treatment.

ACKNOWLEDGEMENTS

The authors are grateful to the Department of Energy, Office of Basic Energy Sciences, for support of this work, under Grant No. DE-FG05-84ER45063. We also thank the staff of the National Center for Small-Angle Scattering Research for their assistance in this project.

APPENDIX

Standard methods for analyzing small-angle scattering data were used to determine the radius of gyration, R_G, the Porod radius, R_p, and the total cavity volume, V_c/V. The equations employed in the analyses are presented below. Reference 19 should be consulted for a more complete description of these methods, and for an explanation of scattering theory. References 11 and 12 should be consulted for a description of the subtraction techniques employed.

For the case of a dilute distribution of non-interacting scatterers the invariant is proportional to the total cavity volume as

$$\int_0^\infty \frac{d\Sigma}{d\Omega} q^2 \, dq = 2\pi^2 (\Delta\rho)^2 \frac{V_c}{V} \tag{A1}$$

where $d\Sigma/d\Omega$ is the macroscopic differential scattering cross-section and $\Delta\rho$ is the scattering length density difference between a cavity and the matrix. Since the measured data extended into both the Guinier and Porod regions, it was possible to extrapolate the scattering curves such that the q range from zero to infinity was covered, and thus permit evaluation of the invariant.

The Porod radius was determined from

$$R_p = \frac{\frac{3}{\pi} \int_0^\infty q^2 \frac{d\Sigma}{d\Omega} dq}{\lim_{q \to \infty} q^4 \frac{d\Sigma}{d\Omega}} \tag{A2}$$

In eqn (A2) the Porod radius is equal to $\langle R^3 \rangle / \langle R^2 \rangle$, where R is the void radius and $\langle \ \rangle$ denotes an average over the ensemble.

A second measure of the size of the pores, the radius of gyration, was calculated from the slope of $\ln(d\Sigma/d\Omega)$ vs q^2 in the Guinier region as

$$\ln \frac{d\Sigma}{d\Omega} = A - \frac{R_G^2}{3} q^2 \tag{A3}$$

For spherical scatterers, the square of the radius of gyration is equal to $3\langle R^8 \rangle / 5\langle R^6 \rangle$. Hence, both R_p and R_G are moments which lie toward the high end of the size distribution.

Cavity size distributions were obtained from the SANS data by the transformation method developed by Letcher and Schmidt[20] and Fedorova and Schmidt.[21] For the case of single scattering from spherical pores the number density function, $N(D)$, is given by

$$N(D) = \frac{1}{D^2} \int_0^\infty \left[q^2 \frac{d\Sigma}{d\Omega}(q) - C_4 \right] \phi(qD) \, dq \tag{A4}$$

where

$$\phi(x) = \cos 2x\left[1 - \frac{2}{x^2}\right] - \frac{2\sin 2x}{x}\left[1 - \frac{1}{2x^2}\right] \tag{A5}$$

and C_4 is the Porod constant. Equation (A4) was numerically evaluated using the measured $d\Sigma/d\Omega$ values over the q range available and extrapolating the $d\Sigma/d\Omega$ values in the high q regime by the method developed by Brill and Schmidt,[22] and by the Guinier approximation in the low q regime. Absolute values of $N(D)$ were obtained by normalizing with respect to the total surface area determined independently from the Porod constant.

The number of cavities per unit volume, N_c/V, was obtained by integrating the absolute number density function with respect to D, the cavity diameter.

$$\frac{N_c}{V} = \int_0^\infty N(D)\,dD \tag{A6}$$

REFERENCES

1. Evans, A. G. and Rana, A., High temperature failure mechanisms in ceramics, *Acta Met.*, **28** (1980) 129–41.
2. Hull, D. and Rimmer, D. E., The growth of grain boundary voids under stress, *Phil. Mag.*, **4** (1959) 673–89.
3. Raj, R. and Dang, C. H., De-adhesion by the growth of penny-shaped bubbles in an adhesive layer, *Phil. Mag.*, **32** (1975) 909–22.
4. Hendricks, R. W., Schelten, J. and Schmatz, W., Studies of voids in neutron-irradiated aluminum single crystals—II. Small angle neutron scattering, *Phil. Mag.*, **30** (1974) 819–37.
5. Saegusa, T., Weertman, J. R., Cohen, J. B. and Roth, M., Small-angle neutron scattering from pores produced in high-temperature fatigue, *J. Appl. Cryst.*, **11** (1978) 602–4.
6. Kettunen, P. O., Lepisto, T., Kostorz, G. and Goltz, G., Voids produced by fatigue in copper single crystals of ⟨111⟩-orientation, *Acta Met.*, **29** (1981) 969–72.
7. Page, R. A., Weertman, J. R. and Roth, M., Small-angle neutron scattering study of fatigue induced grain boundary cavities, *Acta Met.*, **30** (1982) 1357–66.
8. Yoo, M. H., Ogle, J. C., Borie, B. S., Lee, E. H. and Hendricks, R. W., Small-angle neutron scattering study of fatigue induced cavities in nickel, *Acta Met.*, **30** (1982) 1733–42.
9. Cabanas-Moreno, J. G., Yang, M. S., Weertman, J. R., Roth, M., Zhang, Z. H., Wignall, G. D. and Koehler, W. C., Studies of grain boundary cavitation by small-angle neutron scattering, in *Fatigue Mechanisms: Advances in Quantitative Measurement of Physical Damage*, ASTM STP 811, Eds J.

Lankford, D. L. Davidson, W. L. Morris and R. P. Wei, ASTM, Philadelphia, 1983, 95–114.
10. Page, R. A. and Lankford, J., Characterization of creep cavitation by small-angle neutron scattering, *J. Am. Ceram. Soc.*, **66** (1983) C-146–8.
11. Page, R. A., Lankford, J. and Spooner, S., Small-angle neutron scattering study of creep cavity nucleation and growth in sintered alumina, *J. Mat. Sci.*, **19** (1984) 3360–74.
12. Page, R. A., Lankford, J. and Spooner, S., Nucleation and early-stage growth of creep cavities in hot-pressed silicon carbide, *Acta Met.*, **32** (1984) 1275–86.
13. Koehler, W. C. and Hendricks, R. W., The United States national small-angle neutron scattering facility, *J. Appl. Phys.*, **50** (1979) 1951.
14. Dyson, B. F., Profuse decohesion at grain boundaries in nimonic 80A, *Can. Met. Quart.*, **13** (1974) 237–43.
15. Dyson, B. F. and Rodgers, M. J., Prestrain, cavitation, and creep ductility, *Metal Sci.*, **8** (1974) 261–6.
16. Saegusa, T., Uemura, M. and Weertman, J. R., Grain boundary void nucleation in astroloy produced by room temperature deformation and anneal, *Met. Trans.*, **11A** (1980) 1453–8.
17. Stevens, R. A. and Flewitt, P. E. J., The role of hydrostatic pressure on the sintering of creep cavities in a nickel–2 % chromium alloy, *Acta Met.*, **27** (1979) 67–77.
18. Raj, R. and Ghosh, A. K., Stress rupture, *Met. Trans.*, **12A** (1981) 1291–302.
19. Weertman, J. R., Identification by small-angle neutron scattering of microstructural changes in metals and alloys, in *Nondestructive Evaluation: Microstructural Characterization and Reliability Strategies*, Eds. O. Buck and S. M. Wolf, AIME, New York, 1981, 147–68.
20. Letcher, J. H. and Schmidt, P. W., Small-angle X-ray scattering determination of particle-diameter distributions in polydisperse suspensions of spherical particles, *J. Appl. Phys.*, **37** (1966) 649–55.
21. Fedorova, I. S. and Schmidt, P. W., A general analytical method for calculating particle-dimension distributions from scattering data, *J. Appl. Crystallogr.*, **11** (1978) 405–11.
22. Brill, O. L. and Schmidt, P. W., Small-angle X-ray-scattering determination of diameter distributions, *J. Appl. Phys.*, **39** (1968) 2274–81.

Received 17 January 1986; accepted 26 March 1986

Int. J. High Technology Ceramics **2** (1986) 195–206

Importance of Homogeneous Composition in Sintering Behaviour of $Ba_2Ti_9O_{20}$ Ceramics

T. Jaakola, A. Uusimäki and S. Leppävuori

Microelectronics Laboratory, University of Oulu, SF-90570 Oulu, Finland

SUMMARY

The densification behaviour of $Ba_2Ti_9O_{20}$ (B_2T_9) ceramics prepared from two different powder combinations—(i) $2BaCO_3 + 9TiO_2$; (ii) $2BaTiO_3 + 7TiO_2$—was investigated. It was observed that during calcination of the raw material mixture containing barium titanate ($BaTiO_3$), complete formation of B_2T_9, as well as good powder morphology, was readily obtained; in contrast, in the case of the powder containing barium carbonate ($BaCO_3$), good powder characteristics could only be obtained at the expense of achieving conversion to B_2T_9. Dilatometric measurements made at a constant heating rate showed that in the case of the powder starting with $BaCO_3$ the densification of the incompletely reacted powder slowed down temporarily at around 1250°C, while simultaneously, according to X-ray diffractometry (XRD), formation of B_2T_9 occurred.

Observations of the microstructure showed that anisotropic particle growth took place during this stage. It is argued that microstructural coarsening accounts for the observation that higher temperatures are necessary to densify the powders based on $BaCO_3$, as compared with those necessary to densify the powders based on $BaTiO_3$.

1. INTRODUCTION

Single-phase $Ba_2Ti_9O_{20}$ (B_2T_9) is a ceramic having a high dielectric constant, low temperature coefficient of dielectric constant, and low dielectric loss, all of which combine to make it a useful material for microwave applications.[1,2] This compound was first reported by Jonker and Kwestroo[3] in their study of the BaO–TiO_2 system, and later O'Bryan *et al.*[4,5] determined its microwave properties and their dependence on

Int. J. High Technology Ceramics 0267-3762/86/$03·50

processing parameters. Recently the crystal structure of B_2T_9 has been determined.[6]

Preparation of B_2T_9 ceramic by the conventional method involves the usual two processing steps, namely calcination of the starting materials and sintering to form the ceramic. During calcination the B_2T_9 phase partly forms, and the extent to which it does, and other factors, are known to influence the following sintering stage, the final microstructure and dielectric properties. For example, O'Bryan *et al.*[5] suggest that during the calcination stage barium-rich intermediates, such as $Ba_4Ti_{13}O_{30}$, $Ba_6Ti_{17}O_{40}$ and $BaTi_2O_5$, form; during the higher temperature sintering stage these can lead to the development of non-equilibrium liquid phases which can, in turn, concentrate impurities and cause microcracking, both of which are detrimental to dielectric properties. O'Bryan and Thomson[7] found it necessary to form some B_2T_9 during the calcination stage if a single-phase B_2T_9 ceramic is to develop in reasonable time during the sintering stage. Later studies[8] have revealed curvature of the B_2T_9 equilibrium phase boundary at high temperatures, and this is an additional complicating factor.

In more general terms densification and development of the microstructure during ceramic processing are affected by characteristics of the powder as well as the microstructure of the green compacts. Usually a combination of small particle size, non-agglomerated powder, and a homogeneous chemical composition is necessary to obtain an ideal sinterable powder.[9]

The primary aim of the present study was to determine the effect of incomplete formation of B_2T_9 during the calcination stage on the sintering behaviour, since this has immediate relevance to the manufacture of an important microwave dielectric. Initially, the dependence of B_2T_9 formation, for two starting materials, on both temperature and time was examined and the parameters for complete formation were determined. Subsequently, the shrinkage behaviour and evolution of the microstructure of the calcined powder compacts during sintering were examined.

2. EXPERIMENTAL PROCEDURE

The starting materials used for the preparation of B_2T_9 were reagent grade $BaCO_3$, $BaTiO_3$, and TiO_2 (anatase), the average particle sizes being in the range of approximately 1 μm, 1 μm and 0·1 μm, respectively. These oxides were mixed in two combinations: ($2BaCO_3 + 9TiO_2$) and ($2BaTiO_3 + 7TiO_2$). The mixing was carried out in distilled water for a period of 4 h in a plastic ball mill using agate balls. After drying the milled mixture, the powders were reacted at temperatures in the range 900 to 1200 °C, the particular temperature being dependent on the formulation. The reacted

powders were then reground and 1 wt% polyvinyl alcohol (PVA) added. Compacts were uniaxially pressed at 100 MPa into discs 10 mm in diameter and 4 mm thick. Sintering of the pressed discs was carried out at temperatures ranging from 1150 to 1380 °C for a period of 6 h, in air or oxygen.

Quantitative X-ray diffraction (XRD) analysis as described by Chung[10] was used to follow the formation of the B_2T_9 phase. The 2θ values of the reflections used in the measurements were 29·3° for B_2T_9 and 30·1° for $BaTi_4O_9(BT_4)$; these were chosen since there was no overlapping and the reflections were quite intense. All the powders examined were found to contain only B_2T_9, and TiO_2 phases. It is likely that small amounts of phases such as $Ba_6Ti_{17}O_{40}$ were also present but, for sake of simplicity, their amounts were assumed to be negligible. Following Chung, the ratio B_2T_9/BT_4 was determined from which the weight fraction of B_2T_9 could be calculated with the help of the reaction equation ($2BT_4 + TiO_2 \rightarrow B_2T_9$).

Samples for the XRD measurements were prepared by rapidly heating the homogenised mixture (100 °C min^{-1}) to the desired reaction temperature and then rapidly cooling at the end of the predetermined reaction time. The powders were then thoroughly ground and the samples for the XRD measurements made according to the procedure described by Klug and Alexander.[11] To make intensity measurements of the peaks and background, Ni-filtered Cu–Kα radiation and a counting time of 100 s were used.

The densification behaviour of the compacted powders was followed continuously using a high temperature dilatometer in which the shrinkage was transmitted to a linear voltage displacement transducer by an alumina push-rod, and the temperature monitored using a Pt–Pt/Rh thermocouple. Expansion of the alumina push-rod and specimen holder was compensated electronically. The specimens used for the dilatometric measurements were 10 mm in diameter and 25·4 mm thick, the heating rate was 5 °C min^{-1} and the measurements were made in flowing oxygen. The evolution of the pore structure in the initial and intermediate stages of the sintering process was followed using a mercury porosimeter with a capability of measuring pore sizes between 120 and 0·006 μm. The microstructure of the partially and completely sintered specimens was examined using a scanning electron microscope, and the density values determined directly from weight and volume.

3. RESULTS

3.1. B_2T_9 formation and powder properties

The dependence of B_2T_9 formation on the temperature and time of reaction was studied in order to establish suitable reaction conditions for the two

powder mixtures under investigation, namely ($2BaCO_3 + 9TiO_2$) and ($2BaTiO_3 + 7TiO_2$). A reaction temperature of 1150 °C or higher was required for B_2T_9 formation to occur within a reasonable time span in the case of the mixture containing $BaCO_3$. At such temperatures a mixture of BT_4 and TiO_2 phases was quickly formed and, following reaction between the two components, produced B_2T_9. Formation of the B_2T_9 phase as a function of the reaction time at two different temperatures (1150 and 1200 °C) is shown in Fig. 1(a). From the curves it can be seen that in order to achieve B_2T_9 concentrations higher than 90 wt%, a reaction time greater than 24 h was required at 1150 °C, while at 1200 °C the corresponding time was 12 h.

Faster reaction kinetics occur for the mixture of $BaTiO_3$ and TiO_2, for which the reaction temperature for an equivalent reaction rate was lower by over 250°C. The reaction kinetics at the two temperatures are shown in Fig. 1(b). In order to achieve conversions of over 90 wt% at 1000°C, a time of 1 h was sufficient, while at 950 °C it was 4 h.

Table 1 shows the processing conditions selected for the preparation of the B_2T_9 powders, together with principal characteristics. The calcining schedules for powders A1 and B were chosen so as to obtain greater than 90 wt% conversion to B_2T_9. Examples of powder morphologies are shown in Fig. 2, and, as evident from Fig. 2(a), it proved difficult to grind A1 to a fine particle size with a narrow particle size distribution; better characteristics were obtained for the other powders.

Pore size distribution and specific surface area measurements were made on pressed compacts using the mercury porosimeter, the data showing that

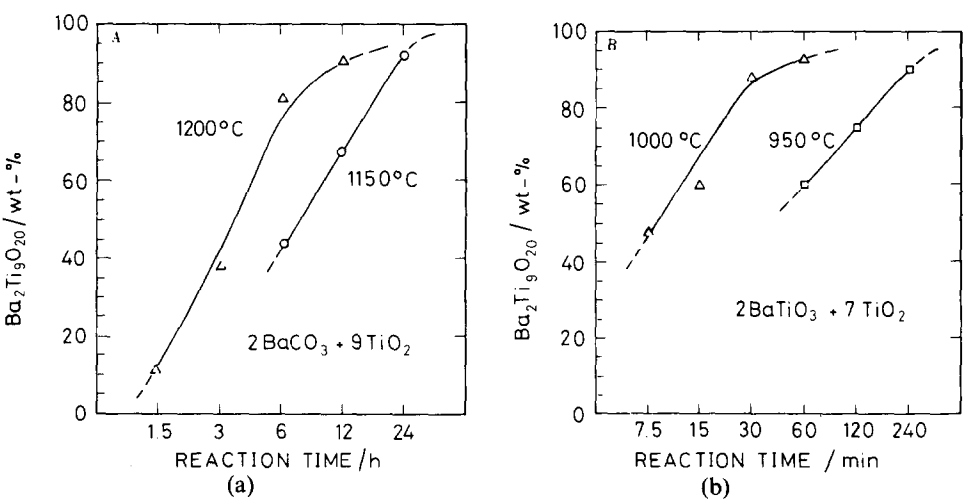

Fig. 1. Formation of $Ba_2Ti_9O_{20}$ from a mixture of (a) $BaCO_3$ and TiO_2, and (b) $BaTiO_3$ and TiO_2.

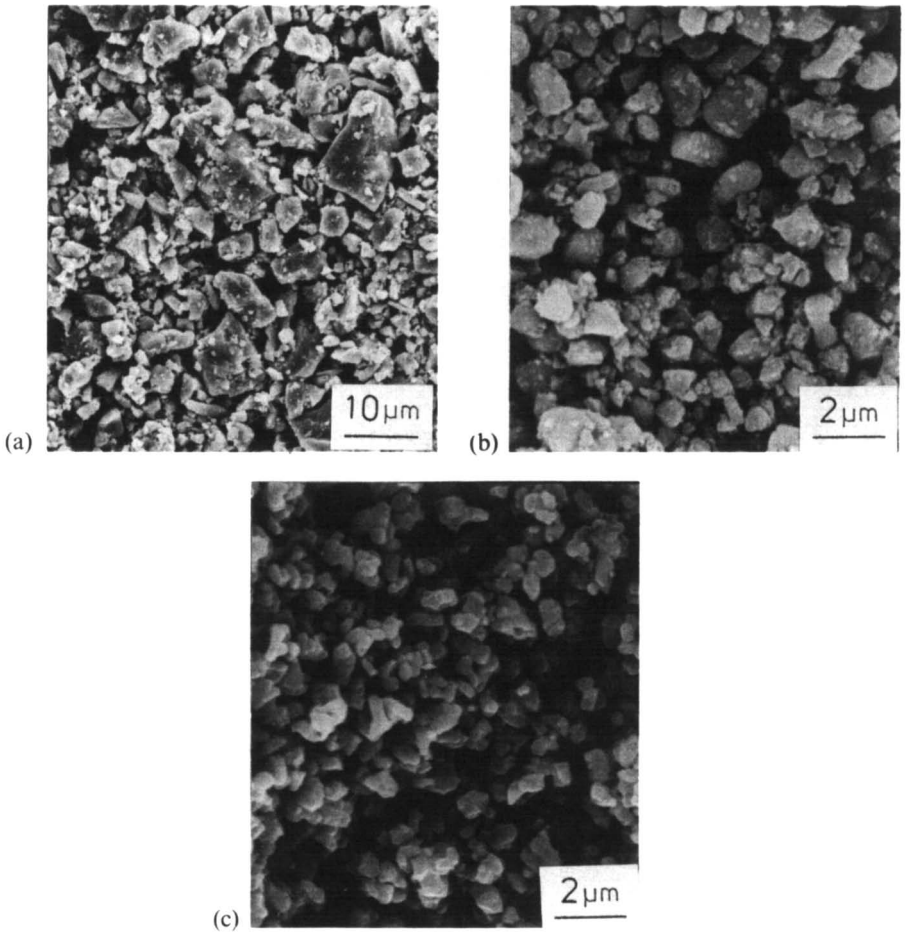

Fig. 2. SEM micrographs of calcined powders; (a) A1; (b) A2; (c) B.

the narrowest distribution was obtained with powder B and the broadest with powder A1. Specific surface area values for powders A2 and B were similar, and considerably higher than that of powder A1, as evident from Table 1. All these data appear consistent with Fig. 2.

3.2. Densification and development of microstructure

Figure 3 shows the densification of calcined powders measured by the dilatometer. Compared to the other powders, type A1, which had the largest particle size, required higher temperatures to achieve equivalent shrinkage. Powder compacts A2 and B showed similar initial densification rates as expected from their similar particle sizes. However, from approximately 1200 °C to 1300 °C the rate of densification of the partially reacted

TABLE 1
Processing Conditions and Powder Characteristics

Powder	*Processing conditions*		*Characteristics*		
	Temperature $T_c/°C$	*Time* t/h	$S/m^2 g^{-1}$	$d/\mu m$	$B_2T_9/wt\%$
A1	1 150	30	1·1	1–10	>90
A2	1 150	3	4·1	0·5–2	20
B	1 000	2	3·5	1	>90

A = $BaCO_3 + TiO_2$ based powder
B = $BaTiO_3 + TiO_2$ based powder
S = specific surface area
d = particle size

powder, A2, decreased, and XRD showed this to be accompanied by the formation of B_2T_9.

The densities of compacts sintered for 6 h in air at various temperatures are shown in Fig. 4. As evident from Fig. 3, compacts of powder B sintered to a higher density at a lower temperature than compacts of either powder A1 or A2. In fact, the highest density achieved with B was at 1200 °C, there being a small decrease in density for compacts sintered to above this temperature. The density of powder compact A1 was comparable to that of the A2 compact despite the large difference in the starting particle sizes. At 1380 °C the densities of A1 and A2 powder compacts were comparable

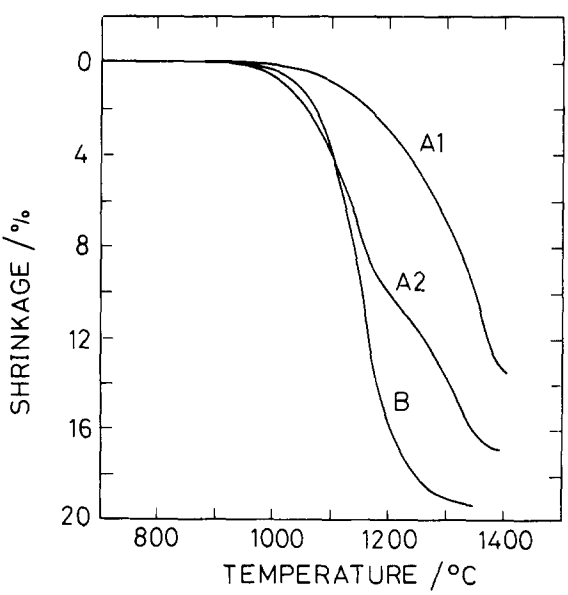

Fig. 3. Variation in non-isothermal shrinkage of compacts of powders. 'Green' compact densities: A1 = 62%, A2 = 56%, B = 52% (all based on theoretical density of B_2T_9).

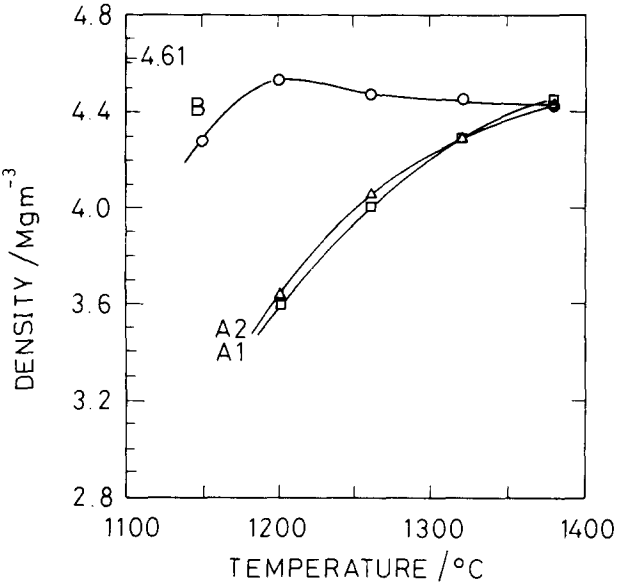

Fig. 4. Dependence of sintered density of powder compacts on temperature for a sintering time of 6 h in air. Theoretical density of B_2T_9 (4·61 Mg m^{-3}) is indicated.

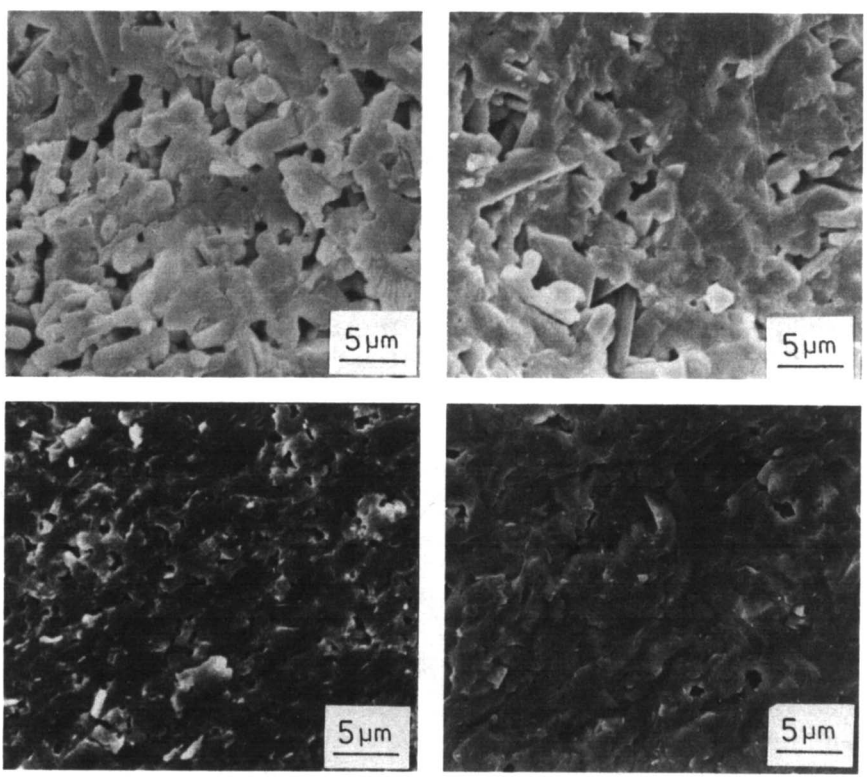

Fig. 5. Fracture surfaces of compacts A2 (above) and B (below) heated to temperatures 1200°C (left) and 1300°C (right).

to the density of the powder B compact. By sintering in an oxygen atmosphere rather than in air it was possible to attain higher final densities; for example, it was noted that at a temperature of 1380 °C and for compact A2, the density increased from 96% to 98% of theoretical.

In order to study the evolution of microstructure during densification, compacts were heated to temperatures of 1200 °C and 1300 °C using a constant rate of heating (5 °C min^{-1}) followed by rapid cooling. Fracture surfaces of the sintered ceramics are shown in Fig. 5. A significant difference between the structures is apparent and evidently related to the slowing down of the densification observed in Fig. 3. It can be seen that the pore size of the ceramic from powder B is significantly smaller than that from A2, and also that the ceramic sintered at 1300°C contains inhomogeneously densified regions where some elongated grains are visible.

4. DISCUSSION

The object of calcining the starting materials in ceramic processing is to obtain a chemically homogeneous material which, in addition, possesses the property of easy grindability to a fine particle size having narrow particle size distribution; this usually ensures good sinterability. Reaction to a homogeneous calcine is desirable since chemical homogenisation occurring simultaneously with sintering may disturb the process of densification.[12] In the case of B_2T_9 prepared from $BaCO_3$ with TiO_2 it was difficult to obtain both the above characteristics. High reaction rates required a high temperature or a long time span which led to poor grindability of the calcined powders, as can be seen by comparison of Figs 2(a) and 2(c). Characteristics closest to the ideal were attained with the B_2T_9 powder prepared from a mixture of $BaTiO_3$ with TiO_2. This was, of course, due to the much lower temperature that was required for complete reaction to occur and consequently to the formation of a relatively soft calcine. Additionally, compacts formed from this powder had the narrowest pore size distribution, which is important for achieving high density during sintering.[13]

The very significantly lower reaction temperature for the $BaTiO_3$ and TiO_2 raw material mixture compared to that for the $BaCO_3/TiO_2$ mixture (Fig. 1) was surprising. A possible explanation is that because the $BaTiO_3$ of the former mixture is closer to B_2T_9 in Ti content than $BaCO_3$, the diffusion distances involved to effect the solid state reaction are relatively short; clearly such conditions favour the development of a homogeneous ceramic. A further reason might be the formation of the intermediate BT_4, when $BaCO_3$ is one of the starting materials. Because the kinetics of BT_4

formation are known to be faster than those for the formation of B_2T_9,[14] the development of the mixture $BT_4 + TiO_2$ would occur prior to that of B_2T_9. This would be especially true were there to be incomplete mixing of the starting materials, possibly because of the presence of agglomerates. This effect was observed when $BaCO_3$ was one of the starting materials, since a nearly complete reaction to a mixture of $BT_4 + TiO_2$ intermediates preceded the formation of B_2T_9, which then occurred according to the reaction equation ($2BT_4 + TiO_2 \rightarrow B_2T_9$). The TiO_2 content at the onset of this reaction was about 10 vol% and so it is apparent that the diffusion distances increase as the reaction proceeds. It is known[7] that if complete ($BT_4 + TiO_2$) formation is allowed to occur, by calcining for 3 h at 1100 °C, then long times are required for single-phase B_2T_9 formation, even at a temperature of 1400 °C.

The slowing down of the densification rate measured for the incompletely reacted powder at around 1250 °C, and the observed simultaneous completion of the formation of B_2T_9 indicates that these processes are related.

The nature of the process occurring in an incompletely reacted B_2T_9 compact becomes clear from Fig. 6, where a series of samples which were heated for different times at a temperature of 1150 °C are shown. Strongly anisotropic grain growth was observed to take place. The uniform equiaxed particles of the starting compact changed to particles with a relatively high aspect ratio. The phenomenon was not surface-dependent since the same effect is evident in fracture surfaces. According to the XRD data the formation of B_2T_9 was completed after 320 min. Densification of the compacts was slight but the average pore size increased significantly from 0·5 μm after 5 min to 1·3 μm after 320 min.

On the basis of these observations an explanation for the anomalous densification behaviour is suggested. The solid state reaction ($2BT_4 + TiO_2 \rightarrow B_2T_9$) that occurs simultaneously with the densification causes the particle size and the pore size to increase, which in turn decreases the driving force for further densification. The structure of the compact becomes coarser and higher temperatures are then required for densification to proceed further. This effect could explain the quite similar densification data in Fig. 4, obtained for compacts A1 and A2, despite the very different starting powder particle sizes.

With powder B the coarsening of the structure of the compacts was not a problem and so attaining a high density even at a temperature as low as 1200 °C was possible; surprisingly, this is lower than what appeared to be the minimum (1275 °C) necessary to achieve full density in an interesting study of the continuous hot-pressing of B_2T_9 prepared from $BaCO_3$ and TiO_2.[15] The decrease in the final densities observed for the compacts of B as the sintering temperature was increased is most probably due to the

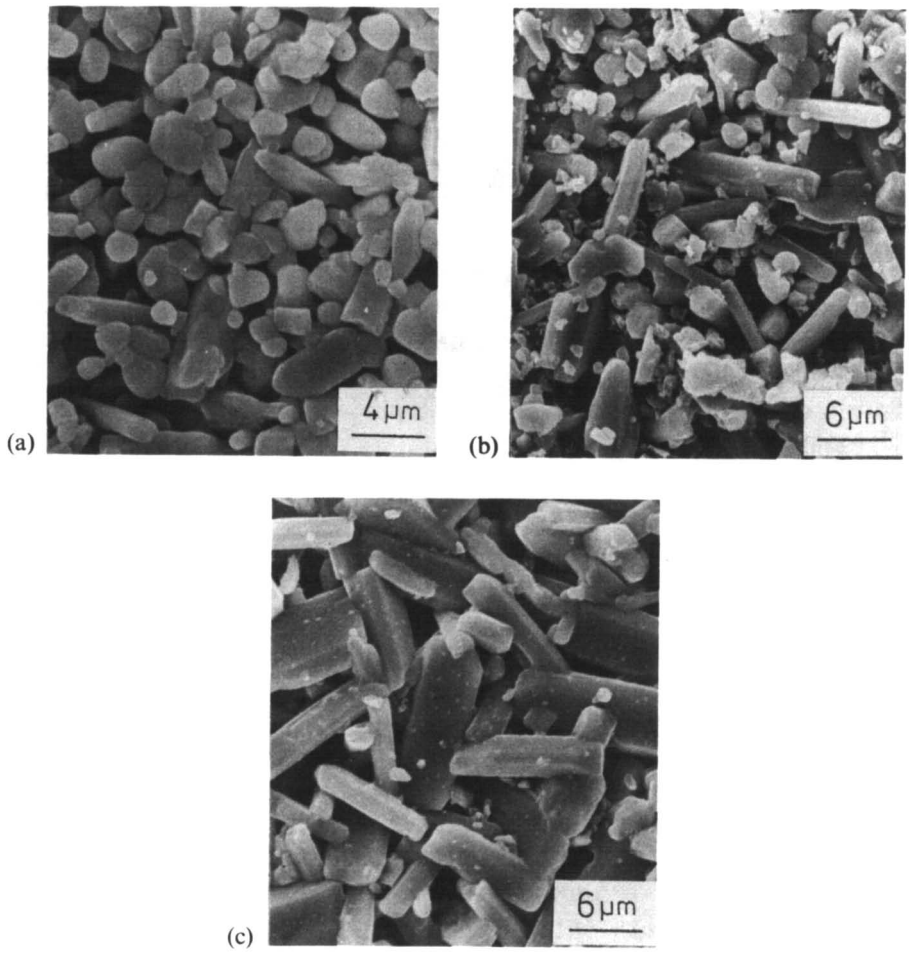

Fig. 6. Surfaces of compacts of powder A2 heated at 1150°C: (a) for 5 min; (b) for 80 min; (c) for 240 min. Densities of compacts after these time periods were 62%, 65% and 66% of the theoretical values, respectively.

coalescence of the pores at the grain boundaries which occurs simultaneously with grain growth.

5. CONCLUSION

The results of the study indicate that in fabricating B_2T_9 ceramics from powders having particle sizes of approximately 1 μm, the compositional homogeneity of the powder has a considerable effect on densification behaviour. In chemically inhomogeneous powders, completion of formation of the B_2T_9 phase, which occurred during densification, was found

to be accompanied by microstructural coarsening. This is believed to be the main reason for the observed decrease in densification rate and for the considerably higher sintering temperatures required.

By using as starting powders $BaTiO_3$ and TiO_2 instead of $BaCO_3$ and TiO_2, it was possible to obtain a homogeneous B_2T_9 powder that sintered to a density of 98% of theoretical at a temperature as low as 1200 °C.

ACKNOWLEDGEMENT

The authors are pleased to acknowledge the financial assistance of the Finnish Academy of Sciences.

REFERENCES

1. Plourde, J. K., Linn, D. F., O'Bryan, H. M. and Thomson, J., $Ba_2Ti_9O_{20}$ as a microwave dielectric resonator, *J. Am. Ceram. Soc.*, **58**(9–10) (1975) 418–20.
2. Plourde, J. K. and Ren, C., Application of dielectric resonators in microwave components, *IEEE Trans. Microwave Theory Tech.*, **MTT-29** (1981) 754–70.
3. Jonker, G. H. and Kwestroo, W., The ternary systems BaO–TiO_2–SnO_2, *J. Am. Ceram. Soc.*, **41**(10) (1958) 390–4.
4. O'Bryan, H. M., Thomson, J., Plourde, J. K., A new BaO–TiO_2 compound with temperature-stable high permittivity and low microwave loss, *J. Am. Ceram. Soc.*, **57**(10) (1974) 450–3.
5. O'Bryan, H. M., Thomson, J. and Plourde, J. K., Effects of chemical treatment on loss quality of microwave dielectric ceramics, *Ber. Dt. Keram. Ges.*, **55**(7) (1978) 348–51.
6. Tillmanns, E., Hofmeister, W. and Baur, W. H., Crystal structure of the microwave dielectric resonator $Ba_2Ti_9O_{20}$, *J. Am. Ceram. Soc.*, **66**(4) (1983) 268–71.
7. O'Bryan, H. M. and Thomson, J., Phase equilibria in the TiO_2-rich region of the system BaO–TiO_2, *J. Am. Ceram. Soc.*, **57**(12) (1974) 522–6.
8. O'Bryan, H. M. and Thomson, J., $Ba_2Ti_9O_{20}$ phase equilibria, *J. Am. Ceram. Soc.*, **66**(1) (1983) 66–8.
9. Yan, M. F., Microstructural control in the processing of electronic ceramics, *Mat. Sci. Eng.*, **48** (1981) 53–72.
10. Chung, F. H., Quantitative interpretation of X-ray diffraction patterns of mixtures. I. Matrix-flushing method for quantitative multicomponent analysis, *J. Appl. Cryst*, **7** (1974) 519–25.
11. Klug, H. P. and Alexander, L. E., *X-ray Diffraction Procedures*, John Wiley, New York, 1959, p. 412.
12. Paulus, M., in *Processing of Crystalline Ceramics*, Eds H. Palmour III, R. F. Davis and T. M. Hare, Plenum Press, New York, 1978, pp. 17–31.

13. Yan, M. F. and Rhodes, W. W., Low temperature sintering of TiO_2, *Mat. Sci. Eng.*, **61** (1983) 59–66.
14. O'Bryan, H. M. and Yan, M. F., Second-phase development in Ba-doped rutile, *J. Am. Ceram. Soc.*, **65**(12) (1982) 616–19.
15. Thomson, J. and Rhodes, W. W., Continuous hot pressing of $Ba_2Ti_9O_{20}$ and its evaluation, *Am. Ceram. Soc. Bull.*, **55**(3) (1976) 308–10.

Received 10 March 1986; accepted 9 May 1986

Int. J. High Technology Ceramics **2** (1986) 207–219

Toughened Ceramics in the System Al_2O_3:Cr_2O_3/ZrO_2:HfO_2

T. Y. Tien, T. K. Brog and A. K. Li

Materials Science and Engineering, The University of Michigan, Ann Arbor, Michigan 48109, USA

SUMMARY

Composites of Al_2O_3:Cr_2O_3 solid solution matrix with ZrO_2:HfO_2 solid solution dispersed particles were prepared and their properties studied. Thermal conductivity of compositions containing 20 mol% or more of chromia was found to be lower than that of partially stabilized zirconia at temperatures above 700°C. Specimens in this system were annealed at 1000°C for longer than 500 h and no mechanical property degradation was observed. Modulus of elasticity, bend strength and fracture toughness of these composites depend strongly on composition, volume fraction, size and the crystallographic modification of the dispersed particles. Best average bend strength of the composites is 490 MPa and the best average fracture toughness observed for these composites was 7·4 MPa $m^{1/2}$. It was found that the fracture toughness of some of the compositions increased with increasing temperature reaching a maximum of 300–500°C, and returned to the room temperature value at 1000°C. From the results obtained these composites can be considered as a potential candidate for advanced heat engine applications.

1. INTRODUCTION

Partially stabilized zirconia (PSZ) has been considered to be the leading candidate for the structural components of the adiabatic diesel engines.[1] However, it has been demonstrated that the currently available PSZ deteriorates at the operating temperatures of the diesel engine in a time period which is much less than that required for automotive applications.[2]

Int. J. High Technology Ceramics 0267-3762/86/$03·50

Alumina toughened with zirconia dispersions has been reported in the literature.[3] The fracture toughness and bend strength of this material are sufficient for it to be considered as a candidate for heat engine applications. However, the thermal conductivity of this material is too high for insulation purposes.[4] The fracture toughness of the alumina/zirconia composite decreases with increasing temperature[5] and the toughening effect diminishes at the operating temperatures of the heat engines. It was suggested that this material be modified to reduce its thermal conductivity by solid solution formation (chromia in alumina)[6] and the temperature dependence of the toughness modified by introducing hafnia in solid solution in the dispersed zirconia particles. It is known that the tetragonal–monoclinic transformation temperatures of the zirconia:hafnia solid solutions are higher than that of pure zirconia.[7] In an effort to optimize the mechanical and physical properties of the possible candidate material for structural applications at elevated temperature, a research program was initiated to study the toughened ceramics in the system Al_2O_3:Cr_2O_3/ZrO_2:HfO_2. The ultimate goal of this project is to develop a material suitable for high temperature applications in advanced heat engines. This paper summarizes the results of these studies.

2. EXPERIMENTS AND RESULTS

Composite specimens in the system Al_2O_3:Cr_2O_3/ZrO_2:HfO_2 were prepared and their properties measured. The properties measured include: thermal conductivity, thermal stability, modulus of elasticity, bend strength and fracture toughness. The specimens were prepared by three different methods, detailed below, depending on the properties to be studied. The sintering and growth kinetics of both the matrix grains and the dispersed particles in the system were also studied in order to develop an optimum microstructure, and, consequently, optimum properties of the composites.

2.1. Thermal conductivity

Specimens for thermal conductivity measurements were hot pressed. Prereacted Al_2O_3:Cr_2O_3 and ZrO_2:HfO_2 powders were ball milled and hot pressed at 1500 °C for 30 min under a uniaxial pressure of 35 MPa using BN-coated graphite dies in a graphite resistance furnace. Thermal diffusivity of these specimens was measured by the 'laser flash' method.[8] Literature data on specific heat were used and the thermal conductivities of these specimens were calculated. The results are given in Fig. 1. The thermal conductivities of some PSZ[9] are also included in the figure for comparison.

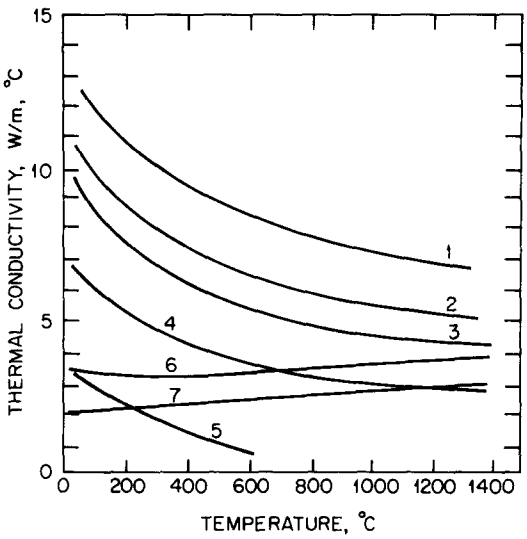

Fig. 1. Thermal conductivity of composites in the system Al_2O_3:Cr_2O_3/ZrO_2:HfO_2. Curve 1, hot pressed Al_2O_3; Curve 2, Al_2O_3/15 vol% ZrO_2; Curve 3, Al_2O_3:20 mol% Cr_2O_3/15 vol% ZrO_2, fine grained; Curve 4, Al_2O_3:20 mol% Cr_2O_3/15 vol% ZrO_2, coarse grained; Curve 5, Al_2O_3:50 mol% Cr_2O_3/15 vol% ZrO_2, coarse grained; Curve 6, ZrO_2:3 mol% Y_2O_3, tetragonal; Curve 7, ZrO_2:6 mol% Y_2O_3, cubic.

2.2. Mechanical properties

Specimens for mechanical property measurements were prepared by dry pressing and sintering. Pre-reacted alumina:chromia and zirconia:hafnia solid solution powders were attrition milled separately (in propanol). Submicron powders of both the matrix and the dispersed phases were mixed in a ball mill (in water). Dried mixtures were granulated (-60 mesh) and isostatically pressed (28 MPa) in thin rubber bags. Pellets, 10 mm in diameter and 5 mm thick, and round bars, 5 mm in diameter and 60 mm long, were made for characterization and property measurements. Dry pressed specimens were sintered at 1550 °C for 2 h under an argon atmosphere in an induction furnace with a graphite susceptor. All of the specimens used for property measurements were fully dense.

The average size of the dispersed particles was measured by the linear intercept method[10] and the results showed that the zirconia:hafnia particle size varied with the matrix composition and volume fraction of the dispersed phase. The results are given in Figs 2 and 3, respectively. The dispersed particles in all sintered specimens contain both tetragonal and monoclinic modifications of the zirconia. The fraction of the tetragonal phase[11] in the sintered specimens depends on the composition of the composites. Some of the results are given in Fig. 4.

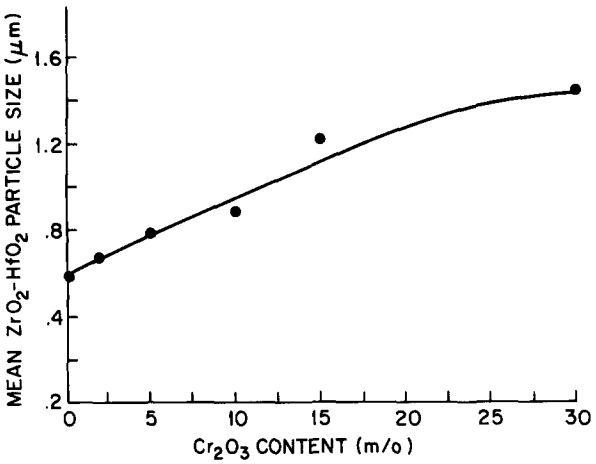

Fig. 2. Mean particle size of the dispersed phase as a function of the Cr_2O_3 content in the matrix phase. The composites contain 10 vol% of ZrO_2:10 mol% HfO_2.

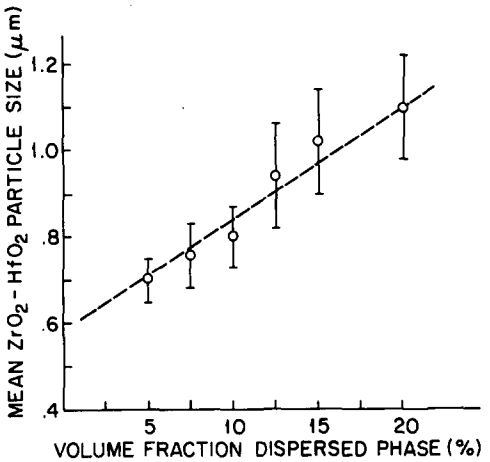

Fig. 3. Mean ZrO_2:HfO_2 particle size in the composites as a function of the volume fraction of the dispersed phase. The matrix phase contains 5 mol% of Cr_2O_3 in Al_2O_3.

The elastic modulus of the sintered bars was measured using the sonic method.* Results of these measurements are given in Fig. 5. The modulus of the composites decreased as the amount of the dispersed phase increased following the rule of mixtures.[5] A sudden decrease in the modulus was observed at high zirconia containing compositions. The drop of the modulus at the high dispersed phase containing compositions indicates the

* Modulus measurements were made by Dr L. Schioler of the Army Materials Technology Laboratory.

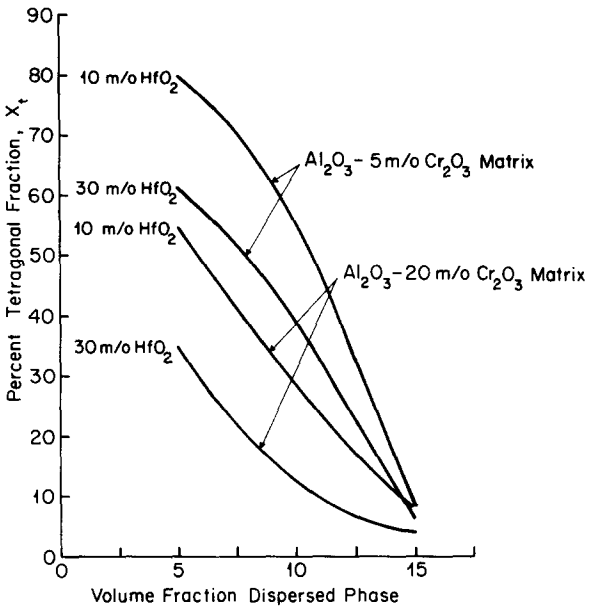

Fig. 4. Tetragonal fraction of the ZrO_2:HfO_2 dispersed phase in the composites.

existence of microcracks in the specimens.[5] The microcracks are the result of the volume change[12] of the dispersed particles during the tetragonal–monoclinic transformation. For composites containing the same volume fraction of dispersed phase, the composite containing 30 mol% of hafnia in solid solution with zirconia has a higher modulus than that of the specimens containing 10 mol% of hafnia. This indicates that the 30 mol% hafnia samples contain a lower density of microcracks. The specimens

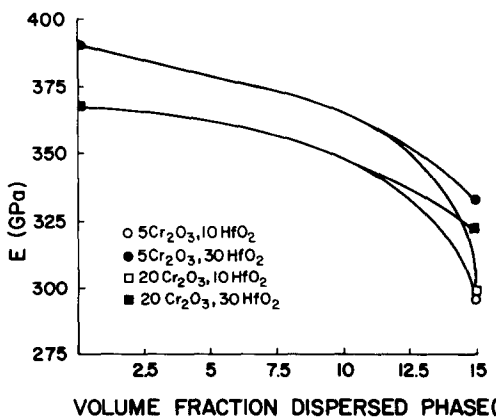

Fig. 5. Elastic modulus of the composites as a function of volume fraction of the dispersed particles.

used for the strength measurements were machined to a nominal dimension of 2·06 × 2·80 × 50 mm^3. The test fixture has an inner span of 9·5 mm and an outer span of 19·0 mm. The results of the 4-points bend strength measurements (average values of 6 or more tests for each composition) are given in Fig. 6. Similar to the modulus measurements, the strength of 30 mol% hafnia specimens at higher volume fractions of dispersed phase is higher than that of the 10 mol% hafnia samples. These results suggested

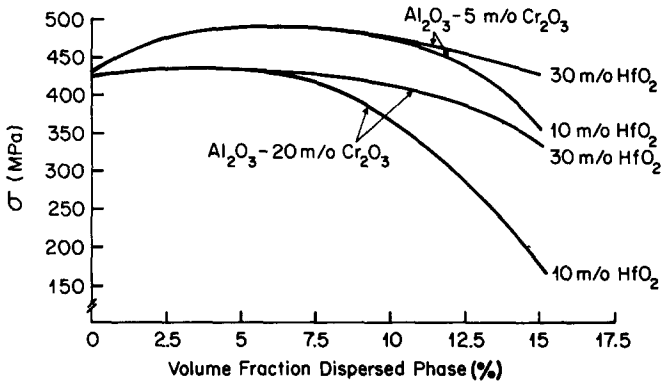

Fig. 6. Bend strength of the composites as a function of volume fraction of the dispersed particles.

that the 30 mol% hafnia samples contained a lower density of microcracks than the 10 mol% hafnia samples. This can be interpreted as showing that the volume change during the tetragonal–monoclinic transformation is lower for the higher hafnia containing zirconia solid solution particles than that of the lower hafnia containing zirconia solid solutions. The volume change of the solid solution particles during phase transformation was measured by thermal expansion of the composites.[13]

Fracture toughness was measured by the indentation in bend strength method.[14] The results are given in Fig. 7. The toughness value of the specimens increased as a function of volume fraction of the dispersed phase and declined after reaching a maximum.

Combining the data in Fig. 7 and Fig. 4, a graph as shown in Fig. 8 was obtained. This graph suggested that higher toughness values could be obtained for compositions containing 10, 12·5 and 15 vol% disperse phase by reducing the value of the volume of the monoclinic phase ($X_m V_f$). For specimens with a constant volume fraction of the dispersed particles (V_f), the $X_m V_f$ value can be reduced by reducing the fraction of the monoclinic form (X_m) of the dispersed zirconia phase. For a given V_f, when $X_m V_f = V_f/2$, a maximum on the toughness curve can be expected.

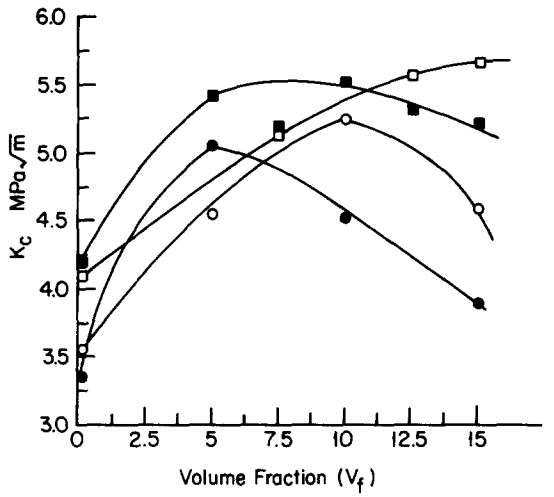

Fig. 7. Fracture toughness of the composites as a function of the volume fraction of the dispersed particles. ○, Al_2O_3:20 mol% Cr_2O_3/ZrO_2:10 mol% HfO_2; ●, Al_2O_3:20 mol% Cr_2O_3/ZrO_2:30 mol% HfO_2; □, Al_2O_3:5 mol% Cr_2O_3/ZrO_2:10 mol% HfO_2; ■, Al_2O_3:5 mol% Cr_2O_3/ZrO_2:30 mol% HfO_2.

Comparing Figs 2, 3 and Fig. 4, X_m can be reduced by reducing the mean particle size of the dispersed phase.

2.3. Thermal stability

Specimens of alumina, 10 and 20 mol% chromia in the matrix phase containing 10 vol% of 10 and 20 mol% hafnia containing zirconia particles, were held at 1000 °C for more than 500 h in air and no degradation

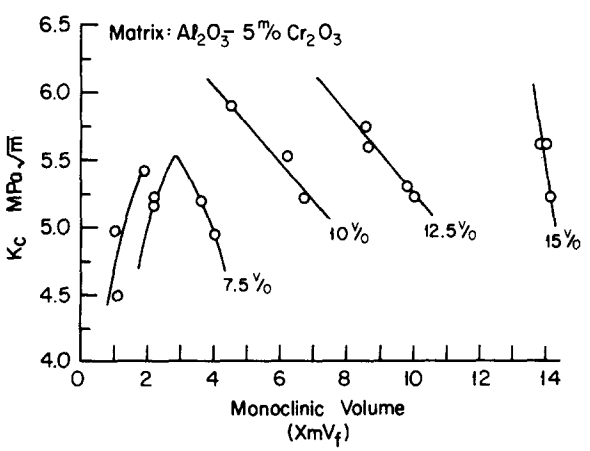

Fig. 8. Fracture toughness of the composites as a function of the monoclinic volume of the dispersed ZrO_2:HfO_2 particles.

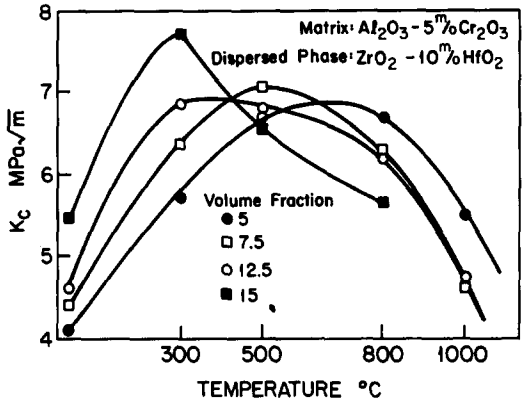

Fig. 9. Temperature dependence of the fracture toughness of composites.

in density, elastic modulus, bend strength and fracture toughness was observed.[15]

2.4. Temperature dependence of fracture toughness

The fracture toughness of some compositions was measured at elevated temperatures. These results are given in Fig. 9. The fracture toughness was measured using the indentation-strength-in-bend test.[14] The mechanism for the toughness increase with increasing temperature is not understood at this time.

2.5. Sintering and growth kinetics of the matrix grains and dispersed particles

Starting powders for these studies were prepared by coprecipitation. Aqueous solutions of aluminum nitrate, chromium nitrate, zirconium oxychloride and hafnium oxychloride were mixed in ratios according to the compositions to be prepared. The mixed metal ions were precipitated by NH_4OH solution. Precipitates were dried and calcined at 1050 °C to convert the hydroxides to oxides. Calcined powders were isostatically pressed and sintered in an induction furnace using a graphite susceptor. The densities of the sintered specimens were measured by Archimedes' principle. The results indicated that specimens sintered at 1550 °C reached the theoretical density when the furnace reached the sintering temperature without holding time. Polished surfaces were thermally etched and the grain sizes and particle sizes were measured by the linear intercept technique.[10] The results are given in Fig. 10. These show that composites with a mean zirconia particle size smaller than 0·5 μm can be obtained in fully dense samples.

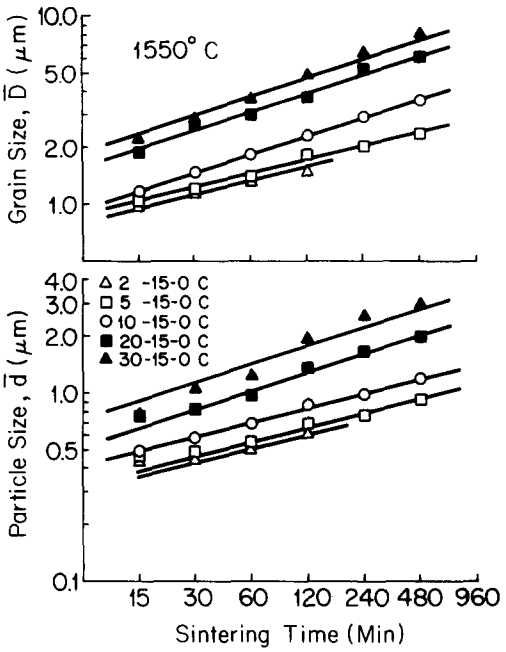

Fig. 10. Matrix grain and dispersed particle growth kinetics for composites containing 15 vol% of dispersed particles, sintered at 1550 °C. Composition designation: Cr_2O_3 content–vol% ZrO_2–HfO_2 content.

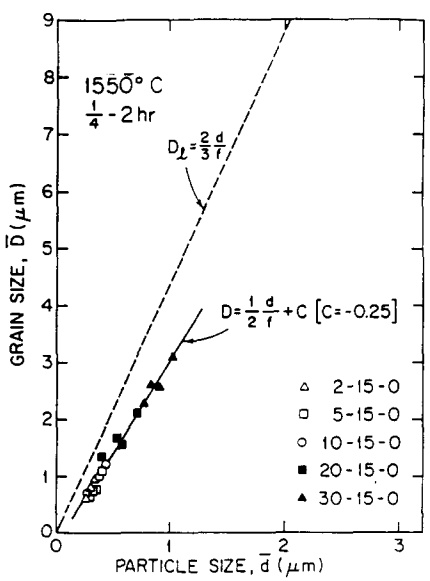

Fig. 11. Grain size vs particle size for specimens sintered at 1550 °C. Composition designation: Cr_2O_3 content–vol% ZrO_2–HfO_2 content.

Growth kinetics of the matrix grains and the dispersed particles were also measured at 1450, 1500, 1550 and 1600 °C. The results are reported in Table 1 in the form of:

$$\ln(D/t^n) = \ln D_0 - Q/RT \qquad \text{and} \qquad \ln(d/t^n) = \ln d_0 - Q/RT$$

where D is the grain size of the matrix phase, d is the particle size of the dispersed phase, n is the time exponent, Q is activation energy for growth, R is the gas constant, and T is absolute temperature.

Grain sizes are plotted against the particle sizes in Fig. 11. This shows a straight line relationship. This relationship follows Zener's suggestion[16] that the limiting grain size (D_f) is related to the size of the inclusions (d) and their volume fraction (f) in a composite following the form: $D_f = d/f$.

As shown in Table 1, both the grain and the particle growth rates

TABLE 1

The Growth Rates of the Matrix Grains and the Dispersed Particles Expressed in the Form of $\ln(D/t^n) = \ln D_0 - (Q/RT)$

Composition[a]	n	$\ln D_0$	Q	*Correlation coefficient*
For matrix grains:				
2–15–0	0·213	1·608	44·4	−0·999
5–15–0	0·244	4·580	55·5	−0·957
10–15–0	0·324	0·422	42·2	−0·999
20–15–0	0·339	7·264	65·7	−0·999
30–15–0	0·385	10·839	79·5	−0·998
0–15–10	0·230	11·474	33·7	−0·962
0–15–20	0·230	11·474	33·7	−0·962
0–15–30	0·230	11·474	33·7	−0·962
For dispersed particles:				
2–15–0	0·140	3·275	51·5	−0·975
5–15–0	0·207	1·314	45·9	−0·947
10–15–0	0·253	2·071	49·3	−0·961
20–15–0	0·296	6·199	64·4	−0·993
30–15–0	0·408	7·660	72·1	−0·986
0–15–10	0·143	−4·137	27·8	−0·990
0–15–20	0·143	−4·137	27·8	−0·990
0–15–30	0·143	−4·137	27·8	−0·990

[a] Composition designations: X–Y–Z. X = mol% of Cr_2O_3 in the matrix Al_2O_3 solid solution phase, Y = vol% of dispersed phase in the composites, and Z = mol% of HfO_2 in the dispersed ZrO_2 solid solution phase.

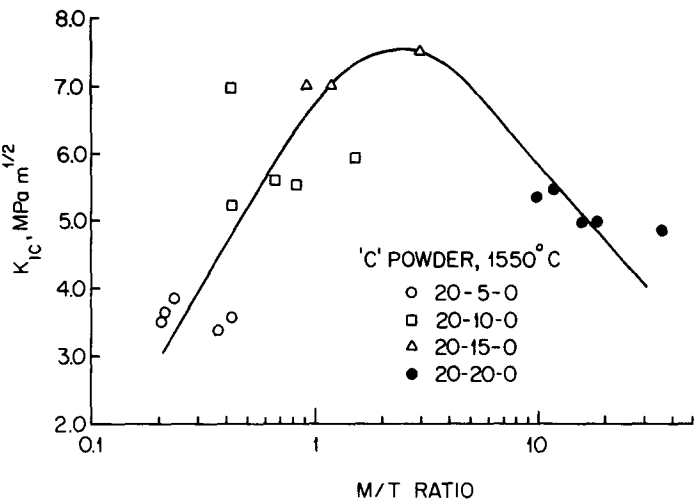

Fig. 12. Fracture toughness of composites as a function of monoclinic to tetragonal ratio of the dispersed ZrO_2 particles. Specimens were prepared using coprecipitated powders as precursors. The composition identification: The first number indicates mol% of Cr_2O_3 in Al_2O_3 and the second number indicates vol% of the dispersed phase in the composite. (For instance 20–15 indicates 20 mol of Cr_2O_3 in Al_2O_3 and 15 vol% of ZrO_2.)

increased as the chromia contents in the matrix phase increased, whereas the growth rate of the particles remained unchanged while the hafnia content changed in the dispersed phase. This result suggested that Ostwald ripening played a less important role in the particle growth than the coalescence.[17]

The fracture toughness of some specimens was measured. The tetragonal zirconia contents were measured and the results indicated that higher toughness values were observed when the zirconia particles had a monoclinic to tetragonal ratio in the range of 1:1 to 1:2 (Fig. 12). These results indicated that multiple toughening mechanisms are active in this system. At lower monoclinic zirconia volume, stress-induced transformation toughening and crack deflection are active, and for high monoclinic zirconia volume, microcrack nucleation/growth and crack deflection are active.[13]

3. CONCLUSION

The modulus of elasticity, bend strength and fracture toughness of composites composed of an Al_2O_3:Cr_2O_3 solid solution matrix containing ZrO_2:HfO_2 solid solution dispersed particles were studied. The results show that the modulus of elasticity, bend strength and fracture toughness

strongly depend on the volume fraction and size of the dispersed zirconia solid solution particles. From these results it can be concluded that an optimum composite should contain a higher volume fraction of the dispersed zirconia particles with a monoclinic to tetragonal ratio in the range of 1:1 to 1:2. The strength degradation of the composite with higher amounts of dispersed particles can be minimized by introducing hafnia in solid solution with zirconia.

Composites containing more than 20 mol% of Cr_2O_3 in the solid solution in the matrix alumina had a thermal conductivity lower than that of partially stabilized zirconia at temperatures higher than 300 °C. Composites were annealed at 1000 and 1200 °C for more than 300 h and no degradation of mechanical properties was observed. The results of these studies suggest that these composites are potential candidates for heat engine applications.

ACKNOWLEDGEMENTS

The authors wish to thank Drs J. S. Wallace, P. F. Becher and R. N. Katz for helpful discussions. The financial support for this investigation was provided by the US Department of Energy, Division of Transportation Energy Conservation; Office of Vehicle and Engine Research and Development, Ceramics Technology for Advanced Heat Engines Programs; administered by the Army Materials Technology Laboratory.

REFERENCES

1. Katz, R. N. and Lenoe, E. M., Ceramics for light duty diesel engines: a technology assessment, *Automotive Technology Development Contractors Coordination Meeting*, Dearborn, Michigan, October 1981, 551.
2. Schioler, L. J., Quinn, G. D. and Katz, R. N., Time–temperature dependence of the strength of commercial zirconia ceramics, *Proc. 21st Automotive Technology Development Contractors' Coordination Meeting*, Dearborn, Michigan, 14–17 November 1983, P-138, 183–91.
3. Claussen, N. E., Fracture toughness of Al_2O_3 with an unstabilized ZrO_2 dispersed phase, *J. Am. Ceram. Soc.*, **59**(1–2) (1976) 49–51.
4. Greve, D., Claussen, N. E., Hasselman, D. P. H. and Youngblood, G. E., Thermal diffusivity/conductivity of alumina with a zirconia dispersed phase, *Am. Ceram. Soc. Bull.*, **56**(5) (1977) 514–15.
5. Lange, F. F., Transformation toughening: Part 5. Effect of temperature and alloy on fracture toughness, *J. Mat. Sci.*, **17**(1) (1982) 255–63.
6. Kingery, D. W., Bowen, H. K. and Uhlmann, D. R., *Introduction to Ceramics*, John Wiley, New York, 1976.

7. Ruh, R., Garrett, H. J., Domagala, T. F. and Tallan, N. M., The system zirconia–hafnia, *J. Am. Ceram. Soc.*, **51**(1) (1968) 23–7.
8. Hasselman, D. P. H., Syed, R. and Tien, T. Y., The thermal diffusivity and conductivity of transformation-toughened solid solution of alumina and chromia, *J. Mat. Sci.*, **20** (1985) 2549–56.
9. Tsukuma, K., Kubota, Y. and Nobugai, K., Thermal and mechanical properties of Y_2O_3 partially stabilized zirconia, *Yogyo-Kyokai-Shi*, **92**(5) (1984) 233–41.
10. Wurst, J. C. and Nelsen, J. A., Linear intercept technique for measuring grain size in two-phase polycrystalline ceramics, *J. Am. Ceram. Soc.*, **55**(2) (1972) 109.
11. Porter, D. L. and Heuer, A. H., Microstructural development in MgO stabilized zirconia (Mg–PSZ), *J. Am. Ceram. Soc.*, **62**(5–6) (1979) 298–305.
12. Subbarao, E. C., Zirconia—an overview, in *Advanced Ceramics—Vol. 3, Science and Technology of Zirconia*, Eds A. H. Heuer and L. W. Hobbs, American Ceramic Society, Columbus, Ohio, 1981.
13. Brog, T. K., *Transformation Toughening in the Al_2O_3:Cr_2O_3/ZrO_2:HfO_2 System*, PhD Dissertation, University of Michigan, 1986.
14. Chantikul, P., Anstis, G. R., Lawn, B. R. and Marshall, D. B., A critical evaluation of indentation technique for measuring fracture toughness: II. Strength method, *J. Am. Ceram. Soc.*, **64**(9) (1981) 539–43.
15. Schioler, L. J., Katz, R. N., Brog, T. K. and Tien, T. Y., Mechanical properties of zirconia-toughened alumina, *Ceramic Engineering and Science*, **6**(7–8) (1985) 822–5.
16. Zener, C. quoted by C. S. Smith, Grains, phases, and interfaces; an interpretation of microstructure, *Metals Technol.*, **15**(4); *Trans. Met. Soc. AIME*, **175**, (1948) 15–51.
17. Li, A. K., *Sintering and Growth Kinetics of the Matrix Grains and the Dispersed Particles in the Al_2O_3:Cr_2O_3/ZrO_2:HfO_2 Composites*, PhD Dissertation, University of Michigan, 1986.

Received 14 April 1986; accepted 6 May 1986

Int. J. High Technology Ceramics **2** (1986) 221–229

Comparison of Indentation and Notched Bar Toughness of TZP Ceramics: Relevance to Models of the Fracture Process

A. W. Paterson

National Institute for Materials Research, CSIR, PO Box 395, Pretoria 0001, South Africa

and

R. Stevens

Department of Ceramics, University of Leeds, Leeds LS2 9JT, England

SUMMARY

Indentation and notched bar (SENB) toughness were determined for two compositions, sintered using different schedules designed to develop different toughness.

Experimental results indicate that the indentation technique tends to give higher values of toughness than SENB specimens with narrow notches. This is attributed to the extensive transformation that takes place in the region of the indentation.

The effect of notch width in tetragonal zirconia polycrystalline (TZP) materials was examined and found to be pronounced; measured K_{Ic} *values varied between* ~ 7 *and 17 MPa* $m^{1/2}$ *for notch widths between 0·1 and 1 mm. X-ray diffractometry (XRD) was used to determine the extent of the tetragonal to monoclinic phase transformation on fracture surfaces. These data, correlated with the* K_{Ic} *data, permit an experimental assessment of the toughening increment,* ΔK^{T}_{Ic}*, due to the transformation, to be made. The experimental value shows good agreement with the theoretical model of Seyler and his co-workers, based on the deviatoric component of the shear transformation.*

A modified equation permits a conservative estimate of the toughness to be made, if the extent of transformation is known.

Int. J. High Technology Ceramics 0267-3762/86/$03·50

1. INTRODUCTION

The simplification of fracture toughness measurement in ceramic materials by the introduction and refinement of the indentation technique[1] has led to its application on materials that were not widely available when the technique was developed.

Tetragonal zirconia polycrystalline (TZP) ceramics based on the Y_2O_3–ZrO_2 system have a structure that can consist of 100% tetragonal grains retained metastably, at room temperature. Many favoured compositions used for engineering applications contain 10–20% of the cubic phase or of a non-transformable tetragonal phase, t', produced from the high temperature cubic phase on cooling.[2]

High voltage transmission electron microscopy (TEM) studies[3] of TZP fracture in a thin foil have shown that some tetragonal grains do not transform in the crack tip stress field and its wake. In addition, certain workers[4] have reported relatively low levels for the $t \rightarrow m$ transformation measured using X-ray diffractometry (XRD) methods.

The literature also indicates a growing distinction between the toughening mechanism of partially stabilised zirconia (PSZ) and TZP materials. This is related to the relative importance of the hydrostatic and deviatoric components of the transformation,[5–7] an aspect that will be explored further in this paper.

Fracture toughness measurements employing indentation techniques have been used on TZP materials by a number of researchers.[4,8–11] In contrast, notched bar (SENB) techniques have been applied by relatively few researchers[12] who worked with mixed-oxide powders.

The importance of notch width in notched bar (SENB) specimens has been widely recognised in studies of alumina.[13,14] In addition a number of other materials have been shown to have K_{Ic} dependence on notch width, including silicon nitride, silicon carbide, porcelain and glass.[15] Zirconia ceramics with a PSZ structure showed an increase in K_{Ic} of 38% with increase in notch width from 0·2 mm to 1·2 mm.[16] In the study by Munz on aluminas, K_{Ic} increased from 4 MPa $m^{1/2}$ with a 50 μm notch to approximately 5·7 MPa $m^{1/2}$ with notches in the range 0·3–1 mm (43% increase). It has been found that SENB specimens with sharp cracks have K_{Ic} values which are equal to those of bars with a notch tip radius of 0·08 mm[15] or a notch width of 50 μm,[14] but the minimum K_{Ic} may be conservatively estimated, by extrapolation, to be at zero notch width.[16] In the present study the effect of notch width in TZP was investigated because of the complicating factors relating to the transformation in the region of both a static crack and one propagating under an applied stress.

A consequence of the passage of a crack is the development of a

transformed layer and thus the extent of transformation in TZP fracture surfaces has been determined in order to correlate this parameter with K_{Ic} values.

2. EXPERIMENTAL

Homogeneous co-precipitated Y_2O_3–ZrO_2 powders 2Y and 2·5Y, Toyo Soda Manufacturing Co., Tokyo, Japan, with 2 and 2·5 mol% Y_2O_3 were uniaxially pressed in a 42-mm die at 25 MPa. The discs were sintered using a range of firing schedules, cut into bars and notched for testing. The bars were then annealed for 10 min at 1100°C in order to minimise transformation effects due to machining. The geometry of the bars is listed in Table 1.

The specimens were broken in 3-point bending in an Instron testing machine with a cross-head speed of 0·1 mm min^{-1} and a load cell full scale deflection of 1 kN. K_{Ic} values were calculated using the equation of Richerson.[17]

TABLE 1
Single Edge Notch Bar Geometry

Dimension	*Size/mm*
Width	5
Breadth	2·5
Notch depth	1·5
Span	19
Notch width	0·1, 0·5, 1

Indentation fracture toughness measurements were performed with a load of 10 kg on a Zwick microhardness tester and the indentation diagonals and crack lengths were measured directly. Five to ten indentations were performed on each specimen. Indentations with loads above 10 kg were made using a Vickers hardness tester and were again measured directly. The equation of Anstis *et al.*[1] was used to compute K_{Ic} from the length of the indent diagonals and the crack length, with values of the elastic modulus determined by a sonic method.

Fracture surfaces were X-rayed to determine the monoclinic phase content using a Philips diffractometer with Cu–Kα radiation. The nature of the monoclinic phase in the fracture surface is discussed elsewhere.[7]

3. RESULTS

Table 2 shows the toughness as determined by the notched beam technique (with different notch widths) and the indentation techniques for the different compositions and sintering conditions used in this study. It is clear that toughness tends to increase with sintering temperature and is higher for the 2 mol% Y_2O_3 composition than for the 2·5 mol% composition. Both SENB and indentation techniques show the same trend for the change in toughness with sintering and composition. However, the individual values of toughness vary strongly as a function of notch width and differ between the SENB technique and the indentation technique.

TABLE 2

Composition/mol% Y_2O_3	*Sintering treatment/°C: h*	*SENB K_{Ic}/MPa $m^{1/2}$*			*Indentation K_{Ic}/MPA $m^{1/2}$*
		0·1	*0·5*	*1*	
2	1 675: 2	7·67	15·91	17	10·0
2·5	1 675: 2	6·88	13·40		8·9
2	1 575: 0·5	6·99	13·71	17	9·3
2	1 400: 2	6·44	12·69	16	9·0
2·5	1 400: 2	5·56	10·11		5·7

Of particular note is the observation that SENB toughness with a 0·1 mm notch is considerably lower than the indentation toughness for the 2 mol% Y_2O_3 sintered at 1675°C.

The test bars with the 1 mm wide notches showed considerable variation between individual specimens (averaging 5 MPa $m^{1/2}$), whilst the scatter in the K_{Ic} values for test bars with 0·1 mm notches is $<0{\cdot}4$ MPa $m^{1/2}$. The increase in notch width causes the measured K_{Ic} values to increase by more than 100%, indicating the importance of this experimental variable to the measurements.

Following the XRD analysis of the fracture surfaces and the determination of the monoclinic content, it became possible to plot the increase in toughness as a function of the extent of the monoclinic transformation directly. These results are shown in Fig. 1.

It is apparent that the toughness measured is dependent on the width of the notch and that specimens with similar sintering schedules exhibit less transformation to the monoclinic phase with the narrow (0·1 mm) notches when compared to the 0·5 mm notches.

For the 0·1 mm and 0·5 mm notch width fracture toughness data there is a linear relationship between K_{Ic} and the monoclinic content.

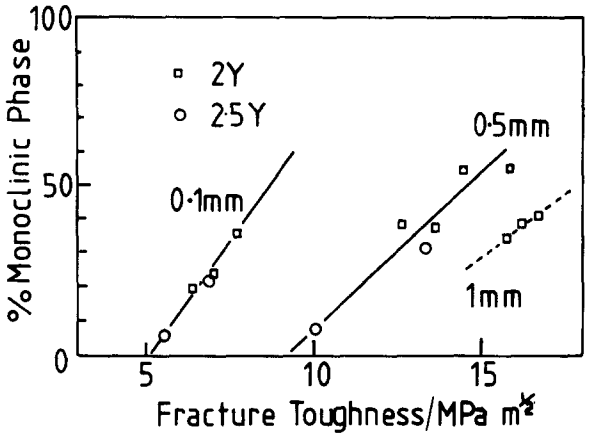

Fig. 1. Percentage monoclinic phase in fracture surface vs toughness for three notch widths, 0·1, 0·5 and 1 mm, and two compositions (□, 2Y; ○, 2·5Y).

Extrapolation of this line for the 0·1 mm notch width specimens to the K_{Ic} axis indicates a toughness for tetragonal material of about 5 MPa $m^{1/2}$ where no transformation occurs.

In order to obtain a set of data over a range of notch widths, test bars with 1 mm wide notches were made. However, no further conclusions can be drawn from the data on this specimen configuration.

4. DISCUSSION

4.1. Comparison of SENB and indentation techniques

The most surprising result of this study has been the discovery that SENB specimens with 0·1 mm notches have K_{Ic} values considerably smaller than the indentation K_{Ic} values for the same materials. It is not yet clear whether further reduction in notch width (for example to 40 μm) will result in a further reduction in K_{Ic}. The evidence from other studies[13] indicates this to be the case. Further, the study of Haberko and Pampuch[4] while it is not directly comparable, showed a minimum value of K_{Ic} by indentation of $\sim$2 MPa $m^{1/2}$. This may be partly attributable to the low value of the Young's modulus, E, indicative of the higher porosity ceramic used in their study.

A 6 mol% Y_2O_3 material examined in conjunction with the present work proved to have an indentation toughness of 2·2 MPa $m^{1/2}$, and yet after abrasion showed no evidence of the presence of transformable tetragonal material. However, there could well be a lowering in toughness

with an increase in yttrium oxide concentration not related to the transformation process. A 3 mol% Y_2O_3 material sintered at low temperature to produce a fine grain size, and therefore in a relatively untransformable condition, has a toughness of 3·9 MPa $m^{1/2}$. These results indicate that K_{Ic} values of certain TZP ceramics may be even lower than the present study indicates. If a value of 4 MPa $m^{1/2}$ is assumed to be the toughness of tetragonal zirconia of low yttrium oxide content in the absence of the transformation, the data in Fig. 1 indicate that the maximum toughness measured by the notched beam technique on a specimen undergoing 100% transformation would be of the order of 12·5 MPa $m^{1/2}$. However, it is clear that such extensive transformation rarely occurs in materials based on the homogeneous co-precipitated powders used in this study. The 2Y material sintered at 1675°C for 2 h has a grain size of the order of 1·5–2 μm but only undergoes 40% transformation in the fracture surfaces with a 0·1 mm notch.

From the results and the preceding discussion it is apparent that the toughness of TZP materials determined by indentation is overestimated when extensive transformation occurs. This may be due in part to the induced transformation taking place in regions of the ceramic adjacent to the indent. Such transformation together with the accompanying volume expansion would tend to close the radial cracks and inhibit their propagation, resulting in overestimation of the toughness. By contrast, cracks in annealed SENB specimens with fine notches may begin to propagate in the tensile stress field before there is a sufficient stress intensity to initiate transformation ahead of the crack tip. Thus the 'material-independent' constant for well behaved materials in the indentation equation of Anstis *et al.*[1] clearly requires revision where transformation takes place and the condition of the metastable material in the region of the crack requires quantitative characterisation.

4.2. The effect of notch width on K_{Ic} in TZP

The effect of increase in notch width on measured K_{Ic} in TZP, compared to that in studies of other ceramic materials (including PSZ), is very large where extensive transformation takes place. Over the range of notch widths studied, increases in K_{Ic} of the order of 120% are observed. This is three times the increase observed for aluminas and PSZ materials. The size of this increase must be related to the induced transformation in the notch tip zone prior to crack initiation and is analogous to excessive plastic yielding due to overload during crack initiation in metals.

The large increase in the scatter of K_{Ic} results with increase in notch width suggested that fracture initiation at the base of large notches may

be controlled by both the transformation and statistical variations in the flaw population associated with the notch. As the notch width is increased, the flaw distribution in the base of the notch dominates the load required to initiate failure and, hence, gives rise to large variability in the results. Furthermore, the increased radius of curvature of the notch will allow a large volume under stress in the notch tip, which on transformation can develop transformation-induced flaws, caused by the link up of microcracks associated with the transformation, or by their interaction with pre-existing processing flaws.

4.3. Estimation of K_{Ic} increment due to transformation

Earlier work indicated that the shear component of the transformation dominates in the fracture toughness increment of TZP ceramics.[7] Seyler and his co-workers[6] have analysed this problem and suggested that the toughening increment for transformation can be determined by

$$\Delta K_I^T = \frac{E\gamma^T}{(1-\nu^2)} w^{1/2} 0{\cdot}21 \ (\sin 2\phi)$$

where γ^T is the shear strain, E is Young's modulus, w is the zone diameter, ϕ is the angle between the crack plane and the shear direction, and ν is Poisson's ratio. This relation can be used to predict the toughening increment for a fully transformed zone (assuming all grains are favourably oriented).

Using

$E = 203$ GPa (determined using a longitudinal resonance technique)

$\nu = \sim 0{\cdot}32$ (Ingel *et al.*[9])

$w = 2\,\mu$m (the maximum grain size of the material observed by SEM)

$\phi = 45°$ (to maximise the expression)

$\gamma^T = 0{\cdot}08$ (Rühle *et al.*[18])

$\Delta K_I^T = 5{\cdot}37$ MPa m$^{1/2}$

This relatively simple analysis compares quite well with the increment estimated from experimental data in this study, which is

$$\Delta K_I^T = 7{\cdot}5 \text{ MPa m}^{1/2} \text{ (for 100\% transformation)}$$

There is also a hydrostatic and a microcracking contribution to the toughening[19] which would make up for the conservativeness of the theoretical prediction. Seyler's expression can therefore be modified to take account of the incompleteness of the transformation by introducing a term for the extent of the transformation, V_f.

Thus

$$\Delta K_I^T = 0{\cdot}21 \frac{E\gamma^T}{1-\nu^2} w^{1/2} . V_f$$

The $(\sin 2\phi)$ term is omitted since only favourably oriented grains are observed to transform.

If the fracture toughness in the absence of transformation is assumed to be 4 MPa $m^{1/2}$ for materials in the compositional range 2–3 mol% Y_2O_3, it is possible, using the above expression, to make a conservative estimate of the toughness of the material. It requires a knowledge of the grain size and the extent of transformation in the fracture surface, which can be determined by XRD and SEM of MOR specimens.

The modified expression is similar in form to that of Evans:[5]

$$\Delta K = 0{\cdot}2G\gamma^T V_f w^{1/2}$$

where G is the shear modulus.

5. CONCLUSIONS

1. The indentation technique for determining K_{Ic} is inappropriate for TZP materials and overestimates the toughness by at least 25% where substantial transformation occurs on fracture.
2. There is a considerable dependence of SENB K_{Ic} values on the width of the notch. The narrow (0·1 mm) notch used in this study gives K_{Ic} values lower than those given by indentation techniques.
3. There is a linear relationship between toughness increment and the extent of transformation, which can be predicted by the expression

$$\Delta K_I^T = 0{\cdot}21 \frac{E\gamma^T}{(1-\nu^2)} w^{1/2} V_f$$

when the zone size (w) is considered to be of the same dimension as the grain size of the transforming material.

REFERENCES

1. Anstis, G. R., Chantikul, P., Lawn, B. R. and Marshall, D. B., A critical evaluation of indentation techniques for measuring fracture toughness: I, Direct crack measurement, *J. Am. Ceram. Soc.*, **64** (1981) 533–8.
2. Paterson, A. W. and Stevens, R., Phase analysis of sintered yttria–zirconia ceramics by X-ray diffraction, *J. Mat. Res.*, **1** (1986) in press.
3. Rühle, M., Kraus, B., Shecker, A. and Waidlech, D., *In-situ* observations of stress-induced phase transformations in ZrO_2-containing ceramics, in *Advances in Ceramics 12*, Eds N. Claussen, M. Rühle and A. H. Heuer, American Ceramic Society, Columbus, Ohio, 1984, 256–74.

4. Haberko, K. and Pampuch, R., Influence of yttria content on phase composition and mechanical properties of Y-PSZ, *Ceramics Int.*, **9** (1983) 8–12.
5. Evans, A. G., Toughening mechanisms in zirconia alloys, in *Advances in Ceramics 12*, Eds N. Claussen, M. Rühle and A. H. Heuer, American Ceramic Society, Columbus, Ohio, 1984, 193–212.
6. Seyler, R. J., Lee, S. and Burns, S. J., A thermodynamic approach to fracture toughness in PSZ, in *Advances in Ceramics 12*, Eds N. Claussen, M. Rühle and A. H. Heuer, American Ceramic Society, Columbus, Ohio, 1984, 213–24.
7. Paterson, A. W. and Stevens, R., Preferred orientation of the transformed monoclinic phase in fracture surfaces of Y–TZP ceramics, *Int. J. High Tech. Ceram.*, **2** (1986) 135–42.
8. Tsukuma, K. and Shimada, M., Hot isostatic pressing of Y_2O_3 partially stabilized zirconia, *Am. Ceram. Soc. Bull.*, **64** (1985) 310–13.
9. Ingel, R. P., Lewis, D., Bender, B. A. and Rice, R. W., Physical, microstructural and thermomechanical properties of ZrO_2 single crystals, in *Advances in Ceramics 12*, Eds N. Claussen, M. Rühle and A. Heuer, American Ceramic Society, Columbus, Ohio, 1984, 408–14.
10. Lange, F. F., Transformation toughening. Part 3, Experimental observations in the ZrO_2–Y_2O_3 system, *J. Mat. Sci.*, **17** (1982) 240–6.
11. Tsukuma, K., Kubota, Y. and Tsukidate, T., Thermal and mechanical properties of Y_2O_3-stabilized tetragonal polycrystals, in *Advances in Ceramics 12*, Eds N. Claussen, M. Rühle and A. Heuer, American Ceramic Society, Columbus, Ohio, 1984, 391–8.
12. Watanabe, M., Iio, S. and Fukuura, I., Aging behaviour of Y-TZP, in *Advances in Ceramics 12*, Eds N. Claussen, M. Rühle and A. Heuer, American Ceramic Society, Columbus, Ohio, 1984, 391–8.
13. Claussen, N., Pabst, R. and Lahmann, C. P., Influence of microstructure of Al_2O_3 and ZrO_2 on K_{Ic}, *Proc. Brit. Ceram. Soc.*, **25** (1975) 139–49.
14. Munz, D., Effect of specimen type on measured values of fracture toughness of brittle ceramics, in *Fracture Mechanics of Ceramics 6*, Eds R. C. Bradt, A. G. Evans, D. P. H. Hasselman and F. F. Lange, Plenum Press, New York, 1983, 1–26.
15. Gogotsi, G. A., Zavada, V. P. and Petrenko, V. P., Determination of the crack resistance of a ceramic in bending of beams with a notch, translation of *Proshkovaya Metallurgia*, **1**(265) (1985) 67–72.
16. Garvie, R. C., Hannink, R. H. M. and Urbani, C., Fracture mechanics study of transformation toughened zirconia alloy in the CaO–ZrO_2 system, *Ceramurgia Int.*, **6** (1985) 19–24.
17. Richerson, D. W., *Modern Ceramic Engineering—Properties, Processing and Use in Design*, Marcel Dekker Inc., New York, 1982, 96.
18. Rühle, M. and Heuer, A. H., Phase transformation in ZrO_2-containing Ceramics: II, The martensitic reaction in t-ZrO_2, in *Advances in Ceramics 12*, Eds N. Claussen, M. Rühle and A. H. Heuer, American Ceramic Society, Columbus, Ohio, 1984, 14–32.
19. Rühle, M., Claussen, N. and Heuer, A., Microstructural studies of Y_2O_3-containing tetragonal ZrO_2 polycrystals (Y-TZP), in *Advances in Ceramics 12*, Eds N. Claussen, M. Rühle and A. Heuer, American Ceramic Society, Columbus, Ohio, 1984, 352–70.

Received 3 February 1986; accepted 18 June 1986

Int. J. High Technology Ceramics **2** (1986) 231–232

Book Review

Ceramic Containing Systems: Mechanical Aspects of Interfaces and Surfaces. Edited by A. G. Evans. Noyes Publications, New Jersey, 1986. Price: $36.00.

This volume is a collection of 12 papers covering five aspects of the mechanical behaviour of materials: monolithic ceramics; ceramic matrix composites; ceramic/metal bonded systems; polymers; and water drop impact. The book was prepared from another volume written in 1984. The logic for the selection of topics is no more than the research projects awarded to Professor Evans by the US Office of Naval Research. The Editor is in fact co-author of all the papers.

The first section concerns monolithic ceramics. An analysis is provided of the microcracking in polycrystalline ceramics of anisotropic crystal structure due to the combined influence of residual stresses and applied loads. This leads to the prediction of microcrack densities and hence the stress/strain curves of microcracking materials. This information is then used to consider microcrack toughening, involving computations of the fracture toughness from the stress/strain data. Toughness variations with grain size are discussed in terms of the model. Discussion then turns to a thermal stressing technique to evaluate surface and corner flaw populations in barium titanate multi-layer capacitors. Corner flaws are identified as the major source of failure during typical in-service thermal cycling.

The second section deals with ceramic matrix composites. Unidirectional silicon carbide fibre/glass ceramic composites were investigated during tensile and bend loading. Behaviour is discussed in terms of multiple matrix cracking followed by fibre fracture and pullout. The relevance of

Int. J. High Technology Ceramics (2) (1986)—

fracture mechanics principles to the systems is discussed, and the principles then applied in more detail to such systems. The matrix cracking stress is calculated from a stress intensity approach, influenced by the fibres that bridge the matrix crack. It is possible to relate the matrix cracking stress with material properties.

Some important aspects of ceramic/metal bonded systems are discussed in the next section. The mechanics of failure are considered and implications for optimised strengths of ceramic/metal bonds are given. Calculations are presented for the residual stresses that develop during cooling of metal/ceramic strips. A second geometry considered, as relevant to microelectronics packaging systems, is a cylindrical metal cylinder through a ceramic matrix.

In the fourth section attention is turned to polymers, with discussions of the mechanisms of toughening in rubber-toughened polymers and of the toughness of particulate-filled polymers. Quantitative predictions are made for various toughening mechanisms which should aid the development of tougher materials. The co-authors of the papers in this section appear to be associated with the University of Cambridge, England, although no acknowledgement of this fact is given.

The final section is concerned with water drop impact. A computer simulation is given for the impact damage process which gives information about the crack patterns in the impact zone. Further theory estimates the inner radius of the crack damage field during impact, and this is expressed as a function of drop size, impact velocity and Rayleigh velocity of the target.

Each of the papers presented is a good balance between background theory, which is generally developed expressly for the topic under consideration, and a comparison with relevant experimental data. The volume is a clear testament to the innovative and broadly based research interests of Professor Evans. As a book it must be regarded less favourably and of rather limited usefulness. Much of this work, in some form or other, has been published independently in the technical literature. The breadth of subject matter is unsuitable for a single subject volume (although probably no more varied than some conference proceedings). The publishers claim that advanced composition and production methods and special techniques have been used as aids to speed of production and reduction in costs. This involves use of camera-ready text but the papers are produced in a wide range of styles and the general result is extremely untidy. The reproduction of photographs is particularly poor; these and a lot of the text give the impression of a second or third generation photo-copy.

R. W. Davidge

Int. J. High Technology Ceramics **2** (1986) 233–234

CALENDAR

1986 Meetings

Nov. 10–12	ISO3, 3rd International Conference/Exhibition on Isostatic Pressing, London, UK
Nov. 17–21	Engineering Foundation Conference on Bio-ceramics, USA
Nov. 25–27	The 3rd Annual ME Conference, London, UK
Dec. 1–6	MRS 1986 Fall Meeting. Symp. E: Advances in Structural Ceramics, Boston, Massachusetts, USA
Dec. 17–19	Engineering with Ceramics—Institute of Ceramics Basic Science Section Meeting, London, UK

1987 Meetings

Jan. 18–21	11th Annual Conference on Composites and Advanced Ceramics, Cocoa Beach, Florida, USA
Mar. 4–6	German–French Meeting on Technical Ceramics, Aachen, FRG
Mar. 29–Apr. 3	Chemical Vapour Deposition, Jerusalem, Israel
Apr. 5–9	International Conference on Wear of Materials, Houston, Texas, USA
Apr. 8–10	High Technology in the Ceramic Industry, Canterbury, UK

Int. J. High Technology Ceramics (**2**) (1986)—

Apr. 26–29	American Ceramic Society Annual Meeting, Pittsburgh, Pennsylvania, USA
Jun. 15–16	Hot Isostatic Pressing, Luleå, Sweden
Sept. 7–9	Science of Ceramics 14, Canterbury, UK
Nov. 4–6	Science and Technology of Sintering, Tokyo, Japan
Nov. 9–13	Science of Hard Materials, Nassau, Bahamas

Selected Abstracts from *Yogyo-Kyokai-Shi*

As a service to readers and with the agreement of The Ceramic Society of Japan, selected English language Abstracts of the papers appearing in the *Journal of the Ceramic Society of Japan* (*Yogyo-Kyokai-Shi*) are reproduced here. The selection was made by Drs R. Stevens and P. Popper.

Yogyko-Kyokai-Shi **94**(1) (1986)
Special Issue Non-Oxide Materials

The page numbers of the papers appear at the end of the abstract.

The Synthesis of Ultrafine Si_3N_4 in a Hybrid Plasma

Toshihiko TANI*, Toyonobu YOSHIDA and Kazuo AKASHI

Department of Metallurgy and Materials Science,
Faculty of Engineering, The University of Tokyo
7-3-1, Bunkyo-ku 113
* Present address : Toyota Research and Development Laboratories, Inc.

Ultrafine silicon nitride powders were prepared in a hybrid plasma, which is characterized by the superposition of a radio-frequency plasma and an arc jet. The reactants of $SiCl_4$ and NH_3 were injected into an arc jet and a tail flame of the hybrid plasma, respectively. The purity of the prepared powder largely depended upon the flow rate of NH_3. Especially, the nitrogen content in the products increased drastically when the flow rate of NH_3 exceeded about 10 *l*/min, and reached the value of about 37 wt% at the flow rate of 20 *l*/min. The prepared powder was soft, fluffy, pure white, and completely amorphous. Moreover, the particle size was from 10 to 30 nm. For a better understanding of the process, thermodynamic equilibrium compositions for the Ar-H_2-NH_3-$SiCl_4$ system were calculated up to 3500 K. Under the assumed conditions, condensed phase of Si is present at the temperature higher than the condensation temperature of Si_3N_4. A lower flow rate of NH_3 widens the temperature range of the Si existence and promotes the formation of $SiCl_2$ by recombination processes. These results suggested that the effective "Reactive Quenching" is the key to success for the synthesis of ideal ultrafine Si_3N_4 powder in this process. [Received July 31, 1985]

pp. 1–6

Synthesis and Characterization of Ultrafine Silicon Nitride Powder Produced by a Hybrid Plasma Technique

Shoji FUTAKI, Katsuzo SHIRAISHI, Tadayoshi SHIMIZU and Toyonobu YOSHIDA*

Central Research Laboratory, Sumitomo Metal Mining Co., Ltd.
3-18-5, Nakakokubun, Ichikawa-shi 272
* Department of Metallurgy and Materials Science, Faculty of Engineering, The University of Tokyo

Ultrafine powder of silicon nitride has been synthesized from the system $SiCl_4$-H_2-NH_3 in a hybrid plasma at the production rate of 100 g/h. The powder was white and fluffy. The X-ray diffraction pattern and the infrared absorption spectrum showed that the ultrafine powder was amorphous Si_3N_4. The crystallization temperature was as high as 1500°C which suggests the high purity of the powder. Chemical composition of the powder was $Si_3N_{3.88}O_{0.35}H_{0.19}$ and the presence of silicon diimide was not detected. The specific surface area of the powder was 60-70 m^2/g and the particle diameter was expected about 300 Å. The powder particles were spherical and the surface was covered with oxidized film of 6-7 Å in thickness. It was observed that amorphous Si_3N_4 ultrafine powder was gradually oxidized in air. [Received July 31, 1985]

pp. 7–11

Preparation of Si_3N_4-SiC Films by Plasma CVD

Kiichiro KAMATA, Yuuji MAEDA, Kanji YASUI and Minoru MORIYAMA*

Faculty of Engineering, Technological University of Nagaoka
1603-1, Nagamine, Kamitomioka-cho, Nagaoka-shi 949-54
* Nagano College of Technology

This paper reports Si_3N_4-SiC films prepared by plasma CVD from SiH_4(90% Ar), NH_3, C_2H_4 and H_2 gas mixtures. Compositions of the films were varied roughly from stoichiometric Si_3N_4 to SiC by changing the flow rate ratio of these gases. Amorphous films with smooth surface were prepared under the pressure of 66.7 Pa(0.5 Torr) at 400°C and a deposition rate about 0.4 $nm \cdot sec^{-1}$. Properties of the films such as thickness, composition, refractive index, structure, texture, infrared absorption and visible ultraviolet absorption spectra were evaluated. Nitrogen and carbon contents in the films were found to be proportional to the flow rate ratio of the raw gases. The wave number of infrared absorption peak shifted from 860(Si-N bond) to 780(Si-C bond)cm^{-1} with increasing carbon content in the films. The optical band gap determined from visible ultraviolet absorption edge shifted from 3.7(Si_3N_4) to 2.4(SiC)eV, also. From above results and TEM observations, it is anticipated that nitrogen and carbon atoms in the films are distributed in an atomic scale in contrast to those in Si_3N_4-C ceramics hitherto prepared by pyrolytic CVD. [Received August 19, 1985]

pp. 12–18

Vapor Phase Growth of β-Sialon Whisker by Nitridation of the System SiO_2-C-Na_3AlF_6

Takashi HAYASHI, Shigehisa KAWABE* and Hajime SAITO**

Department of Applied Chemistry, Faculty of Engineering, Nagoya University, Furo-cho, Chikusa-ku, Nagoya-shi 464
* Now with NEC Corporation
** Now with Toyota Technological Institute

The vapor phase growth of β-sialon whisker was investigated by nitridation of the system SiO_2-C-Na_3AlF_6 in a flow of N_2 gas at 1350° and 1400°C. Whiskers were grown both inside and outside graphite sample cylinder with caps. In the former, α-Si_3N_4 whisker grew mainly, while in the latter, β-sialon ($Si_{6-z}Al_zO_zN_{8-z}$) whisker grew along with a small amount of α-Si_3N_4 whisker. Although the amount of the whiskers formed at the outside increased with an increase in molar ratio Na_3AlF_6/SiO_2, the fraction of β-sialon whisker decreased and that of α-Si_3N_4 whisker increased. The β-sialon/α-Si_3N_4 ratio in the whiskers formed at outside depended also on the reaction temperature and N_2 gas flow rate. Under optimum condition, the whiskers containing about 85% β-sialon, up to 10 mm long and 1.0～10 μm thick, were obtained in about 20% yield. It was considered that β-sialon whiskers with droplets at the tips grew by the VLS growth mechanism by the precipitation from the supersaturated solution of SiO, CO, AlF_3 and N_2 gas in the droplets. The composition of β-sialon whiskers was estimated to be $z \fallingdotseq 1.8$-2.0 on the basis of XRD data. [Received August 8, 1985]

pp. 19–25

Pressureless Sintering of Ultrafine SiC Powder Produced by Gas Evaporation Method

Masato OHKOHCHI and Yoshinori ANDO

Department of Physics, Faculty of Science and Technology, Meijo University
Shiogamaguchi, Tenpaku-ku, Nagoya-shi 468

Pressureless sintering of ultrafine powders of β-SiC prepared by a gas evaporation method was carried out in the atmosphere of Ar. When the raw material was sintered without sintering aids, only the grain growth occurred without significant densification. It was proved that the simultaneous addition of boron and carbon is effective for the densification of present ultrafine powder produced by gas evaporation method also. The addition of carbon as a sintering aid is not always necessary, because the raw materials contain a few percent of free carbon. The highest density, 97% theoretical, was obtained with the aids of 1.0 wt% boron and 4.3 wt% free carbon at 2200°C. In the following two cases, plate-like crystals (6H-type SiC) larger than 50 μm grew and the densification was significantly prevented : (1) The raw material including a considerable amount of free silicon was sintered with the aids of boron 1.0 wt% above 1900°C. (2) The raw material containing free carbon less than 3.0 wt% was sintered with the excess aids of boron more than 1.0 wt% above 2100°C. [Received July 15, 1985]

pp. 26–34

Synthesis of Submicron SiC Powder from Carbonization of Iminodisilanenitrile

Nobuhiro KODAMA, Toshihiko ARAKAWA, Yuji TOKUNAGA and Takaaki TSUKIDATE

(Tokyo Research Center, Toyo Soda Manufacturing Co., Ltd.
2743-1, Hayakawa, Ayase-shi 252)

The formation of silicon carbide powder by carbonization of iminodisilanenitrile (Si_2N_3H) has been investigated. Submicron SiC powder was produced by heating the mixture of carbon black and amorphous Si_4N_3H for 0.5-4 h at 1350°-1650°C under reduced pressure. The crystallinity of the products increased with increasing the reaction temperature and reaction time. The particles were spherical and had maximum size of 0.2-0.4 μm in diameter. A reaction process consisting of the formation of Si_3N_4 particles as an intermediate and the subsequent carbonization was proposed for the formation of present SiC particles. [Received August 8, 1985]

pp. 35–7

Formation and Crystallization of Oxynitride Glasses in the System Si, Al, Mg/O, N

Takashi HAYASHI* and T.Y. TIEN

(Materials and Metallurgical Engineering, The University of Michigan
Ann Arbor, MI 48109, USA
*Now with Department of Applied Chemistry, Faculty of Engineering, Nagoya University
Furo-cho, Chikusa-ku, Nagoya-shi 464)

Mg-Sialon oxynitride glasses were prepared from the mixtures of Si_3N_4, AlN, SiO_2, Al_2O_3 and MgO, and the glass forming regions were determined in the system Si, Al, Mg/O, N on cooling from 1550°C. Glasses containing up to 6.5 at% N were obtained. The substitution of nitrogen for oxygen in cordierite-based composition glasses resulted in significant increase of density, glass transition temperature, Vickers hardness and refractive index, and decrease of thermal expansion coefficient. In DTA curves, exothermic peak due to the crystallization of cordierite was observed in the range of 1000°C to 1200°C. The effect of heating time and temperature and Pt as a nucleation agent on the crystallization of the glasses was studied. It was found that optimum temperature to precipitate cordierite crystals was 1200°C and Pt was effective in controlling of the microstructure. The Mg-sialon glasses are considered to be self-nucleating and can, therefore, form finer-grained glass ceramics, compared with the corresponding oxide glasses. A microstructure of cordierite crystals dispersed in a oxynitride glass matrix was observed on the crystallization. Mg-sialon glass ceramics had thermal expansion coefficients comparable to its values of Si_3N_4 ceramics.

[Received August 2, 1985]

pp. 44–52

Reduction of Dewaxing Time by Pressurized Atmosphere in the Ceramics Injection Molding Process

Makoto INOUE, Tadamoto SAKAI and Taro KATAGIRI*

Machinery and Electronics Technology Center, The Japan Steel Works, Ltd.
6-1, Minami 1-chome, Funakoshi, Aki-ku, Hiroshima-shi 736
* Tokai Konetsu Kogyo Co., Ltd.

The effects of the pressurized nitrogen atmosphere on the dewaxing time of injection molded Si_3N_4 green parts have been studied. As-molded parts of complex shapes, such as cutter blades and turbocharger rotors were used, and were dewaxed within one or two days at the heating rate of 10°-20°C/h in the pressurized (5 kg/cm^{2}G) nitrogen gas atmosphere. On the other hand, dewaxing needed 6-20 days by the conventional method with the non-pressurized condition because of the limited heating rate of 1°-3°C/h. The extensive reduction in dewaxing time is explained in terms of the prevention of binder boiling and control of evolved gas volume.

[Received July 31, 1985]

pp. 78–80

Pressureless Sintering of Si_3N_4 with CeO_2, Y_2O_3 and Al_2O_3

Hisao SUZUKI and Hajime SAITO

Department of Mechanical Systems Engineering, Toyota Technological Institute
2-12-1, Hisakata, Tenpaku-ku, Nagoya-shi 468

Pressureless sintering of Si_3N_4 with CeO_2, Y_2O_3 and Al_2O_3 as sintering aids was carried out at 1750°C for 2 h in N_2 atmosphere. The amount of Al_2O_3 as an additive was 1.5 wt% and that of others ($CeO_2 + Y_2O_3$) was 15 wt%. The powder bed technique was used to suppress the decomposition of Si_3N_4. The addition of more than 7.5 wt% CeO_2 yielded Si_3N_4 materials having more than 95% relative density and flexural strengths of about 600 MPa at room temperature. These Si_3N_4 materials containing $Ce_5(SiO_4)_3N$, $Y_5(SiO_4)_3N$ and glassy phase as grain boundary phases were expected to have excellent high-temperature properties, such as superior oxidation resistance and high flexural strength at elevated temperature. With increasing the amount of CeO_2 addition, the fraction of α-Si_3N_4 solid solution, $\alpha'/(\alpha'+\beta)$, increased and reached about 65% for more than 10 wt% CeO_2 addition. The densification mechanism in this system was considered to be liquid phase sintering combined with reaction sintering in which α-Si_3N_4 solid solution was formed. With increasing temperature, α-Si_3N_4 solid solution transformed into β-Si_3N_4. The flexural strength of Si_3N_4 material containing 10 wt% of CeO_2 at 1300°C was as high as 500 MPa. The critical stress intensity factors (K_{IC}) of Si_3N_4 materials by the indentation microfracture method were about 6 MN/m$^{3/2}$.

[Received July 30, 1985]

pp. 81–9

Sintering Behavior of Si_3N_4 with Y_2O_3 and Al_2O_3 Addition

Mamoru MITOMO and Ken-ichi MIZUNO*

(National Institute for Research in Inorganic Materials
1-1, Namiki, Sakura-mura, Niihari-gun, Ibaraki 305
*Present address : NGK Spark Plugs Co., Ltd.,)

The densification behavior of Si_3N_4 with 5 wt% Y_2O_3 and 2 wt% Al_2O_3 was investigated using a dilatometer during heating for 1 h from 1750° to 1800°C in 1 atm N_2 (pressureless sintering) and from 1800° to 1980°C in 10 atm N_2 (gas pressure sintering). In the pressureless sintering, the densification occurred from 1600° to 1800°C. At 1800°C, the densification stopped after heating for 30 min due to the thermal decomposition of Si_3N_4. The maximum density of 71.7% theoretical was obtained in the pressureless sintering. In gas pressure sintering, the thermal decomposition was depressed and chemical reactions to increase the amount of liquid phase took place. The density of material was increased at 1800°-1980°C by a solution-reprecipitation process. The contribution of the process increased at higher sintering temperature. High density materials (relative density> 97%) were fabricated at 1930°-1980°C. The maximum density of 99.4% was obtained at 1950°C. Abnormal grain growth was observed during the densification at high temperatures which resulted in fibrous grains. [Received August 8, 1985]

pp. 96–101

Joining of Silicon Nitride by Solder System La_2O_3-Y_2O_3-Al_2O_3

Shigeru YAMAZAKI, Mitsuru KITAGAWA, Katsumi TAKATSU and Yoshinobu SUEHIRO

(Research and Development Division, Iwasaki Electric Co., Ltd.
1-20, Fujimi-cho, Gyouda-shi 361)

Silicon nitride-to-silicon nitride joints were made by using pre-baked oxide pellet solder composed of La_2O_3·Y_2O_3·Al_2O_3·SiO_2 and BeO which were mixed, ground, and then made pellet form. Joining was carried out under a nitrogen pressure of 40-53 kPa at 1400°C to 1500°C by heating and cooling temperature rate from 50° to 1800°C/min to find out the optimum joining condition. From the result of microscopic examination, no void and crack were observed in the jointed layer. The results of EPMA in the cross-section of the jointed region indicated that some elements of adhesive (La, Y, Al) diffused into Si_3N_4 to form a diffusion layer, while a small amount of N was found in the joining layer. From the results of the three-point bending measurements, a joining strength of 290 MPa was obtained for the sample bonded at comparatively low temperature 1450°C. Distructed part is considered to start at the diffusion layer, indicating that the joining strength will be much higher than that value. The Vickers hardness of diffused layer was stronger than that of Si_3N_4 itself. [Received August 9, 1985]

pp. 102–7

Metallizing of Silicon Nitride Ceramics

Akio SAYANO, Shun-ichiro TANAKA and Kazuo IKEDA

(Toshiba Corp., Metal Products Div.
8, Shinsugita, Isogo-ku, Yokohama-shi 235)

It was found that a metallized layer can be formed on Si_3N_4 ceramics using the paste containing Li_2MoO_4 and TiO_2. X-ray diffraction pattern and SEM observations revealed that the metallized layer consisted of Mo, TiN, $Y_2O_3 \cdot 2SiO_2$, etc., and that the thickness was around 7 μm. Metallized Si_3N_4 specimens were bonded to steel by Ag-Cu solder after Ni plating. The shear strength of the bonded specimens was about 130 MPa at room temperature, 100 MPa at 300°C and 50 MPa at 500°C. [Received August 8, 1985]

pp. 108–10

Oxidation Resistance of AlN Coated Graphite Prepared by Plasma Enhanced CVD

Hideaki ITOH, Mamoru KATO and Kohzo SUGIYAMA

(Department of Applied Chemistry, Faculty of Engineering, Nagoya University
Furo-cho, Chikusa-ku, Nagoya-shi 464)

Uniform and adherent aluminum nitride (AlN) films were coated on graphite substrate by plasma enhanced chemical vapor deposition using a reaction gas mixture of $AlBr_3$, N_2, H_2 and Ar. The oxidation resistance test of AlN coated graphite specimen (15×10×1 mm) was carried out in air (relative humidity : ~50%) in the temperature range from room temperature to 1200°C. Thermogravimetric analysis of the specimen showed that the oxidation resistance depends upon the preferred orientation and the film thickness of the AlN film. No oxidation of the graphite substrate occurred even at 1200°C, when the specimen was coated uniformly by the thick AlN film (thickness >15 μm) with a high preferred orientation to the c axis. At elevated temperatures (1050°-1200°C), these films followed the parabolic oxidation law. The oxidized surface layer of α-Al_2O_3 was confirmed to act as a passivation film for further oxidation of AlN film. However, the AlN films having low preferred orientation, were oxidized at 1200°C approximately linearly with the oxidation time. The latter film was unfavorable for the oxidation-resistant film of graphite. [Received July 30, 1985]

pp. 135–40

Thermal Shock Testing of Dense SiC by Water-Quenching

Masashi MIDORIKAWA* and Takayoshi ISEKI

(Research Laboratory for Nuclear Reactors, Tokyo Institute of Technology
O-okayama, Meguro-ku 152
* Now with : NIKKEI Techno-Research Co., Ltd.)

For the evaluation of thermal shock resistance of ceramics, water quench test in which a critical temperature difference, ΔT_c, is measured by degradation of strength has often been applied, although

many experimental conditions may influence the result. The main reason for using this method is that the test can be easily carried out. In this report, the effect of variation of heat transfer coefficient on the result was analyzed. Reaction-sintered (RB-) and pressureless-sintered (S-) SiC were used. A semicircular crack was introduced by Knoop hardness indentation on a polished surface of the specimen of 5×36×(2-5)mm. Each specimen was quenched in a 50 cm-deep water bath kept at 290± 2 K and then its bending strength was measured in 4-point bending. The value of ΔT_c was determined from a diagram of bending strength and quench temperature difference. Generally RB-SiC showed larger resistance than S-SiC, mainly because of much higher thermal conductivity of RB-SiC. Thermal stress generated by quenching at the indentation site and the surface heat transfer coefficient h was calculated from the following relation,

$$\sigma=\frac{E\alpha\Delta T}{1-\nu}f(\beta)$$

where σ is the stress generated, α the thermal expansion coefficient, E Young's modulus, ΔT the temperature change, ν Poisson's ratio and $\beta(=ah/k)$ is Biot's modulus, with k the material's thermal conductivity and a the characteristic length. Contrary to the above, the thermal stress generated was calculated as a function of quench temperature difference using the h value. Consequently Knoop indented specimen gives more than two ΔT_c's in some case and no well defined ΔT_c in other case.

[Received July 26, 1985]

pp. 141–5

Thermal Expansion of Chemically Vapor-Deposited Si_3N_4

Koichi NIIHARA and Toshio HIRAI

(The Research Institute for Iron, Steel and Other Metals, Tohoku University
2-1-1 Katahira, Sendai-shi 980)

The thermal expansion of chemically vapor-deposited (CVD) Si_3N_4 was investigated from 20° to 1000°C. X-ray and TEM analyses revealed that CVD-Si_3N_4 samples prepared from a mixture of $SiCl_4$, NH_3 and H_2 were only α-Si_3N_4 and free from impurity phases even at grain boundaries. The thermal expansion was measured using dilatometry, and X-ray diffraction techniques. The bulk CVD-Si_3N_4 specimens with (110) and (210) orientations indicated a lower coefficient of thermal expansion than those for the specimens with (222) orientation. This difference in thermal expansion may be the effect of the crystallographic anisotropy. In fact, X-ray diffraction technique revealed that the coefficient of thermal expansion of α-Si_3N_4 is lower in the a axis than in the c axis.

[Received August 12, 1985]

pp. 146–8

Thermal Conductivity of Pressureless-Sintered SiC with B_4C and C

Hiroshi NAKAJO and Yoshikazu UTSUMI

(Materials & Electronic Device Laboratory, Mitsubishi Electric Corporation
1-1-57, Miyashimo, Sagamihara-shi 229)

The effects of amount of additives B_4C and C on the thermal conductivity and bulk density, and the relation between the thermal conductivity and bulk density were described. SiC con-

taining B_4C and C was sintered at 2000° to 2150°C for 60 minutes by pressureless sintering. The thermal conductivity of dense SiC with a relative density of 98% reached 160 to 180 W/m·K by 1.5 wt% C and 2.0 wt% B_4C addition. Moreover, it was found that the additives in compact SiC were localized at grain boundaries and within grains. The non-uniform distribution of additives enhanced the thermal conductivity effectively. [Received August 21, 1985]
pp. 149–52

Sintering and Mechanical Properties of Silicon Nitride Crystallized from Amorphous Powder

——Effect of Yttria Addition——

Shuzo KANZAKI, Osami ABE and Hideyo TABATA

(Government Industrial Research Institute, Nagoya
1-1, Hirate-cho, Kita-ku, Nagoya-shi 462)

Sintering and mechanical properties of hot-pressed silicon nitride which was crystallized from amorphous powder with the addition of Y_2O_3 have been studied. The crystallization was performed by calcination at 1200°-1500°C in a nitrogen atmosphere with and without Y_2O_3 addition. The calcined powder was hot-pressed at 1750°C for 1h under a pressure of 49 MPa. Addition of Y_2O_3 promoted the crystallization of amorphous Si_3N_4 to α-phase and increased the rate of α/β transformation. The crystallized powder by calcining after Y_2O_3 addition consisted of fairly fine particles with uniform size distribution, while the calcination without additives resulted in powder of large particle size with various morphologies. The bulk density and the flexural strength tested at room temperature and at 1200°C increased with increasing initial α-phase content for the powders incorporated with Y_2O_3 before calcination, but decreased with decreasing α-phase content for the powder added with Y_2O_3 after calcination. The initial α-phase content had no significant effect on either the bulk density or the flexural strength of the hot-pressed bodies when the starting powder was prepared by crystallization of amorphous powder with the addition of Y_2O_3. It was found that the factors which control sinterability, mechanical properties and microstructure of the hot-pressed silicon nitride ceramics are morphology of the powder particles and the reaction products between Y_2O_3 and Si_3N_4 rather than the α-phase content. [Received August 8, 1985]
pp. 159–66

Preferred Orientation and Mechanical Properties of Pressureless Sintered Silicon Nitride

Yasuhiro GOTO*, Hiroyasu OHTA, Michiyasu KOMATSU and Katsutoshi KOMEYA

(Metal Products Div. Toshiba Corporation
Shinsugita-cho, Isogo-ku, Yokohama-shi 235
* Toshiba Research & Development Center)

Mixtures of granular α-and needle-like β-silicon nitride particles could be obtained by adequate heat treatment of α-silicon nitride. By cold-pressing and pressureless sintering, the c-axis of the

β-Si_3N_4 has a preferred orientation perpendicular to the cold-press direction. This orientation varied sharply in the vicinity of the specimen surface because of the β-Si_3N_4 grain growth along the surface. The degree of preferred orientation was related to the content of β-Si_3N_4 in the starting powder and to the molding pressure. Vickers microhardness and 3-point bending strength showed anisotropy due to the crystal orientation. [Received August 27, 1985]

pp. 167–71

Crystallinity of SiC Coated on Carbon Fiber

Kuniaki HONJO and Akio SHINDO

(Government Industrial Research Institute, Osaka
1-8-31, Midorigaoka, Ikeda-shi, Osaka 563)

The structure, crystallinity and preferred orientation of the SiC coated on carbon fiber at 1200°C from mixtures of monomethyltrichlorosilane, hydrogen, methane and argon were studied by X-ray and selected area electron diffractometries. The SiC was identified to be 3C type, in which the stacking sequence of the closest packed layers is highly disordered along one of the [111] directions. Moreover, it was found that a decrease in hydrogen concentration or an increase in methane concentration enhances the orientation of these layers parallel to the fiber surface, and increases the crystallite size. Such changes in the orientation and the crystallite size are considered to be due to the increase in methane concentration in the reaction zone.

[Received August 2, 1985]

pp. 172–8

Room Temperature Strength of β-Sialon Fabricated from Aluminum-iso-propoxide and α-Si_3N_4

Kazushi KISHI, Seiki UMEBAYASHI, Eiji TANI and Kazuo KOBAYASHI

(Government Industrial Research Institute, Kyushu
Shuku-machi, Tosu-shi 841)

β-sialon with $z = 0.5$ was fabricated from Al(Oi-Pr)$_3$/n-C_6H_{14} solution containing α-Si_3N_4 particles. The solution was ball-milled and spray-dried. The powder mixture of α-Si_3N_4 and Al(Oi-Pr)$_3$ was calcined and then hot-pressed. Three-point bending strength of the materials was measured at room temperature. The fracture origin was investigated by an optical microscope. Sintered β-sialon with $z = 0.5$ was consisted of β-sialon and a small amount of O'-sialon. The bending strength was 81 kg/mm^2 for the specimens ground with # 270 diamond wheel, 85 kg/mm^2 for those ground with # 600 diamond wheel and 97 kg/mm^2 for those polished with # 1500 SiC abrasive paper. The annealing at 1200°C for 1h in air increasing the strength remarkably up to 140kg/mm^2 (160kg/mm^2 in maximum). Most specimens fractured at surface flaw caused by machining. [Received July 29, 1985]

pp. 179–82

Properties of α-Sialon Ceramics

Kenki ISHIZAWA, Nobuo AYUZAWA, Akira SHIRANITA, Masamichi TAKAI, Norimasa UCHIDA and Mamoru MITOMO*

(Shinagawa Refractories Co., Ltd.
707, Imbe, Bizen-shi 705
* National Institute for Research in Inorganic Materials)

α-Sialon ceramics in the system of Si_3N_4-AlN-Y_2O_3 were fabricated by pressureless sintering. The solid solubility range, microstructure and mechanical properties such as fracture strength, hardness, fracture toughness were measured. In the Y-α-Sialon ceramics, there existed a composition range containing a small amount of additive named "partially stabilized α-Sialon" in which α-Sialon and β-Si_3N_4 coexist. α-Sialon ceramics with excellent mechanical properties can be obtained in this composition range by controlling composition and microtexture.

[Received August 1, 1985]
pp. 183–5

Fracture Energies of Sintered Boron Nitride

Michio INAGAKI, Kazuhiro URASHIMA, Shinsuke TOYOMASU and Mototsugu SAKAI

(Materials Science, Toyohashi University of Technology
Tempaku-cho, Toyohashi-shi 440)

Fracture energies of a sintered boron nitride were measured using chevron-notched compact tension type specimens. During stable crack growth unloading-reloading processes were repeated in order to evaluate the plastic deformation. From load P-loadpoint displacement u diagram, total fracture energy (work of fracture) γ_{WOF} was determined as 26.2 J/m^2 with error of less than 5%, close to a half of which (about 45%) was found to be dissipated by plastic deformation. The results were discussed in the relation with those on graphite materials.

[Received July 29, 1985]
pp. 186–7

Wear of Hot-Pressed Aluminum Nitride

Mikio IWASA and Tsutomu MURAO*

(Government Industrial Research Institute, Osaka
Midorigaoka 1-chome, Ikeda-shi 563
* Now with : Tatsuta Electric Wire & Cable Co., Ltd.)

Aluminum nitride ceramics were fabricated by hot-pressing at 1700°-2000°C, and their friction and wear properties were measured with a pin-on-disk tester. The sliding velocity dependence of wear was also investigated with a Sawin-type tester. AlN hot-pressed at 1700°C has some residual porosities, so its fracture toughness and Vickers hardness are relatively low. But they

become almost constant for AlN hot-pressed above 1800°C. Substantial grain growth was observed with increasing hot-pressing temperature. The friction coefficient and specific wear rate measured with the pin-on-disk tester increased with increasing hot-pressing temperature. Wear particles consisting of small AlN grains may act as a solid lubricant when sliding conditions are relatively mild. The specific wear rate measured with the Sawin-type tester was low at low sliding velocities, but showed a sharp maximum at the high velocity region. The peak is lower for AlN hot-pressed at higher temperatures. The wear in this region is supposed to be caused by the small fractures at contact points. As a result, AlN ceramics with higher fracture toughness and hardness show higher wear-resistance. [Received July 10, 1985]

pp. 188–93

Mirror Finish Grinding of β-Sialon with Fine Grained Diamond Wheels

Yoshio ICHIDA, Kozo KISHI, Tomoshige HANIDA, Yusuke IYORI* and Hisao HARA*

Faculty of Engineering, Utsunomiya University
2753, Ishiimachi, Utsunomomiya-shi 321
* Magnetic and Electronic Materials Research Laboratory, Hitachi Metals, Ltd.

The surface grinding tests for normal sintered β-sialon were carried out with various fine grained diamond wheels, and the influence of grain size on the characteristics of mirror finish grinding for the sintered sialon was investigated. When the sintered sialon was ground using fine grained wheels with a grain size of less than 6/12 μm, fine flow-type chips were formed. It has been confirmed that the formation of the chips and the removal of material proceed, in a large measure, by plastic deformation. In grinding the sintered sialon with fine grained wheels with a grain size of less than 6/12 μm, a mirror finished surface with a very small area of fractured surface could be obtained. For instance, when the sintered sialon was ground by a wheel with a grain size of 0.5/3 μm, a mirror finished surface with a surface roughness of about 0.03 μm R_{max} was obtained. The grinding force component, specific grinding energy U_e and maximum grinding wheel temperature θ_m increase with a decrease in grain size. When the mean grain diameter $\bar{d}$ does not exceed about 20 μm, U_e and θ_m are proportional to $(-\log \bar{d})$ approximately.

pp. 194–200

Grindability of Silicon Nitride Ceramics

Yoshihito KONDO, Yasuyuki KUROSHIMA, Akira TSUKUDA and Shōjirō OKADA

Kagawa Prefectural Industrial Technology Center
Gōtō-chō, Takamatsu-shi 761

A hot pressed silicon nitride ceramic is very difficult to grind and it is expected to be widely applied to the heavy duty use, which does not permit the slightest machining damage. Therefore, the efficient grinding without machining damage is very necessary. In this study, the said ceramic

was ground by several diamond grinding wheels in order to find out the relation between material removal rate and machining damage. According to the test results, the efficient grinding was performed using a vitrified diamond wheel of 170/200 grain size and the damaged layer was removed using a resinoid diamond grinding wheel of 270/325. [Received August 1, 1985]

pp. 201–3

Electrical Discharge Machining of ZrB_2-Based Composite Ceramics

Kazuo MANNAMI, Kohzo SAKAI and Masataro OKUMIYA

(Research & Development Div., Asahi Glass Co., Ltd.
Hazawa, Kanagawa-ku, Yokohama-shi 221)

ZrB_2 ceramics has high melting point, high hardness, low electrical resistance and high corrosion resistance against molten metal and slag. Because of the low electrical resistance, electrical discharge machining is available for ZrB_2-based composite ceramics. Electrical discharge machining (wire-type and ram-type) for ZrB_2-based composite ceramics has been studied. Cutting rate of ZrB_2-based composite ceramics is 50-70% of conventional steel and 1.5-2 times of cemented carbide. This is the commercial base cutting rate. Machining mechanism is melting and brittle fracture of ZrB_2-based composite ceramics by electrical discharging. Wear of positively polarized electrodes is more remarkable than those of negatively polarized one. ZrB_2 ceramics adhere to the electrode during electrical discharge machining. Because of this adhering, wear of the electrode decreases. [Received August 14, 1985]

pp. 204–13

Electrical Resistivity of SiC-ZrB_2 Electro-Conductive Ceramic Composites

Ken TAKAHASHI, Ryutarou JIMBOU, Yasuo MATSUSHITA and Tetsuo KOSUGI

(Hitachi Research Laboratory, Hitachi, Ltd.
1-1, Saiwai-cho 3-chome, Hitachi-shi 317)

Relations between the composition of SiC-ZrB_2 electro-conductive ceramic composites and their electrical resistivity, as well as their temperature dependences, were investigated. The resistivity of hot-pressed composites was measured by the Pauw method in the temperature range of RT to 800°C. The resistivity of the composites decreases with increasing the volume fraction of ZrB_2, and that was observed to be comparable to the value of Ni-Cr alloys or 18-8 stainless steel above 30 vol% ZrB_2. The effective medium theory can explain the relationship between the resistivity and the composition of the composites with ZrB_2 of more than 40 vol%, indicating the absence of correlation between the geometrical compositions of SiC and ZrB_2 grains in the composite. The resistivity of the composites with ZrB_2 between 23 vol% and 40 vol%, on the other hand, can be interpreted using the percolation theory. The resistivity versus temperature curves indicate the formation of local chains of ZrB_2 particles giving lower resistivities for the composites with ZrB_2 of less than 23 vol% than those expected by the percolation theory. [Received August 9, 1985]

pp. 214–18

Electrical Conduction in Sintered SiC

Kazuo OKANO

(Department of Electricity, Oyama Vocational Training College
612-1, Aza Mitake, Oaza Yokokura, Oyama-shi 323)

Relationship between sintering condition and electrical properties was investigated for sintered SiC. SiC powder containing boron and carbon was sintered in the temperature range of 1950°-2200°C in vacuum and cooled at 5 and 35°C/min. The electrical properties of specimens depended on the sintering temperature. The electrical conductivity of specimens sintered below 2000°C was independent of measuring temperature and applied voltage. Whereas, the conductivity of specimens sintered above 2050°C depended on the temperature and voltage. To explain these results, two electrical conduction mechanisms were proposed ; (1) current along grain boundaries which was dominant in specimens sintered below 2000°C, and (2) current across grain boundaries, which was dominant in specimens sintered above 2050°C. The effects of cooling rate on the electrical conductivity were remarkable for specimens sintered above 2050°C. Conductivity of rapidly cooled (35°C/min) specimens was higher than that of slowly cooled (5°C/min) specimens, and this effect was remarkable below room temperature. A symmetry Schottky barrier model depicting high density localized states was proposed, and cooling rate dependence of conductivity was explained in terms of difference in density of localized states.

[Received July 31, 1985]

pp. 219–25

Int. J. High Technology Ceramics **2** (1986) 249–278

Review: Fabrication of Engineering Ceramics by Injection Moulding. II. Techniques

M. J. Edirisinghe and J. R. G. Evans

Department of Materials Technology, Brunel University,
Uxbridge, Middlesex, England

SUMMARY

The development of injection moulding techniques and their application to ceramic suspensions is described, with particular attention being paid to the mixing of suspensions prior to moulding and to the origin of moulding defects. Methods for the removal of the organic component of the injection moulding blend are reviewed.

1. INTRODUCTION

The injection moulding process evolved from metal die-casting technology and has been used for over a century for shaping polymers. The first ceramic articles were produced in this way half a century ago. Today, many substantial research programmes worldwide aim to perfect the fabrication of fine engineering ceramics by this versatile technique.[1]

A ceramic blend must be prepared prior to injection moulding and therefore dispersive mixing of the ceramic powder in an organic vehicle is an important initial step. Technical developments in mixing therefore impinge on ceramics fabrication by determining the uniformity of particle assemblies in prefired bodies and therefore uniformity and extent of shrinkage.

In the present review the main technical developments in injection moulding machine design are described, including recent developments which allow control over solidification in the mould.

Int. J. High Technology Ceramics 0267-3762/86/$03·50

The process of flow of the suspension into the cavity and of solidification is qualitatively described. The complexity of such processes still prevents the development of models which yield useful information for the practitioner. It is at this stage that moulding defects or residual stresses develop in moulded parts.

The polymer removal stage is often considered the most challenging technical aspect of the process. This may be because detailed study of this complex process has only recently begun. The techniques that have been applied to the problem, in so far as they have been published, are discussed below.

2. MIXING OF CERAMIC INJECTION MOULDING BLENDS

2.1. Characteristics of mixtures

The mixing of polymer–ceramic blends for injection moulding has received scant attention in ceramic literature but is considered of great importance in the preparation of filled polymers and polymer blends.[2–4] It will be shown below that it is also of considerable importance to ceramists because failure to disperse ceramic powder in a vehicle at an early stage in the process may result in non-uniform shrinkage at a microscopic or even macroscopic scale during subsequent sintering. The principles of mixing in so far as they apply to ceramic systems in general have been reviewed by Messer.[5]

It is generally insufficient to consider ceramic injection moulding blends as simply two-phase systems of ceramic in a polymer matrix. It has been shown[1] that the matrix is frequently a multicomponent polymer blend itself. Frequently it consists of a low-viscosity polymer or oil and a viscous thermoplastic. In most cases incomplete solubility can be expected to prevail and the degree of dispersion of one polymer phase in the other will influence the properties of the blend; in particular its decomposition kinetics. Thus the mixing of ceramic injection moulding blends involves the dispersion of ceramic particles and a minor polymer binder in a continuous matrix of the major polymer binder.

Mixing is defined as a process that reduces compositional non-uniformity and in viscous polymeric fluids the influence of molecular and eddy diffusion is generally negligible for useful timescales, leaving forced convective flow as the main mixing process.[2] If convection causes the movement of fluid or solid particles from one spatial location to another such that the interfacial area between liquid particles and the matrix

increases, or that solid particles are distributed throughout the matrix, then *distributive* mixing is said to have occurred.

Distributive mixing is influenced by the strain imposed on the mixture. However, in the case of viscoelastic polymers and agglomerated fine particles which show yield point characteristics, the application of strain is necessary, but insufficient, to achieve mixing. The strain rate and hence shear stress imposed on the material determine the extent of mixing and this is known as *dispersive* mixing.[2]

The importance of dispersive mixing in ceramic systems is illustrated by the recent work of Lange[6] on uniformity of prefired density in ceramics. If agglomerates start at a different prefired density from the dispersed particles in a ceramic body then very high stresses are set up during firing[7] and these can produce circumferential or radial cracks in the region of agglomerates[8] depending on whether the agglomerates shrink faster or slower than the matrix respectively.[9] Furthermore failure to disperse agglomerates may influence the sintering kinetics and reduce the fired density by leaving thermodynamically stable pores with a large grain co-ordination number.[10]

In defining mixture quality the *characteristic volume*, sometimes called the *scale of segregation*, is an important parameter. Characteristic volume may be defined[5] as the amount of material at every location throughout the mixture within which the position of individual particles is unimportant. Its size depends on the properties demanded of the mixture. For example the characteristic volume of an engineering ceramic injection moulding composition could be calculated from the dimensions of the flaw size defined by Griffiths' equation for a desired mechanical strength. This would mean that compositional uniformity would be expected among random samples of typically 1000 μm^3 volume. Since such samples are well below the limits of practical analysis, resort to microscopical methods[11,12] is necessary in defining mixture quality. Since flaws produced by firing agglomerated powders are typically of the same dimensions as the starting agglomerates[9] the characteristic volume will be smaller than the volume of agglomerates often found in ceramic powders.[12] The breakdown of agglomerates in shear flow is described quantitatively by Tadmor and Gogos.[13]

There is increasing interest in ultrafine monosized spherical powders which can be packed into ordered arrays for ceramic fabrication.[14,15] In this case the characteristic volume would be of particle dimensions. The best that can be expected from injection moulding of such particles is a uniform random packing throughout.

Numerous indices to quantify the extent of mixing have been proposed and these are reviewed by Fan and co-workers.[16,17] In general these are

based on the standard deviation s or the variance s^2 of the composition of spot samples taken from the mixture. The simplest such index[18] is given by

$$m_1 = \frac{\sigma_R}{s}$$

when σ_R is the standard deviation of composition for a random homogeneous mixture (RHM). A RHM is defined as a mixture in which the probability of finding a particle of a given component is the same at all locations in the mixture and σ_R is equal to $\sqrt{P(1-P)/n}$ for a binary mixture of particles. P is the proportion of one component and n is the number of particles in the sample.[18] The sampling of mixtures and treatment of results is extensively reviewed by Weidenbaum.[19]

A further aspect of mixture quality is the distinction between *ordered* and *random* mixtures. Ordered mixing occurs when fine particles of one component find interstices between large particles of another component.[5] Another example of interest in ceramics fabrication is where fibres mixed into a ceramic moulding composition exhibit preferred orientation or texture in the product. For single crystal fibres X-ray diffraction methods allow fibre orientation to be defined by a stereographic projection. For fibres amorphous to X-rays the preferred orientation in two dimensions can be defined by microscopical or microradiographical methods and the orientation in the third dimension is defined by the aspect ratio of the elipse created in the section plane by the fibre and can be found by quantitative microscopy.

2.2. Mixing techniques

Mixing devices for high-viscosity fluid are reviewed in several reputable texts.[4,20,21] The simplest mixers are so-called motionless mixers in which a fluid is pumped through intricately designed internal passages which create strain in the fluid and induce distributive mixing. Such mixers consist of a battery of mixing elements and these introduce a substantial pressure drop. The high viscosity of polymer–ceramic blends has thus restricted the use of such mixers.

Lower-viscosity fluids (10–100 Pa s) are frequently mixed in single-blade stirred tank devices which incorporate either propellers, turbines or paddles and produce distributive mixing.[4]

An advance on this process is the range of double-blade batch mixers such as the 'Z' or 'sigma' blade mixers which have been applied extensively to the blending of ceramic injection moulding material. Blade profiles and power requirements of such mixers are detailed by Irving and Saxton.[20]

Early experts on ceramic injection moulding such as Schwartzwalder[22] and Taylor[23] favoured such mixers and some recent research has also relied on these types.[24] The limitations of the double-blade mixers are the tendency for filled thermoplastics which show yield point behaviour to reside in dead spaces in the mixer and there is insufficient dispersive mixing to break down ceramic powder agglomerates.[12]

Banbury-type mixers provide higher intensity batch mixing and are used on high-viscosity fluids for pigment and filler dispersion. They consist of a figure-of-eight section mixing chamber containing two counter-rotating lobed rotors. Quackenbush *et al.*[25] employed a torque rheometer of similar design to prepare ceramic moulding compositions.

The two-roll mill is also a mixer ideally suited to the processing of high-viscosity materials. It consists of two counter-rotating differential speed rolls with an adjustable nip and imposes intense shear stresses on the material as it passes the nip. There is little transverse mixing and thus constant operator attention is needed to displace the strip transversely. This process can be partially automated for polymers. A two-roll mill was used by Birchall *et al.*[26] to produce very high solids content mouldable cement pastes.

Two types of extruder are used for mixing: single- and twin-screw extruders. Single-screw devices with a helical screw rotating inside a heated barrel are not efficient mixing devices[20] and are sometimes enhanced by the incorporation of mixing discs, torpedoes or planetary gears into the screw configuration. The total strain imparted to an element of material is strongly dependent on its position and therefore mixing tends to be non-uniform across the screw channel. Unlike the more complex extruders the helical flow behaviour in single-screw machines is well characterized[27] and machines are well documented in textbooks.[28,29]

Flow in single-screw extruders relies on adhesion of the material to the barrel wall and it was to overcome this limitation that twin-screw extruders evolved.[30] There are four types depending on whether the screws co-rotate or counter-rotate and whether the screws intermesh or not. The first device was an intermeshing co-rotating extruder invented in 1939, and patented in 1949.[31] Considerable variation of screw design is possible to balance pumping and mixing characteristics.[32] Intermeshing extruders provide positive displacement pumping unlike single-screw machines and the output in volume per unit time is given by the difference between the theoretical flow rate and the sum of the leakage flows described in Fig. 1:

$$Q = Q_{th} - Q_L = 2mNV - (Q_f + Q_c + Q_t + Q_s)$$

where m is the number of thread starts per screw, V is the volume of the 'C'-shaped channel between the flanks of successive flights and N is the

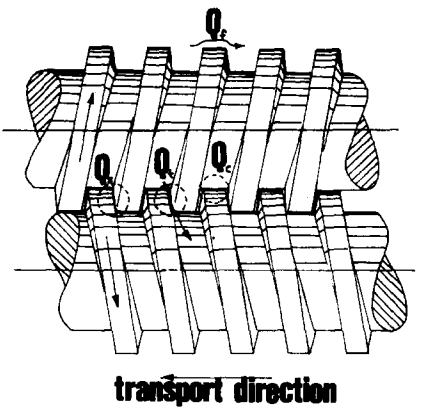

Fig. 1. Leakage flow paths in an intermeshing twin-screw extruder; after Janssen.[30]

rotation rate. Q_f is the leakage between screw flight and barrel wall, Q_c is the leakage between the screw flight and the other screw, Q_t is the leakage between the flanks of screw flights and Q_s is the leakage between flanks perpendicular to the plane through the screw axis.[30] The leakage paths have a strong influence on residence time in the extruder. Flow characteristics of such extruders have not been well defined and machine development has been largely empirical. As with single-screw devices mixing discs and kneading discs can be incorporated into the screw configuration.[33]

Twin-screw extrusion has been used for the preparation of particle-filled polymers[11] for reinforcement, flame retardancy, fabrication of prosthetic materials[34] or incorporation of magnetic or dielectric solids. The polymer degradation during processing can be controlled by screw design[35] and is found to be less severe than degradation induced by two-roll milling.[34] The degree of dispersive mixing obtained by twin-screw extrusion compounding is greater than that achieved by using a double-blade mixer.[12]

2.3. Composites

Of particular recent interest is the fabrication of ceramic matrix composites. This involves particular problems of mixing in which ceramic fibres or whiskers are dispersed along with ceramic powder in a fluid phase.

The theory of ceramic matrix composites was reviewed by Donald and McMillan in 1976.[36] Since then the reinforcement of engineering ceramics with ceramic fibres has acquired renewed interest as a toughening method.[37] Injection moulding has been used for short fibre reinforced polymers for many years[38,39] and considerable control is now possible over fibre orientation.[40] The main problem to be overcome when fibres or whiskers are incorporated in a ceramic suspension is control of fibre length

degradation during the mixing process and during flow in the moulding machine. This difficulty has led to interest in fabricating ceramics from polymeric precursors.[41]

3. DEVELOPMENT OF INJECTION MOULDING TECHNOLOGY

A study of the adaptation of metal die-casting technology to polymer moulding shows how the problems of defective mouldings were slowly overcome as attention was directed to key components of the moulding machine. Many of the problems associated with that technology transfer were similar to those encountered in modern attempts to mould ceramics.

The injection moulding process had its origins in the die-casting technique invented by Sturges in 1849[42] for non-ferrous alloys and therefore the designs of the first injection moulding machines for polymers were based upon die-casting methods. The first machine was used to fabricate cellulose nitrate plasticized with camphor and was patented by Hyatt in 1872.[43] In this machine a ram applied pressure to the material in a heated chamber, extruding it through a nozzle into a cooled mould to produce continuous rod, sheet or tube. The first moulding process used a multi-cavity mould to coat metal parts with Celluloid.[44,45] The key early developments were by Richards,[46] Eichengrun[47,48] and Buchholz,[49] and a more detailed account of early work is reported in several texts.[50-52] Some of the first materials moulded were filled with glass but the filler was abandoned because of poor results![50] The first semi-automatic machines emerged in Germany and America in 1929 and were activated by compressed air.[50] Although suitable for small articles these devices were limited by low material and clamp pressures.

An hydraulically activated machine appeared in 1934[53] and in the same period British machines appeared with hydraulic or pneumatic ram pressure.[50] Hydraulic mould clamping was introduced by Piperoux and Radburn in 1933[54] and this overcame the flashing inherent in earlier designs. The introduction of toggle mould clamping on the Isoma machines (1936) allowed superior mould locking. Uniform heating of the material was a problem in these early ram machines but improvements were achieved by incorporating a spreader into the flow channel patented by Gastrow.[55] Many of the characteristics of modern machines appeared in the rapid developments of the 1930s, including early automation made possible by temperature controllers, timers and dosing devices. Better control over injection pressure, mould closing and barrel heating facilitated the fabrication of large components. This in turn gave rise to larger

moulding machines, including the large multi-nozzle machines with vertical clamping which appeared in 1936. Serious problems of reproducibility of components remained, and to solve this problem an early automatic machine was patented by Burroughs.[56] Thus by 1940 machines had developed to include an hydraulic ram acting in a heated thermostatted cylinder with an internal spreader and injecting into a vertically or horizontally clamped mould with hydraulic and toggle clamping and automatic ejection.

By 1944 a machine was available capable of moulding both thermoplastic and thermosetting materials.[50] Mould closing and clamping by hydraulic and toggle methods were perfected by 1944. Large scale machines for thermosets were developed at this time,[57,58] and a device combining injection and compression moulding was in use.[59]

Machines are characterized by the injection end rather than the clamp geometry and two major classes of machine are commonly used: the plunger machine and the reciprocating screw machine.[45]

A typical single-stage plunger machine is shown in Fig. 2(a). A metered quantity of material enters the heated barrel from the feed hopper and, as the piston advances, flows over a torpedo or spreader designed to improve heat transfer.[60] Such machines suffered from the following disadvantages.[61] There was little mixing of the molten material, giving rise to inhomogeneity. The pressure at the nozzle could vary considerably from cycle to cycle as the plunger compressed material which ranged from solid granules to viscous fluid. Since viscosity of polymer melts is pressure sensitive, erratic pressures increased the mould filling variability. The torpedo caused a significant pressure drop. The shot size was difficult to meter accurately.

A preplasticizing system overcame some of these disadvantages.[62-64] Such machines had twin barrels and in the case of a two-stage plunger device material was plasticized in the first barrel before being fed into the second barrel via a non-return valve. The torpedo could then be omitted from the injection barrel. Homogeneity was assisted by passing the material

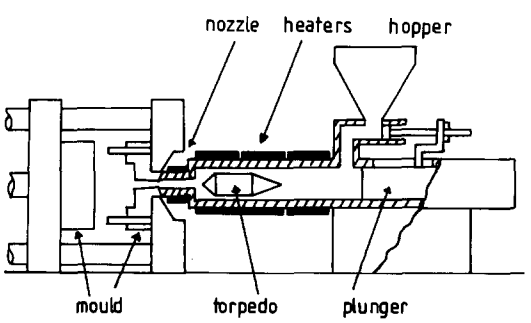

Fig. 2(a). Plunger-type injection moulding machine.

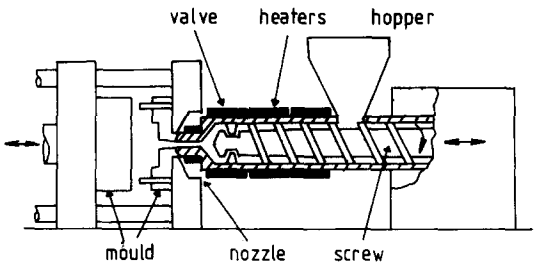

Fig. 2(b). Reciprocating screw-type injection moulding machine.

through the interconnecting nozzle. Shot size was metered by using limit switches on the primary barrel. In screw-plunger machines the primary plunger was replaced by a rotating screw.

The development of the reciprocating screw machine overcame many of the problems of plunger machines. The use of a rotating screw to heat and convey material was first introduced in Germany in 1943.[65] A typical reciprocating screw machine is shown in Fig. 2(b). Adhesion to the barrel wall allows the rotating screw to pump material forward, simultaneously mixing and heating the fluid to achieve uniformity. An adjustable pressure applied to the screw controls the reverse drift of the screw in the barrel and thus the plasticization of the material. The screw then ceases to rotate and behaves as a plunger, injecting material into the mould. A check ring or ball valve prevents leakage of material past the end of the screw. The screw remains in the forward position applying a hold pressure to compensate for shrinkage of the material in the cavity. The screw then again rotates recharging the injection chamber while the mould remains closed.

The fundamental improvement in the screw machine is the preplasticizing action[66–68] which causes direct Joule heating of the material. High shear rates produce lower viscosities in pseudoplastic fluids. Lower injection and clamp pressures can be used because of greater homogeneity of the material resulting from non-laminar flow. Degradation problems are less severe because of lower residence times and better heat transfer. This is especially advantageous in the processing of heat-sensitive materials. Finally, screw machines are more efficiently purged as the material is changed.

4. TECHNICAL DEVELOPMENTS IN MOULDING OF CERAMICS

One of the earliest reported applications of ceramic injection moulding was the manufacture of spark plug insulators in 1937.[22] Since then there

has been considerable and varied experimentation with different moulding techniques.

4.1. Machine types

The ideal design of moulding equipment depends on the nature of the organic vehicle system and this can be classified as[69] thermoplastic, thermoplastic wax or thermosetting.

Both plunger and reciprocating screw injection moulding machines routinely used for unfilled polymers are also used for ceramic suspensions after minor modification.[25,40,69-73] Reciprocating screw machines are often favoured[71,73] as they provide better metering, homogeneity, injection pressure control, reproducibility and lower cycle time. In plunger machines flow moulding is not possible and part size is limited by the maximum volume of the plunger stroke.[72] Nevertheless plunger-type machines are often favoured on the grounds of longer machine life because of less wear.[25,69,70] They also tend to require less capital investment.[70]

Plunger machines can be vertical injection, vertical press type with attainable cavity pressures up to 170 MPa[69] or of the horizontal type.[70] They are generally fully microprocessor controlled and equipped with a shuttle table to allow die transfer.

Reciprocating screw machines specifically developed for ceramic injection moulding are also currently marketed.[70,71] These are based on conventional designs and are again fully automated. Some machines contain circuits which permit fine control of injection and hold pressures which is considered essential for ceramic moulding.[74]

Wax-based systems tend to have much lower viscosities (<200 Pa s) than high polymer systems and are often injection moulded on plunger machines[69] known as wax injectors.[75] The suspension is stored in an agitated heated chamber prior to transfer to an injection chamber where an hydraulically controlled piston injects it into a mould. Such machines vary in size from the small (12 000 kg) horizontally clamped devices to 300 000 kg vertical press machines.

Thus for thermoplastic and wax systems direct injection processes are used in which the heated suspension is forced into a colder mould under pressure and then subjected to a hold pressure as it solidifies.[69,76] For thermosetting systems, however, transfer moulding is used in which the softened suspension is transferred by a plunger or screw to a heated mould where the resin cross-links.[69,77,78] In both cases the polymer phase undergoes a shrinkage as it changes state and this can introduce defects.

4.2. Process control

There is considerable interest in modelling the flow of non-Newtonian unfilled polymers under non-isothermal conditions through sprue and runners of varying dimensions but the problems are considerable. It is an achievement to be able to predict approximately the flow behaviour of polymers[79] and ceramic suspensions are complicated by the reduced thermal capacity and increased thermal conductivity which causes rapid cooling in the runner and mould. Furthermore the yield point behaviour of the suspension changes the flow behaviour at low shear rates. Viscosities of suspensions tend to be much higher than of unfilled polymers[80] and for these reasons the correct choice of machine parameters is important if sound mouldings are to be obtained.[71]

Peshek[69] has listed several requirements for ceramic moulding; optimization of pressure, temperature and injection speed is essential. Quackenbush *et al.*[25] pay particular attention to mould temperature and pressure hold times. It is thought that injection speed has a pronounced effect on ceramic moulding[71] because of the rapid chilling of the melt, described above. Reliability of temperature control is important with correct choice of thermocouple locations to avoid hot or cold spots. Pressure control mechanisms should be hydraulic and allow repeatable and accurate control over a wide range. Injection pressures are typically in the range 35–140 MPa.[72]

Internal stresses in moulded ceramic articles can produce internal defects both during solidification in the cavity or shortly after removal. This is enhanced by the solidification and cooling of a pocket of fluid trapped in the moulding after the sprue or gate has frozen off. Attempts to solve the problem therefore centre on ways of keeping the sprue molten until the interior of the moulding has completely solidified.

Extremely high pressures should compensate for thermal contraction[81] and this approach has been used to produce polyethylene mouldings with net internal compressive stresses.[82] However, the pressures used (up to 450 MPa) are impractically high.

Hot runner moulds have been used for moulding plastics[83] and these allow the moulding to solidify completely under the applied hold pressure.[84] However, they generally demand very small gates which are unsuitable for ceramic suspensions.

Menges *et al.*[85] used an oscillating hold pressure for polymer mouldings designed to compensate for internal shrinkage. Another design for applying oscillating pressure to a ceramic suspension in the mould is described in a German patent.[86] The reciprocating screw is bored to receive an oscillating

piston activated from the screw drive end of the machine. Another part of the device applies oscillating pressure to the ceramic material in the mould and this oscillation is claimed to enhance pressure transmission.

Oscillating pressure applied to the moulded material in place of a static hold pressure was used by Allan and Bevis[87,88] to keep the sprue and runners molten during mould cooling and thereby to make 40 × 50 mm thick section mouldings of unfilled polyethylene without sink marks or internal voiding. The oscillating pressure causes viscoelastic heating in the sprue and runners and this allows the interior of the moulding to be filled, compensating for shrinkage. Continuous monitoring of cavity pressure allows the process to be controlled.

The same technique has been applied to short fibre reinforced thermoplastics[89] and ceramics[90] although the device is subject to wear when used with ceramics.

Defects introduced by entrapped air or adsorbed moisture in ceramic injection moulding mixtures have been overcome by using an injection moulding machine in which the feed reservoir and the mould are held under vacuum by a series of valves, a vacuum pump and vacuum reservoir.[91,92]

4.3. Tooling

Design of injection moulding tooling plays a major role in ceramic fabrication. Stanciu[93] outlined the main parameters in tool design. These include a consideration of flow in runners, part geometry, ease of automation and cost. In addition, tool wear is an important factor when moulding abrasive materials.

Incorrect mould design is one of the main causes of weld or knit lines in single gated moulds although incorrect machine settings can also cause this defect. Ideally the gate should be in a position where plug flow into the main part of the moulding is preferred.[25] Stanciu[93] suggests that gates should be placed at the bottom of the cavity to ensure flow against gravity and thus avoid air entrapment, but this is likely to be important only for low-viscosity fluids or low injection speeds. Venting of the die is important in avoiding air entrapment. Venting can proceed through ejector pin clearances or through machined grooves on the die face. Quackenbush *et al.*[25] have suggested that die design should incorporate overflow chambers beyond the die cavity. This allows the initial chilled material entering the mould to be excluded from the moulding.

The conventional mould clamping arrangement of hydraulic ram and toggle has been dismissed by some manufacturers who prefer simple mechanical mould locking for ceramic materials.[94] This is claimed to

simplify the machine frame and allow greater versatility in mould design.

Injection moulding of detailed geometries is expensive to automate but automation has been achieved for complex silicon nitride stators.[95]

5. MACHINE WEAR

Wear and corrosion of machine parts and tooling is regarded as a problem in ceramics injection moulding.[69,71,93] The barrel, screw, non-return valve, nozzle and mould are areas especially at risk.[96] The difference in hardness between ceramic particles and metal or cermet parts (Table 1) is a main factor in abrasive wear.[97] A further factor in determining ploughing action

TABLE 1
A Comparison of Hardness Values for Typical Ceramics and Some Wear-resistant Materials

	Hardness (GPa)
Ceramics	
Zirconia	14
Sialon	20
Alumina	22
Silicon nitride	25
Silicon carbide	33
Wear-resistant metals and cermets	
Carbon tool steels	8·5
High-speed steels	9·0
Nitrided steels	10·0
Tungsten carbide—16% cobalt	11·5
Tungsten carbide—6% cobalt	15·5

is the particle size and size distribution of the ceramic.[98] Pressure on material has a pronounced influence on machine wear and this tends to localize the severity of damage.[98]

Studies of machine wear caused by filled polymers[99] suggest that material hardness is not a good indicator of wear resistance. Particles produced more severe wear than fibres in the conveying zone but fibres were more damaging in the metering zone. On arrival in the metering zone it is considered that particles would be coated with molten polymer.

Nitrided barrels and chromium-plated steel screws were subjected to severe wear[71] and enhanced leakage flow between flights and barrel made

process control impossible. Japan Steel Works incorporated corrosion–abrasion resistant screws although the material is not specified. The barrels were lined with a nickel-based iron–chromium boride composite with a hardness of approximately 7·6 GPa.[71] This reduced damage to the mating screw surfaces compared to metallic cylinders. Also barrel wear with a silicon carbide composition was 20% of that seen on nitrided steel.

Non-return valves of the check ring type have also been subjected to appreciable wear[100] as shown in Fig. 3. Nozzle and nozzle seat wear has

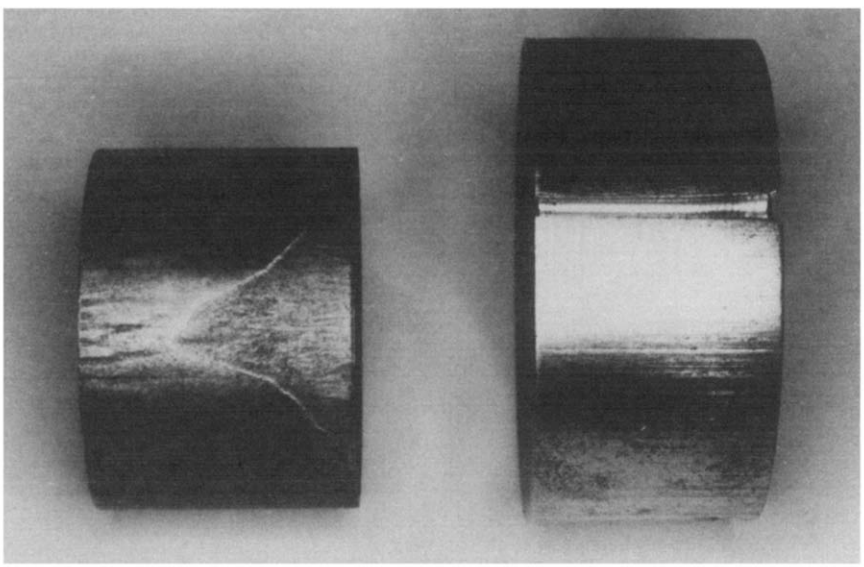

Fig. 3. Wear in check ring-type non-return valves.[100]

been observed[98] on a carbon steel of hardness 4·7 GPa as shown in Fig. 4 but was considerably reduced by using a tool steel of hardness 7·5 GPa.

Tooling should also be constructed of wear-resistant material and resistance to chipping is also important.[93] Thus high carbon–chromium tool steels have been preferred to high wear-resistant but brittle carbide cermets and for the same reason steel-bonded carbide has been rejected.

Since 1974 high pressures (35–140 MPa) have been used extensively for ceramic injection moulding[101] and this tends to enhance machine wear. Furthermore, with incorrectly formulated compositions dilatancy effects can be induced by high material pressures causing separation of fluid from powder.[25,78] These difficulties have led to the use of lower pressures in the range 0·2–0·6 MPa.[72] The low pressure process originated over 30 years ago in the electronics industry[102] and machines using the same principles

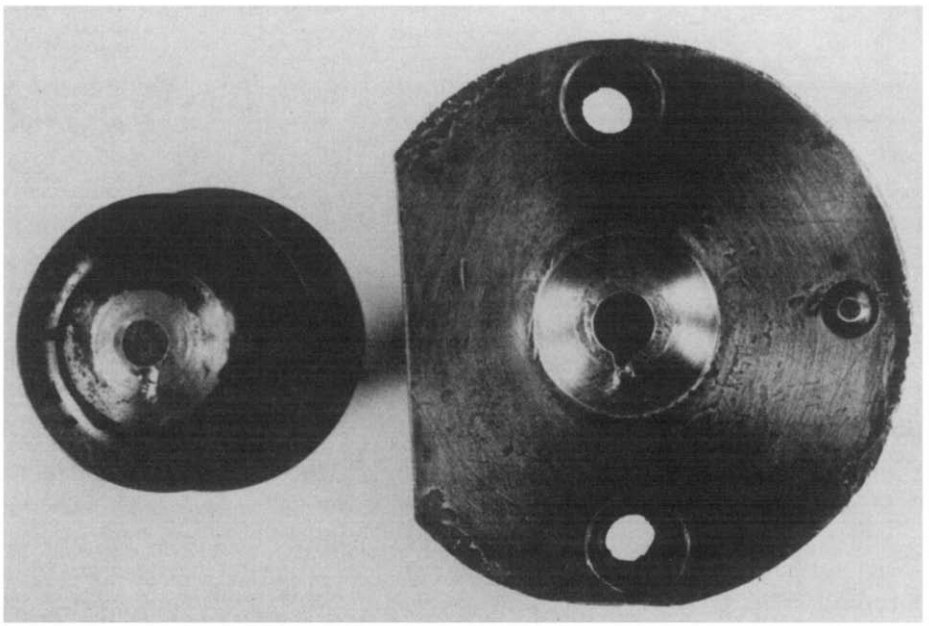

Fig. 4. Wear groove in nozzle and nozzle seat.

are marketed today for ceramic injection moulding.[103] In such machines moving parts such as screws or plungers are absent and energy consumption is small (1–3 kW). Dies are generally small and may be constructed from aluminium or wood because of the low pressures.[72]

Low viscosities ($\simeq$100 Pa s) are achieved by using wax-based systems which are mixed in a thermostatted tank incorporating a planetary mixer. Injection of the die is achieved by imposing air pressure on the material in the tank causing it to flow along a feeder pipe into the mould. The method has been used for silicon nitride, silicon carbide and oxide ceramics[72] but it is not clear how shrinkage defects in thick section mouldings are avoided.

6. DEFECTS IN CERAMIC INJECTION MOULDINGS

Moulding defects may originate at the mould filling stage or during solidification in the cavity. The former include incomplete cavity filling and the incidence of weld or knit lines. The latter are defects which originate from volume shrinkage effects or from unrelieved polymer orientation and consist typically of voids, microvoids, gross cracking or microcracking. Such defects can provide initiation sites for defects found in powder assemblies after polymer removal.

6.1. Mould filling

The entry of fluid into a cavity in an injection moulding machine involves non-isothermal flow of a non-Newtonian fluid through a variety of channel sections under high pressure which itself influences both fluidity and crystalline melting point.[104] It is not therefore a process which can easily be modelled. The enhanced thermal conductivity and lower specific heat of a polymer which has been filled with large volume fraction of ceramic powder means that chilling of the melt is rapid. Incomplete mould filling, especially of thin sections, may result from low material fluidity, low mould temperatures, low barrel temperatures or low injection speeds or pressures. Material fluidity is limited by the need to incorporate large loadings of powder. Higher mould temperatures are limited by the need to eject the component without distortion and barrel temperatures are limited by the degradation of the vehicle during residence.

Filled polymers do not exhibit die swell[105] and show a greater tendency to jet into the cavity producing a coil and resulting in weld lines within the moulding.[71,106] Weld lines are regions of weakness and decrease the toughness.[107] They may persist as defects in the fired ceramic. They are almost inevitable in multi-gated cavities[108] but can also occur in single gated articles if the melt front splits to overcome an obstacle. Gate position can have an important bearing on whether or not welds will occur. In general welds can be avoided on single gated moulds by side gating the cavity to generate plug flow.[25,106]

6.2. Solidification

The development of cracking or voiding in ceramic injection mouldings is related to non-uniform shrinkage.[108] During the early stages of cooling the thickness of the solid skin of material adjacent to the mould wall increases and residual stress may appear, but volume shrinkage is compensated for by the static hold pressure on the fluid material imposed by the plunger or screw. However, at some time after injection the material in the gate freezes and the remaining pocket of fluid in the core of the moulding solidifies, undergoing crystallization and/or thermal contraction. The resulting stresses produce, in many thermoplastics, characteristic sink marks in the surface of the mouldings. In ceramic suspensions, however, such stresses are preferentially relieved by the appearance of voids or cracks. Examples of such defects in injection moulded modulus of rupture bars are shown in Fig. 5. The tendency to produce voids or cracks is influenced by the machine settings but also by the crack arrest temperature of the polymer.[109] The nucleation of voids is particle size dependent[109]

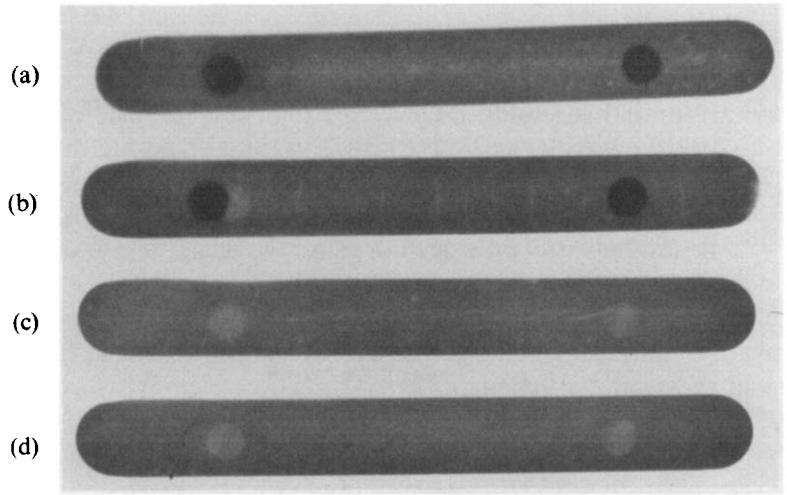

Fig. 5. Defects in injection moulded modulus of rupture bars revealed by X-ray radiography. (a) Shrinkage voids, (b) transverse cracks, (c) longitudinal cracks, (d) free of injection moulding defects.

and takes a Griffith form with stress to nucleate a void being proportional to the reciprocal root of the particle diameter.[110]

For these reasons, post injection hold pressure is an important parameter and indeed for unfilled materials very high pressures (450 MPa) have produced residual compressive stress in the centre of mouldings.[82] Runner and gate geometry is clearly important and large gates are favoured[81] to extend the freeze off time. Ram forward time should be sufficient to apply pressure until the gate freezes. High mould temperatures reduce the differential stresses resulting from rapid cooling rates.[81] High barrel temperatures reduce viscosity sufficiently to enhance pressure transmission.[81] The properties of moulding formulations themselves also influence the incidence of defects.[108] In particular a low temperature dependence of viscosity allows greater pressure transmission to the cavity.[81] These problems are enhanced in regions of mouldings with large sections.

Preferred molecular orientation combined with residual stresses can cause cracking or voiding.[108] During flow in the cavity polymer chains keyed by the solid skin are extended by polymer flow, producing alignment. Orientation is avoided by high melt and mould temperatures which allow recovery to take place. Reduction in injection pressure and speed also reduce the high shear stresses experienced by the material in the mould. In this case thick sections tend to suffer less from polymer orientation effects because of slower cooling.

A recent technique which allows greater control over solidification in the moulding, and therefore allows the production of thick section

thermoplastic mouldings, uses an oscillating rather than a static post injection pressure. The methods of achieving this effect are described above and have been used to mould large sections of polyethylene without sink marks or voids.[87,88] More recently short fibre reinforced thermoplastics[89] have been moulded in this way and the technique is being applied to ceramics.[90] The technique causes pressures in the sprue to oscillate at a preset frequency between predetermined limits. The energy absorbed by the material causes the sprue to remain molten and material to enter the interior of the moulding for long and controllable periods after injection. By constantly monitoring the cavity pressure, the shrinkage and resulting stresses in the moulded part can be controlled.

7. POLYMER REMOVAL TECHNIQUES

The thermal and oxidative degradation of polymers has been extensively investigated and is well reviewed.[111–113] Thermal degradation may involve depolymerization, in which the carbon–carbon backbone of the molecule is severed, decreasing the molecular weight, or substituent reactions in which side groups are attacked, typified by the stripping of HCl from polyvinylchloride. The former may occur either by a random process leaving large molecular weight fragments (and this is the case for most polyolefins) or by scission at reactive sites yielding mainly monomer but having little initial effect on molecular weight (and this is the case for polyoxymethylene). Polystyrene is intermediate in behaviour. If oxygen is present, a series of chemical reactions between the polymer and oxygen or oxygen-containing radicals becomes possible and these may be strongly exothermic.

The polymer removal stage of the process involves the extraction of typically 30–40 vol.% of vehicle. Five polymer removal techniques can be identified: (a) thermal degradation of the organic binder in an inert atmosphere,[114] (b) oxidative degradation,[115] (c) capillary flow into a finer powder,[72] (d) evaporation,[116] (e) solvent extraction.[117]

7.1. Thermal degradation

This is the most widely used technique. It involves a very slow heating rate and this leads to long cycle times which could be several weeks for complex shapes.[25,114] If the temperature is not accurately controlled, decomposition of the polymer occurs within a narrow temperature range resulting in high degradation product vapour pressures producing swelling and cracking.[71] Initially the moulding may be heated to its softening point

fairly rapidly whereupon the vehicle becomes fluid.[25,118] An exception is where residual stresses are present in mouldings and a low temperature stress relieving treatment is preferred.[114] Subsequently an extremely slow heating rate is required at the early stages of decomposition.[114] Quackenbush *et al.*[25] heated articles at $10°C\,h^{-1}$ up to the flow point of the binder and then decreased the rate to $2°C\,h^{-1}$ between 150 and 450°C. The rate could be increased to $10°C\,h^{-1}$ towards the end of the process when a substantial void volume was present.

Vacuum or inert gas atmospheres are preferred[24,114] during polymer removal. Pressures of 7–14 Pa have been found acceptable.[114] This avoids the strong exothermic reaction of polymers with oxygen which hinders process control.

Attempts have been made to use a blend of polymers with different molecular weight characteristics in order to broaden the burn-out region.[114,119] It is significant that for nitrogen ceramics, carbon residue is undesirable. Similarly ash content of the polymer becomes important in some applications where very low silicate or sodium levels are required and in particular for optical property control.

It is a common practice to embed injection moulded articles in a fine powder such as alumina during polymer removal.[24,25,71,114,120–122] The powder bed may perform several functions. It may allow temperature uniformity in the furnace, avoiding surface radiant heating. It may, under certain circumstances, extract fluid from the article by capillary action. It may reduce the steep gas partial pressure gradients at the surface of the moulding. It may also support the moulding in its softened state and prevent sagging.[71] Unfortunately the condensation of polymer degradation products in the powder bed may give errors in weight loss measurements and thus interfere with process control.[114]

Peltsman and Peltsman[72] used a powder bed to extract binder from the component surface by capillary action. They used a low-viscosity wax but the same technique may be less effective with high polymers. They initiated the capillary extraction process between 50 and 60°C and continued heating to 120°C. Evaporation of the remaining binder continued up to 300°C. Ideally in this method the powder bed should be composed of a somewhat finer powder than that of the moulded article. Its success with mouldings of ultrafine precipitated powders has not yet been demonstrated.

The early Bendix process for polymer removal took many days. The binder was a blend of polyethylene, paraffin wax and beeswax[116] and speeding up the process resulted in cracking and blistering. Strivens[120] increased the burn-out rates of this process by incorporating thermosets into the formulation and reduced the removal time to 20 h. It is suggested that the incorporation of thermosetting resins increased the inter-particle

adhesion at elevated temperatures. Thus Wiech[116] suggests that the internal energy of the binder decomposition products must be less than the cohesive energy of the particle assembly if defects are to be avoided at this stage.

7.2. Oxidative degradation

Mutsuddy[115] has reported that after investigating alternative approaches to binder removal, oxidative degradation of polyolefins is the most effective. Polyolefins, either as waxes or high polymers, have been used extensively as ceramic injection moulding vehicles[1] and their degradation,[123–125] reaction products[126–128] and catalytic influences[129,130] have been well documented. Some general points deserve emphasis. Although tacticity of polyolefins does not influence thermal degradation, atactic polypropylene reacts with more oxygen than the isotactic polymer because more tertiary carbons are accessible.[131] The tertiary carbons produced by side chain branching are very susceptible to attack and for this reason polypropylene is much less stable than polyethylene. Of particular interest is the influence of sample thickness on the oxidation of polyolefins. An effect of thickness caused by oxygen diffusion is found in degradation studies, when sample thickness exceeds 250 μm.[132] Not only does the rate of reaction depend on oxygen partial pressure but the nature of the reaction sequence also changes.[133] Since most injection moulded articles are much larger than 250 μm the oxygen diffusion step controls the kinetics and the complexity of reaction sequences and hinders the application of known kinetic data to the problem of process control. Thus Mutsuddy[115] states that temperature–time schedules have to be modified for changes in size and shape of component as well as minor changes in the binder. However, he has attempted to identify reaction sequences in polyethylene binder removal by gas analysis in order to help devise burn-out schedules.[115]

Johnsson *et al.*[114] used weight loss measurement to control the heating rate of a burn-out oven under vacuum. The temperature followed a preset ramp provided the weight loss was below a critical value. The furnace temperature was reduced if this value was exceeded. In this way 13 wt% of polyethylene was removed from silicon nitride mouldings in 30 h for 10 mm thick cylinders and 35 h for a 20 mm thick cylinder. This represents at least a 50% reduction in cycle time compared to linear heating rates. These authors claim that supporting the moulding in a powder bed was not necessary.

Flaw generation during binder removal by thermal degradation can occur early in the cycle.[25] When the binder becomes fluid, flaws can be generated by expansion of air compressed into the component during injection moulding. Blistering and cracking of the components can occur

if the temperature is increased too steeply due to rapid evolution of volatiles.[25]

Delamination or internal cracking is a more serious type of burn-out flaw.[25] It is claimed to be independent of the binder removal rate and depends on powder loading and morphology of the powder.[25] It can also be related to the use of certain organic vehicle systems.[25] Control over this type of flaw has been achieved by modifying powder loading levels and by selecting suitable surfactants.[25] The binder is preferentially removed from the surface of mouldings but subsequently, as polymer emerges from the interior, the resulting slight shrinkage generates tensile stresses and causes internal cracks. 'Skin' formation is another defect frequently observed.[71] This can produce surface cracks and blistering. This has not been fully explained but may be related to preferential polymer degradation at the surface.

7.3. Evaporation

Weich[116] has preferred evaporation or sublimation of binders. The moulded articles were placed in a chamber with control of binder partial pressure and of temperature. Thus control of diffusion and evaporation was achieved. The volatile binder was recondensed and reused. This method has been demonstrated with 3–5 μm metal powders and low molecular weight organic binders. Controlled drying also becomes possible where water-soluble or water-based emulsion polymer systems are used.[1]

7.4. Solvent extraction

A two-component vehicle was used wherein one component was soluble in the extraction solvent and the other insoluble.[117] Combinations of thermoplastic waxes and thermosetting resins have been employed.[117,120] Extraction was effected by immersion in, or washing with, boiling solvent prior to drying. The process can be automated by using a conveyor belt which passes through a solvent wash and drying zones. A wide range of solvents have been used,[117] many of which require expensive plant to control.

The advantage claimed for solvent extraction was faster removal of the organic vehicle.[117] It was also claimed to be more economical, requiring less expensive plant. To meet modern safety regulations this may no longer be valid. The solvent can be distilled and reused.

7.5. Polymer precursors

It is natural to question the need to remove the fluid phase in its entirety from ceramic mouldings and for this reason the current interest in polymer

precursors for ceramics[134] impinges on injection moulding. Silicone oils have been used in moulding compositions to produce silica in the fired ceramic.[135,136] The use of polymer precursors for ceramics was first suggested by Chantrell and Popper.[137] Such techniques have found most use in the fabrication of ceramic fibres.[138,139] There is, however, considerable interest in the fabrication of monolithic ceramics of silicon carbide and boron carbide from polymers.[140] The use of such materials in the binder formulation would have several major advantages; a reduction in the volume of gaseous product to be removed, an increase in the prefired strength of the powder assembly and a reduction in shrinkage during burn-out. Polymers which efficiently deposit ceramic residues are currently being developed[141–143] and this makes the direct fabrication of monolithic ceramics feasible. Such a procedure would avoid the rheological and mixing problems of moulding suspensions and it would eliminate the problem of severe machine wear.

8. CONCLUSIONS

The concept of injection moulding began with metals technology, was transferred to plastics engineering and is now increasingly used for ceramics fabrication. Many of the techniques developed for polymer, and especially reinforced polymer, processing can be applied to ceramics forming.

Dispersive mixing of powders in a polymer blend by machines whose configuration imposes high shear stress is the preferred mixing method. There are three common machine types and each uses two principal moving parts: two-roll mills, double-cam mixers and twin-screw extruders.

A wide range of injection moulding machines can be used for components of small cross-section but the real challenge to ceramic injection moulding technology is the ability to produce thick sections which will survive solidification in the cavity and subsequent polymer removal without the incidence of defects. Solutions to the former problem include techniques for keeping the sprues and runners molten during the post injection stage to allow extended mould filling and thus control shrinkage stresses during solidification and cooling.

Available reports suggest that the wear of ceramic moulding machinery tends to be localized and that specific machine parts require special and often expensive materials. The complex screw does not necessarily experience the most severe wear.

Numerous ingenious methods have been devised to remove the polymer vehicle. In addition to thermal and oxidative degradation, these include solvent washing, capillary extraction and evaporation or sublimation.

While each method has its disadvantages, thermal degradation has been the most frequently cited method. Weight loss–temperature control loops on furnaces allow the polymer extraction time to be minimized. There remains little quantitative understanding of the process; diffusivities of low molecular weight components or degradation products in molten polymer blends are largely uncharted. The mechanical strength of the powder assembly and the extent of shrinkage which it undergoes during polymer removal both influence the incidence of defects.

The problems presented by this technology impinge on many specialisms within materials technology, engineering and chemistry and thus skills in collaborative research planning have tended to yield the most significant developments.

REFERENCES

1. Edirisinghe, M. J. and Evans, J. R. G., Review: fabrication of engineering ceramics by injection moulding. I. Materials selection, *Int. J. High Tech. Ceram.*, **2** (1986) 1–31.
2. Tadmor, Z. and Gogos, C. G., *Principles of Polymer Processing*, Wiley, New York, 1979, Chapter 7.
3. Uhl, V. W. and Gray, J. B. (Eds), *Mixing: Theory and Practice II*, Academic Press, New York, 1967, Chapter 8.
4. Middleman, S., *Fundamentals of Polymer Processing*, McGraw-Hill, New York, 1977, Chapter 12.
5. Messer, P. F., *Milling and Mixing*, to be published.
6. Lange, F. F., Processing-related fracture origins I. Observations in sintered and isostatically hot-pressed Al_2O_3–ZrO_2 composites, *J. Am. Ceram. Soc.*, **66** (1983) 393–8.
7. Kellet, B. and Lange, F. F., Stresses induced by differential sintering in powder compacts, *J. Am. Ceram. Soc.*, **67** (1984) 369–71.
8. Lange, F. F. and Metcalf, F., Processing-related fracture origins II. Agglomerate motion and cracklike internal surfaces, *J. Am. Ceram. Soc.*, **66** (1983) 398–406.
9. Lange, F. F., Davis, B. E. and Aksay, I. A., Processing-related fracture origins III. Differential sintering of ZrO_2 agglomerates, *J. Am. Ceram. Soc.*, **66** (1983) 407–8.
10. Lange, F. F., Sinterability of agglomerated powders, *J. Am. Ceram. Soc.*, **67** (1984) 83–9.
11. Hornsby, P. R., Design and application of a laboratory twin-screw compounding extruder, *Plastics Compounding*, **6** (1983) 65–70.
12. Edirisinghe, M. J. and Evans, J. R. G., *Proc. Brit. Ceram. Soc.*, to be published.
13. Tadmor, Z. and Gogos, C. G., *Principles of Polymer Processing*, Wiley, New York, 1979, p. 434 et seq.
14. Barringer, E. A. and Bowen, H. K., Formation, packing and sintering of monodisperse TiO_2 powders, *J. Am. Ceram. Soc.*, **65** (1982) C199–201.

15. Milne, S. J., *Proc. Brit. Ceram. Soc.*, to be published.
16. Fan, L. T., Chen, S. J. and Watson, C. A., Solids mixing, *Ind. Eng. Chem.*, **62** (1970) 53–69.
17. Fan, L. T. and Wang, R. H., On mixing indices, *Powder Technology*, **11** (1975) 27–32.
18. Lacey, P. M. C., Developments in the theory of particle mixing, *J. Appl. Chem.*, **4** (1954) 257–68.
19. Weidenbaum, S. S., Mixing of solids, in *Advances in Chemical Engineering II*, Eds T. B. Drew and J. W. Hooper, Academic Press, New York, 1958, 211–321.
20. Irving, H. F. and Saxton, R. L., Mixing of high viscosity materials, in *Mixing Theory and Practice II*, Eds V. W. Uhl and J. B. Gray, Academic Press, New York, 1967, Chapter 8.
21. Tadmor, Z. and Gogos, C. G., *Principles of Polymer Processing*, Wiley, New York, 1979, Chapter 8.
22. Schwartzwalder, K., Injection moulding of ceramic materials, *Am. Ceram. Soc. Bull.*, **28** (1949) 459–61.
23. Taylor, H. D., Injection moulding intricate ceramic shapes, *Am. Ceram. Soc. Bull.*, **45** (1966) 768–70.
24. Mann, D. L., *Injection Moulding of Sinterable Silicon-Base Non-Oxide Ceramics*, Technical Report AFML-TR-78-200, Dec. 1978.
25. Quackenbush, C. L., French, K. and Neil, J. T., Fabrication of sinterable silicon nitride by injection moulding, *Ceram. Eng. Sci. Proc.*, **3** (1982) 20–34.
26. Birchall, J. D., Howard, A. J. and Kendall, K., Imperial Chemical Industries Ltd, UK, *Cementitious product*, Eur. Patent 0021682, 7 Jan. 1981. Date of filing: 6 Jun. 1980.
27. Fenner, R. T., *Principles of Polymer Processing.* Macmillan, London, 1979, Chapter 6.
28. Fisher, E. G., *Extrusion of Plastics*, Butterworths, London, 1976.
29. Tadmor, Z. and Klein, I., *Engineering Principles of Plasticating Extrusion*, R. E. Krieger Publ. Co., New York, 1978.
30. Janssen, L. P. B. M., *Twin-Screw Extrusion*, Elsevier, Amsterdam, 1978.
31. SpA Plastic Materials Laboratory, *Improvements in or relating to moulding thermoplastic synthetic resins by extrusion*, UK Patent 629 109, 13 Sept. 1949. Date of filing: 2 May 1946.
32. Martelli, F., *Twin Screw Extruders*, Van Nostrand, New York, 1983.
33. UK laboratory compounding extruder sets high standards, *European Plastics News*, June (1982) 9.
34. Abram, J., Bowman, J., Behiri, J. C. and Bonfield, W., The influence of compounding route on the mechanical properties of highly loaded particulate filled polyethylene composites, *Plast. and Rubb. Proc. and Appl.*, **4** (1984) 261–9.
35. Hornsby, P. R. and Sothern, G. R., Polymer degradation during twin screw extrusion compounding, *Plast. and Rubb. Proc. and Appl.*, **4** (1984) 165–71.
36. Donald, I. W. and McMillan, P. W., Review: ceramic–matrix composites, *J. Mat. Sci.*, **11** (1976) 949–72.
37. Schioler, L. J. and Stiglich, J. J., Ceramic matrix composites: a literature review, *Am. Ceram. Soc. Bull.*, **65** (1986) 289–92.

38. Folkes, M. J., *Short Fibre Reinforced Thermoplastics*, Wiley, New York, 1982.
39. Delmonte, J., *Technology of Carbon and Graphite Fibre Composites*, Van Nostrand Reinhold, New York, 1981.
40. Bevis, M. J., Gaspar, E., Allan, P. and Hornsby, P. R., Brunel University, UK, *Forming articles from composite materials*, UK Patent Application 8511152. Date of filing: 2 May 1984.
41. Willis, R. R., Markle, R. A. and Mukherjee, S. P., Siloxanes, silanes and silazanes in the preparation of ceramics and glasses, *Am. Ceram. Soc. Bull.*, **62** (1983) 904–11.
42. Sturges, R. F., *Manufacture of candlesticks and lamp pillars*, UK Patent 12480, 14 Aug. 1849. Date of filing: 14 Feb. 1849.
43. Hyatt, I. S. and Hyatt, J. W., Celluloid Manufacturing Co., USA, *Improvements in processes and apparatus for manufacturing pyroxyline*, US Patent 133229, 19 Nov. 1872.
44. Hyatt, J. W., Celluloid Manufacturing Co., USA, *Improvements in coating articles with celluloid and carbon*, US Patent 202441, 16 Apr. 1878. Date of filing: 25 Mar. 1878.
45. Rubin, I. I., *Injection Moulding Theory and Practice*, Wiley, New York, 1972, 1.
46. Richards, F. H., *Apparatus for moulding playing balls*, US Patent 791649, 6 Jun. 1905. Date of filing: 10 Feb. 1903.
47. Eichengrun, A., Cellon Works, Germany, *Process for the production of moulded articles from cellulose acetate*, UK Patent 147904, 9 Nov. 1921. Date of filing: 9 Jul. 1920.
48. Eichengrun, A., Cellon Works, Germany, *Process for the production of moulded articles from cellulose acetate and the like cellulose derivatives*, UK Patent 171432, 9 Nov. 1921. Date of filing: 9 Jul. 1920.
49. Buchholz, H., *Process of making moulded articles*, US Patent 1810126, 16 Jun. 1931. Date of filing: 14 Nov. 1923.
50. Thomas, I., *Injection Moulding of Plastics*, Reinhold, New York, 1947, Chapters 1 and 2.
51. Gaspar, E., Polymer history: the injection moulding process, *Shell Polymers*, **5** (1981) 40–2.
52. Walker, J. S. and Martin, E. R., *Injection Moulding of Plastics*, Iliffe, London, 1966, 2.
53. Jeffrey, H. L., Grotelite Co., USA, *Moulding machine*, US Patent 2111857, 22 Mar. 1938. Date of filing: 5 Apr. 1932.
54. Piperoux, R. P. and Radburn, N. J., Celluloid Corp., USA, *Extruded article and device for making same*, US Patent 2161588, 6 Jun. 1939. Date of filing: 22 Mar. 1935.
55. Gastrow, H., *Improvements in and relating to apparatus for moulding plastic material*, UK Patent 424369, 20 Feb. 1935. Date of filing: 11 Dec. 1933.
56. Burroughs, C. F., *Injection moulding apparatus*, US Patent 2202140, 28 May 1940. Date of filing: 4 Aug. 1936.
57. Rapid, continuous injection of thermosetting materials, *Modern Plastics*, **21** (1944) 90–1.
58. Stanley, F. B. (Ed.), Three newcomers, *Modern Plastics*, **21** (1944) 121–3 and 188.

59. Injection–compression moulding of acrylic feeder heads, *Modern Plastics*, **23** (1945) 146–50.
60. Rakas, N. J. and Cousino, W. B., A multi-purpose moulding machine, *Modern Plastics*, **22** (1944) 133–41 and 196.
61. Crawford, R. J., *Progress in Plastics Engineering*, Pergamon Press, London, 1981, 169–70.
62. Fisher, E. G. and Maslen, W. A., Preplasticising in injection moulding. Part I. The principles of preplasticising and the history of its development, *British Plastics*, **32** (1959) 417–22.
63. Wood, R., Preplasticising in injection moulding. Part II. A classification of plunger and screw type machines and equipment in use, *British Plastics*, **32** (1959) 468–74.
64. Fisher, E. G. and Maslen, W. A., Preplasticising in injection moulding. Part III. Comparison of extruding systems and suggested requirements of an ideal system, *British Plastics*, **32** (1959) 516–20.
65. Simonds, H. R. (Ed.), *The Encyclopedia of Plastics Equipment*, Reinhold, New York, 1964, 306.
66. Kriner, W. G., Graphic comparison of screw and plunger machine performance, *Modern Plastics*, **39** (1962) 121–32 and 214.
67. Weir, C. L. and Zimmerman, P. T., Facts and figures on ram versus screw injection, *Modern Plastics*, **40** (1962) 122–5 and 220.
68. Weir, C. L. and Zimmerman, P. T., Ram versus screw injection Part II, *Modern Plastics*, **40** (1962) 123–8, 133 and 190.
69. Peshek, J. R., Machinery for injection moulding of ceramic shapes, in *Advances in Ceramics*, Vol. 9, Ed. J. Mangels, 1984, 234–8.
70. *Special Purpose Machines*, Mercia Machinery Sales Ltd, UK, Trade literature, 1986.
71. *Injection Moulding Machine for New Ceramics*, Japan Steel Works (Hiroshima Plant), Trade literature, 1984.
72. Peltsman, I. and Peltsman, M., Low pressure moulding of ceramic materials, *Interceram*, **4** (1984) 56.
73. Rottenkolber, P., Langer, M., Storm, R. S. and Frechette, F., *Design, Fabrication and Testing of an Experimental Alpha Silicon Carbide Turbocharger Rotor*, Society of Automotive Engineers, USA, Publication No. 810523, 1981.
74. Uchida, I. and Inami, T., The control system and the program of 'μPACS-2000' for injection moulding machine, *Nihon Seihojo Giho*, **41** (1982) 21–35.
75. Mangels, J. A., Injection moulding ceramics, *Ceram. Eng. and Sci. Proc.*, **3** (1982) 529–37.
76. Crossley, I. A., Kirk, G. E., Anthony, N. H. and Bamber, D. R., Rolls-Royce Ltd, London, UK, *Injection of a ceramic into a mould cavity*, US Patent 3 882 210, 6 May 1975, Date of filing: 17 Nov. 1972.
77. Ohnsorg, R. W., The Carborundum Co., USA, *Composition and process for injection moulding ceramic materials*, US Patent 4 144 207, 13 Mar. 1979. Date of filing: 27 Dec. 1977.
78. Ohnsorg, R. W., The Carborundum Co., USA, *Process for injection moulding sinterable carbide ceramic materials*, US Patent 4 233 256, 11 Nov. 1980. Date of filing: 18 Dec. 1978.
79. Cox, H. W., Mentzer, C. C. and Custer, R. C., The flow of thermoplastic melts—Experimental and predicted, *SPE Antec*, **29** (1983) 694–7.

80. Farris, R. J., Prediction of the viscosity of multimodal suspensions from unimodal viscosity data, *Trans. Soc. Rheol.*, **12** (1968) 281–301.
81. Rubin, I. I., *Injection Moulding Theory and Practice*, Wiley, New York, 1972, 270–317.
82. Kubat, I. and Rigdahl, M., Influence of high injection pressures on the internal stress level in injection moulded specimens, *Polymer*, **16** (1975) 925–9.
83. Rubin, I. I., *Injection Moulding Theory and Practice*, Wiley, New York, 1972, 104.
84. Morrison, R. V., Discovision Assoc., USA, *Hot sprue assembly for an injection moulding machine*, US Patent 4 412 805, 1 Nov. 1983. Date of filing: 23 Sept. 1981.
85. Menges, G., Koenig, D., Luettgens, R., Sarholz, R. and Schuermann, E., Follow up pressure pulsation in the manufacture of thick walled high strength thermoplastic components, *Plastverarbeiter*, **31** (1980) 185–93.
86. Demag Kunststofftechnik, Federal Republic of Germany, *Method of apparatus for moulding plastic ceramic materials*, UK Patent 1 553 924, 10 Oct. 1979. Date of filing: 23 Dec. 1976.
87. Allan, P. S. and Bevis, M., The production of void-free thick-section injection-flow mouldings I. Shot-weight and dimensional reproducibility, *Plast. and Rubb. Proc. and Appl.*, **3** (1983) 85–91.
88. Allan, P. S. and Bevis, M., The production of void-free thick-section injection-flow mouldings II. Preferred orientation and residual stress measurements, *Plast. and Rubb. Proc. and Appl.*, **3** (1983) 331–6.
89. Allan, P. S. and Bevis, M., Producing void-free thick-section thermoplastic and fibre reinforced thermoplastic mouldings, *Plas. Rubb. Int.*, **9** (1984) 32–6.
90. Edirisinghe, M. J. and Evans, J. R. G., *J. Mater. Sci. Lett.* (1986), in press.
91. Huther, W., Motor and Turbine Union, Federal Republic of Germany, *Injection moulding apparatus*, UK Patent 2 086 796, 19 May 1982. Date of filing: 27 Oct. 1981.
92. Huther, W., Motor and Turbine Union, Federal Republic of Germany, *Apparatus for injection moulding of precision parts*, US Patent 4 412 804, 1 Nov. 1983. Date of filing: 4 Nov. 1981.
93. Stanciu, V. V., Tooling for ceramic injection moulding, in *Advances in Ceramics*, Vol. 9, Ed. J. Mangels, 1984, 239–40.
94. IFO AB, Sweden, *Improvements in or relating to injection moulding machines*, UK Patent 1 433 638, 28 Apr. 1976. Date of filing: 20 Jul. 1973.
95. Johnson, C. F. and Mohr, T. G., Injection moulding 2·7 g/cc silicon nitride turbine rotor blade rings utilising automatic control, in *Ceramics for High Performance Applications II*, Eds J. J. Burke, E. N. Lenoe and R. N. Katz, Brook Hill Publishing Co., Chestnut Hill, MA, 1978, 193–206.
96. Honstrater, R. A., A practical approach to screw and barrel wear and repair, *Plastics Engineering*, **37** (1981) 35–8.
97. Bowden, F. P. and Tabor, D., *The Friction and Lubrication of Solids*, Clarendon Press, Oxford, 1950, 294.
98. Edirisinghe, M. J. and Evans, J. R. G., to be published.
99. Reinhard, M., Ways of wear reduction in plastics processing, *SPE Antec*, **30** (1984) 798–802.
100. Dawson, D., A.E. Turbine Components Ltd, UK, private communication.

101. Mutsuddy, B. C., Injection moulding research paves way to ceramic engine parts, *J. Ind. Res. and Dev.*, **25** (1983) 76–80.
102. Gribovsky, P. O., *Hot Moulding of Ceramic Parts*, G.E.I., Moscow-Leningrad, 1961, 400.
103. Peltsman, I. and Peltsman, M., Improvements in machinery for hot moulding of ceramics under low pressure, *Ceram. Eng. and Sci. Proc.*, **3** (1982) 865–8.
104. Wunderlick, B. (Ed.), *Macromolecular Physics III*, Academic Press, New York, 1980, 91.
105. Sugano, T., Materials for injection moulding silicon carbide, in *Proceedings of the 1st Symposium on Research and Development of Basic Technology for Future Industry*, Fine Ceramics Project, Japan Tech. Assoc., Tokyo, 1983, 67–84.
106. Mangels, J. A. and Trela, W., Ceramic components by injection moulding, in *Advances in Ceramics*, Vol. 9, Ed. J. Mangels, 1984, 220–3.
107. Criens, R. M. and Moste, H. G., On the influence of knit lines on the mechanical behaviour of injection moulded structural elements, *SPE Antec*, **28** (1982) 22–4.
108. Crawford, R. J., *Progress in Plastics Engineering*, Pergamon Press, London, 1981, 189–97.
109. Su, K. B. and Suh, N. P., Void nucleation of particulate filled polymeric materials, *SPE Antec*, **27** (1981) 46–9.
110. Gent, A. N. and Park, B., Failure processes in elastomers at or near a rigid spherical inclusion, *J. Mat. Sci.*, **19** (1984) 1947–56.
111. Grassie, N., Degradation, in *Polymer Science*, Vol. II, Ed. A. D. Jenkins, North Holland, Amsterdam, 1972.
112. Reich, L. and Stivala, S. S., *Elements of Polymer Degradation*, McGraw-Hill, New York, 1971.
113. Conley, R. T. (Ed.), *Thermal Stability of Polymers*, Marcel Dekker, New York, 1970.
114. Johnsson, A., Carlstrom, E., Hermansson, L. and Carlsson, R., Minimization of the extraction time for injection moulded ceramics, *Proc. Brit. Ceram. Soc.*, **33** (1983) 139–7.
115. Mutsuddy, B. C., Oxidative removal of organic binders from injection moulded ceramics, *International Conference on Non-Oxide Technical and Engineering Ceramics*, National Institute of Higher Education, Limerick, Ireland, 10–12 July 1985.
116. Wiech, R. E., *Method and means for removing binder from a green body*, US Patent 4 305 756, 15 Dec. 1981. Date of filing: 14 Jan. 1980.
117. Strivens, M. A., Standard Telephones and Cables Ltd, UK, *Improvement in or relating to the formation of moulded articles from sinterable materials*, UK Patent 808 583, 4 Feb. 1959. Date of filing: 13 Jul. 1956.
118. Wiech, R. E., Parmatech Corp., USA, *Manufacture of parts from particulate material*, UK Patent 1 516 079, 28 Jun. 1978. Date of filing: 30 Mar. 1977.
119. Litman, A. M., Schott, N. R. and Tozlowski, S. W., Rheological properties of highly filled polyolefin/ceramic systems suited for injection moulding, *Soc. Plas. Eng. Tech.*, **22** (1976) 549–51.
120. Strivens, M. A., Standard Telephones and Cables, UK, *Improvements in or relating to the formation of moulded articles from sinterable materials*, UK Patent 779 242, 17 Jul. 1957. Date of filing: 7 Aug. 1953.

121. Watanabe, K., Special Ceramics Co., Japan, *Ceramic binder removal method*, Japanese Patent 100973, 23 Jun. 1982. Date of filing: 10 Dec. 1980.
122. Curry, J. D., Leco Corp., USA, *Apparatus and method of manufacture of article containing controlled amounts of binder*, US Patent 4011291, 8 Mar. 1977. Date of filing: 2 Sept. 1975.
123. Sedlazek, B., Verberger, C. G., Mark, H. F. and Fox, T. G. (Eds), Degradation and stabilization of polyolefins, *J. Polym. Sci. Polymer Symposium No. 57*, Wiley, New York, 1976.
124. Luongo, J. P., Infra-red study of oxygenated groups formed in polyethylene during oxidation, *J. Polym. Sci.*, **42** (1960) 139–50.
125. Canterino, P. J., Ethylene polymers, in *Encyclopedia of Polymer Science and Technology*, Vol. 6, Eds H. F. Mark and N. G. Gaylord, Wiley, New York, 1967, 275–454.
126. Adams, J. H., Analysis of non-volatile oxidation products of polyethylene, *J. Polym. Sci.*, **8** (1970), 1077–90.
127. Tsuchiya, Y. and Sumi, K., Thermal decomposition products of polypropylene, *J. Polym. Sci.*, **7** (1969), 1599–1607.
128. Tsuchiya, Y. and Sumi, K., Thermal decomposition products of polyethylene, *J. Polym. Sci.*, **6** (1968) 415–24.
129. Chaudhri, S. A., The metal salt catalysed antioxidation of atactic polypropylene in solution II. Behaviour of Co, Ni, Fe and Cu salts as catalysts, *Polymer*, **9** (1968) 604–8.
130. Hansen, R. H., Thermal and oxidative degradation of polyethylene, polypropylene and related olefin polymers, in *Thermal Stability of Polymers*, Ed. R. T. Conley, Marcel Dekker, New York, 1970, 153–88.
131. Hansen, R. H., Thermal and oxidative degradation of polyethylene, polypropylene and related olefin polymers, in *Thermal Stability of Polymers*, Ed. R. T. Conley, Marcel Dekker, New York, 1970, 162.
132. Hansen, R. H., Thermal and oxidative degradation of polyethylene, polypropylene and related olefin polymers, in *Thermal Stability of Polymers*, Ed. R. T. Conley, Marcel Dekker, New York, 1970, 158–60.
133. Reich, L. and Stivala, S. S., *Elements of Polymer Degradation*, McGraw-Hill, New York, 1971, 10.
134. Rice, R. W., Ceramics from polymer pyrolysis. Opportunities and needs, *Am. Ceram. Soc. Bull.*, **62** (1983) 889–92.
135. Burroughs, J. E. and Thornton, H. R., Refractory aerospace structural components by plastic moulding process, *Am. Ceram. Soc. Bull.*, **45** (1966) 187–92.
136. Matkin, D. I., Denton, I. E., Valentine, T. M. and Warrington, P., The fabrication of silicon nitride by ceramic/plastic technology, *Proc. Brit. Ceram. Soc.*, **22** (1973) 291–304.
137. Chantrell, P. G. and Popper, P., Inorganic polymers and ceramics, in *Special Ceramics*, Ed. P. Popper, Academic Press, New York, 1965, 87–103.
138. Hasegawa, Y., Limura, M. and Yajima, S., Synthesis of continuous silicon carbide fibre, *J. Mat. Sci.*, **15** (1980) 720–8.
139. Yajima, S., Hasegawa, Y., Ohamura, K. and Matsuzawa, T., Development of high tensile strength silicon carbide fibre using an organosilicon polymer precursor, *Nature*, **273** (1978) 525–7.
140. Walker, B. E., Rice, R. W., Becker, P. F., Bender, B. A. and Coblenz, W. S.,

Preparation and properties of monolithic and composite ceramics produced by polymer pyrolysis, *Am. Ceram. Soc. Bull.*, **62** (1983) 916–23.
141. Seyferth, D. and Wiseman, G. H., High yield synthesis of Si_3N_4/SiC ceramic materials by pyrolysis of a novel polyorganosilane, *J. Am. Ceram. Soc.*, **67** (1984) C132–7.
142. Yajima, S., Special heat resisting materials from organometallic polymers, *Am. Ceram. Soc. Bull.*, **62** (1983) 893–915.
143. Schilling, C. L., Wesson, J. P. and Williams, T. C., Polycarbosilane precursors for silicon carbide, *Am. Ceram. Soc. Bull.*, **62** (1983) 912–15.

Received 17 June 1986; accepted 30 July 1986

Int. J. High Technology Ceramics **2** (1986) 279–290

Corrosion of SiC, Si_3N_4 and AlN in Molten K_2SO_4–K_2CO_3 Salts

Tsugio Sato, Yoshimi Kanno and Masahiko Shimada*

Department of Applied Chemistry, Faculty of Engineering,
Tohoku University, Sendai 980, Japan

SUMMARY

Silicon carbide, silicon nitride and aluminium nitride ceramics were immersed in potassium sulphate–potassium carbonate melts in air or in a nitrogen atmosphere at 1013–1200°C to examine their corrosion behaviour. Aluminium nitride ceramics exhibited great resistance to corrosive attack from potassium salts under these conditions, exhibiting only a slight weight loss. Silicon carbide ceramics dissolved slowly in molten potassium carbonate (K_2CO_3), but rapidly dissolved in both potassium sulphate (K_2SO_4) and 50 mol% K_2SO_4–50 mol% K_2CO_3 melts. The weight loss of silicon carbide in these potassium salt melts was larger in air than in nitrogen. Silicon carbide ceramics reacted with K_2SO_4 melt quantitatively and the stoichiometry of K_2SO_4/SiC was 0·8. On the other hand, the weight loss of silicon nitride ceramics was appreciable in all potassium salt melts. The reaction between Si_3N_4 and K_2SO_4 or K_2CO_3 proceeded quantitatively and the stoichiometry of K_2SO_4/Si_3N_4 and K_2CO_3/SI_3N_4 was 1·6 and 3·5, respectively. The presence of oxygen accelerated the reaction between Si_3N_4 and K_2CO_3, but greatly retarded the reaction between Si_3N_4 and K_2SO_4, due to the formation of a protective film. The oxidation mechanisms of Si_3N_4 and SiC with K_2SO_4 and K_2CO_3 melts are discussed on the basis of the experimental results.

1. INTRODUCTION

Considerable efforts have been made recently to develop new energy conversion systems with increased fuel efficiencies, such as magnetohydrodynamic (MHD) generation, high temperature gas turbines, etc., in which the operating temperatures are much higher than metal alloys would

* To whom correspondence should be addressed.

Int. J. High Technology Ceramics 0267-3762/86/$03·50

permit. Consequently, only certain ceramic materials are good candidates for use as structural materials. However, in an MHD generator, the electrodes and insulating walls are exposed to a high temperature potassium-seeded plasma. Since the plasma contains about 1 wt% of seed materials such as K_2CO_3 and K_2SO_4, potassium salts condense on the wall and cause severe corrosion. It is also well known that in a high temperature gas turbine system, condensed NaCl and Na_2SO_4 salts may cause corrosion. Therefore, the structural materials used for energy conversion systems should not only have excellent thermal and mechanical properties but must also be resistant to the oxidation–reduction reaction in the corrosive environment of elements such as K, Na, V, S, etc.

Since ceramics based on silicon carbide, silicon nitride and aluminium nitride can retain outstanding fracture strength to high temperatures and are remarkably resistant to thermal shock and oxidizing combustion environments, they are considered good candidates for structural applications at high temperatures. Many investigators have studied the physical and mechanical properties of these ceramics; however, only limited data on their corrosion mechanism in molten salts have been reported.[1–10] McKee and Chatterji,[1] Mayer and Riley,[2] Brooks *et al.*[3] and Erdoes and Altorfer[4] have investigated the behaviour of silicon carbide and silicon nitride in a variety of molten salt/gas environments. According to their reports, the oxygen potential at the surface of silicon carbide and silicon nitride was a critical parameter for the 'active' and 'passive' oxidation in gaseous and molten salt environments. Tressler *et al.*[5] reported that the degree of corrosion of silicon carbide and silicon nitride with molten Na_2SO_4–NaCl salts depended on the concentration of free oxide ions in the molten salts. Becher[8] studied the fracture strength degradation of silicon carbide and silicon nitride ceramics resulting from the exposure to coal slags at high temperatures, and he reported that the corrosion behaviour of silicon carbide and silicon nitride ceramics depended on the chemical constitution of the coal slags, and that silicon carbide ceramics generally exhibited greater resistance to corrosive attack than silicon nitride ceramics. In the previous investigations, however, only qualitative experimental results on chemical reaction have been reported, so that the details of the corrosion reactions are still not clear. In the present work, a series of corrosive reaction experiments was conducted to obtain more detailed information of the corrosion behaviour of silicon carbide, silicon nitride and aluminium nitride ceramics in K_2SO_4–K_2CO_3 melts.

2. EXPERIMENTAL

The materials selected were silicon carbide and silicon nitride, fabricated by pressureless sintering using additives of boron and carbon for silicon

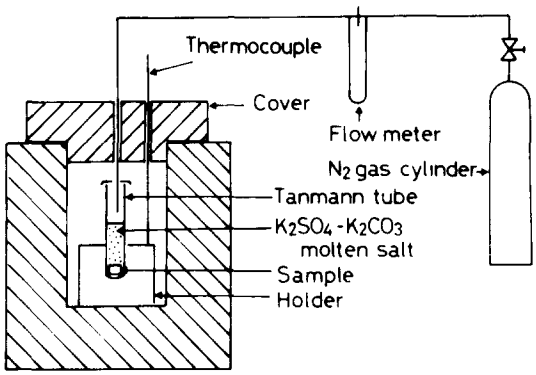

Fig. 1. Schematic diagram of the reaction apparatus.

carbide, and yttrium oxide and aluminium oxide for silicon nitride (made by the NGK Spark Plug Co. Ltd), and aluminium nitride without additives, fabricated by high pressure hot pressing at the Institute of Scientific and Industrial Research, Osaka University. These materials were cut into bars of rectangular cross-section (typically 5 mm × 4 mm × 8 mm). Figure 1 shows diagrammatically the apparatus for the corrosion tests. In each experiment a weighed sample and powdered reagent-grade K_2SO_4 and/or K_2CO_3 were put into a Tanmann tube of high purity alumina, 16 mm in diameter and 170 mm in length, which was then placed into an electric furnace controlled at a desired temperature. The reaction temperature, T, was set to the value of $T/T_m = 1{\cdot}1$ (T_m = the melting point (K) of each salt). Nitrogen gas of higher than 99·99% purity was injected into the Tanmann tube at the rate of 20 ml min^{-1} when the corrosion test was carried out in a nitrogen gas atmosphere. After maintaining the desired temperature for a given time, the Tanmann tube was removed from the electric furnace and quickly cooled to room temperature. The samples were washed in hot water, dried and weighed. Crystalline phases and microstructures on the surface of the samples exposed to the molten potassium salts were examined by X-ray diffraction analysis (XRD), scanning electron microscopy (SEM) and electron probe microanalysis (EPMA).

3. RESULTS AND DISCUSSION

3.1. Thermodynamic aspects of the stability of silicon carbide, silicon nitride and aluminium nitride ceramics in molten K_2SO_4–K_2CO_3 salts

The oxidation reactions of silicon carbide, silicon nitride and aluminium nitride and the reducing reactions of K_2SO_4 and K_2CO_3 can be expressed

as eqns (1)–(10), when the reactions are expressed on the basis of the transfer of oxygen.

Oxidation reactions:

$$2/3\,SiC(s) + O_2(g) \longrightarrow 2/3\,SiO_2(s) + 2/3\,CO(g) \quad (1)$$

$$SiC(s) + O_2(g) \longrightarrow SiO(g) + CO(g) \quad (2)$$

$$1/3\,Si_3N_4(s) + O_2(g) \longrightarrow SiO_2(s) + 2/3\,N_2(g) \quad (3)$$

$$4/3\,Si_3N_4(s) + O_2(g) \longrightarrow 2Si_2N_2O(s) + 2/3\,N_2(g) \quad (4)$$

$$2/3\,Si_3N_4(s) + O_2(g) \longrightarrow 2SiO(g) + 4/3\,N_2(g) \quad (5)$$

$$4/3\,AlN(s) + O_2(g) \longrightarrow 2/3\,Al_2O_3(s) + 2/3\,N_2(g) \quad (6)$$

Reducing reactions:

$$1/2\,K_2SO_4(l) \longrightarrow 1/2\,K_2S(l) + O_2(g) \quad (7)$$

$$2K_2SO_4(l) \longrightarrow 2K_2SO_3(l) + O_2(g) \quad (8)$$

$$2K_2CO_3(l) \longrightarrow 2K_2O(l) + 2CO(g) + O_2(g) \quad (9)$$

$$K_2CO_3(l) \longrightarrow 2K(l) + CO(g) + O_2(g) \quad (10)$$

$$1/2K_2S(s) + O_2(g) \longrightarrow 1/2\,K_2SO_4(s) \quad (7')$$

$$2K_2SO_3(s) + O_2(g) \longrightarrow 2K_2SO_4(s) \quad (8')$$

$$2K_2O(s) + 2CO(g) + O_2(g) \longrightarrow 2K_2CO_3(s) \quad (9')$$

$$2K(s) + CO(g) + O_2(g) \longrightarrow K_2CO_3(s) \quad (10')$$

Chemical free energy change of the oxidation reactions written by eqns (1)–(6) and (7′)–(10′) are shown as a function of temperature in Fig. 2.

Although all the compounds, K_2SO_4, K_2CO_3, K_2S, K_2SO_3 and K_2O, melted at the experimental temperature, the free energy changes of these compounds were calculated on the basis of the solid–gas reactions expressed by eqns (7′)–(10′) because of the lack of thermodynamic data for the molten K_2S, K_2SO_3 and K_2O salts. If the dashed lines in Fig. 2, which are derived from eqns (7′)–(10′), are above the full lines, which represent the reactions expressed by eqns (1)–(6), the oxidation of SiC, Si_3N_4 and AlN by K_2SO_4 and K_2CO_3 is thermodynamically favourable. Potassium sulphate possesses a strong oxidizing activity and might oxidize SiC, Si_3N_4 and AlN. Further, the reduction of K_2SO_4 to K_2S is more advantageous than that to K_2SO_3, and the reduction of K_2CO_3 to K and CO is more advantageous than that to K_2O and CO.

3.2. Weight loss of SiC, Si_3N_4 and AlN in molten K_2SO_4–K_2CO_3 salts

SiC, Si_3N_4 and AlN specimens were immersed into K_2SO_4, 50 mol% K_2SO_4–50 mol% K_2CO_3 and K_2CO_3 melts exposed to air at 1200, 1068 and 1013 °C, respectively. The weight losses of these specimens by corrosion with potassium melts are shown in Figs 3, 4 and 5.

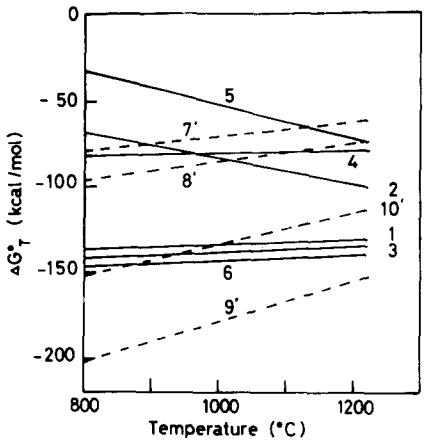

Fig. 2. Chemical free energy changes as a function of temperature for the possible oxidation reactions in the system of SiC, Si_3N_4 or AlN and K_2CO_3 or K_2SO_4. (Lines 1–6 and 7′–10′ refer to eqns (1)–(6) and (7′)–(10′) given in text.)

Silicon carbide dissolved very slowly in K_2CO_3 melts, but rapidly in K_2SO_4 and 50 mol% K_2SO_4–50 mol% K_2CO_3 melts. The rate of the weight loss of the silicon carbide specimen in 50 mol% K_2SO_4–50 mol% K_2CO_3 was much faster than that in the K_2SO_4 melt. It is expected that the rate of solution of silicon carbide in potassium salt melts depends not only on the oxidizing activity but also on the basicity of the melts.[1,2]

On the other hand, the weight loss of silicon nitride was appreciable in all potassium salts used. The rate of weight loss was the fastest in the K_2CO_3 melt, and decreased with increasing concentration of K_2SO_4 in the melts.

It is notable that aluminium nitride exhibited good resistance to

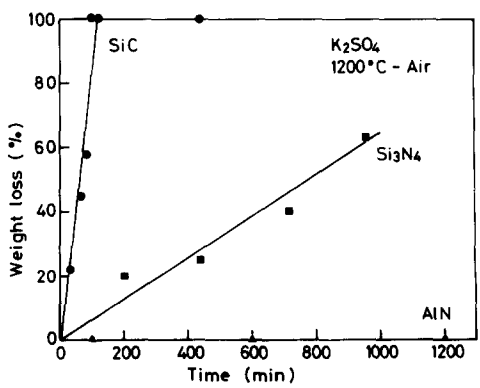

Fig. 3. Weight loss of SiC, Si_3N_4 and AlN specimens in molten K_2SO_4 exposed to air at 1200 °C.

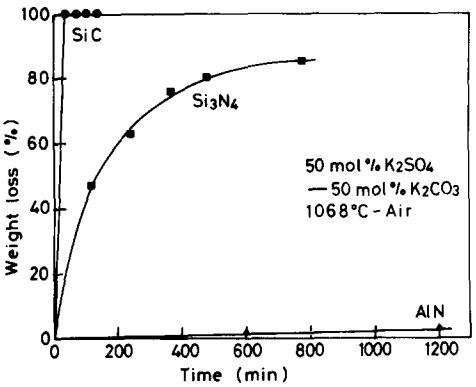

Fig. 4. Weight loss of SiC, Si_3N_4 and AlN specimens in molten 50 mol.% K_2SO_4–50 mol% K_2CO_3 exposed to air at 1068 °C.

potassium melts and little weight loss was observed in all potassium salts used. The present results are in good agreement with those reported by Sata and Kasukawa.[10]

3.3. Stoichiometry of the reaction of SiC and Si_3N_4 with K_2SO_4 and K_2CO_3 melts

A series of experiments was conducted in which silicon carbide and silicon nitride specimens were immersed into K_2CO_3 and K_2SO_4 melts, exposed to air or nitrogen atmospheres for 20 h; the initial molar ratio of K_2CO_3 or K_2SO_4 per SiC or Si_3N_4 was systematically changed from 0·5 to 5·0. The results of XRD from the surface of the reacted specimens showed only the diffraction peaks corresponding to SiC or Si_3N_4, but $K_2O.4SiO_2$

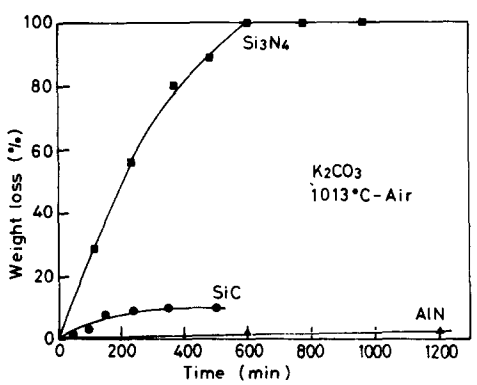

Fig. 5. Weight loss of SiC, Si_3N_4 and AlN specimens in molten K_2CO_3 exposed to air at 1013 °C.

was detected by XRD in the flux. Further, sulphide was detected by qualitative analysis using $AgNO_3$ solution in the flux of the K_2SO_4–SiC and K_2SO_4–Si_3N_4 systems. The SEM photographs of the SiC and Si_3N_4 specimens corroded in K_2SO_4 melts exposed to air and nitrogen are shown in Fig. 6. Extensive roughening of the surface and bubbles of evolved gas were observed for the SiC– and Si_3N_4–melt interfaces. As seen in Fig. 6(D), a film of about 50 μm was formed below the roughened surface of the specimen when silicon nitride was immersed in the K_2SO_4 melt exposed to air. This may be the protective film which is described later.

The amount of the weight loss of silicon carbide and silicon nitride specimens for each test is shown in Figs 7 and 8. As seen in Fig. 7(A), the weight loss of silicon carbide increased linearly with increasing initial molar ratio of K_2SO_4/SiC; the reaction of SiC and K_2SO_4 seemed to proceed quantitatively under the reaction conditions. The stoichiometry of K_2SO_4/SiC was determined to be 0·8 from the plots of weight loss versus initial molar ratio of K_2SO_4/SiC for the melt exposed to nitrogen

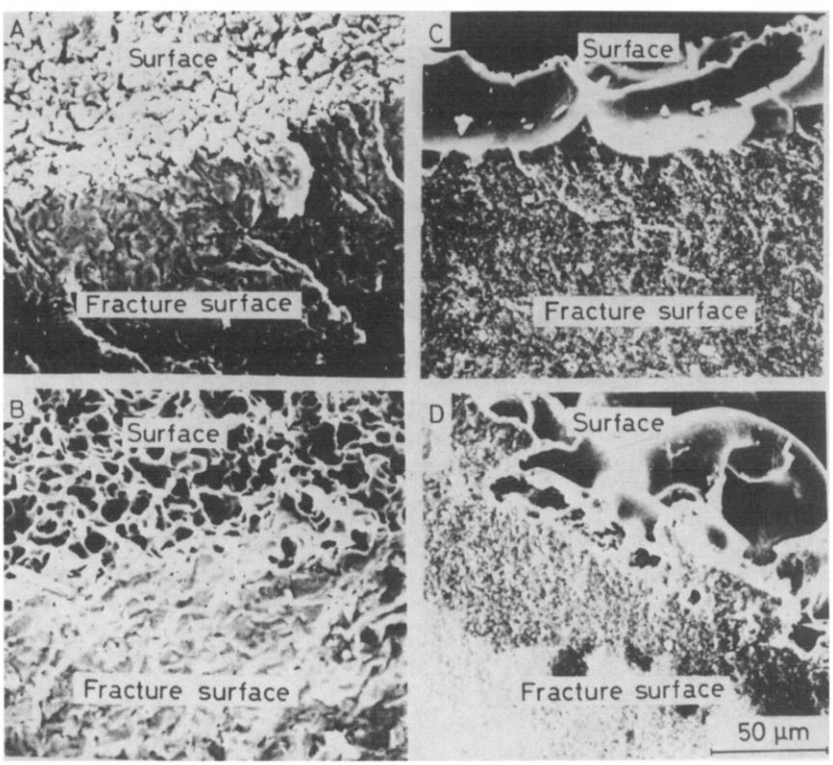

Fig. 6. Microstructural characteristics of SiC and Si_3N_4 specimens immersed in molten K_2SO_4 exposed to air or nitrogen: (A) SiC–K_2SO_4–N_2; (B) SiC–K_2SO_4–air; (C) Si_3N_4–K_2SO_4–N_2; (D) Si_3N_4–K_2SO_4–air.

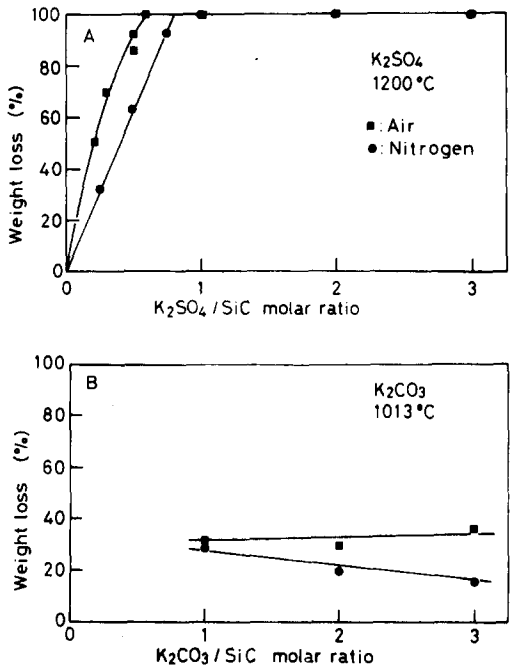

Fig. 7. Relations between weight loss of the SiC specimens and the initial molar ratios of (A) K_2SO_4/SiC and (B) K_2CO_3/SiC.

gas. The stoichiometry value for the K_2SO_4 melt exposed to air was 0·6, which implied that SiC was partially oxidized by oxygen. The value of 0·8 for the stoichiometry of K_2SO_4/SiC was quite close to the value of 0·75 corresponding to the simplified reaction expressed by eqn (11):

$$4SiC + 3K_2SO_4 \rightarrow 4SiO_2 + 4CO + 3K_2S \quad (K_2SO_4/SiC = 0{\cdot}75) \quad (11)$$

Equation (11) is the combination of the reactions shown by eqns (1) and (7). It is expected that SiO_2 dissolved in the salt melt as potassium silicate and no free SiO_2 could be observed on the surface of the remaining specimen by EPMA and XRD. Since potassium silicates, $K_2O\,.\,nSiO_2$ ($n < 5$), and potassium polysulphides, K_2S_x ($x < 6$), could form liquid phases at 1200°C, the following reactions were considered:

$$5SiC + 4K_2SO_4 \rightarrow K_2O\,.\,5SiO_2 + 5CO + K_2S + 2K_2S_2 \quad (12)$$
$$(K_2SO_4/SiC = 0{\cdot}8)$$

$$16SiC + 13K_2SO_4 \rightarrow 4(K_2O\,.\,4SiO_2) + 16CO + 5K_2S + 4K_2S_2 \quad (13)$$
$$(K_2SO_4/SiC = 0{\cdot}81)$$

Although further studies should be carried out to confirm the species of

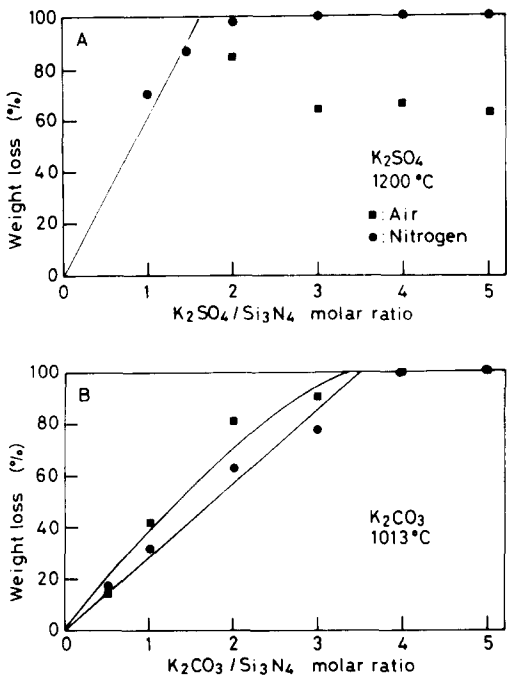

Fig. 8. Relations between weight loss of Si_3N_4 specimens and the initial molar ratios of (A) K_2SO_4/Si_3N_4 and (B) K_2CO_3/Si_3N_4.

polysulphide, the present results indicate that the first step of the reduction of sulphate was not the formation of sulphite but of sulphide.

McKee and Chatterji[1] and Tressler *et al.*[5] reported the formation of SO_2 by the reaction between SiC or Si_3N_4 and Na_2SO_4–NaCl melts. No reaction equation was given in their report. It is considered that the formation of SO_2 is possible, due to the reaction between the initial production of sulphides and residual sulphate in the SiC or Si_3N_4–Na_2SO_4 melt system:

$$3Na_2SO_4 + Na_2S \rightarrow 4Na_2O + 4SO_2 \qquad (14)$$

Reaction (14) is based on the results reported by Turkdogan and Vinters[11] in the excess $CaSO_4$–C system. In the present experiments no formation of SO_2 occurred in the system of SiC–K_2SO_4 melts when K_2SO_4/SiC was less than 0·8; however, above 1·0 the formation of SO_2 would have occurred.

As seen in Fig. 7(B), the reaction between SiC and K_2CO_3 was much less than in either K_2SO_4 or the mixed salts and no relation was found between the weight loss of the SiC specimen and the initial molar ratio of K_2CO_3/SiC. Silicon carbide might not react with K_2CO_3 directly and the

weight loss of the SiC specimen in K_2CO_3 melt might be caused by the oxidation of SiC to SiO_2 owing to dissolved oxygen. The following dissolution of SiO_2 into K_2CO_3 was expected:

$$2SiC + 3O_2 \rightarrow 2SiO_2 + 2CO \tag{15}$$

$$4SiO_2 + K_2CO_3 \rightarrow K_2O \cdot 4SiO_2 + CO_2 \tag{16}$$

The reaction between Si_3N_4 and K_2SO_4 exposed to nitrogen proceeded quantitatively as seen in Fig. 8(A). The stoichiometry of K_2SO_4/Si_3N_4 was 1·6, which was close to that of the simplified reaction expressed by eqn (17):

$$2Si_3N_4 + 3K_2SO_4 \rightarrow 6SiO_2 + 4N_2 + 3K_2S \quad (K_2SO_4/Si_3N_4 = 1{\cdot}5) \tag{17}$$

Therefore, the reactions shown by eqns (18) and (19) are actually expected to proceed:

$$20Si_3N_4 + 33K_2SO_4 \rightarrow 12(K_2O \cdot 5SiO_2) + 40N_2 + 9K_2S + 12K_2S_2 \quad (K_2SO_4/Si_3N_4 = 1{\cdot}65) \tag{18}$$

$$16Si_3N_4 + 27K_2SO_4 \rightarrow 12(K_2O \cdot 4SiO_2) + 32N_2 + 3K_2S + 12K_2S_2 \quad (K_2SO_4/Si_3N_4 = 1{\cdot}68) \tag{19}$$

On the other hand, when a Si_3N_4 specimen was immersed into K_2SO_4 melt exposed to air, the reaction did not proceed quantitatively. In Fig. 6(D), an intermediate thin layer in the microstructure between the roughened surface and the unreacted inside body was observed; a protective layer of SiO_2 which did not react with the acidic melt of K_2SO_4 might be formed on the surface of Si_3N_4 grains in the presence of oxygen.

In contrast with the results of the reaction of SiC and K_2CO_3, Si_3N_4 reacted with K_2CO_3 melts quantitatively. The stoichiometry of K_2CO_3/Si_3N_4 was determined to be 3·5 by the reaction of the Si_3N_4 specimen with K_2CO_3 melt exposed to nitrogen gas, which was close to that of the simplified reaction of eqn (20):

$$3K_2CO_3 + Si_3N_4 \rightarrow 3SiO_2 + 2N_2 + 3CO + 6K \quad (K_2CO_3/Si_3N_4 = 3{\cdot}0) \tag{20}$$

A similar reaction has been confirmed to proceed in carbonates–SiO_2–Si_3N_4 systems.[9] As mentioned before, since SiO_2 dissolves as potassium silicates in the K_2CO_3 melts, the following reactions could be postulated:

$$7K_2CO_3 + 2Si_3N_4 \rightarrow 2(K_2O \cdot 3SiO_2) + 4N_2 + 7CO + 10K \quad (K_2CO_3/Si_3N_4 = 3{\cdot}5) \tag{21}$$

$$81K_2CO_3 + 24Si_3N_4 \rightarrow 18(K_2O \cdot 4SiO_2) + 48N_2 + 81CO + 126K \quad (K_2CO_3/Si_3N_4 = 3{\cdot}4) \tag{22}$$

Since K_2CO_3 slowly evaporated under the present reaction conditions a further study is necessary to confirm the stoichiometry of K_2CO_3/Si_3N_4.

4. CONCLUSIONS

1. Aluminium nitride ceramics exhibited good resistance to molten potassium salts.
2. Silicon carbide dissolved rapidly in molten potassium salts in the presence of K_2SO_4.
3. Silicon carbide reacted with K_2SO_4 melt quantitatively and the stoichiometry of K_2SO_4/SiC was 0·8.
4. Silicon nitride dissolved rapidly in all potassium melts.
5. The reactions of silicon nitride with K_2SO_4 melt were prevented by the formation of a protective film in the presence of oxygen.
6. Silicon nitride reacted with K_2SO_4 and K_2CO_3 quantitatively and the stoichiometries of K_2SO_4/Si_3N_4 and K_2CO_3/Si_3N_4 were 1·6 and 3·5, respectively.

ACKNOWLEDGEMENTS

The authors are indebted to the management of NGK Spark Plug Co. Ltd for supplying the test pieces of SiC and Si_3N_4 used in this study. This work has been carried out partially with the support of the grant-in-aid for energy research of the Japanese Ministry of Education.

REFERENCES

1. McKee, D. W. and Chatterji, D., Corrosion of silicon carbide in gases and alkaline melts, *J. Am. Ceram. Soc.*, **59** (1976) 441–4.
2. Mayer, M. I. and Riley, F. L., Sodium-assisted oxidation of reaction-bonded silicon nitride, *J. Mater. Sci.*, **13** (1978) 1319–28.
3. Brooks, S. M., Ferguson, J. M., Meadowcroft, D. B. and Stevens, C. G., Corrosion above 700 °C in oil-fired combustion, in *Materials and Coatings to Resist High Temperature Corrosion*, Eds D. R. Holmes and A. Rahmel, Elsevier Applied Science Publishers, London, 1977, 121–38.
4. Erdoes, E. and Altorfer, H., Corrosion behavior of hot-pressed and reaction-bonded silicon nitride in condensed phase, in *Materials and Coatings to Resist High Temperature Corrosion*, Eds D. R. Holmes and A. Rahmel, Elsevier Applied Science Publishers, London, 1977, 161–74.
5. Tressler, R. E., Meiser, M. D. and Yonushonis, T., Molten salt corrosion of SiC and Si_3N_4 ceramics, *J. Am. Ceram. Soc.*, **59** (1976) 278–9.

6. Bourne, W. C. and Tressler, R. E., Molten salt degradation of Si_3N_4 ceramics, *Am. Ceram. Soc. Bull.*, **59** (1980) 443–6, 452.
7. Ferber, M. K. and Tennery, V. J., Behavior of tubular ceramics heat exchanger materials in acidic coal ash from coal-oil-mixture combustion, *Am. Ceram. Soc. Bull.*, **62** (1983) 236–43.
8. Becher, P. F., Strength degradation in SiC and Si_3N_4 ceramics by exposure to coal slags at high temperatures, *J. Mater. Sci.*, **19** (1984) 2805–14.
9. Wusirika, R., Problems associated with the melting of oxynitride glasses, *J. Am. Ceram. Soc.*, **63** (1984) 232–3.
10. Sata, T. and Kasukawa, K., Alkali corrosion and vaporization of MHD materials, *Rev. Int. Hautes Tempér. Réfrect., Fr*, **17** (1980) 174–83.
11. Turkdogan, E. T. and Vinters, J. V., Reduction of calcium sulphate by carbon, *Trans. Inst. Min. Metal.*, **C85** (1976) 117–23.

Received 22 April 1985; amended version received 21 October 1985; accepted 15 May 1986

Int. J. High Technology Ceramics **2** (1986) 291–307

Synthesis and Hot-pressing of Single-phase ZrC_xO_y and Two-phase ZrC_xO_y–ZrO_2 Materials

P. Barnier and F. Thévenot

Ecole Nationale Supérieure des Mines de Saint-Etienne Équipe 'Céramiques Spéciales' and Centre de Recherches Rhône-Alpes des Céramiques Spéciales (CRRACS), 158 Cours Fauriel, F 42023 Saint-Etienne Cédex 2, France

SUMMARY

Single-phase zirconium oxycarbide and a two-phase material, zirconium oxycarbide–zirconia, were synthesized by the reaction between zirconium carbide and zirconia powders at 2000°C under vacuum (4 Pa). ZrC_xO_y has the same cubic face centered (c.f.c.) crystallographic structure as zirconium carbide. The insertion of O increases the metal–non-metal bond strength and causes a decrease of the lattice parameter. $ZrC_{0.64}O_{0.26}$ with a = 4·66 Å is the composition of zirconium oxycarbide at the phase boundary with free zirconium dioxide.

The sinterability of these new materials was studied by hot-pressing under argon. Dense specimens without change of composition were obtained after hot-pressing. The hot-pressing temperature necessary to reach a relative density of 0·97 in 1 h was more than 300°C lower (at 1765°C) for zirconium oxycarbide saturated with oxygen than for zirconium carbide. Likewise, an increasing amount of ZrO_2 in the two-phase materials permitted a decrease of the hot-pressing temperature: between 0 and 17 mass% of ZrO_2 the hot-pressing temperature required decreased by more than 200 to 1550°C.

1. INTRODUCTION

Authors[1,2] who have studied the transition-metal carbides of the fourth, fifth and sixth groups of the periodic table have noticed the difficulty of producing these materials without the presence of dissolved oxygen. Zirconium carbide especially[3] shows a great affinity for oxygen. Several

Int. J. High Technology Ceramics 0267-3762/86/$03·50

investigations have been carried out on the reaction between zirconium dioxide and carbon,[4-10] and between zirconium oxide and zirconium carbide.[11-14] Different authors give a partial phase diagram for the Zr–O–C system[15-19] with a homogeneity range of the zirconium oxycarbide phase. However, these studies led to different or contradictory results; this can be explained by the different experimental conditions concerning temperature and atmosphere (argon, vacuum, partial pressure of carbon monoxide). Certain authors conclude that zirconium oxycarbide is unstable,[12,13] whereas Ogawa[20] affirms that the oxycarbides, i.e. the carbides containing dissolved oxygen, of the group IV and actinide elements are so stable that it is hard to obtain the oxygen-free carbides. The most complete study was carried out by Ouensanga and Dodé,[19] who give a phase diagram for the Zr–O–C system at 1555°C.

Until now workers have been interested primarily in the chemical and thermodynamic aspect of the formation of zirconium oxycarbide. We have been interested in the preparation of dense specimens in order to study their properties. Thus, the main aim of this work was the synthesis of powders of single-phase zirconium oxycarbide, and of two-phase material, zirconium oxycarbide–zirconia, by reaction between zirconium dioxide and zirconium carbide at 2000°C under vacuum, and the study of their sinterability by hot-pressing.

These materials had previously never been studied in a densified form and their mechanical properties in particular were unknown. Several possible applications exist: zirconium oxycarbide can be of value as a material for structural applications at very high temperature, or as a component in cemented carbides. If toughening of zirconium oxycarbide by zirconia is induced, the two-phase material could find cutting tool applications.

2. STUDY OF THE REACTION BETWEEN ZrO_2 AND ZrC

2.1. Starting materials

Zirconium carbide (ZrC) powder of high purity was supplied by H. C. Starck ('vacuum quality', low Hf content). The amounts of the principal impurities are in mass%: Fe = 0·012, O = 0·106 and N = 0·253. The formula determined by chemical analysis is $ZrC_{0.963}$. The BET specific surface area was $0{\cdot}5\,m^2\,g^{-1}$. Zirconium dioxide (ZrO_2) powder without stabilizer was supplied by Criceram (UPH V). The specific surface area of this powder was $6{\cdot}6\,m^2\,g^{-1}$. X-ray diffraction analysis showed the presence of both monoclinic and tetragonal zirconium dioxide.

2.2. Procedure

The reaction was studied at 2000°C under a steady-state vacuum of 4 Pa ($\simeq 3 \times 10^{-2}$ torr). Mixtures of ZrO_2 and ZrC powders with the different compositions (molar basis) $ZrO_2 + \alpha ZrC$, with $\alpha = 19, 8, 6, 4, 3{\cdot}25, 2{\cdot}5, 2$, were intimately mixed in ethanol using a 'Turrax' turbine and dried under vacuum at 110°C. Cylindrical specimens (diameter = 20 mm, height $\simeq$ 15 mm) were obtained by uniaxial cold-pressing. Reaction was allowed to proceed at 2000°C for 4 h: this time was sufficient to reach the thermodynamic equilibrium (longer annealing at 2000°C did not change the composition) except for the mixture $ZrO_2 + 19ZrC$. This material therefore was re-milled, cold-pressed and heated again at 2000°C for 4 h in order to achieve complete reaction. After annealing, specimens were crushed in a steel mortar for X-ray diffraction and chemical analysis.

The main elements zirconium, carbon and oxygen were analysed. Zr was determined by combustion of the powder at 1000°C in air for 1 h. After oxidation, only zirconium dioxide remains; hence it is possible to determine the Zr content. To determine the carbon content, the powder was combusted at 1600°C in a 'LECO 523' with the aid of fluxes, and the amount of carbon monoxide was determined using conductimetry. Oxygen was assumed to account for the residual mass.

The amount of zirconium dioxide in the two-phase powders (ZrC_xO_y–ZrO_2) was obtained by quantitative X-ray analysis. After crushing, ZrO_2 was entirely monoclinic. For low contents (<10 mass%), ZrO_2 was determined by extrapolation to the origin of the straight line, $I_{11\bar{1}}ZrO_2/I_{111}ZrC_xO_y$, versus content of added ZrO_2 in the powder to be analysed, with

$I_{11\bar{1}}ZrO_2$: intensity of the principal diffraction peak ($11\bar{1}$) of monoclinic ZrO_2

$I_{111}ZrC_xO_y$: intensity of the principal diffraction peak (111) of ZrC_xO_y

Monoclinic zirconium dioxide supplied by Magnesium Elektron was used for additions. For high contents (>10 mass%), ZrO_2 was obtained from a standard curve plotting $I_{11\bar{1}}ZrO_2/I_{111}ZrC_xO_y$ versus content of ZrO_2 additions to pure ZrC_xO_y.

2.3. Theoretical study of the reaction

For starting mixtures rich in zirconium carbide, the reaction can be written as follows:

$$ZrO_2 + \alpha ZrC \rightarrow (1 + \alpha)ZrC_xO_y + XCO \quad (1)$$

(to simplify, it is assumed that zirconium carbide is stoichiometric).

Considering the reaction equilibrium, the following relations are derived from (1):

$$x = \frac{\alpha - X}{1 + \alpha} \tag{2}$$

$$y = \frac{2 - X}{1 + \alpha} \tag{3}$$

X can be determined by measuring the mass loss of the specimen during reaction (it is supposed that the mass loss is due only to the formation of carbon monoxide). Consequently, the composition of zirconium oxycarbide can be calculated by using the composition of the starting mixture and the measure of the mass loss during reaction.

For the starting mixtures weaker in zirconium carbide, the reaction becomes

$$ZrO_2 + \alpha ZrC \rightarrow (1 + \alpha - A)ZrC_{x_0}O_{y_0} + A\,ZrO_2 + X CO \tag{4}$$

In this case, the zirconium oxycarbide is saturated with oxygen and is therefore in thermodynamic equilibrium with the residual zirconium dioxide. The composition of zirconium oxycarbide at the phase boundary ($A = 0$) is given by the following relations from (2) and (3):

$$x_0 = \frac{\alpha_0 - X_0}{1 + \alpha_0} \tag{5}$$

$$y_0 = \frac{2 - X_0}{1 + \alpha_0} \tag{6}$$

where α_0 is the number of moles of ZrC in the starting mixture to give pure zirconium oxycarbide saturated with oxygen and X_0 is the number of moles of saturated CO formed.

From (5) and (6), the following relation can be written:

$$x_0 - y_0 = \frac{\alpha_0 - 2}{1 + \alpha_0} \tag{7}$$

Considering the reaction equilibrium (4), the following relation is derived:

$$x_0 - y_0 = \frac{\alpha - 2 + 2A}{1 + \alpha - A} \tag{8}$$

From (7) and (8), the number of moles of residual zirconia A is given by the following equation:

$$A = 1 - \frac{\alpha}{\alpha_0}$$

TABLE 1

Composition of ZrC_xO_y and ZrC_xO_y–ZrO_2 in the Reaction Products, According to Chemical X-ray Diffraction Analysis and Calculation from the Weight Loss Measurement During Reaction; Lattice Parameter of Oxycarbide

α	*Starting mixture: mole% ZrC*	*Mass loss/ %*	*Total elemental chemical analysis in*			*X-ray determination: mass% ZrO_2*	$x = \frac{C}{Zr}$	$y = \frac{O}{Zr}$	*x calculated*	*y calculated*	*Mass% ZrO_2 calculated*	*Lattice parameter of ZrC_xO_y/ Å*
			Mass% Zr	*Mass% C*	*Mass% O (by difference)*							
19	95	2·20	89·26	10·32	0·42	0	0·88	0·027	0·87	0·018	—	4·692
8	88·89	2·98	89·14	9·25	1·61	0	0·79	0·10	0·78	0·11	—	4·682
6	85·71	3·54	89·00	8·70	2·30	0	0·74	0·15	0·72	0·15	—	4·677
4	80	4·17	88·76	7·79	3·45	0	0·67	0·22	0·64	0·24	—	4·665
3·25	76·47	5·07	88·25	7·35	4·40	1·8	—	—	—	—	0·8	4·661
2·5	71·43	5·60	87·39	6·79	5·82	7·9	—	—	—	—	8·5	4·660
2	66·67	5·11	86·73	6·32	6·95	13·2	—	—	—	—	15·7	4·659

2.4. Results and discussion

According to the composition of the starting mixture, the solid reaction products, analysed by X-ray diffraction, are only zirconium oxycarbide or a mixture of zirconium oxycarbide and zirconium dioxide (Table 1). ZrC_xO_y has a crystallographic structure which is identical with that of zirconium carbide: c.f.c. (NaCl type). Carbon and oxygen atoms occupy the octahedral interstitial vacancies of the metallic lattice. The zirconium dioxide is entirely in its monoclinic form.

The variation of the lattice parameter of the oxycarbide phase is plotted as a function of the molar content of zirconium carbide in the starting mixture (Fig. 1). Two different domains are observed. On the right side of the figure, we observe a gradual decrease of the lattice parameter with the diminution of the zirconium carbide concentration of the starting mixture. This corresponds to the monophase domain. The lattice parameter decreases with the progressive introduction of oxygen in the metallic lattice. Zirconium oxycarbide is grey-like ZrC, or reddish for specimens rich in oxygen ($x < 0{\cdot}74$ and $y > 0{\cdot}15$).

Below a limiting content of zirconium carbide in the starting material, the lattice parameter of ZrC_xO_y is constant. Two phases are in thermodynamic

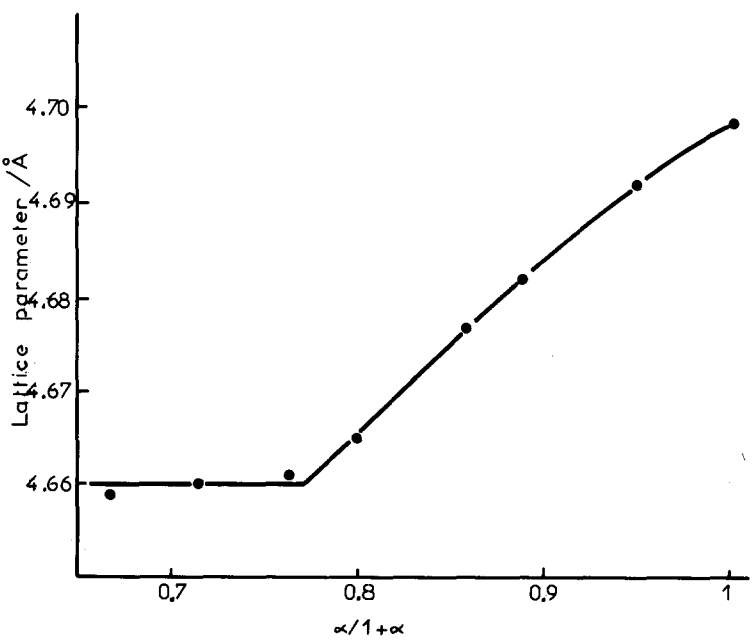

Fig. 1. Variation of the lattice parameter of zirconium oxycarbide after reaction of mixtures ($ZrO_2 + \alpha ZrC$) at 2000°C as a function of the starting molar concentration of zirconium carbide [$\alpha/(1 + \alpha)$].

equilibrium: zirconium oxycarbide saturated with oxygen and zirconium dioxide.

The chemical composition of the specimens is given in Table 1. The amounts of O and C calculated from the weight loss using the relations given above are close to the values obtained by chemical analysis. The phase boundary of the zirconium oxycarbide is obtained for a starting mixture of $ZrO_2 + 3{\cdot}37ZrC$ (see Fig. 1).

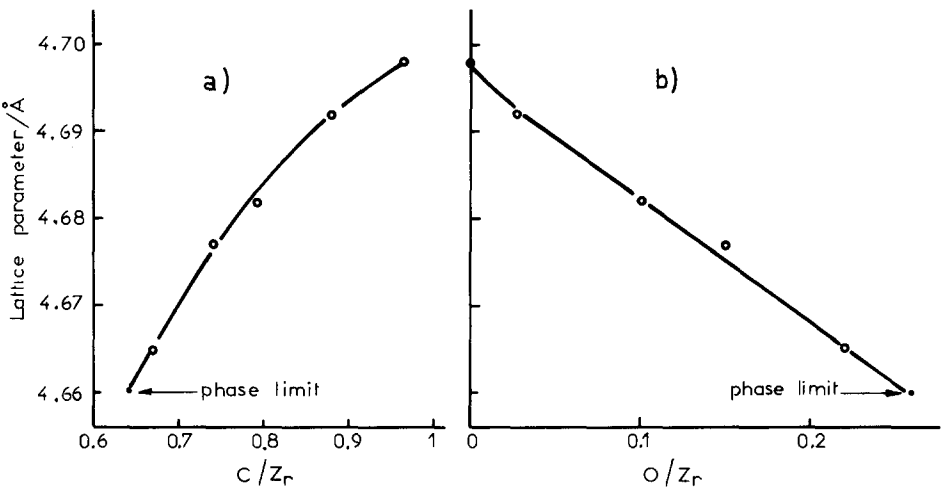

Fig. 2. Variation of the lattice parameter of zirconium oxycarbide as a function of (a) carbon and (b) oxygen concentration.

In Fig. 2 the variation of the lattice parameter of ZrC_xO_y is plotted as a function of the oxygen and carbon content. It can be seen that an increase of the oxygen content or a decrease of the carbon content leads to a decrease of the lattice parameter. The composition of zirconium oxycarbide saturated in oxygen is determined by extrapolation, $ZrC_{0{\cdot}64}O_{0{\cdot}26}$, using the limit parameter 4·66 Å found in Fig. 1. It can be seen that the insertion of oxygen is accompanied by an increase in the concentration of octahedral vacancies ($x + y < 1$ and decreases when y increases). To determine the real influence of oxygen, we compared the variation of the lattice parameter as a function of the occupation of the octahedral vacancies for the oxycarbide phase and for non-stoichiometric zirconium carbide according to Ramqvist[3] (Fig. 3). It can be seen that, in this interval of concentration of octahedral vacancies, the lattice parameter of ZrC_x is almost constant. The lattice parameter of ZrC_xO_y is always less than that of ZrC_x and the difference between the two parameters increases with increasing y. This proves that the Zr–O bond (certainly partially

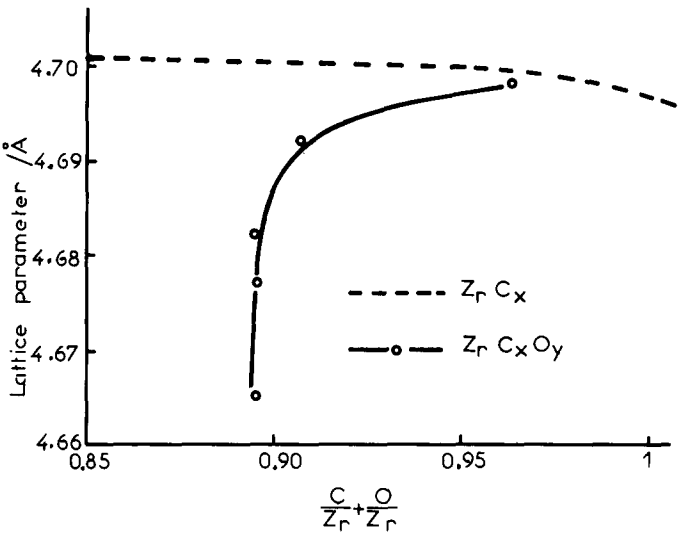

Fig. 3. Comparison of the lattice parameter of the oxycarbide phase and of non-stoichiometric zirconium carbide according to Ramqvist,[3] as a function of the degree of occupation of the octahedral vacancies.

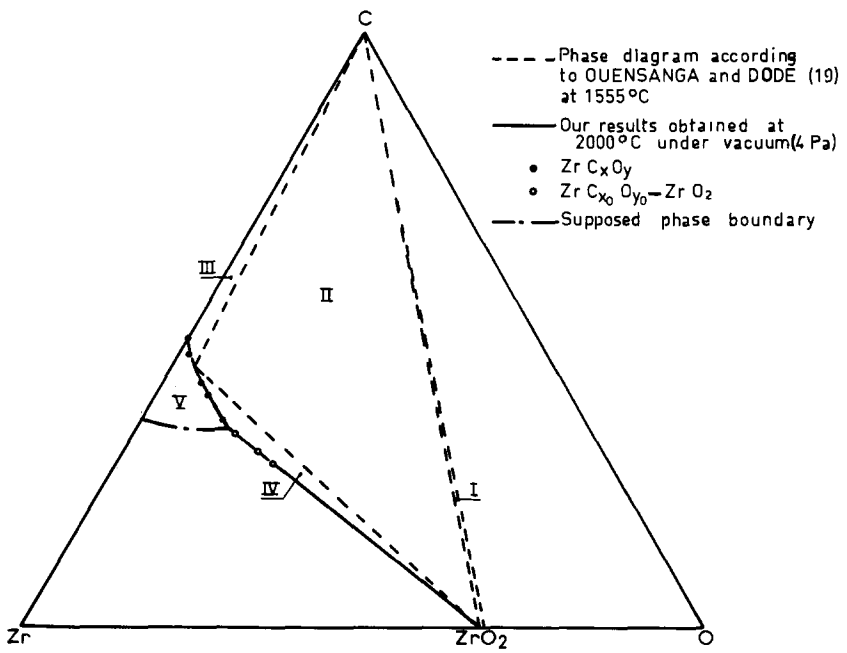

Fig. 4. Results obtained in this study at 2000°C plotted on the Zr–O–C diagram. Diagram given by Ouensanga and Dodé[19] obtained at 1555°C with five domains (I, 'ZrO_2'–C, $P_{CO} > 4 \times 10^4$ Pa (300 torr); II, 'ZrO_2'–C–ZrC_xO_y, $P_{CO} = 4 \times 10^4$ Pa; III, ZrC_xO_y–C, $P_{CO} < 4 \times 10^4$ Pa; IV, ZrC_xO_y–'ZrO_2', $P_{CO} < 4 \times 10^4$ Pa; V, ZrC_xO_y).

ionic) is stronger than the covalent Zr–C bond, and leads to a contraction of the lattice.

The results obtained are plotted in a Zr–O–C diagram (Fig. 4). We also show the results of the work of Ouensanga and Dodé[19] obtained at 1555°C. There is good agreement between the two studies. At 2000°C it is possible to insert more oxygen in the oxycarbide lattice ($ZrC_{0.64}O_{0.26}$) than at 1555°C ($ZrC_{0.73}O_{0.14}$). On the other hand, oxycarbides in the single-phase domain produced by Ouensanga and Dodé at 1555°C under a pressure of 1·3 mPa (10^{-5} torr) (the points are not plotted in Fig. 4) have compositions close to our results obtained at 2000°C under a pressure of 4 Pa (3×10^{-2} torr). The phase boundary (Zr side) of the zirconium oxycarbide domain was supposed to be a line between $ZrC_{0.575}$ (phase boundary of non-stoichiometric zirconium carbide with zirconium according to Ramqvist[3]) and $ZrC_{0.64}O_{0.26}$ (phase boundary of zirconium oxycarbide with zirconium dioxide).

3. HOT-PRESSING OF ZrC_xO_y AND ZrC_xO_y–ZrO_2

3.1. Powder preparation and characterization

After reaction, the specimens were milled in ethanol in a 'Dangoumau' mill, using a stainless steel jar and balls, for 4 h. The contamination by iron was removed by washing in concentrated hydrochloric acid at temperatures between 80°C and boiling point for 0·5 h. The acid, and iron salts, were removed by rinsing with water, followed by acetone, before drying. The operation was repeated twice to ensure the complete elimination of iron. For powders rich in oxygen, a (non-negligible) solution of zirconium oxycarbide was noticed: washing was carried out at 80°C to minimize the solution. For composite powders, the zirconium dioxide content was determined a second time, after washing, by quantitative X-ray diffraction analysis.

The BET specific surface area was measured for all powders (Table 2) and showed values between 0·5 and 1 $m^2 g^{-1}$.

The theoretical density of zirconium oxycarbide was calculated from the chemical analysis and from the determination of the lattice parameter. For two-phase materials, X-ray diffraction analyses of polished specimens show that the zirconium dioxide is certainly entirely monoclinic. Hence, the following relation was used for calculating the theoretical density of the two-phase material:

$$d = \frac{100}{\frac{t}{d_1} + \frac{(100 - t)}{d_2}}$$

TABLE 2

Characterization of the Starting Powders and Results of Hot-pressing of ZrC_xO_y and ZrC_xO_y–ZrO_2

Composition of the starting powder	*Mass% ZrO_2*	*BET specific area/ $m^2 g^{-1}$*	*Lattice parameter of ZrC_xO_y/ Å*	*Theoretical density/ $Mg m^{-3}$*	*Hot-pressing temperature/ °C*	*Sintering time/ h*	*Pressure/ MPa*	*Lattice parameter after hot-pressing/ Å*	*Final density/*		*Hot-pressing temperature required for 0·97 theoretical density (time = 1 h)/ °C*
									$Mg m^{-3}$	*% theoretical density*	
$ZrC_{0·963}$	0	0·5	4·698	6·58	1 900	1	40	4·697	6·07	(92·2)	2 100
					2 000	1	40	4·699	6·35	(96·5)	
					2 100	1	40	4·698	6·38	(97·0)	
					2 200	1	40	—	6·40	(97·3)	
$ZrC_{0·88}O_{0·027}$	0	1	4·692	6·57	1 800	1	32	4·691	5·82	(88·6)	1 915
					1 900	1	32	4·693	6·36	(96·8)	
					1 950	0·75	32	4·690	6·27	(95·4)	
					2 000	1	32	4·692	6·48	(98·6)	
$ZrC_{0·79}O_{0·10}$	0	1	4·682	6·62	1 800	1	32	4·683	6·22	(94·0)	1 870
					1 900	0·5	32	4·682	6·53	(98·6)	
					1 900	1	32	4·683	6·50	(98·2)	
					2 000	0·5	32	4·681	6·44	(97·3)	
					2 000	1	32	4·680	6·55	(98·9)	
$ZrC_{0·74}O_{0·15}$	0	0·6	4·677	6·65	1 800	1	32	4·678	6·39	(96·1)	1 830
					1 850	1	32	4·676	6·49	(97·6)	
					1 900	0·5	32	4·678	6·56	(98·6)	
					1 900	1	32	4·677	6·64	(99·8)	
					2 000	1	32	4·678	6·63	(99·7)	

$ZrC_{0.67}O_{0.22}$	0	0·6	4·665	6·72	1 700	1	32	4·667	6·42	(95·5)	1 765
					1 750	1	32	4·664	6·47	(96·3)	
					1 800	1	32	4·667	6·58	(97·9)	
					1 850	0·75	32	4·666	6·68	(99·4)	
					1 900	0·5	32	4·665	6·71	(99·9)	
					1 900	1	32	4·666	6·72	(100)	
					2 000	1	32	4·663	6·71	(99·9)	
	2·4	0·6	4·661	6·73	1 600	1	32	4·660	6·42	(95·4)	1 625
					1 650	1	32	4·661	6·60	(98·1)	
					1 750	1	32	4·660	6·68	(99·3)	
					1 800	0·5	32	4·660	6·70	(99·6)	
					1 800	1	32	4·665	6·71	(99·7)	
					1 850	1	32	4·663	6·72	(99·9)	
$ZrC_{0.64}O_{0.26}$ + ZrO_2	10·1	0·9	4·660	6·62	1 600	1	32	4·661	6·36	(96·1)	1 640
					1 700	1	32	4·662	6·52	(98·5)	
					1 750	1	32	4·661	6·54	(98·8)	
					1 800	0·5	32	4·663	6·58	(99·4)	
					1 800	1	32	4·664	6·59	(99·5)	
	17·0	0·9	4·559	6·52	1 500	1	32	4·660	6·20	(95·1)	1 550
					1 600	0·5	32	4·661	6·28	(96·3)	
					1 600	1	32	4·661	6·44	(98·8)	
					1 750	1	32	4·662	6·49	(99·5)	

where d is the density of the two-phase material; d_1 is the density of monoclinic zirconium dioxide, $d_1 = 5{\cdot}56\,\mathrm{Mg\,M^{-3}}$; d_2 is the density of zirconium oxycarbide saturated with oxygen, $d_2 = 6{\cdot}76\,\mathrm{Mg\,m^{-3}}$; and t is the mass% of ZrO_2.

3.2. Hot-pressing procedure

The hot-press used has already been described in previous papers.[21-23] Graphite dies and punches were used to obtain cylindrical-shaped specimens 20 mm in diameter and 8 to 12 mm in height after hot-pressing. The hot-pressing results for zirconium carbide are taken from a previous study.[24]

For ZrC_xO_y and ZrC_xO_y–ZrO_2, a chemical barrier is necessary to avoid reaction of the specimen with carbon. The powder is encapsulated in tantalum foil (thickness = 0·025 mm), and is then embedded in hexagonal boron nitride. This method has already been used with success to produce dense boron and boron suboxide.[22,25] During hot-pressing, the temperature was raised linearly with time at 30°C $\mathrm{min^{-1}}$ with a low applied pressure of 8 MPa, under vacuum up to 1000°C and under argon at higher temperature. At its maximum, the temperature was held for 0·5 to 1 h and a pressure of 32 MPa was applied (40 MPa for zirconium carbide). Then the temperature was decreased linearly with time at 30°C $\mathrm{min^{-1}}$ without pressure for ZrC_xO_y and at a speed of 10°C $\mathrm{min^{-1}}$ in the case of ZrO_2-containing material to avoid the formation of macrocracks during the martensitic transformation of zirconium dioxide which involves an increase in volume.

After hot-pressing, the surface of the specimens was polished before measuring the density and before X-ray examination. The lattice parameter of ZrC_xO_y was calculated and compared with the parameter of the initial powder.

3.3. Results and discussion

The results of the hot-pressing experiments are summarized in Table 2. No appreciable change of the lattice parameters of the oxycarbide was observed in the single-phase domain. This proves that the chemical composition of the zirconium oxycarbide phase remains constant and the stability of this phase can be confirmed under the conditions of this investigation. At higher hot-pressing temperatures ($T > 1800$°C), the lattice parameter of zirconium oxycarbide in the two-phase system increased slightly. This can be explained by the slightly different conditions of the thermodynamic equilibrium for the reaction of the powders (vacuum) on the one hand

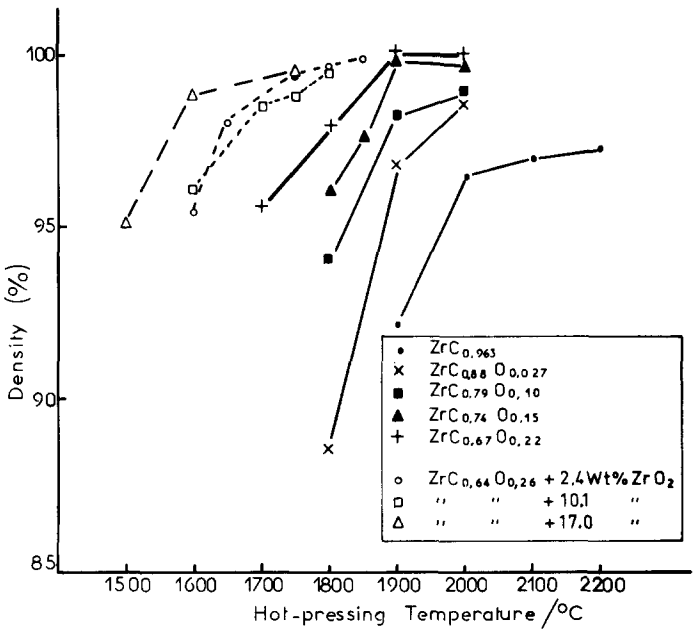

Fig. 5. Variation of the relative density of ZrC_xO_y and ZrC_xO_y–ZrO_2 as a function of the hot-pressing temperature (sintering time = 1 h).

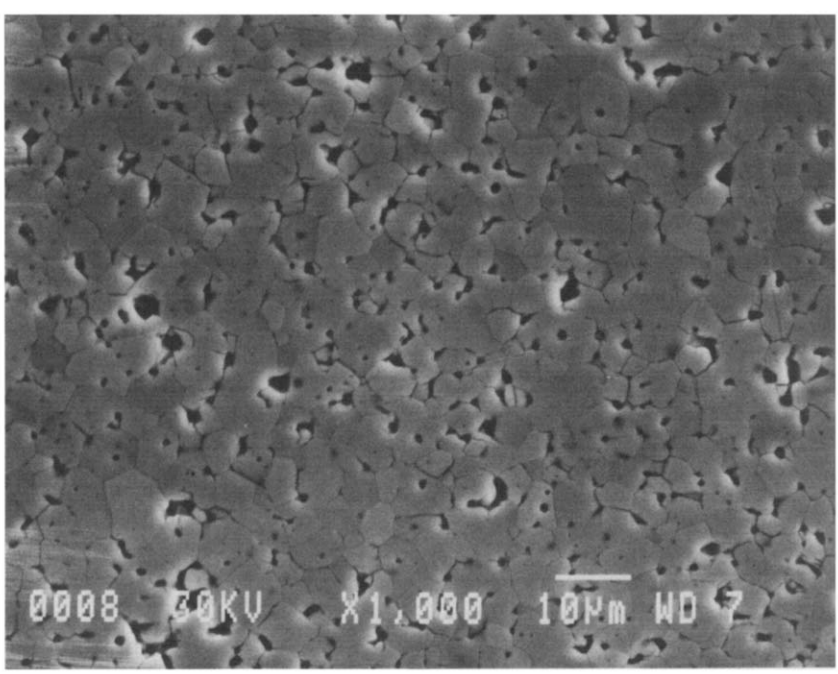

Fig. 6. Scanning electron micrograph of $ZrC_{0{\cdot}74}O_{0{\cdot}15}$ hot-pressed at 1900°C for 30 min, using secondary electrons (chemical etching).

and for hot-pressing (argon atmosphere and application of pressure) on the other hand. At lower temperatures there is no variation of the lattice parameter, since the reaction kinetics is very slow and the reaction equilibrium is metastable.

For all compositions it was possible to obtain specimens of high density. The variation of the relative density with different hot-pressing temperatures is shown in Fig. 5. It can be seen that the sinterability of zirconium oxycarbide increases, when the oxygen content increases. In Table 2 is noted the hot-pressing temperature necessary to reach a relative density of 97% in 1 h: for zirconium oxycarbide rich in oxygen ($ZrC_{0\cdot67}O_{0\cdot22}$), the temperature necessary (1765°C) is 335°C lower than the temperature necessary for zirconium carbide (2100°C). For materials with a low amount of ZrO_2 (2·4 mass%) the hot-pressing temperature necessary to reach a density of 97% is only 1625°C, whereas 1765°C is required for $ZrC_{0\cdot67}O_{0\cdot22}$. Materials with 10·1 mass% of ZrO_2 have a slightly worse sinterability but only 1550°C is necessary to reach a density of 97% for materials with 17·0 mass% of ZrO_2.

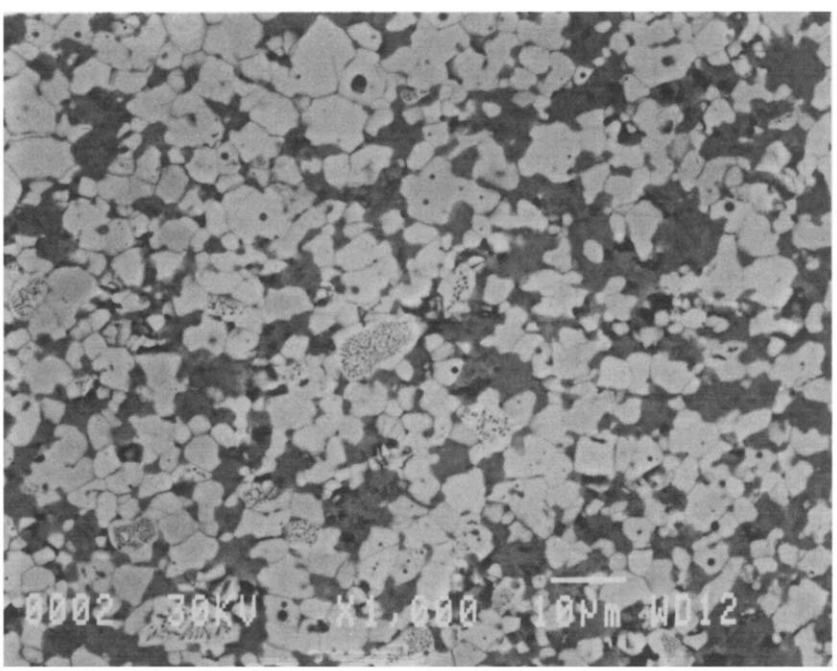

Fig. 7. Scanning electron micrograph of the two-phase material $ZrC_{0\cdot64}O_{0\cdot26}$–17·0 mass% ZrO_2, hot-pressed at 1600°C for 60 min, using back-scattered electrons (without chemical etching; zirconium oxycarbide, zirconium dioxide and porosity appear respectively as light, grey and dark).

Metallographic examinations of polished specimens were made by SEM; Fig. 6 shows the microstructure of $ZrC_{0.74}O_{0.15}$ hot-pressed at 1900°C for 0·5 h. The surface was etched with a solution of nitric and hydrofluoric acids: grain boundaries are well etched but attack by acids increases the size of holes due to porosity or caused by abrasion. Figure 7 shows the microstructure of a two-phase material ($ZrC_{0.64}O_{0.26}$ + 17·0 mass% ZrO_2) hot-pressed at 1600°C for 1 h. Polishing is sufficient to reveal the grain boundaries. The image was taken using back-scattered electrons in order to obtain better phase contrast.

4. CONCLUSION

The synthesis of powders of single-phase ZrC_xO_y and of two-phase ZrC_xO_y–ZrO_2 was achieved by reaction between zirconium carbide and zirconium dioxide powders at 2000°C under vacuum (4 Pa).

The sintering of these new materials has been studied for the first time by hot-pressing under argon. Specimens with good density and without change of composition during hot-pressing were obtained. The sinterability of oxycarbide increased considerably with the oxygen content, and increased still further for materials containing ZrO_2, even when the amount of ZrO_2 was low.

The thermomechanical properties of these new materials will now be investigated. The possibility in particular of toughening zirconium oxycarbide by zirconia will be studied.

REFERENCES

1. Toth, L. E., *Transition Metal Carbides and Nitrides*, Academic Press, New York and London, 1971.
2. Storms, E. K., *The Refractory Carbides*, Academic Press, New York, 1967.
3. Ramqvist, L., Variation of lattice parameter and hardness with carbon content of group 4b metal carbides, *Jerkont. Ann.*, **152** (1968) 517–23.
4. Henney, J. and Jones, J. W. S., Phases in the zirconium–carbon–oxygen system, in *Special Ceramics*, Ed. P. Popper, Academic Press, London, 1964, 35–43.
5. Leprince-Ringuet, F., Contribution à l'étude de l'action du carbone sur les oxydes réfractaires à haute température, *Ann. Chim.*, **2** (1967) 297–306.
6. Ouensanga, A., Vermesse, C. and Dodé, M., Contribution à l'étude thermodynamique du système Zr–O–C à haute température, *Rev. Chim. Miner.*, **9** (1972) 473–81.
7. Ouensanga, A. and Dodé, M., Etude à 1555°C de la solubilité de l'oxygène dans le carbure de zirconium en présence de carbone libre et dans les conditions

d'équilibre thermodynamique, *Rev. Int. Hautes Temp. et Réfract.*, **11** (1974) 35–9.
8. Ouensanga, A., Pialoux, A. and Dodé, M., Etude aux rayons X à haute température du système Zr–O–C dans les conditions d'équilibre thermodynamique, puis sous vide, *Rev. Int. Hautes Temp. et Réfract.*, **11** (1974) 289–93.
9. Kutsev, V. S. and Zhelankin, V. I., Thermodynamics of carbothermal reduction of zirconium and hafnium oxides, *Izv. Akad. Nauk SSSR, Neorg. Mater.*, **14** (1978) 593–5.
10. Lyubimov, V. D., Shveikin, G. P. and Alyamovskii, S. I., Mechanism of the direct reduction of tantalum, hafnium, and zirconium oxides, *Zh. Neorg. Khim.*, **27** (1982) 3015–19.
11. Fedorus, V. B., Kosolapova, T. Ya. and Kuzma, Yu. B., Interaction of carbides of transition metals of groups IV–VI of periodic system of elements with zirconium oxide, *Rev. Int. Hautes Temp. et Réfract.*, **6** (1969) 193–7.
12. Gropyanov, V. M., Kovaleskaya, T. A. and Yudin, B. F., Stability of oxycarbides in the system ZrC–ZrO_2, *Izv. Akad. Nauk SSSR, Neorg. Mater.*, **8** (1972) 88–91.
13. Gropyanov, V. P., Kovalevskaya, T. A. and Razumovskii, S. N., Crystal structure of zirconium oxycarbides in the system ZrC–ZrO_2, *Izv. Akad. Nauk SSSR, Neorg. Mater.*, **8** (1972) 92–5.
14. Granov, V. I. and Glaskov, A. V., Theoretical analysis of the reaction of zirconium dioxide with zirconium carbide, *Izv. Akad. Nauk SSSR, Neorg. Mater.*, **11** (1975) 226–9.
15. Alyamovskii, S. I., Zainulin, Yu. G., Schveikin, G. P. and Gel'd, P. V., Concentration range corresponding to the stability of the cubic (NaCl type) zirconium oxide carbide and the degree of filling of its unit cell, *Zh. Neorg. Khim.*, **6** (1971) 7–11.
16. Klimashin, G. M., Kozlovskii, L. V. and Chiu, A. K., Region of existence of an oxycarbide phase in the system Zr–C–O, *Zh. Prikl. Khim.*, **44** (1971) 1644–6.
17. Klimashin, G. M., Avgustinik, A. I. and Smirnov, G. V., Carbonitride and oxycarbide phases of titanium and zirconium, *Izv. Akad. Nauk SSSR, Neorg. Mater.*, **8** (1972) 843–5.
18. Constant, K., Kieffer, R. and Ettmayer, P., Über des pseudoternäre System 'ZrO'–ZrN–ZrC, *Monatsh. Chem.*, **106** (1975) 823–32.
19. Ouensanga, A. H. and Dodé, M., Etude thermodynamique et structurale à haute température dy système Zr–C–O. Diagramme de phases à 1555°C, *J. Nucl. Mater.*, **59** (1976) 49–60.
20. Ogawa, T., Method to assess the equilibrium MO_x–'MC_y'–C–CO. The system ZrO_2–'ZrC'–C–CO, *J. Chem. Eng. Data*, **27** (1982) 186–8.
21. Brodhag, C. and Thévenot, F., Utilisation d'un système de traitement informatique interactif APL pour le suivi de la fabrication de pièces frittées par compression à chaud, in *Proc. Colloque sur le Contrôle de Qualité et l'Assurance de la Qualité en Métallurgie des Poudres*, Société Française de Métallurgie, Paris, September 1980, Vol. 10, 1–6.
22. Brodhag, C., *Etudes sur le Bore et les Composés Interstitiels du Bore Alpha—Traitement Infographique des Cinétiques de Frittage sous Charge*, Thesis, University of Limoges, France, 1983.

23. Brodhag, C., Bouchacourt, M. and Thévenot, F., La cinétique de la compression à chaud de céramiques spéciales, *Silicates Ind.*, **4–5** (1981) 91–101.
24. Barnier, P., Brodhag, C. and Thévenot, F., Hot-pressing kinetics of zirconium carbide, *J. Mat. Sci.*, **21** (1986) 2547–52.
25. Bouchacourt, M., Brodhag, C. and Thévenot, F., The hot pressing of boron and boron rich compounds, *Science of Ceramics 11*, Stenungsund, Sweden, 14–17 June, 1981, 231–6.

Received 14 February 1986; revised version received 14 July 1986; accepted 3 August 1986

Int. J. High Technology Ceramics **2** (1986) 309–313

Conference Reports

WORLD CONGRESS ON HIGH TECH CERAMICS, MILAN, ITALY (23–28 JUNE, 1986)

This was the 6th meeting in the CIMTEC series, an intermittent series, which, until this present meeting, had been held in Rimini, Italy. It was a very ambitious undertaking as is obvious from the stated objectives:

(i) Review the science of ceramic processes for advanced materials and the 'state-of-the-art' in terms of the most recent progress and understanding of the phenomena involved.
(ii) Discuss strategies for high technology applications and critical limiting factors.
(iii) Report on present national research projects and plans for high tech ceramics in the more advanced countries.
(iv) Provide an insight into the present market for advanced ceramics on a world basis and the expected areas of development in the medium term.
(v) Assess the impact of advanced ceramics on key industrial sectors such as energy generation, conversion, distribution and storage, high temperature engineering, process engineering, electronics–nuclear–space technology and biotechnology.

The congress was held under the auspices of the Italian Ministry for Science and Technology and was co-sponsored by almost all the national ceramic societies world-wide. Since Rimini could not provide the required facilities of multiple simultaneous sessions, the congress was held at the new and very impressive Congress Centre of the World Trade Centre at

Int. J. High Technology Ceramics (2) (1986)—

Milanofiori. As this must have been the largest conference in the field of ceramics held in Europe, reminiscent of the Annual Meetings of the American Ceramic Society, it is worth considering the advantages and disadvantages of such large meetings and of the choice of venue.

From an attendee's point of view, the programme of lectures (3 opening, 10 invited, 10 general, 182 contributed) and posters (199) offered plenty of interest in his particular field. In fact, probably too much, as often he would wish to hear lectures taking place simultaneously and an agonizing choice had to be made. Being unable to attend an event of one's particular interest always leaves a bad feeling of having missed something important. Fortunately, the posters were displayed all through the conference so that they could be studied in relative leisure although the authors were not always available at the set times when they were expected to attend.

From the organizer's point of view, financial considerations demand that there be a very large number of contributions in order to obtain sufficient funds from the conference fees. In addition, the organizer has to invite a number of lecturers to review certain fields whose names will attract additional registrations.

The large number of delegates (over 700) caused considerable logistic problems. They had to be accommodated in various hotels, some in the centre of Milan, some in the outskirts, with buses providing transport; these were liable to be delayed by heavy traffic on the 'tangenziale' and at least on one occasion one bus was an hour late in the morning.

There was an International Advisory Board of 34 well-known personalities but, without doubt, the whole organization of the scientific and technical programme was ultimately in the hands of the Congress Chairman, P. Vincenzini. The detailed organization was carried out by a commercial agency; their efforts were not particularly impressive. Thus, there was no list of participants issued, although a list was pinned on a board. It was not clear who attended, as we were told that because of fear of terrorist activities 60% cancellations were received from the USA. The number of posters actually displayed, i.e. 112 out of the 199 listed in the programme, indicated a 43% withdrawal. Whether this percentage was the same for the lectures was impossible to tell; it certainly did not apply to the invited and general lectures all of which were presented. A serious drawback resulted from chairmen carrying on with their programme in a continuous manner even when lectures were cancelled. This led to the situation that when one arrived at the scheduled time to hear a particular lecture one only heard the closing remarks because the lecture had started early as one of the previous speakers had not turned up. In an event with simultaneous sessions it is imperative to adhere strictly to the printed time schedule. Another annoying feature was that although the official language was said to be English, several speakers spoke in an 'unofficial' language.

Headphones were supplied to those who wished to listen to the simultaneous translations from English, but those who understood English did not bother to collect these and therefore sometimes found themselves unable to understand those speakers using an 'unofficial' language.

It is of course impossible to mention the contents and quality of each of the many lectures and posters; almost every subject was covered. Some of the review lectures of key areas were very informative and Dr Vincenzini must be congratulated on having assembled presenters for such a vast amount of information. The proceedings of the congress will be published by Elsevier, North Holland in 2 volumes running for several thousands of pages. The prospect of being able to read the contributions one missed is eagerly anticipated, although with some trepidation about the cost of the publication.

One has to ask oneself whether meetings on this scale are desirable. I remember an American colleague saying to me at an American Ceramic Society Meeting when I mentioned that the trouble was that I would like to be in three places at the same time: 'I am not coming for the lecture, I come to meet people and see the exhibition'. This brings me to the small exhibition which, save for the stand by ASEA on isostatic pressing, was really not very interesting. The main reason for this is that the high technology activity in Italy is almost non-existent and potential foreign exhibitors would therefore consider the cost involved as a bad investment. Meeting people was not particularly easy. One usually saw people one would have liked to talk to rushing from one lecture location to another. There were no coffee or tea breaks, although there was some opportunity to meet people at the very pleasant evening receptions. However, these were more of a social occasion and in any case one was so exhausted by the end of the day (it was very, very hot outdoors) that one kept one's conversation away from ceramics. The congress was concluded by a very pleasant dinner in the Cloisters of St Francis a charming location in alta Bergamo.

In conclusion, the reviewer has formed the opinion that meetings on this scale should only be held if accompanied by a worthwhile exhibition of high technology ceramic materials and equipment for their R & D and production; and this can only be achieved in a country with high activity in this area.

PM 86 INTERNATIONAL CONFERENCE AND EXHIBITION, POWDER METALLURGY DUSSELDORF, FRG (7–11 JULY 1986)

Because the programme indicated much subject matter of relevance to high technology ceramics, the reviewer decided to attend this conference; after

Headphones were supplied to those who wished to listen to the simultaneous translations from English, but those who understood English did not bother to collect these and therefore sometimes found themselves unable to understand those speakers using an 'unofficial' language.

It is of course impossible to mention the contents and quality of each of the many lectures and posters; almost every subject was covered. Some of the review lectures of key areas were very informative and Dr Vincenzini must be congratulated on having assembled presenters for such a vast amount of information. The proceedings of the congress will be published by Elsevier, North Holland in 2 volumes running for several thousands of pages. The prospect of being able to read the contributions one missed is eagerly anticipated, although with some trepidation about the cost of the publication.

One has to ask oneself whether meetings on this scale are desirable. I remember an American colleague saying to me at an American Ceramic Society Meeting when I mentioned that the trouble was that I would like to be in three places at the same time: 'I am not coming for the lecture, I come to meet people and see the exhibition'. This brings me to the small exhibition which, save for the stand by ASEA on isostatic pressing, was really not very interesting. The main reason for this is that the high technology activity in Italy is almost non-existent and potential foreign exhibitors would therefore consider the cost involved as a bad investment. Meeting people was not particularly easy. One usually saw people one would have liked to talk to rushing from one lecture location to another. There were no coffee or tea breaks, although there was some opportunity to meet people at the very pleasant evening receptions. However, these were more of a social occasion and in any case one was so exhausted by the end of the day (it was very, very hot outdoors) that one kept one's conversation away from ceramics. The congress was concluded by a very pleasant dinner in the Cloisters of St Francis a charming location in alta Bergamo.

In conclusion, the reviewer has formed the opinion that meetings on this scale should only be held if accompanied by a worthwhile exhibition of high technology ceramic materials and equipment for their R & D and production; and this can only be achieved in a country with high activity in this area.

PM 86 INTERNATIONAL CONFERENCE AND EXHIBITION, POWDER METALLURGY DUSSELDORF, FRG (7–11 JULY 1986)

Because the programme indicated much subject matter of relevance to high technology ceramics, the reviewer decided to attend this conference; after

all, powder metallurgy and ceramics are both based on the same technology and the science of sintering, and cross-fertilization conceives better products than in-breeding.

As this meeting followed very soon after the World Congress on High Technology Ceramics (see above) comparisons come to one's mind. The two meetings were roughly of the same size but this meeting was accompanied by a very impressive exhibition in which there were not only approximately 150 exhibitors with their individual stands but many of these collaborated in a 'state-of-the-art' show covering subjects such as tools, engineering, transport, electronics, etc.

The organization can only be described as superb. On registration one was handed amongst other interesting information 2 volumes of 'Horizons of Powder Metallurgy' running in total to 1345 pages and containing preprints of the papers to be presented. There was also a list of the 620 registrants, covering 36 countries. Most delegates came from the FRG (132), the USA (70), Sweden (64) and Japan (60). The technical programme was covered by 12 plenary lectures, five of which were of definite interest to ceramists; of the latter the review 'New Ceramic Materials—a Challenge for Powder Metallurgy' given by F. Aldinger of Hoechst was outstanding. The remaining 300 plus contributions were covered by what appears to be a new concept, i.e. 'theme zones'. There were 25 altogether, covering: powder production, cutting materials, applications, new shaping methods for components, HIP and joining quality control, new materials, sintering, etc. Three or four theme zones were held simultaneously in different rooms. Between 10 and 20 posters were displayed for a whole day in each theme session. At a set time, all authors of a session assembled around a table and were introduced to the delegates by the chairmen. Authors then moved to their exhibit and were given 45 minutes for individual explanations and discussions. Thereafter, all authors went back to the podium for a further public discussion.

Another new feature was 'students' day'. On one day, students were given free access to the conference and exhibition. Two special lectures entitled 'Why PM?' and 'Examples of Applications of Modern PM Materials' were presented to them. Another day was designated 'users day' when a planning discussion was held with a panel consisting of important industrial users.

One's general impression was that there was much common ground in the handling of metal and ceramic powders, i.e. characterization of powder milling and mixing, granulation, forming equipment, sintering, and micro-structural evaluation. Whilst powder metallurgists seem to have only just woken up to consider the ancient ceramic art of slip casting, they are ahead in non-destructive inspection methods, particularly in the evaluation of density distribution by computer tomography using γ-rays. Freeze drying

was proposed as a forming method but one learned that the problem of die wear was rather serious with ceramic powders.

The organizers, the 'Ausschuss für Pulvermetallurgie' under the chairmanship of Prof. Dr G. Detzon, and the programme committee under Dr W. J. Huppmann must be congratulated for having arranged a most interesting programme for $4\frac{1}{2}$ days.

The social event was a cruise on the river Rhine.

Paul Popper

CALENDAR

1987 Meetings

Jan. 18–21	11th Annual Conference on Composites and Advanced Ceramics, Cocoa Beach, Florida, USA
Mar. 4–6	German–French Meeting on Technical Ceramics, Aachen, FRG
Mar. 29–Apr. 3	Chemical Vapour Deposition, Jerusalem, Israel
Apr. 5–9	International Conference on Wear of Materials, Houston, Texas, USA
Apr. 8–10	High Technology in the Ceramic Industry, Canterbury, UK
Apr. 26–29	American Ceramic Society Annual Meeting, Pittsburgh, Pennsylvania, USA
Jun. 15–16	Hot Isostatic Pressing, Luleå, Sweden
Sept. 7–9	Science of Ceramics 14, Canterbury, UK
Nov. 4–6	Science and Technology of Sintering, Tokyo, Japan
Nov. 9–13	Science of Hard Materials, Nassau, Bahamas

Int. J. High Technology Ceramics (**2**) (1986)—

Selected Abstracts from *Yogyo-Kyokai-Shi*

As a service to readers and with the agreement of The Ceramic Society of Japan, selected English language Abstracts of the papers appearing in the *Journal of the Ceramic Society of Japan* (*Yogyo-Kyokai-Shi*) are reproduced here. The selection was made by Drs R. Stevens and P. Popper.

Yogyo-Kyokai-Shi **94** (1986)

The Effect of Al_2O_3 or SiO_2 Addition on the Thermal Shock Resistance of Y_2O_3-Stabilized ZrO_2 Hiroshi WATANABE and Mitsuo CHIGASAKI, *Yogyo-Kyokai-Shi*, **94**, 255-60 (1986)——Thermal shock resistance of ZrO_2-(4-17)% Y_2O_3 has been investigated. A relatively excellent thermal shock resistance is obtained in partially stabilized ZrO_2-7% Y_2O_3. The effect of Al_2O_3 or SiO_2 addition to ZrO_2-7% Y_2O_3 has been also investigated to enhance its thermal shock resistance. ZrO_2-7% Y_2O_3-(0.5-4)% Al_2O_3 indicated an improved thermal shock resistance. In ZrO_2-7% Y_2O_3, the monoclinic ZrO_2 grains tended to coalesce into large clusters in the cubic ZrO_2 matrix. As a result, large cracks are prone to initiate from the monoclinic phase during the martensitic transformation. On the other hand, the addition of Al_2O_3 results in the isolated spherical grains of monoclinic ZrO_2 phase, leading to an improved thermal shock resistance. 4 figs., 1 table, 19 refs. [H. W.]

Hitachi Research Laboratory, Hitachi Ltd.
3-1-1, Saiwai-cho, Hitachi-shi 317

Firing Shrinkage of Alumina Green Sheet Shozo OHTOMO, Masatoshi KATO and Kimitake KOREKAWA, *Yogyo-Kyokai-Shi*, **94**, 261-66 (1986)——The alumina Green sheet (96% purity; Remainder 4% consists SiO2, CaO and MgO) produced by doctor blade method is popularly used for the electronic ceramic parts. In this study,

the firing shrinkage behavior of almuina green sheet is discussed quantitatively by the mixing of certain ratio of two types of low soda aluminas selected from three commercial types of low soda aluminas. Higher green density is obtained by the mixing of two types. The green density of tape is predictable from particle size distribution. The linear shrinkage is determined by the dimensional distribution ratio which seems to be determined essentially by the anisotropy of alumina particles in the orientation effects by the tape processing equipment. 13 figs., 3 tables, 9 refs. [S. O.]

Narumi Chaina Corporation
Narumi-cho, Midori-ku, Nagoya-shi 458

Milling Effects of Starting Hydrated Aluminum Sulfate on $\eta \rightarrow \alpha$ Phase Transformation and Sinterability of Alumina Keiji DAIMON and Etsuro KATO, *Yogyo-Kyokai-Shi*, **94**, 273-80 (1986)——The milling effects of hydrated aluminum sulfate were studied. Dehydration of milled hydrated sulfate produced broken-egg shell-like particles composed of finer anhydrous sulfate particles through melting of the hydrate on heating. The anhydrous sulfate desulfated into aggregate grains of η-Al_2O_3 with irregular pore size distribution, and the transformation temperature from η- to α-phase transformation was lowered about 100°C. It was confirmed that the enhancement of phase transformation was attributed to accelerated nucleation in η-Al_2O_3 grains, and that the sinterability of α-Al_2O_3 was improved by the increase in the density of green compacts, which was caused by occurrence of many cracks in the skeletal grains of α-Al_2O_3. 11 figs, 1 table, 11 refs. [K. D.]

Nagoya Institute of Technology
Gokiso-cho, Showa-ku, Nagoya-shi 466

Measurement of Thermal Diffusivity of Boron Nitride and Sapphire by Laser Flash Method Hiromichi OHTA and Yoshio WASEDA*, *Yogyo-Kyokai-Shi*, **94**, 295-99 (1986)——In order to measure the thermal diffusivity of ceramics at high temperatures, the correlation factor for radiative heat leak has been estimated with respect to normalized temperature decay rate after its maximum. The thermal diffusivity of boron nitride was obtained at temperature between 1073 and 1773 K with

these correlation factors. The absorber of laser beam and the emitter of heat flux for measuring the temperature response curve by an infrared detector are required in thermal diffusivity measurement of transparent materials. The validity of thin sintered platinum layers formed both sides of specimen was demonstrated by measuring thermal diffusivity of synthetic sapphire at temperature between 1173 and 1773 K. These techniques were found to work basically well at high temperatures. 7 figs., 6 refs. [H. O.]

Department of Metallurgical Engineering, Faculty of Engineering, Ibaraki University
4-12-1, Nakanarusawa, Hitachi-shi 316
*Research Institute of Mineral Dressing and Metallurgy, Tohoku University

Gas Pressure Sintering of Si_3N_4 with an Oxide Addition Eiji TANI, Mitsuhiko NISHIJIMA*, Hiromichi ICHINOSE**, Kazushi KISHI and Seiki UMEBAYASHI, *Yogyo-Kyokai-Shi*, **94**, 300-05 (1986)——Si_3N_4 with Al_2O_3, Y_2O_3, La_2O_3, CeO_2 or Sm_2O_3 was sintered at 1800° to 2000°C under nitrogen of 2 to 4 MPa.

The density of Si_3N_4 with Y_2O_3, La_2O_3 or CeO_2 increased with increasing amount of additives and increasing sintering temperatures. The density and flexural strength of Si_3N_4 sintered at 2000°C and MPa with 10 wt% CeO_2 addition were 3.23 g/cm^3 and about 520 MPa, respectively. 6 figs., 4 tables, 12 refs. [E. T.]

Government Industrial Research Institute, Kyushu
Shuku-machi, Tosu-shi 841
*Kobe Cast Iron Works, Ltd.
**The Saga prefectural Ceramic Research Institute

Sintering Temperature Dependence on Impurities in SiC Ceramics Katsuhisa USAMI, Shizuo UEHARA, Atsuko SOETA and Kunihiro MAEDA, *Yogyo-Kyokai-Shi*, **94**, 306-08 (1986)——The amounts of impurities in hot-pressed SiC ceramics containing 2 wt% AlN or BeO were investigated as a function of sintering temperature. For AlN addition, almost all impurities in raw SiC material remained in the ceramics and their quantities were almost constant in the sintering temperature range of 1800°-2050°C. On the other hand, the behavior of

impurities for BeO addition was different from that for AlN addition. Namely, the quantities decreased above 1850°C and vigorously at around 1950°C. As a result, the quantities of most impurities in ceramics became less than 10 ppm at 2100°C at which the sintering is completed substantially. The residual impurities formed two kinds of phases in ceramics ; a Ti compound including V and a Fe compound including small amounts of Ti, V and Ni. 4 figs., 1 table, 6 refs.

[K. U.]

Hitachi Research Laboratory, Hitachi Ltd.
4026, Kuzicho, Hitachi-shi 319-12

Preparation of Sialon Powder from Kaolinite (Part 2) Sinterability of Sialon Powder Hideyuki YOSHIMATSU, Hisashi MIHASHI and Tatsumi YABUKI, *Yogyo-Kyokai-Shi*, **94**, 309-11 (1986)——Sinterability of a sialon powder prepared from kaolinite and carbon has been studied. The compact of the sialon powder of 93 % conversion sintered densely on heating for 1 h at 1700°C under 1 atm N_2. The bulk density was 3.15 g/cm^3. The sintered sialon was mostly composed of β-sialon. The sialon powder of 98 % convension did not sinter densely. The sialon powder prepared from kaolinite and carbon was more sinterable than the mixture of Si_3N_4, AlN and Al_2O_3. 3 figs., 1 table, 8 refs.

[H. Y.]

Industrial Technology Center of Okayama Prefecture
4-3-18, Ifuku-cho, Okayama-shi 700

Fabrication of Grain-Oriented $Bi_4Ti_3O_{12}$ Ceramics by Normal Sintering (Part 2) Sintering Mechanisms Hirokazu CHAZONO, Toshio KIMURA and Takashi YAMAGUCHI, *Yogyo-Kyokai-Shi*, **94**, 324-29 (1986)——The sintering mechanism of the compacts formed by tapecasting a plate-like $Bi_4Ti_3O_{12}$ powder was studied by densification measurement and microstructure observation. The sintering behavior is characterized as follows : the dominant mechanism responsible for densification is particle rearrangement,

which leads to well-oriented regions of grains and flat and elongated pores, whose long axes are parallel to the sheet plane. The increases in the size of the well-oriented regions and in the contact area between them break up pore connection, resulting in the formation of closed pores at a low density. Grain growth occurs above 1050°C and broadens the grain size distribution. 7 figs., 15 refs. [H. C.]

Faculty of Science and Technology, Keio Universty
3-14-1, Hiyoshi, Kohoku-ku, Yokohama-shi 223

Thermal Shock Resistance of ZrO_2 Ceramics Stabilized by Rare Earth Oxides Hiroshi WATANABE and Mitsuo CHIGASAKI, *Yogyo-Kyokai-Shi*, **94**, 330-35 (1986)——The thermal shock resistance of ZrO_2 stabilized by oxides of rare earth element (La, Nd, Ce, Sm, Gd, Dy, Er, and Yb) has been investigated. Among these ZrO_2 ceramics, only ZrO_2-Yb_2O_3 system shows an improved thermal shock resistance. Specifically ZrO_2-8 wt% Yb_2O_3 exhibits a superior thermal shock resistance to that of ZrO_2-7 wt% Y_2O_3 commonly used in the thermal barrier coating for jet engine components. Furthermore, the addition of 2 wt% Al_2O_3 to the ZrO_2-8 wt% Yb_2O_3 leads to a remarkable thermal shock resistance enhancement. In ZrO_2-8 wt% Yb_2O_3, the monoclinic ZrO_2 grains tended to coalesce into large clusters in the cubic ZrO_2 matrix. As a result, cracks are prone to initiate and propagate within the monoclinic phase during the martensitic transformation. On the other hand, the addition of Al_2O_3 results in the isolated spherical grains of monoclinic ZrO_2 phase, leading to an improved thermal shock resistance. 4 figs., 5 tables, 17 refs. [H. W.]

Hitachi Research Laboratory, Hitachi Ltd.
3-1-1, Saiwai-cho, Hitachi-shi 317

Friction and Wear of Ceramics Measured by a Pin-on-Disk Tester Mikio IWASA and Yasuo TOIBANA*, *Yogyo-Kyokai-Shi*, **94**, 336-43 (1986)——Friction and wear properties of ceramics were measured by a pin-on-disk tester. Four of the most promising fine-ceramics, SiC, Si_3N_4, Al_2O_3 and PSZ were selected, and several samples of each with different raw powders, additives or sintering processes were used in this experiment.

SiC pins showed the lowest coefficient of friction and specific wear rate, followed by Al_2O_3 pins. As Si_3N_4 pins showed a relatively

higher coefficient of friction and specific wear rate, some improvement must be made for practical sliding part applications of Si_3N_4 ceramics. The coefficient of friction and specific wear rate of PSZ pins changed drastically according to disk materials, perhaps as an effect of their thermal conductivity. Wear of any ceramics pins except Al_2O_3 pins was lowest for sliding on SiC disk, followed by Si_3N_4, Al_2O_3 and then PSZ disk. 11 figs., 21 refs. [M. I.]

Government Industrial Research Institute, Osaka
8-31, Midorigaoka 1-chome, Ikeda-shi 563
*Now with Government Industrial Research Institute, Chugoku

Thermal Expansion of High Cordierite and Its Solid Solutions Hiroyuki IKAWA, Tadashi OTAGIRI*, Osamu IMAI*, Kazuyori URABE and Shigekazu UDAGAWA, *Yogyo-Kyokai-Shi*, 94, 344-50 (1986)——High cordierite ($Mg_2Al_4Si_5O_{18}$) and its solid solutions containing Fe, Mn, Ga or Ge were synthesized, and axial thermal expansions of those crystals were measured by means of high temperature X-ray powder diffraction.

The a-parameter increased while the c-parameter decreased with increasing substitution of Fe or Mn for Mg. The thermal expansion along the a-axis decreased whereas the negative expansion along the c-axis increased to positive side with increasing substitution.

The a- and c-parameters increased on the whole with increasing substitution of Ga for Al. The axial thermal expansion behaviours of Ga-bearing crystals with increasing amount of substitution were almost identical to those of Fe and Mn-bearing crystals.

The a- and c-parmameters increased linearly with increasing substitution of Ge for Si. The negative thermal expansion along the c-axis further decreased with increasing substitution, however, the expansion along the a-axis varied in a complex manner the amount of substitution. 10 figs., 2 tables, 29 refs. [H. I.]

Department of Inorganic Materials, Faculty of Engineering, Tokyo Institute of Technology
12-1, Ookayama 2-chome, Meguro-ku, Tokyo 152
*Now with NGK Insulators Ltd.

A Study on the Alumina Ceramics Casting Conditions by the Doctor-Blade Method and Their Effect on the Properties Green Type (Part 1) Kanji OTSUKA, Yoshiyuki OHSAWA* and Koichiro YAMADA**, *Yogyo-Kyokai-Shi*, 94, 351-59 (1986)——The thickness accuracy of the alumina ceramics green tape made by doctor-blade was improved. Calculation and experiment were

compaired. A recommendation of the improvement of the accuracy was conducted as to keep the viscous flow part small and to keep the drift flow part large. From the fluctuation of the machine and atmospheric condition, an accuracy prediction of 6.2 percent at 0.5 mm thickness was derived on the worst case (Table 2). 14 figs., 2 tables, 13 refs. [K. O.]

Device Development Center of Hitachi, Ltd.
2326, Imai, Oome-shi, Tokyo 198
*Kanagawa Works of Hitachi, Ltd.
**Hitachi Reserch Laboratory, Hitachi Ltd.

Some Properties and Sinterability of High Purity Alumina Fine Powders Kenya HAMANO, Takeshi HARA*, Chii-Shyang HWANG, Zenbe-e NAKAGAWA and Minori HASEGAWA, *Yogyo-Kyokai-Shi*, **94**, 372-79 (1986) —— Properties and sintering behaviour of 12 alumina samples of nearly the same grade of high purity and fine powder were compared experimentally. The all samples were α-Al_2O_3 except one which accompanied θ-Al_2O_3. Their apparent crystallite size, specific surface area, distribution of particle size, and shape and appearance of their particles differed considerably with samples. Further, green density of their compacts and sintering behaviour differed markedly with samples, but these difference might be explained well with shape and appearance of particles. From the results obtained, it became clear that to produce dense ceramics, selection of its raw materials is the most effective means. Further, required properties for good sinterable alumina powder were estimated. 9 figs., 4 tables, 3 refs. [K. H.]

Research Laboratory of Engineering Materials, Tokyo Institute of Technology
4259, Nagatsuta, Midori-ku, Yokohama-shi 227
*Asahi Kogyo Co., Ltd.

Synthesis of Hexagonal Plate-Like Corundum Using Hydrated Aluminum Sulfate As Starting Materials Keiji DAIMON and Etsuro KATO, *Yogyo-Kyokai-Shi*, **94**, 380-82 (1986)——Synthesis of hexagonal plate-like corundum crystals by heating η-Al_2O_3 with AlF_3 was studied using different starting aluminum sulfates. It was suggested that a vapour phase formed in the presence of AlF_3

transformed Al_2O_3 from η-Al_2O_3 to the surface of the growing corundum crystals. The relatively large hexagonal plate corundum crystals with a narrow size distribution were obtained when well developed hydrated sulfate crystals were used and dehydrated in vacuum and the crystallization to corundum was performed at 900°C. The experimental results indicate that the elimination of defects of Al^{3+} ion layer structure of hydrated sulfate suppresses the nucleation of α-Al_2O_3 so that large corundum crystals may be formed in the presence of AlF_3. 2 figs., 7 refs. [K. D.]

Nagoya Institute of Technology
Gokiso-cho, Showa-ku, Nagoya-shi 466

Saturation Magnetization of Nickel Ferrites in Relation to Lattice Strain Hiroshi YAMAMURA, Toshihiko KAKIO*, Hajime HANEDA, Akio WATANABE, and Shin-ichi SHIRASAKI, *Yogyo-Kyokai-Shi*, **94**, 393-99 (1986) —— Nickel ferrites, which were prepared by firing the co-precipitated oxalate of Ni^{2+} and Fe^{2+} at various temperatures from 500°to 1000℃ in air, were Fe-deficient spinel-type phase. The samples fired at fairly low temperature have many crystal imperfections such as lattice strain ($\Delta d/d$) and lattice defects, which decreased with increasing firing temperature, and vanished above 800°C. The nickel ferrite having such imperfections has a low saturation magnetization, which increased with increasing firing temperature. On the other hand, the nickel ferrite prepared by solid-state was mechanically ground for extended time period to introduce lattice strain. The saturation magnetization of the sample thus obtained also decreased lineary with increasing lattice strain. These facts suggest that the lattice strain, regardless, its origin, lowers the saturation magnetization. 9 figs., 4 tables, 12 refs. [H. Y.]

National Institute for Research in Inoranic Materials
1-1, Namiki, Sakura-mura, Niihari-gun, Ibaraki 305
*Taki Chemical Co.

Preparation of Codeposited Al_2O_3-TiO_2 Powders by Vapor Phase Reaction Using Combustion Flame Saburo HORI, Yoshio ISHII, Masahiro YOSHIMURA* and Shigeyuki SŌMIYA*, *Yogyo-Kyokai-Shi*, **94**, 400-08 (1986) —— Spherical ultrafine Al_2O_3-TiO_2 powders were prepared by vapor phase reaction using a combustion flame. They consisted pf γ-Al_2O_3 and anatase and rutile TiO_2. β-Al_2TiO_5

was scarcely formed due to the difference between the reactivity of $AlCl_3$ and that of $TiCl_4$. Solutions of Al_2O_3 into TiO_2 and of TiO_2 into Al_2O_3 appeared to influence the stability of phases in the codeposited Al_2O_3-TiO_2 powders. An unknown phase was detected in the powders calcined at 1200°C. It was considered to be a bronze-type compound containing H^+ and Al^{3+}. 7 figs., 4 tables, 21 refs.

[S. H.]

Kureha Chemical Industry Co., Ltd.
16, Ochiai, Nishikimachi, Iwaki-shi 974
*Research Laboratory of Engineering Materials,
Tokyo Institute of Technology

Preparation of Carbon-Ceramic Composite Materials by Use of Raw Coke (Part 4) Oxidation Resistance of C-SiC-B_4C Composite in Air Ichitaro OGAWA , Takayoshi YAMAMOTO*, Tsuyoshi HAGIO, Hisayoshi YOSHIDA and Kazuo KOBAYASHI, *Yogyo-Kyokai-Shi*, **94**, 409-14 (1986)——C-SiC-B_4C composites were made from powder mixtures of raw coke and SiC-B_4C (42 : 58 in weight) by grinding, compacting and baking in Ar gas at 2000°C. Thus, the weight loss of the composite made from the ground powder containing 30 vol% SiC-B_4C was 0.2, 0.6 and 6% after 1000°C-20 h, 1200°C-5 h and 1300°C-5 h heating respectively. X-ray diffraction analysis and IR spectroscopy showed that the specimens were coated with a liquid film of B_2O_3- or SiO_2-B_2O_3 Glass in air. 7 figs., 13 refs. [I. O.]

Government Industrial Research Institute, Kyushu
Shuku-machi, Tosu-shi, Saga 841
*Aso Cement Co., Ltd.

HREM Analysis of SiC Grain Boundary Structure Hideki ICHINOSE, Yoshizo INOMATA* and Yoichi ISHIDA, *Yogyo-Kyokai-Shi*, **94**, 415-18 (1986)——A grain boundary of high purity SiC bicrystal grown by sublimation recrystallization method was examined by high resolution electron microscopy. The boundary was coincided with one of three models which were constructed so that

the number of dangling bond was least throughout the possible atomic arrangement at that orientation relation ship. The reason why only one structure was preferred among three in spite of the number of dangling bond was attributed to the effect of ionic bonding component of SiC crystal. 6 figs., 13 refs. [H. I.]

Institute of Industrial Science, University of Tokyo
22-1, Roppongi 7-chome, Minato-ku, Tokyo 106
*National Institute for Reserch in Inorganic Materials

Debye Length and Gas Sensor Mechanism of Undoped and Sm_2O_3-Doped ZnO Ceramics Seigen RI, Kenya HAMANO and Zenbe-e NAKAGAWA, *Yogyo-Kyokai-Shi*, **94**, 419-24 (1986)——Only specimens, whose neck radii were smaller than the Debye length, showed decrease in electrical resistivity under the admission of propane gas. This mechanism is explained by gate action of pinch-off potential at the necks. 12 figs., 2 tables, 9 refs. [S. R.]

Research Laboratory of Engineering Materials, Tokyo Institute of Technology
4259, Nagatsuta, Midori-ku, Yokohama-shi 227

Fatigue Behavior of Y_2O_3-Partially Stabilized Zirconia Masahiro ASHIZUKA, Hideki KIYOHARA, Eiichi ISHIDA, Makoto KUWABARA, Yoshitaka KUBOTA* and Takaaki TSUKIDATE*, *Yogyo-Kyokai-Shi*, **94**, 432-39 (1986)——The fatigue behavior of 3 mol% Y_2O_3-patially stabilized zirconia with average grain size of 0.4 μm (Z3Y-I) and 1.0 μm (Z3Y-II) and was studied. The crack growth parameter (N) of Z3Y-I and Z3Y-II measured by the dynamic fatigue technique at 20°C was 40.8 and the N value of Z3Y-I at 250°C was 50.5. On the other hand, the N value of Z3Y-II at 250°C was 10.2. The average lifetime of Z3Y-I and Z3Y-II at 20°C and 250°C were predicted from dynamic fatigue data.

The average lifetime of Z3Y-II measured by the static fatigue technique at 250°C was 4 to 6 times the lifetime from dynamic fatigue data. The fracture surface of Z3Y-II tested by the static fatigue technique at 250°C showed fatigue surface near tensile surface and its zone size increased with decreasing applied stress and increasing time to failure. 9 figs., 2 tables, 24 refs. [M. A.]

Kyusyu Institute of Technology
1-1, Sensui-cho, Tobata-ku, Kitakyusyu-shi 804
*Tokyo Soda Manufacturing Co., Ltd.

Lattice Constants of High Cordierite Containing TiO_2 or ZnO
Hiroyuki IKAWA, Kunio SATO*, Masaharu SUZUKI**, Kazuyori URABE and Shigekazu UDAGAWA, *Yogyo-Kyokai-Shi*, **94**, 452-53 (1986) —— The increase in lattice constants of high cordierite on doping with ZnO or TiO_2 were investigated. Gahnite was an impurity crystalline phase when cordierite glasses doped with ZnO were crystallized by heating at 1050°C for 48 h. Just a trace of gahnite was detected when 1.5 wt% of ZnO was added, but it increased with increased amount of the dopant. The unit cell volume of high cordierite increased on doping with ZnO up to 3 wt%, however, the volume did not increase on further doping. Rutile was one of the impurites when TiO_2 was added to the cordierite glass. In this case, however, solubility limit of TiO_2 in high cordierite was not so well defined as for the case of ZnO. That is, the unit cell volume of high cordierite increased continuously with increasing amount of TiO_2 up to 9 wt%, although the rate of increase in unit cell volume diminished with increased doping. Some differences in crystal chemistry between Zn^{2+} and Ti^{4+} ions were considered to be responsible for the observed difference. 1 fig., 1 table, 11 refs. [H. I.]

Departmen of Inorganic Materials, Faculty of Engineering,
Tokyo Institute of Technology
12-1, Ookayama 2-chome, Meguro-ku, Tokyo 152
*Now with Sumitomo Cement Co., Ltd.
**Now with Denki Kagaku Kogyo Co. Ltd.

Int. J. High Technology Ceramics **2** (1986) 326–327

CONTENTS OF VOLUME 2

Number 1

Number 2

Number 3

Number 4

High Technology Ceramics
Papers Published in 1985

CONTENTS OF VOLUME 1

Number 1

Number 2

International Journal of
HIGH TECHNOLOGY CERAMICS

The *International Journal of High Technology Ceramics* will concentrate its attention on research papers which deal with the development, fabrication and utilisation of modern ceramic materials that have technological, as well as commercial potential. The Journal will publish papers of high scientific standard and will provide a much needed interface for scientists, technologists and engineers working with ceramic materials. Attention will also be given to the concept of ceramic engineering, be it for mechanical, electrical, magnetic or other special applications.

Manufacturing-related topics with which this Journal will be concerned include: powder synthesis, processing and fabrication techniques such as slip casting, injection mouldings, isostatic pressing, CVD and hipping.

Materials to be covered in the areas of engineering and electrical ceramics will include silicon carbide, silicon nitride, sialons, alumina, zirconia and zirconates, titanates, ferrites and aluminates.

Papers dealing with the interaction between design, manufacture and microstructural control will be particularly welcome.